AN $^{18}O/^{16}O$, D/H AND K-Ar STUDY OF THE SOUTHERN HALF OF THE IDAHO BATHOLITH

Thesis by

Robert Everett Criss

In Partial Fulfillment of the Requirements

for the Degree of

Doctor of Philosophy

California Institute of Technology

Pasadena, California

1981

(Submitted September 22, 1980)

ACKNOWLEDGEMENT

I learned a great deal from my thesis advisor, Hugh Taylor. He originally suggested this project to me, contributed many valuable ideas and suggestions, and gave me some sound personal advice along the way. The time and care he gave to the thesis manuscript deserve special mention.

Much of the laboratory work was accomplished during my stay at the Branch of Isotope Geology of the U.S. Geological Survey at Menlo Park. Marv Lanphere arranged for me to work in the K-Ar laboratories, provided many helpful instructions and suggestions, and expedited matters in the rare instances when progress was slow. Jim O'Neil made me feel welcome in his stable isotope laboratory, where most of the D/H work was done, and also provided helpful advice and discussion. The collective efforts of these men and my advisor made my Ph.D. experience memorable and unique.

Professors L.T. Silver, H.A. Lowenstam and S. Epstein provided advice during my stay at Caltech, some of which proved to be critically important. I thank Professors John Hower and Sam Savin for my initial interest in geochemistry, and for contributing so much to my excellent undergraduate education at Case Western Reserve University.

In the course of this work I profited from discussions with many geologists and geochemists, including L.T. Silver (C.I.T.), D.E. White (U.S.G.S.), W.R. Greenwood (U.S.G.S.), H.W. Yeh (Univ. of Hawaii), W.E. Hall (U.S.G.S.), R.H. Becker (C.I.T.), B.W. Chappell (A.N.U.) and E.H. Bennett (Idaho Bur. Mines and Geology). Bennett also provided many maps and manuscripts of his work in Idaho in advance of their publication, which greatly helped me interpret the results in the Rocky Bar area. The value of the discussions and help provided by my fellow Caltech students cannot be overstated,

and I particularly want to thank Bob Gregory, Dave Nelson, Duane Champion, Jim Quick, Bob Powell, Dave Cole, Ted Labotka, Stein Jacobsen, John Jones, Cleve Solomon, and Dave Beaty. This incomplete list does little justice to the best group of people I have ever known.

It is also impossible for me to properly state the value of the technical assistance and instruction I received from the Caltech and the U.S.G.S. staffs. Those most directly involved were Jerry von Essen, Art Chodos, Joop Goris, Mike Carr, John Coulson, Bobbie Myers, James Saburomoru, Elliot Sims, Vic Nenow, Doug White, Paul Klock and Joe Christie. Anne Swatfigure did a nice job typing the manuscript, and worked many extra hours when deadlines drew near.

I enjoyed the help and company of Karl Criss, John Jones and Dave Nelson during portions of the field work. Jeff Given provided the important suite of samples collected along the Salmon River. I thank Kim and Dave Kline for their kindness and hospitality whenever I came out of the field, usually dirty, hungry and tired.

Most of all I thank my parents for their continued encouragement, advice and help, and for tending to my personal matters when I could not. It is to them that this thesis is dedicated.

Support for this work was provided by N.S.F. Grants EAR-7816874 and EAR76-21310 and D.O.E. Grant EY-76-G-03-1305.

ABSTRACT

$\delta^{18}O$ and δD measurements provide powerful tools for the study of igneous rock petrogenesis. Among the noteworthy contributions of such studies have been the demonstration that massive quantities of hydrothermal fluids have interacted with considerable portions of the earth's upper crust, that the majority of such fluids are derived from ordinary meteoric surface waters, and that similar fluids appear to be involved in the formation of many ore deposits. This thesis presents the results of a combined $\delta^{18}O$, δD, K-Ar and petrographic study, whose principal goal was to elucidate the characteristics and thermal history of a series of hydrothermal systems developed within the Idaho batholith during the Eocene, about 40-45 m.y. ago.

The hydrothermal activity of concern is related to a period of intense magmatism and tectonism in Idaho termed the Eocene event. This period was characterized by intrusion of epizonal granite batholiths, formation of the cogenetic Challis volcanic field, block faulting, ring faulting, and ore deposition. The effects are very widespread but are most conspicuous in the east-central portion of the southern half (Atlanta lobe) of the Idaho batholith, the region which was studied in most detail.

The effects of the widespread hydrothermal activity are easily monitored against the relatively uniform primary character of the Mesozoic granitoids, which originally had whole-rock $\delta^{18}O$ values of 9.5±1.5 and biotite δD values of -70±5 permil. The Eocene meteoric waters in this region had $\delta^{18}O$ and δD values of about -16 and -120 permil respectively, and interaction and exchange of the rocks with deep circulating fluids derived from these waters produced major heavy isotope depletions in the rocks, such that the whole-rock $\delta^{18}O$ and biotite δD values became as low as -4.5 and -176 permil. However, the rates of isotopic exchange of

various minerals with the fluid are not identical, and the new results prove that feldspar exchanged ^{18}O with the fluid at least four times as fast as did coexisting quartz, and that biotite exchanged D with the fluid at a much faster rate than did coexisting muscovite. These differential effects are important because they allow the primary isotopic compositions to be deduced from altered rocks, and have the still unproven potential of indicating something of the temperature-time history of the hydrothermal interactions.

Widespread propylitization of the rocks occurred concurrently with the $\delta^{18}O$ and δD exchange effects. The most commonly observed petrographic changes are the development of chlorite and sericite, whose quantities generally increase in crude proportion to the amount of ^{18}O exchange. Such hydration effects are generally not conspicuous in previously studied hydrothermal areas associated with gabbroic plutons, which indicates that the hydrothermal interactions in Idaho occurred at relatively low temperatures (generally <350°C, see below).

Systematic mapping of the $\delta^{18}O$ and δD depletions of the rocks has provided some startling new insight on the ancient hydrothermal systems in Idaho. The largest well-studied low-^{18}O anomaly, termed the Sawtooth Ring Zone (SRZ), is a 5 to 15 km wide annulus of low ^{18}O rock (average ~2 permil) which has an outer diameter of 40 X 60 km. D/H effects in the rocks are often discernible more than 25 km outside of the periphery of this feature, the larger size being attributable to the extreme sensitivity of the δD value to alteration under conditions of low water/rock ratios. The low-^{18}O ring is centered on the Eocene Sawtooth batholith and its outlying plutons, and a large aeromagnetic anomaly suggests that Eocene rocks in fact underlie the entire SRZ region. These data provide good evidence that the SRZ is coincident with a high-permeability ring fracture

zone associated with a giant Eocene caldera.

Several smaller low-^{18}O zones have also been mapped in the Atlanta lobe, and their clearcut spatial association with the Eocene intrusives provides an important mapping and interpretative tool in the region. Furthermore, most of the productive mines in the Atlanta lobe are located near the periphery of these low-^{18}O zones (along the "outer" +8 permil $\delta^{18}O$ contour); this association links these deposits with the Tertiary hydrothermal activity and has great potential as an exploration tool.

K-Ar age data provide important complementary information about the geology of the region and on the thermal characteristics of the ancient geothermal systems. The apparent ages of Mesozoic biotites systematically decrease from about 95 m.y. along the east and west margins of the Atlanta lobe to <45 m.y. near the Eocene plutons, the latter ages being approximately concordant with those of the Eocene plutons themselves. However, there is a significant "age gap" between 45 and 53 m.y. No strong correlations of the apparent ages with the $\delta^{18}O$, δD or K_2O contents of the "biotite" separates were noted, and the majority of the apparent ages in any given locality are in fact correlated simply with the elevation. These observations suggest that most of the ages were produced by uniform, constant uplift (~0.15 mm/yr) of the batholithic terrane through the Ar "blocking temperature" (~300°C) during the early Tertiary. This uplift continued through the Eocene but was modified by the formation of a regional dome probably related to the intrusion of a gigantic volume (~25,000 km^3) of Eocene magma. However, rocks collected near the contacts with the Eocene plutons, or at the lowest elevations in the overall region, definitely suffered catastrophic Ar loss during the Eocene; the apparent ages of these rocks do not correlate with the elevation and indicate that temperatures were high (>300°C). A

model of the ancient temperature distribution is derived from these data and indicates that 1) most of the hydrothermal activity occurred at temperatures of 150-350° C and persisted to depths of at least 7 km below the earth's surface, 2) many of the outcropping Eocene intrusives were intruded at depths of 5 to 7 km, and 3) a significant proportion (>1/3) of the heat provided to the circulating fluids was provided by the ordinary geothermal gradient in the older rocks, although the driving force for the circulation was clearly provided by the thermal energy of the Eocene plutons.

All of the above properties bear on the nature of modern geothermal systems at deep levels which are presently inaccessible to view, and a close analogy of the SRZ may be made with the region at Yellowstone, Wyoming. The evidence presented for the extensive lateral migration of fluids, the depth of circulation and the thermal properties of these fluids are of particular importance, and helps explain the incredibly high fluid and thermal discharge rates currently observed within the Yellowstone caldera. The lack of definite evidence for low-^{18}O magmas in Idaho contrasts with the recent discovery of voluminous extrusions of such magmas at Yellowstone, and suggests that such magmas are produced at the top of silicic magma chambers and are inevitably erupted, commonly as H_2O-rich ash flow sheets. Last, the intense deep-level circulation patterns of the annular SRZ zone contrast with the surface intercaldera discharge systems currently observed at Yellowstone, and may indicate that significant geothermal reserves may be tapped at deep levels by drilling into the ring fracture zones of modern caldera-related systems.

TABLE OF CONTENTS

FIGURES page

TABLES page

CHAPTER 1

INTRODUCTION

1.1 Object of the Research

This thesis presents considerable new data on the origin and deep circulation patterns of a series of hydrothermal systems established in the Idaho batholith during the Eocene, about 38-45 m.y. ago. These systems are associated with large masses of rhyolitic volcanic rocks and their associated epizonal batholiths, and are thought to be analogous in many respects to the hydrothermal and magmatic phenomena presently taking place in Yellowstone National Park, Wyoming. Hydrothermal systems are subjects of considerable scientific interest, and they have great economic and social importance as well. Areas of hot water and steam discharge are among the most beautiful and interesting places in the world, as evidenced by the fact that Yellowstone National Park was the first such region established in the United States and to this day remains one of the most appreciated.

The economic significance of the subsurface counterparts of geyser systems was probably first recognized by Agricola (1556), who proposed that many valuable metals were carried and concentrated by these types of aqueous solutions. Current interest in geothermal systems includes all aspects of the chemistry of the waters, the physics of the hydrologic transport process, the character and historical development of the geothermal regions, and the utilization of the fluids as sources of energy and chemicals.

The discovery that much of the region underlain by the Idaho batholith was formerly the site of large scale ($\sim 10^4 km^2$) geothermal activity was made by Taylor and Magaritz (1976; 1978). They used $^{18}O/^{16}O$ and D/H measurements of the granitic rocks to make a reconnaissance map of the

ancient (Eocene) hydrothermal systems, a technique that is also utilized extensively in the present work. Their principal conclusions, other than demonstrating the existence and wide scale of the phenomenon, was that the aqueous solutions were all of meteoric origin and that Eocene plutonic activity provided the requisite heat. They also noted that the areas of ancient hydrothermal activity coincided with large regions of rocks with anomalously young K-Ar ages, as mapped in reconnaissance fashion by Armstrong (1974). Based on the geographic correlation, Taylor and Magaritz (1976) proposed that the Eocene plutonism and associated hydrothermal alteration were in fact the processes responsible for the anomalous K-Ar age pattern discovered by Armstrong (1974).

The goal of the present investigation was to carefully map the $^{18}O/^{16}O$, D/H and K-Ar age distributions in the southern half of the Idaho batholith, and to determine whether any detailed correlations exist among these different variables. It was hoped that such a detailed isotopic study, together with some supportive geologic work, would produce results that might help answer some of the following problems:

(a) The age, size, and shape of the hydrothermally altered areas in the Idaho batholith and their relationships to causal geologic factors.

(b) The nature of the deep portions of analogous modern geothermal systems, such as Yellowstone, Wyoming and the Valles Caldera, New Mexico, using the ancient, deeply dissected terrane in Idaho as a model.

(c) The petrology, isotopic composition and distribution of plutonic and hypabyssal rock types of various ages in the batholith.

(d) The nature of the relationships between petrographic, isotopic, and K-Ar age changes in the rocks.

(e) The mechanism of $^{18}O/^{16}O$ and D/H exchange in the minerals and rocks of the batholith.

(f) The mechanism of radiogenic Ar loss from minerals, and its effect on the the K-Ar age values.

(g) The establishment of new criteria for determining the relationship between K-Ar measurements and the true emplacement age of the plutons.

Considerable progress has been made on all of the above problems except (g). In addition, this work has also provided new information on the following:

(h) The distribution of Eocene intrusive rocks in unmapped portions of the batholith, as well as in the subsurface.

(i) The genesis and localization of Au-Ag mineralization in the batholith, and some indications of potential exploration targets for such mineralization.

(j) The temperature distribution in the batholith during the Eocene, and the relative thermal contributions of the Eocene magmas to the hydrothermal fluids, as compared to the effects of the ordinary geothermal gradient.

(k) An approximate estimate of the volume of the Eocene magma emplaced in the batholith, and some data on the mechanism of emplacement of these epizonal plutons.

(l) The discovery of a relationship between K-Ar apparent ages and elevation in the batholith, which permits calculation of the rate of uplift of the batholithic terrane during the Cenozoic.

Besides providing new stable isotope and K-Ar data, the present work attempts to utilize these data to evaluate and provide a synthesis of the geology and geochemistry of a large portion of southern Idaho over the past 150 m.y. The

following discussion thus concerns itself with a very broad variety of geologic problems, beginning with the multiple episodes of intrusion associated with emplacement of this giant composite batholith, continuing through all the subsolidus and hydrothermal alteration effects superimposed on these rocks, and ending with some conclusions about the uplift and cooling history of the batholith. In order to place these new data in proper context it is necessary to review a variety of previous approaches to these problems, not merely those concerned with the geology and geochemistry of the Idaho batholith, but also those earlier studies that bear on the general problems of K-Ar age re-setting, silicic volcanism and caldera formation, and water/rock interactions associated with convective hydrothermal circulation systems. The next few sections of the thesis therefore review the pertinent previous scientific studies that form an essential foundation for the principal conclusions of the present study.

1.2 Previous Work

1.2.1 $^{18}O/^{16}O$ and D/H Studies of the Idaho Batholith

Lawrence and Taylor (1971, 1972) made an $^{18}O/^{16}O$ and D/H study of soil profiles, two of which were developed on granitic rocks of the south-central portion of the Idaho batholith. They concluded that clastic mineral fragments in the soils retain the isotopic compositions of the parent rocks, but that secondary clay minerals and hydroxides that form in the weathering environment are in approximate isotopic equilibrium with low-temperature meteoric waters. They also made analyses of the parent rocks on which the soils were developed, and this study provided the first indication of unusually low $\delta^{18}O$ (4.0, -6.1) and δD (-152) values in the plutonic igneous

rocks of Idaho. However, Lawrence and Taylor (1971) made no attempt to explain or expand on these data.

Following up the indications discovered by Lawrence and Taylor, Taylor and Magaritz (1976, 1978) made a reconnaissance stable isotope study of the Idaho batholith. Inasmuch as their results are of central importance and reflect the state of knowledge previous to the current study, they are shown on Figs. 1.1-1.4. Taylor and Magaritz recognized that the west-central portion of the batholith was isotopically "undisturbed" and characterized by "normal" δD values of about -70 permil. In this region the $\delta^{18}O$ values of quartz and feldspar give "normal" fractionation factors, but the whole rock $\delta^{18}O$ values are slightly high; they suggested that this reflected the involvement of high $-^{18}O$ sialic crust in the source regions of the original magmas.

East of this "undisturbed" zone, the δD values become lower and more erratic although the $\delta^{18}O$ values remain roughly constant, indicating relatively weak hydrothermal alteration of the rocks. Still further east, in the large (10^4 km^2) zone of Eocene igneous activity and anomalous K-Ar ages, the δD values drop to about -150 and the $\delta^{18}O$ values of feldspar also become very low and extremely erratic; however, the $\delta^{18}O$ value of quartz was only slightly lowered, because of it lower exchange rate. Taylor and Magaritz (1976, 1978) interpreted these marked ^{18}O and D depletions in terms of pervasive meteoric-hydrothermal activity (water/rock about 0.1 to >2.0) developed about the Eocene plutons. They emphasized the spatial correlation between the stable isotopic and K-Ar age data, and proposed that the regional re-setting of K-Ar ages reflected large scale heat transfer and rock alteration by the hydrothermal fluids.

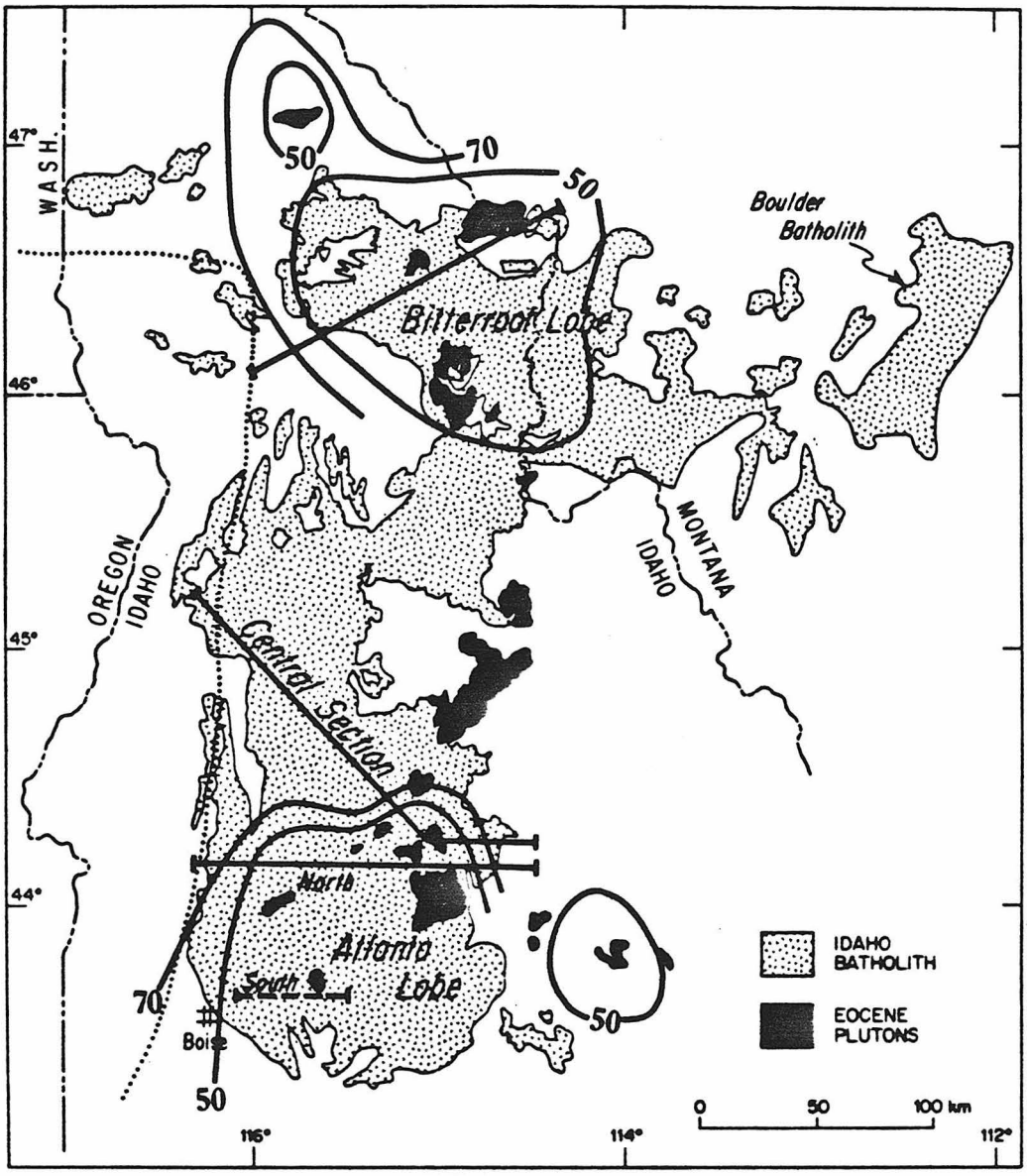

Figure 1.1 Map of the Idaho batholith and Eocene plutons, showing the 70 and 50 m.y. apparent age contours of Armstrong (1974), and the $^{87}Sr/^{86}Sr$ boundary (0.706, dotted line) of Armstrong et al (1977). Section lines refer to Figs. 1.4a, 1.4b, and 1.4c. From Taylor and Magaritz (1978).

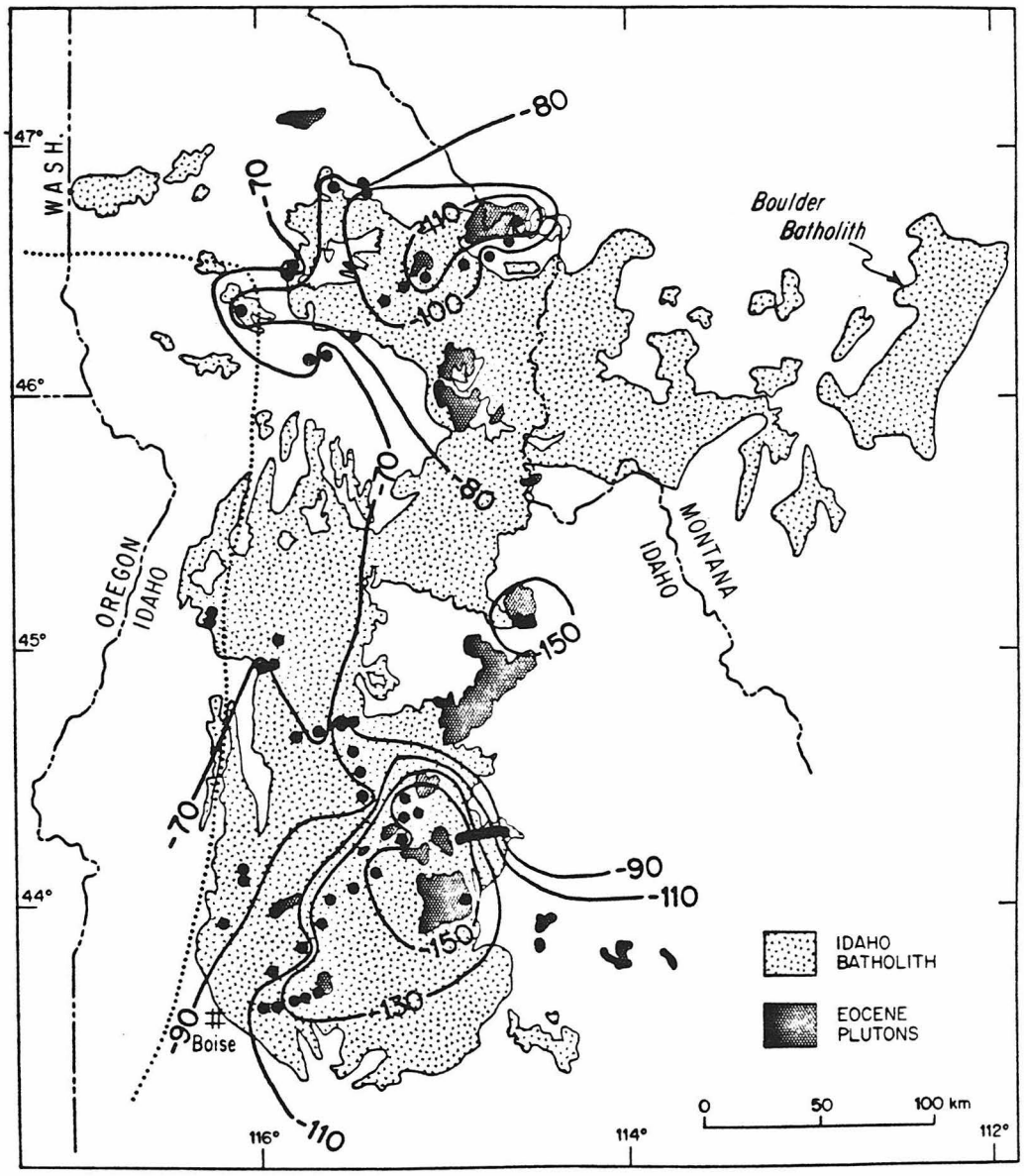

Figure 1.2 Map of the Idaho batholith, showing sample locations (dots) and δD contours for biotite, hornblende, and chlorite. Note the spatial relationship of the δD contours to the Eocene plutons; also compare with Figs. 1.1 and 1.3. From Taylor and Magaritz (1978).

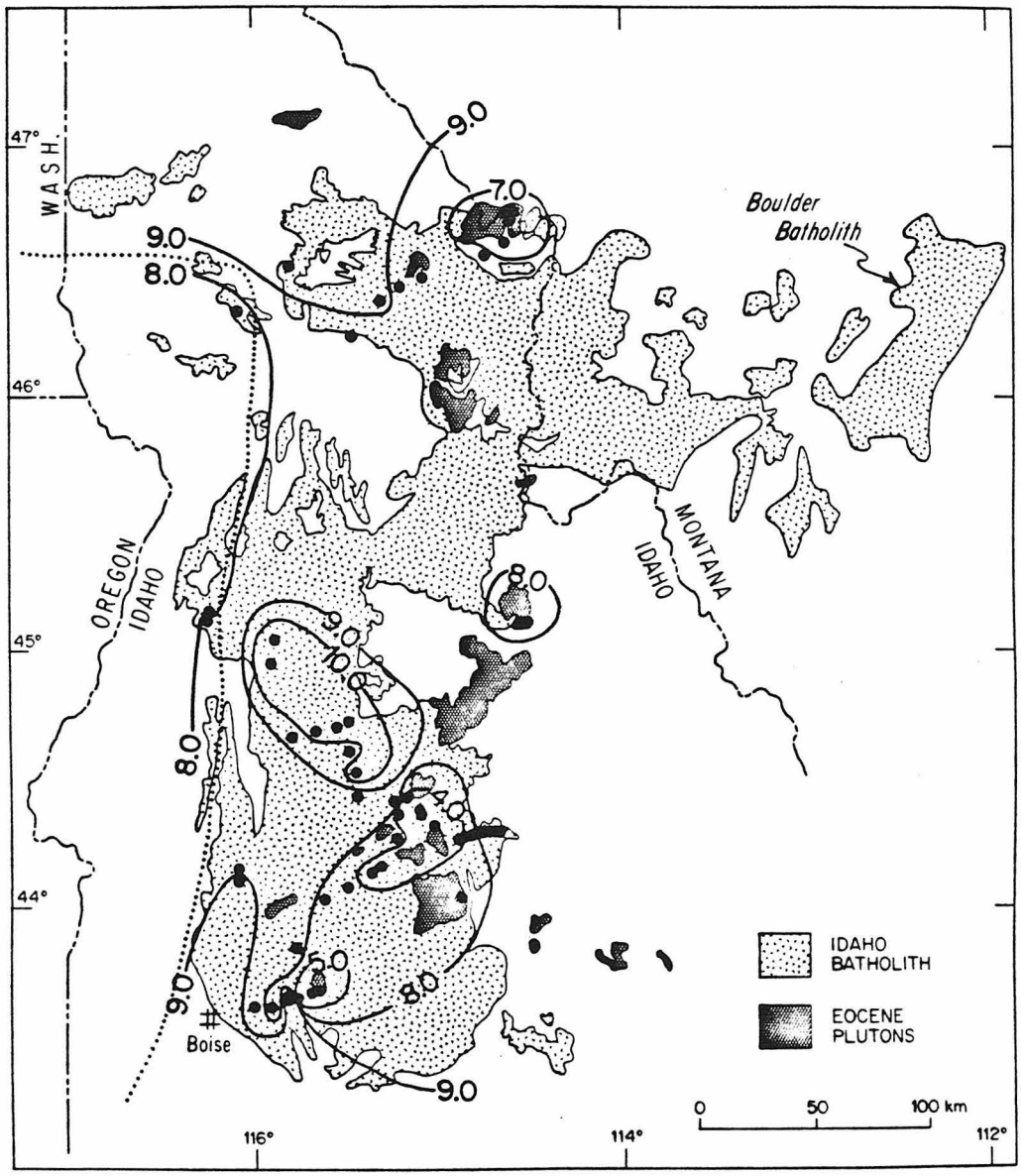

Figure 1.3 Map of the Idaho batholith, showing sample locations (dots) and $\delta^{18}O$ contours for the feldspar and whole-rock samples analyzed by Taylor and Magaritz (1976). Unpublished map provided by H.P. Taylor.

Fig. 1.4 abc $\delta^{18}O$ and δD analyses of Taylor and Magaritz (1976) projected along the three section lines shown in Fig. 1.1, namely the central section (Fig. 1.4a), the northern and southern Atlanta lobe sections (Fig. 1.4b) and the Bitterroot lobe section (Fig. 1.4c). Fig. 1.4b strikingly shows the relative constancy of quartz $\delta^{18}O$, compared to the marked ^{18}O depletions observed in feldspars and the marked deuterium depletions in the hydrous minerals in rocks near the large Eocene plutons. Figures 1.4a and 1.4b are from Taylor and Magaritz (1978); Figure 1.4c is unpublished data provided by H.P. Taylor.

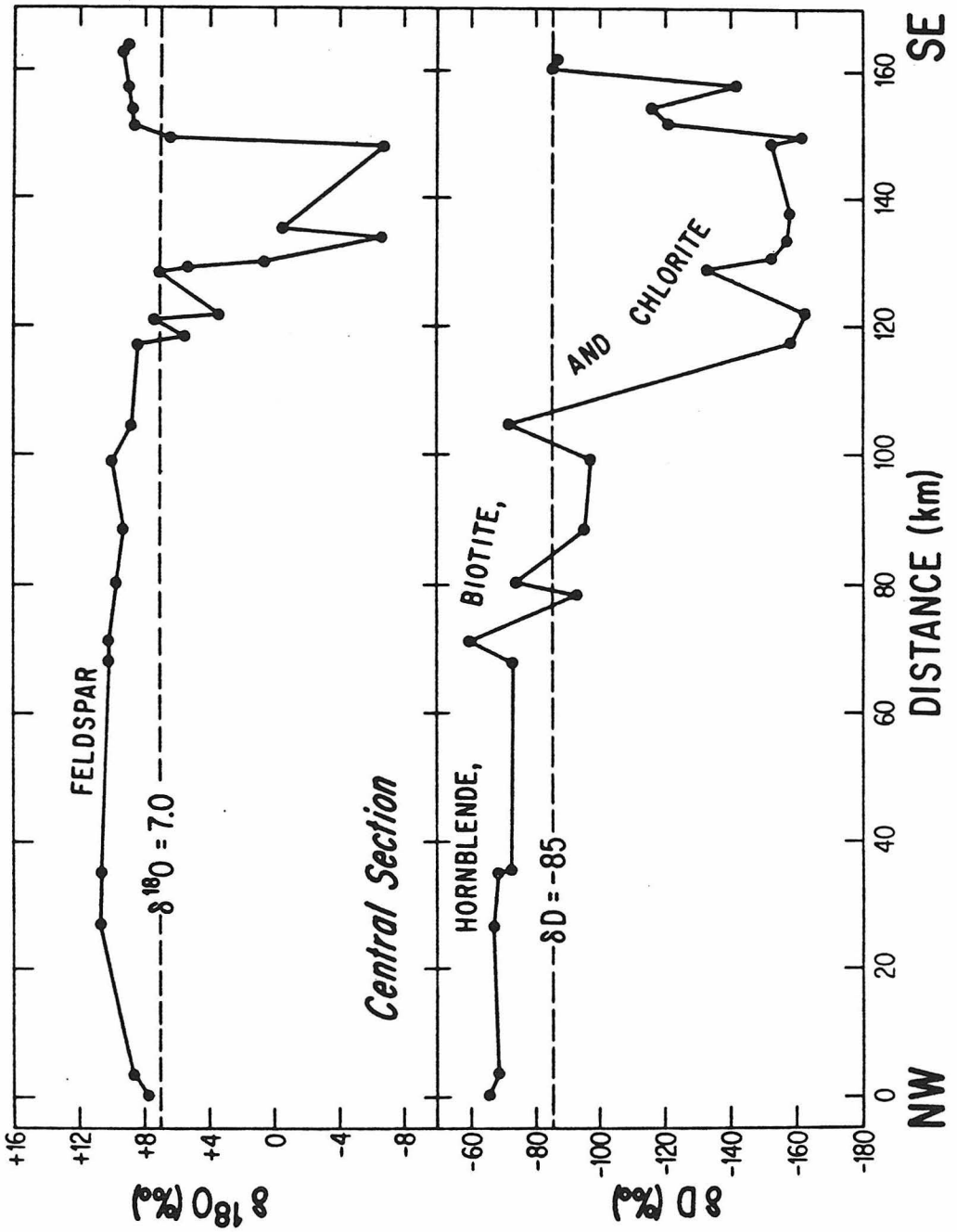
FELDSPAR
$\delta^{18}O = 7.0$
Central Section
HORNBLENDE, BIOTITE, AND CHLORITE
$\delta D = -85$
$\delta^{18}O$ (‰)
δD (‰)
+16
+12
+8
+4
0
-4
-8
-60
-80
-100
-120
-140
-160
-180
0
20
40
60
80
100
120
140
160
NW
SE
DISTANCE (km)

Fig. 1.4a

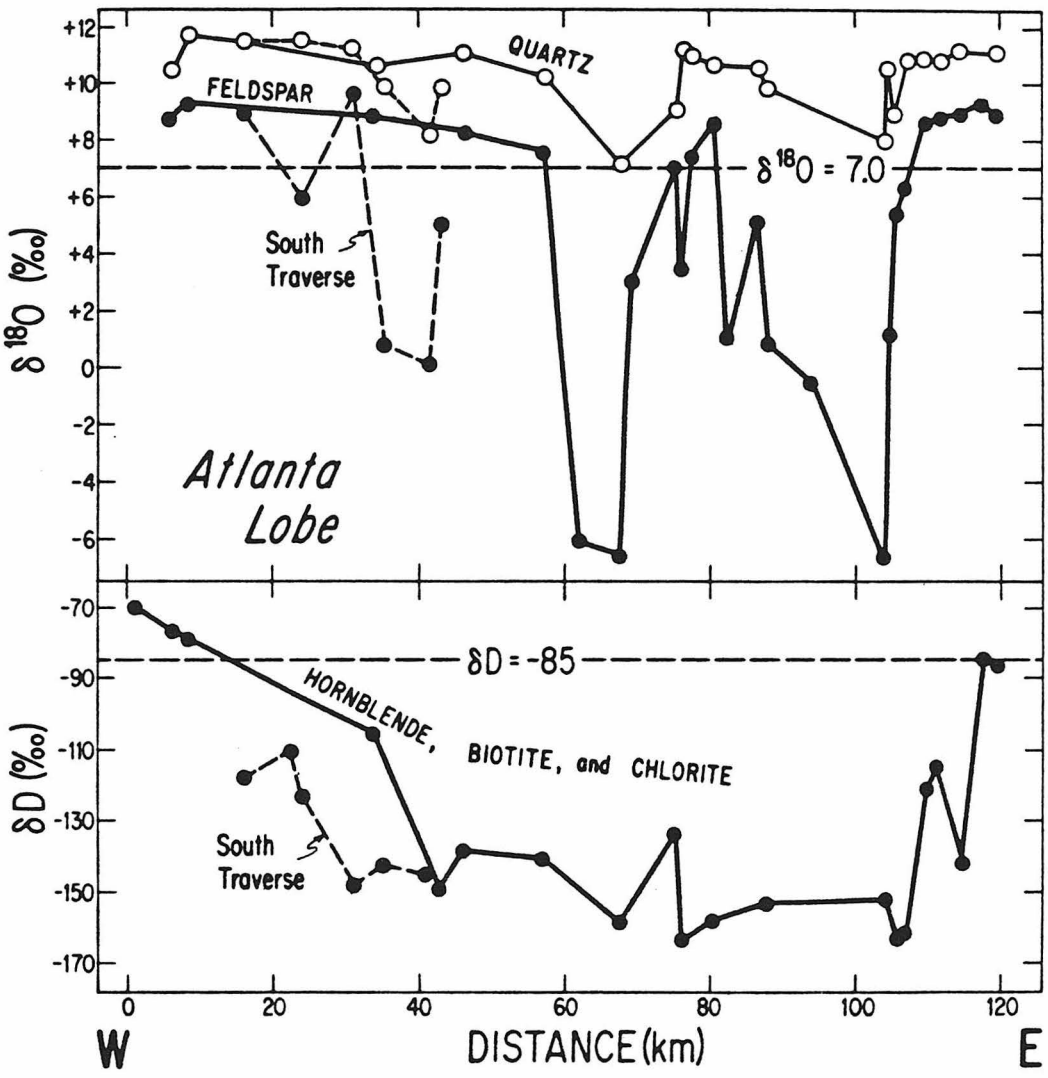
QUARTZ
FELDSPAR
δ18O = 7.0
South Traverse
Atlanta Lobe
δ18O (‰)
+12
+10
+8
+6
+4
+2
0
-2
-4
-6
δD = -85
HORNBLENDE, BIOTITE, and CHLORITE
South Traverse
δD (‰)
-70
-90
-110
-130
-150
-170
0
20
40
60
80
100
120
W
DISTANCE (km)
E

Fig. 1.4b

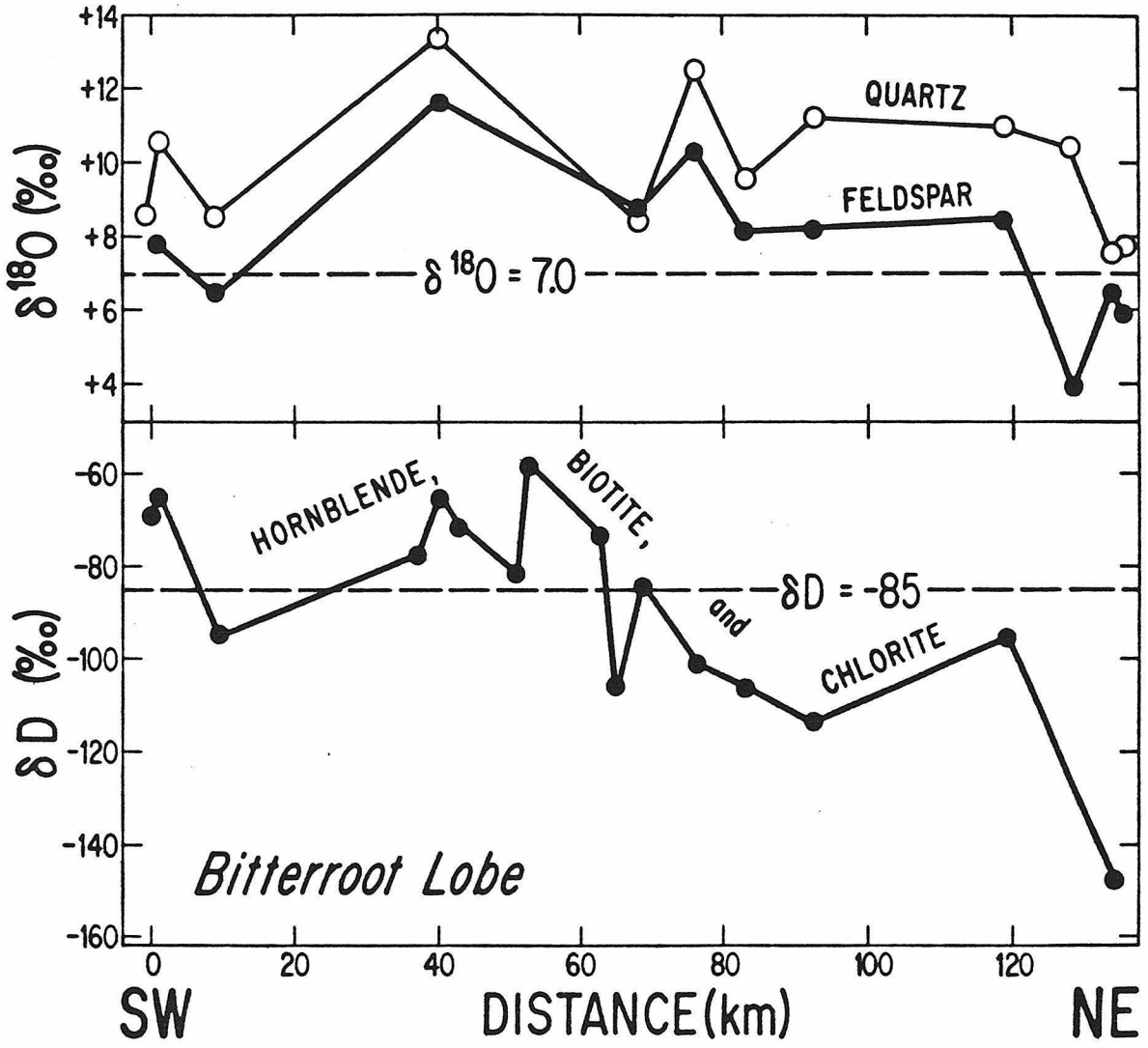
+14
+12
+10
+8
+6
+4
δ18O (‰)
QUARTZ
FELDSPAR
δ 18O = 7.0
-60
-80
-100
-120
-140
-160
δD (‰)
HORNBLENDE,
BIOTITE,
and
CHLORITE
δD = -85
Bitterroot Lobe
0
20
40
60
80
100
120
SW
DISTANCE(km)
NE

Fig. 1.4c

1.2.2 K-Ar Age Studies of the Idaho Batholith

McDowell and Kulp (1969) made the first systematic potassium-argon study of the Idaho batholith, building on the earlier study of McDowell (1966) and on the lead-alpha and petrographic work of Larsen et al (1958) and Larsen and Schmidt (1958). McDowell and Kulp concluded that the primary igneous activity in the region was early Cretaceous (125 m.y.) or older, and that a major intrusive or heating event occurred during the Eocene. Because ten of the thirteen analyzed rocks gave ages between 77 and 38 m.y., McDowell and Kulp (1969) suggested that much of the batholith shows the effects of complete or partial argon loss during the Eocene.

Percious et al (1967) analyzed four samples from a portion of the porphyry belt near the Boise Basin. Ages of biotite from two small porphyry stocks and from one sample of the host Idaho batholith ranged from 44 to 48 m.y., but a whole-rock age of a quartz latite dike was slightly younger (39 m.y.). The authors concluded that the data did not necessarily indicate a period of plutonic activity in the Eocene, because it was also possible that the results were cooling ages which reflected uplift in the region.

Armstrong (1974) contributed much new data on the Idaho batholith and emphasized the importance of the Eocene igneous event. He concluded that the Challis volcanic rocks east of the batholith are predominantly Eocene in age, confirming the work of Axelrod (1966), and he showed that the Sawtooth batholith, the Casto pluton, and many other intrusives were in fact Challis correlatives. He also outlined two huge regions in the Idaho batholith which he interpreted to have been strongly affected by early Cenozoic argon loss (Fig. 1.1).

Ferguson (1975) made a fission track study of part of the northeast portion of the batholith. He proposed that major (~ 12km) regional uplift occurred after emplacement of the Idaho batholith and before or during the Eocene, and that the apatite ages and the available K-Ar age data in his study area reflect this uplift and regional cooling.

Armstrong et al (1977) reviewed all available K-Ar and Rb-Sr data of the Mesozoic rocks in the batholith and the surrounding region, and concluded that the magmatism was episodic. The earliest events occurred along the western side in late Triassic to early Jurassic time (200-217 m.y.), continued through to late Jurassic (~ 150 m.y.), and were followed by late Cretaceous emplacement of most of the southern half (75-100 m.y.) and the northern half (70-80 m.y.) of the Idaho batholith proper. Armstrong et al (1977) also discovered an abrupt discontinuity of initial $^{87}Sr/^{86}Sr$ ratios near the western margin of the batholith, with values of 0.704 or less to the west, and of 0.706 or greater to the east (Fig. 1.1).

Marvin et al (1973) reported a K-Ar age of 87 m.y. for biotite associated with quartz-molybdenite-pyrite stockwork mineralization in a small quartz monzonite stock immediately east of the Idaho batholith. Armstrong et al (1978) obtained a 62 m.y. whole rock K-Ar age from silicified molybdenite-bearing metasediments near the White Cloud stock, and emphasized its post-batholithic but pre-Challis age. Rostad (1978), however, reports several Tertiary K-Ar ages for molybdenite deposits in the "Idaho-Montana porphyry belt", including Challis K-Ar ages (41-44 m.y.) for mineralization at the Cumo and Little Falls prospects in Boise County.

A few pertinent data have also been reported by Hayden and Wehrenberg (1960), Hietanen (1969), Cater et al (1973), Greenwood and Morrison (1973),

and Berry et al (1976). Geochronologic determinations for surrounding areas can be found in Armstrong's (1975a) complete compilation of age data for the state of Idaho.

1.2.3 Oxygen Isotopic Fractionation Factors between Quartz, Feldspar, and Water.

The isotopic fractionation factor (α) between two phases A and B is defined as

$$\alpha = R_A/R_B$$

where (R) refers to the isotopic ratio in each phase (e.g. D/H; $^{18}O/^{16}O$; $^{13}C/^{12}C$). These factors represent the partitioning of isotopic species between the phases and generally have values close to unity. Isotopic mixtures are almost perfectly ideal and, as a consequence, at equilibrium the fractionation factors depend only upon the temperature and the nature of the phases. Pressure effects are negligible, owing to the extremely small volume changes associated with isotopic substitutions (Clayton et al, 1975).

The $^{18}O/^{16}O$ fractionation factors for quartz-water, feldspar-water, and quartz-feldspar are of particular importance to the present study; the quartz-feldspar fractionation, in particular, is an extremely sensitive indicator of hydrothermally altered rocks, and readily distinguishes the latter from normal magmatic rocks. Furthermore, these fractionation factors permit calculation of the isotopic composition of the ancient hydrothermal fluids from isotopic analyses of the altered minerals and vein materials. Unfortunately, in the recent literature there is less than complete agreement between various experimental determinations of these fractionation factors. This section will summarize the available experimental data and will

discuss the geologic implications of some of the discrepancies.

The isotopic fractionation factor between quartz and water has been determined at various temperatures by O'Neil and Clayton (1964), Clayton et al (1972), Blattner and Bird (1974), Matsuhisa et al (1978, 1979) and Matthews and Beckinsale (1979); the results are shown on Fig. 1.5. There is good agreement between the results obtained in the Chicago laboratories by Matsuhisa et al (1978, 1979) and Clayton et al (1972) at temperatures of 250-500°C, and only a small discrepancy at higher temperatures. Theoretical calculations by Becker and Clayton (1976) agree closely with the T vs. 1000 ln α slope of the Clayton et al (1972) relationship. The experimental results of Matthews and Beckinsale (1979) and the single (600°C) determination of Blattner and Bird (1974) are systematically higher than those from the Chicago laboratories.

Figure 1.6 compares the fractionation factors between alkali feldspar and water as determined by O'Neil and Taylor (1967), Blattner and Bird (1974), and Matsuhisa et al (1979). Results for anorthite-water are also shown for comparison. O'Neil and Taylor (1967) showed that although there is no discernible fractionation between Na and K feldspars at any temperature, plagioclase of intermediate compositions lies between the alkali feldspar and anorthite curves. The results of Matsuhisa et al (1979) in general confirm the earlier work, but are appreciably divergent at temperatures above 500°C. Matsuhisa et al (1979) have challenged the validity of O'Neil and Taylor's (1967) results, arguing that the cation exchange method utilized in the earlier study may involve solute-water isotopic effects which were not accounted for. Furthermore, Matsuhisa et al (1979) suggested that the slopes of the O'Neil and Taylor (1967) least-squares lines depend

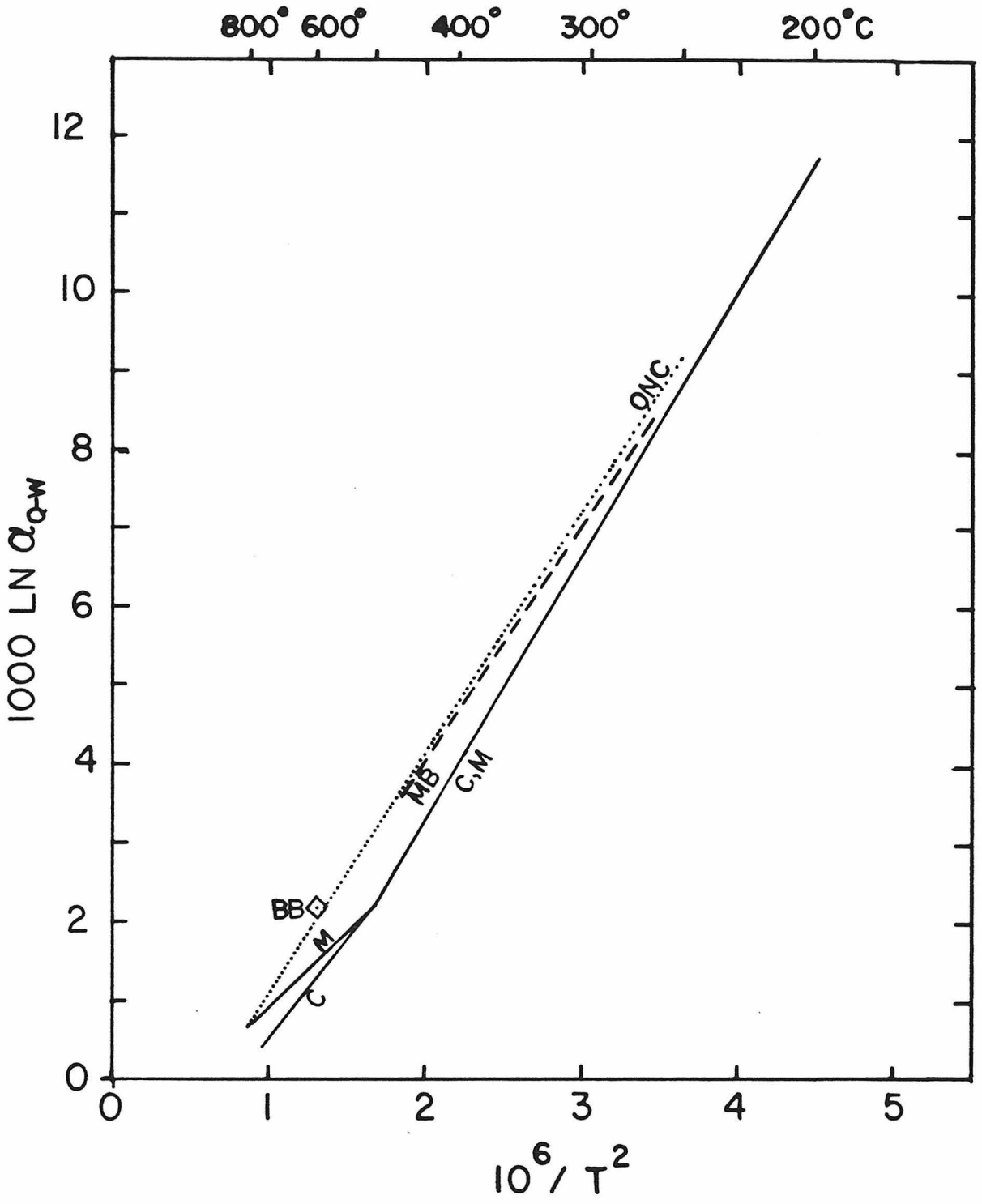

Figure 1.5 Experimental determinations of quartz-water ^{18}O fractionation, reported as 1000 ln α. BB (Blattner and Bird, 1974), C (Clayton et al, 1972), M (Matsuhisa et al, 1979), MB (Matthews and Beckinsale, 1979), ONC (O'Neil and Clayton, 1964).

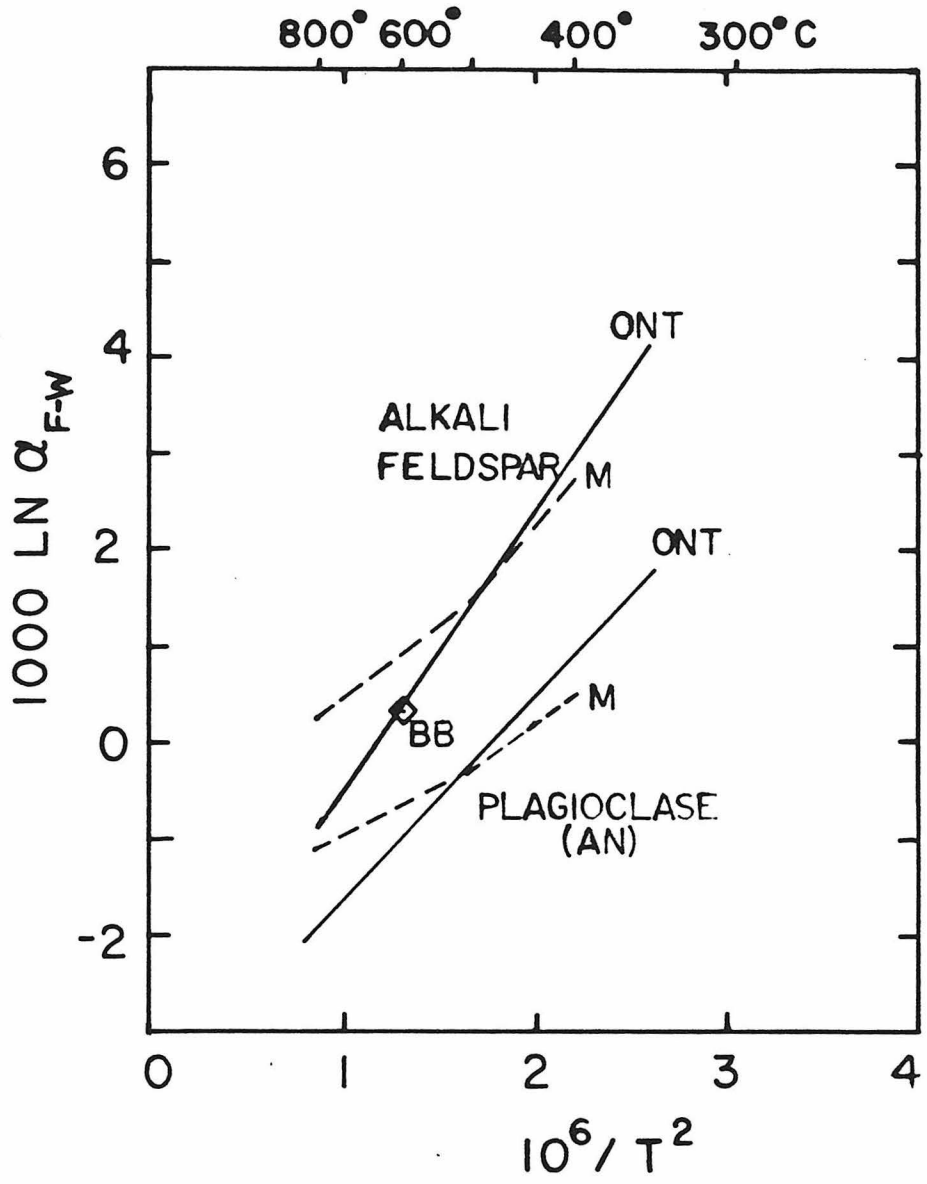

Figure 1.6 Experimental determinations of ^{18}O fractionation between feldspar and water, reported as 1000 ln α. BB (Blattner and Bird, 1974), M (Matsuhisa et al, 1979), ONT (O'Neil and Taylor, 1967).

strongly on the data points at 800°C, where the run duration was severely limited by the corrosion problem of the chloride solutions. Neither statement appears to be valid. Although solute-water isotopic effects have been measured at relatively low temperatures ($\leq$ 275°C) by Truesdell (1974), their existence at higher temperature is unlikely considering that these effects are generally small (< 1 permil) and would probably decrease with temperature. O'Neil and Taylor (1967) in fact demonstrated that the cation exchange results at 500°, 600°, and 800°C are virtually identical with experiments utilizing pure water. The suggestion that the 800°C determination of O'Neil and Taylor (1967) is questionable is certainly not founded for their alkali feldspar-water results, which are restricted in range (-1.29, -0.82, -1.01 permil) and consistent with the results at low temperature. In contrast, two of the three high temperature (800° and 825°C) measurements of Matsuhisa et al (1979) seem to be much too large (by 1 to 2 permil, if one takes into account data on quartz-feldspar $^{18}O/^{16}O$ fractionations in igneous and metamorphic rocks).

The serious nature of what may seem to be minor experimental discrepancies becomes evident when the quartz-water and feldspar-water results are combined to give a quartz-alkali feldspar geothermometer. The Matsuhisa et al (1979) results differ from the combined O'Neil and Taylor (1967) - Matthews and Beckinsale (1979) results by almost 1 permil at high temperatures. Thus, Matsuhisa et al (1979) would interpret an observed quartz-alkali feldspar fractionation of 1.5, which is typical of the "primary" values observed in a fresh, "unaltered" granitic rock, as indicating that the oxygen isotopes in the minerals completely reequilibrated down to temperatures of about 350°C, in spite of the fact that the minerals clearly

formed from magmas at high temperatures (~ 700°C). Such an interpretation would also be favored by Deines (1977) and Giletti et al (1978).

In fact, closed system, subsolidus, high-temperature ^{18}O exchange is definitely known to occur in plutonic rocks such as gabbros during slow cooling (Anderson et al, 1971; Taylor, 1968; Taylor and Forester, 1979). The above argument thus hinges on whether these exchange effects continue down to temperatures well below 400°C, or whether the $\delta^{18}O$ values are "frozen" in at relatively high temperatures. The latter interpretation is generally favored by Taylor (1967) and Bottinga and Javoy (1973, 1975), and by most workers dealing with data on natural samples. These workers generally agree that significant isotopic reequilibration does occur on cooling, especially if the rock is held for long times under wet conditions, but they certainly do not endorse the hypothesis that extreme reequilibration down to temperatures as low as 200°-300°C is typical of all plutonic igneous and metamorphic rocks.

The problem with appealing to extremely low-temperature closed-system exchange in a granitic rock is that under such conditions the feldspar can basically only exchange with the coexisting quartz, as these two minerals are the only appreciable reservoirs of oxygen in the rock. Thus, although feldspar is known to readily exchange down to low temperatures under "wet" conditions, quartz is known to be relatively inert under these same conditions. In an open system, in which hydrothermal fluids migrate into the rock, it is thus very common to see a change in the $\delta^{18}O$ of the feldspar. and virtually no change in the $\delta^{18}O$ of the quartz. In a closed-system environment the ease of exchange of feldspar is thus not pertinent, because if the coexisting quartz is inert, the feldspar will have nothing to

exchange with, and therefore must retain its original high-temperature $\delta^{18}O$ value.

Until the above problems are resolved, there are bound to be some ambiguities in interpreting oxygen isotopic data in igneous rocks. Nonetheless, in this thesis we shall assume that all the plutonic igneous rocks typically started with "normal" quartz-feldspar fractionations of 1.0 to 2.0 permil (i.e. 1.0 to 1.3 for alkali feldspar, and 1.5 to 2.0 for plagioclase, which are the characteristic values measured in most "fresh, unaltered" igneous rocks), thereby making no use of the presently available laboratory data to interpret what the original primary magmatic values may have been. Fortunately, in calculating the $\delta^{18}O$ values of the fluids, none of the above complications are very important because all of the mineral-H_2O fractionation curves agree to $\pm$ 1 permil (Figs. 1.5, 1.6) and at present this effect is far outweighed by the uncertainty in the temperature of alteration.

In summary, at low temperature we will use the extrapolated quartz-water data of Matsuhisa et al (1979) and the alkali feldspar-water fractionation data of O'Neil and Taylor (1967). These seem to be the most complete and internally consistent determinations presently available, and their use at relatively low temperatures where fractionation factors are large does not involve serious geologic contradictions. Note, however, that at high temperatures these independent determinations are not mutually consistent, and result in quartz-feldspar fractionation factors with an absurd temperature dependence.

1.2.4 K-Ar Age Relations in Regions of Orogeny and Uplift (other than in the Idaho batholith)

Many studies have demonstrated that minerals in crystalline rocks often

have K-Ar apparent ages which are younger than the true age. One way in which this happens is by loss of radiogenic Ar, either by diffusion or by recrystallization of the host minerals, in the reheated contact zones of crosscutting plutons, (c.f. Hart, 1964, Hanson and Gast, 1967). It is also possible for rocks to be emplaced or metamorphosed at relatively deep levels in the crust, where ambient temperatures are initially too high to allow accumulation of daughter Ar. This section describes several selected regions where a considerable interval of uplift and cooling separates the time of emplacement (or metamorphism) from the time of Ar retention in the minerals.

1.2.4.1 Swiss Alps

Jäger (1962) reported Rb-Sr age data for 19 mica and whole-rock samples from the Swiss Alps. Although the true ages of most of the samples are Paleozoic and Mesozoic, rocks from the lowest nappe units give ages of 16 to 21 m.y. and were recrystallized to high metamorphic grades (kyanite plus staurolite; sillimanite) during the Alpine Orogeny. Jäger (1962) regarded the 5 m.y. range as real, and proposed that the older ages, which occur south of the 16 m.y. zone, reflect earlier uplift of the southern region followed by rapid erosion and northward tectonic transport of superjacent rocks.

Steiger (1964) showed that K-Ar ages of hornblende in the Gotthard Massif of the Alps are older than the nearby rocks that have ~ 16 m.y. biotite Rb-Sr ages (Jäger, 1962). Steiger separated the rocks into three groups on the basis of the orientation of the hornblende crystals. First generation hornblendes commonly exhibit "partial" orientation and give ages

between 46 and 112 m.y., reflecting either the ocurrrence of excess Ar or (more probably) partial Ar loss in the old minerals. Second generation hornblende crystals are oriented N-S and have "ages" near 46 m.y.; these were thought to have been formed during the main tectonic phase when the massif was overridden by nappes. Third generation hornblende crystals usually exhibit random orientations and show "ages" of 23 to 30 m.y.; Steiger (1964) proposed that the latter formed during the main phase of "anatexis and granitization" immediately to the south. He did not support the uplift and erosion hypothesis of Jäger (1962), and suggested that her biotite Rb-Sr ages reflect E-W compression during a weak, subsequent tectonic event that has a minimum age of 16 m.y.

Armstrong et al (1966) demonstrated that K-Ar and Rb-Sr ages of biotite samples from the Alps are usually concordant within experimental error. They also noted that present-day heat flow is correlated with the Rb-Sr ages, with the youngest ages occurring in regions of high heat flow. They proposed that late uplift in such regions is consistent with both the low ages and the high heat flow, and hence they did not accept Steiger's (1964) hypothesis that the young ages result from a late phase of Alpine metamorphism.

Clark and Jäger (1969) utilized heat flow measurements in five Alpine tunnels to calculate the rate of denudation in the Alps, assuming that K-Ar and Rb-Sr "ages" of biotite at these localities reflect the time since the rocks cooled to the blocking temperature of the radiogenic daughter products. They concluded that denudation rates of 0.3 to 1.1 mm/yr characterize the Alps, and argued that this estimate is in good agreement with proposals based on sedimentation and also with the apparent age discordance

of about 8 m.y. between biotite and muscovite. More refined calculations by Clark (1979) support the earlier conclusions, but restrict the uplift rates to lie between 0.4 and 0.8 mm/yr.

1.2.4.2 Peninsular Ranges Batholith

Krummenacher et al (1975) made an extensive K-Ar study of biotite and hornblende from the Peninsular Ranges batholith of Southern California and Baja California. Their regional contour maps of the apparent ages show that along several 100-km traverses perpendicular to the trend of the batholith, the ages systematically decrease eastward from values of ~ 115 m.y. to 65 m.y., with hornblende ages consistently being about 5 m.y. older than biotite ages. The authors demonstrated K-Ar age concordance for all rocks within a small, geologically complex area containing wallrocks, small stocks, and numerous aplite, pegmatite and amphibolite dikes, even though great intervals of geologic time are probably represented by these diverse lithologies. They also showed that several age contours pass without significant deflection through the giant La Posta tonalite pluton, such that the apparent ages span a range of 15 m.y., with younger ages on the east. Based on these observations and on U-Pb age data of L.T. Silver (unpub.), Krummenacher et al (1975) proposed that the intrusive ages of the rocks are oldest in the west. However, there also was an east-to-west progression of uplift and erosion such that the deepest dissection occurs in the east; therefore the K-Ar ages in some complex manner must reflect both the true emplacement age and the pattern of regional cooling (Armstrong and Suppe, 1973; Krummenacher et al 1975).

Silver et al (1979) have summarized and expanded upon the results of

several previous U-Pb studies on zircons by L.T. Silver and his co-workers. They conclude that zircon U-Pb ages within the batholith represent true emplacement ages, consistent with field relations, and that these ages are a function of geographic position (Fig. 1.7). Zircon ages within the western half of the batholith range from 105 to 120 m.y., with any age or lithology occurring at any position in this belt. In contrast, rocks in the eastern portion all have ages of less than 105 m.y. and show a progressive eastward decrease to about 85 m.y.

Comparison of the zircon ages with available K-Ar results on biotite and hornblende thus show that: (1) Along the west side, cooling was sufficiently rapid that K-Ar biotite and hornblende ages are almost identical and only about 5 m.y. lower than the zircon emplacement ages of the youngest plutons; hence, all of these different age methods give concordant results. This is near the roof of the batholith and was a zone of meteoric-hydrothermal activity, which caused rapid cooling of these epizonal plutons (Taylor and Silver, 1978). (2) Down the center of the batholith, hornblende ages display a distinct ~ 10 m.y. decrease that is roughly coincident with, and superimposed on, the zircon age step. (3) Further east the biotite and hornblende K-Ar ages show a progressively increasing discordance compared to the zircon ages, with biotite ages decreasing fastest, until the easternmost rocks display biotite and hornblende ages which are, respectively, 25 and 20 m.y. lower than the zircon ages. Silver et al (1979) proposed that these data indicate progressive magmatic migration, with larger masses of magma in the east, greater crustal thickening, and consequent higher isostatic recovery in the east. This produced greater uplift and westward regional tilting, and was followed by possible late

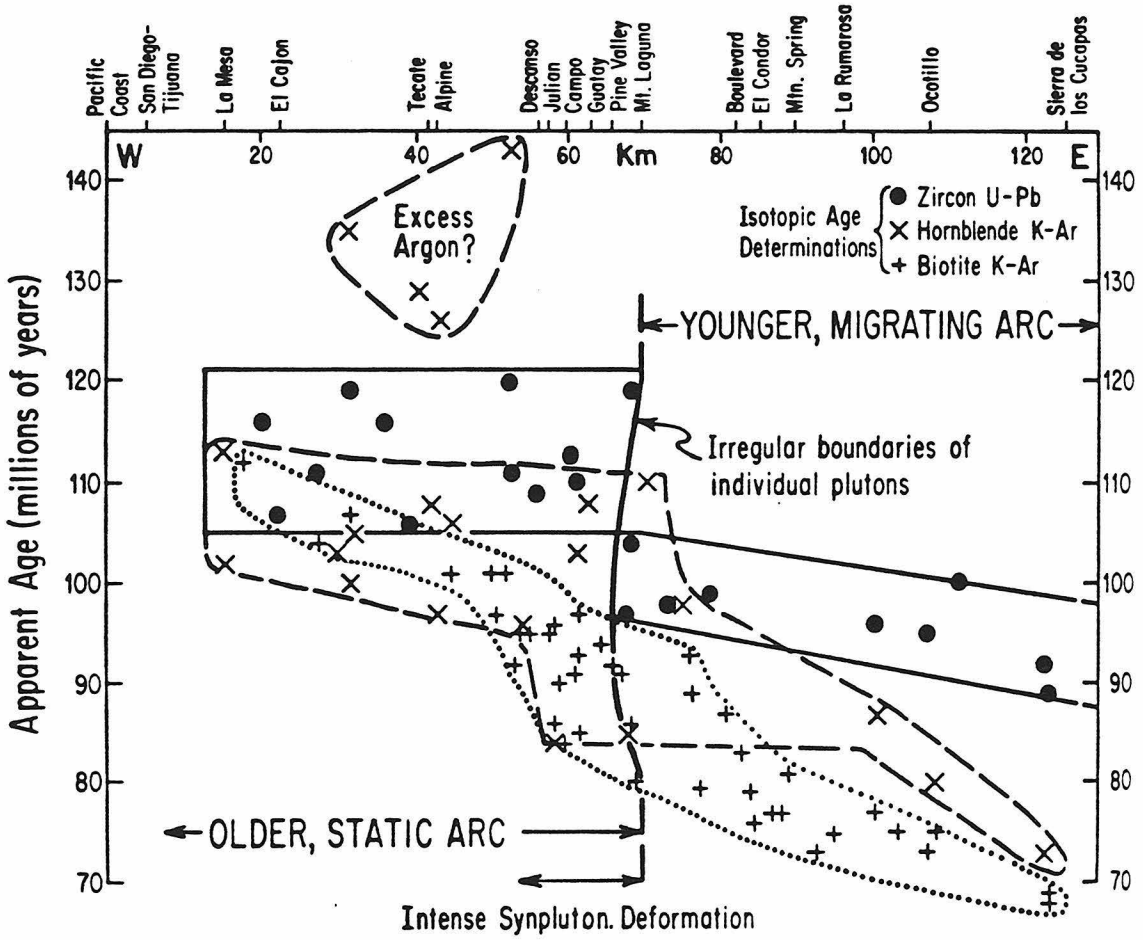

Figure 1.7 E-W profile of isotopic age determinations of the Peninsular Ranges batholith. See text. From Silver et al (1979).

thermal perturbations associated with the Gulf of California rift zone.

1.2.4.3 Other Areas

Hadley (1964) compiled K-Ar and Rb-Sr age data for the Blue Ridge and Piedmont provinces of the Appalachian Mts. He noted that the frequencies of Paleozoic apparent ages correlated well with the thickness of correlative clastic wedge deposits in neighboring basins. Inasmuch as uplift of the crystalline terrane was responsible for the clastic sedimentation, Hadley (1964) proposed that regional cooling associated with the uplift marked the time of radiogenic daughter retention in the crystalline rocks.

Armstrong and Hansen (1966) made a K-Ar study of biotite and muscovite from almandine-amphibolite facies rocks of the eastern Great Basin, Nevada and Utah. Although the metamorphism is known to have occurred in the Mesozoic, the K-Ar ages range from 20 to 57 m.y. and hence are as much as 100 m.y. younger than the true age of the metamorphism. Armstrong and Hansen (1966) proposed that these rocks comprise part of a Cordilleran infrastructure, and attributed the young apparent ages to Tertiary uplift and erosion.

Harper (1967) demonstrated that K-Ar ages within the Dalradian Series of the Scottish Highlands are related to post-metamorphic cooling. The oldest ages (average ~ 470 m.y.) postdate the time of metamorphism, and occur in retentive minerals such as amphibole, as well as in the upper portions of the series. Relatively rapid uplift during the period of F_3 folding occurred between 450 and 430 m.y., as indicated by the predominance of ages in this interval in the main portion of the series. Still younger ages (~ 420 m.y.) are common in the stratigraphically lower Moine Series. These

results suggested that the apparent ages are related to the rate of cooling during uplift. Harper (1967) attributed a few 410-420 m.y. apparent ages to localized heating effects caused by intrusion of the post-tectonic Newer Granites.

Turner and Forbes (1976) report that K-Ar ages of biotite show a linear decrease from 120 m.y. at the surface to 65 m.y. at the bottom of the 2970 m Eielson drill hole in central Alaska. Utilizing the bottom temperature (94.7°C) and the present geothermal gradient (31.5°C/km), the authors calculated that the biotite would give a zero K-Ar age at a temperature of 225°C. They proposed that this represents the Ar blocking temperature of the biotite, and that the linear age vs. depth relation reflects uplift and erosion of the rock column.

CHAPTER 2

GEOLOGY, GEOCHRONOLOGY AND GEOCHEMISTRY OF THE IDAHO BATHOLITH

2.1 Regional Setting and Location

2.1.1 Dimensions of the Batholith

The Idaho batholith is a large (~ 40,000 km^2), composite mass, made up of numerous granitic plutons, located in the northern Rocky Mountains of central Idaho and adjacent portions of Montana (Fig. 2.1). Most of the the batholith lies between longitudes 114° and 116° west and latitudes 43° and 47° north, although small areas on the NE and SW sides lie outside these confines. The batholith is elongate in a N-S direction, with dimensions of approximately 125 km by 375 km.

The outcrop perimeter of the Idaho batholith is irregular in detail, and in plan it has the appearance of a giant hourglass. The constriction in the center divides it into two approximately equal areas, the northern "Bitterroot" lobe and the southern "Atlanta" lobe, as defined by Armstrong et al (1977). Although the present study is largely confined to the Atlanta lobe, some of the introductory remarks will deal with the batholith as a whole.

2.1.2 Geomorphology and Physiography

The region underlain by the Idaho batholith is rugged and mountainous. The elevation ranges from about 3000' (900 m) on the southwest side to almost 11,000' (3350 m) in the Sawtooth Mountains, and averages about 6000' (1800 m) above sea level (Fig. 2.2). Most of the land is covered by a dense forest comprised mainly of lodgepole pine and Douglas fir. However, the highest regions are above the treeline, and large interior valleys and low regions along the periphery of the batholith are covered by sagebrush

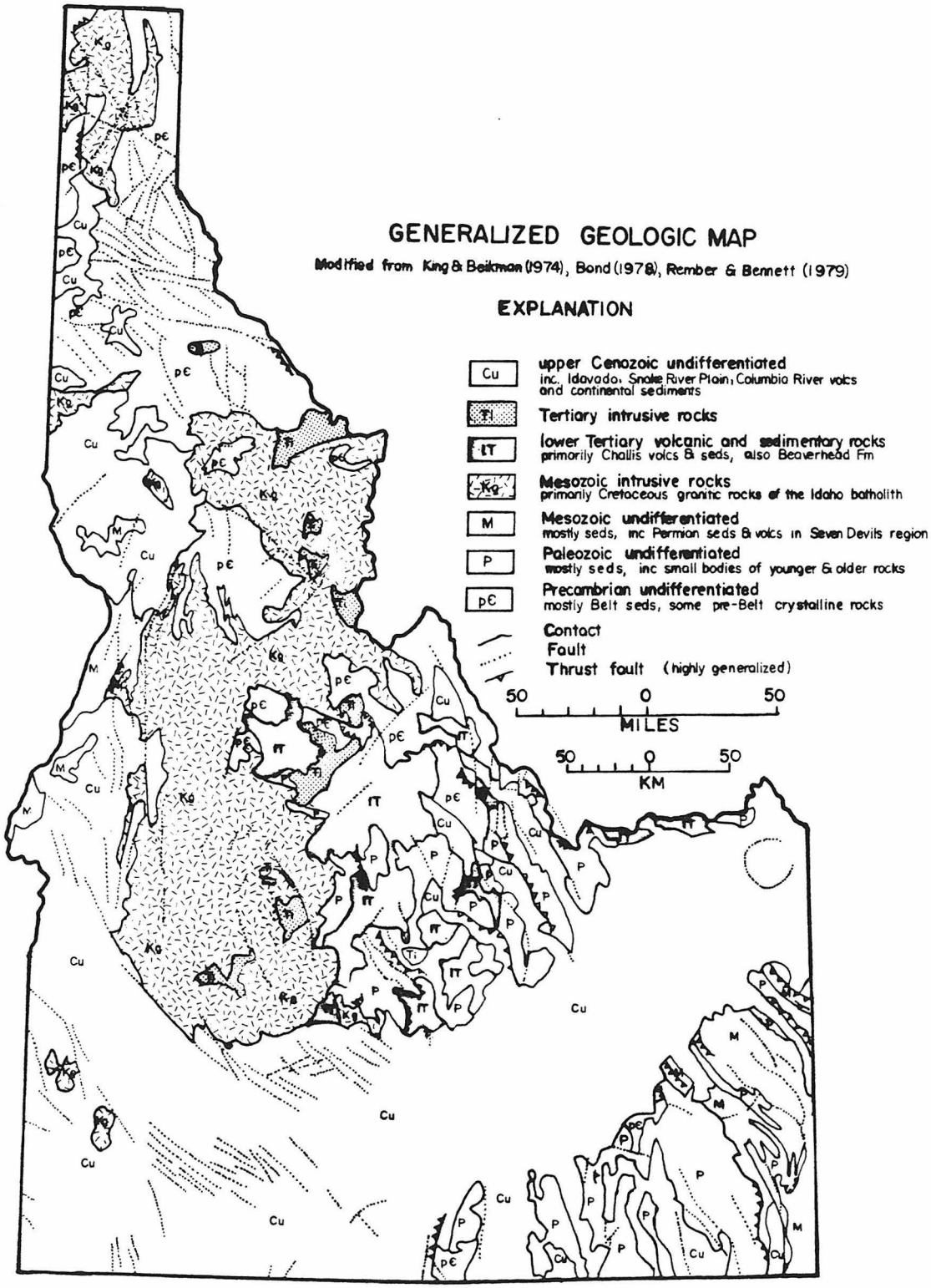
GENERALIZED GEOLOGIC MAP
Modified from King & Beikman (1974), Bond (1978), Rember & Bennett (1979)
EXPLANATION
Cu
upper Cenozoic undifferentiated
inc. Idavado, Snake River Plain, Columbia River volcs and continental sediments
Ti
Tertiary intrusive rocks
lT
lower Tertiary volcanic and sedimentary rocks
primarily Challis volcs & seds, also Beaverhead Fm
Kg
Mesozoic intrusive rocks
primarily Cretaceous granitic rocks of the Idaho batholith
M
Mesozoic undifferentiated
mostly seds, inc Permian seds & volcs in Steven Devils region
P
Paleozoic undifferentiated
mostly seds, inc small bodies of younger & older rocks
pC
Precambrian undifferentiated
mostly Belt seds, some pre-Belt crystalline rocks
Contact
Fault
Thrust fault (highly generalized)
50 0 50
MILES
50 0 50
KM

Figure 2.2 Topography of Atlanta lobe, from U.S.G.S. 1:1,000,000 and 1:250,000 sheets. Contours at 1000 (dashed), 1500 (solid), 2000 (dash-dot), 2500 (dash-dot-dot) and 3000 m (dotted line); heavy solid line indicates the outline of the Atlanta lobe. Note that the elevation systematically increases from west to east.

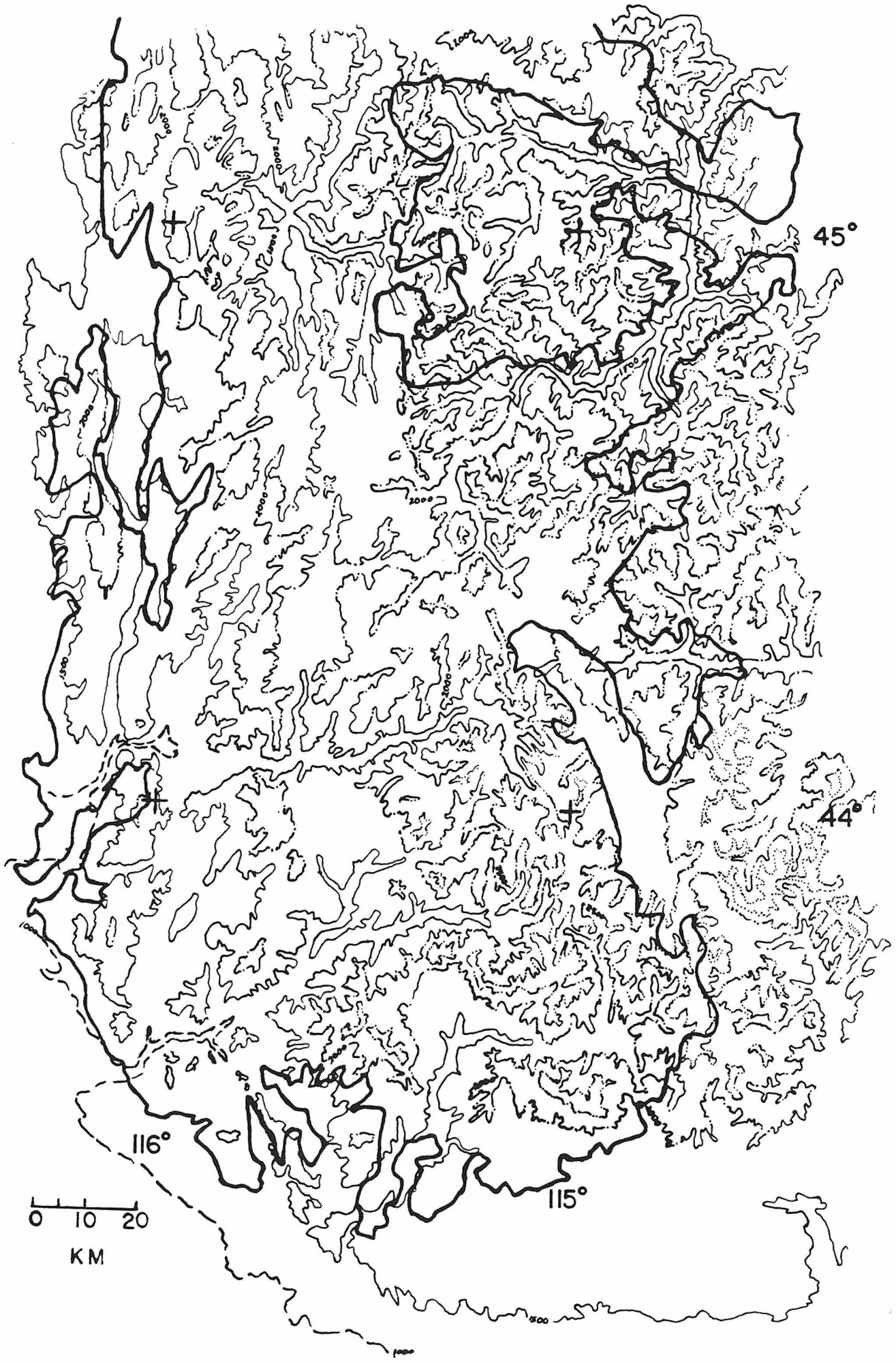
45°
44°
116°
115°
0 10 20
KM

and grass.

Several workers, most recently Schmidt and Mackin (1970), have remarked about the existence of a "rolling upland surface", termed the "Idaho peneplain", which exists on a regional scale at elevations of approximately 7000' to 9000' (2100-2700 m). The age and explanation for this surface are a matter of dispute, ranging from post Challis, Miocene-Pliocene peneplanation (Ross, 1934) to Pleistocene altiplanation (Schmidt and Mackin, 1970). Although there is an apparent accordance of summit elevations in the region, a rude histogram of randomly chosen elevations shows an approximate conformity to a Gaussian distribution. A detailed quantitative study would be interesting.

Regardless of its origin, the "Idaho peneplain" has been disrupted by the more recent downcutting of streams and, more importantly, by the development of block faults having large displacements and general N-S trends. These have broken much of the Atlanta lobe into linear, N-S trending mountain ridges separated by large graben valleys. These faults are often described as "Basin and Range" type, but their age relations are poorly known. Several of them cut Miocene Columbia River Basalt and others cut glacial moraine deposits (Schmidt and Mackin, 1970), but Armstrong (1974) also refers to widespread block faulting during the Eocene. Examples of faults with large demonstrated displacements are the Sawtooth Valley fault (>1200'; Reid, 1963) and the Long Valley fault (10,000'; Schmidt and Mackin, 1970).

Most of the region above about 8000' (2500 m) has been affected by Pleistocene glaciation. Particularly spectacular alpine features characterize the geomorphology of the Sawtooth Mountains, and rock exposure

is excellent (Reid, 1963). Below the level of glacier activity much of the granitic rock is deeply weathered to grus and good outcrops are few. Many of the major valleys between the large mountain blocks contain hundreds or thousands of feet of glacial moraine and outwash deposits (Schmidt and Mackin, 1970; Williams, 1961).

Schmidt and Mackin (1970) have described the North Fork of the Payette River near Cascade as an antecedent stream whose development preceeded the episode of block faulting. It should be pointed out that most N-S streams in the Atlanta lobe have broad, meadow filled valleys with gentle gradients, whereas E-W streams are generally swift, steep and deeply entrenched (Fig. 2.2). The antecedent hypothesis of Schmidt and Mackin (1970) may be applicable to many of the latter streams.

2.1.3 Regional Geologic History

The Idaho batholith comprises a portion of the North American Cordillera, which is one of the world's widest and most complex mountain ranges. The following discussion will focus on the historical development of this area, especially on the relationship of the Idaho batholith to the surrounding rocks. However, it must be emphasized that the geology of the region is extremely complex, that workers in the area have major differences in interpretation of certain features, and consequently that this brief essay cannot provide more than a highly simplified overview of this history.

During upper Proterozoic and Paleozoic time the western margin of the North American craton was the site of geoclinal ("geosynclinal") sedimentation. The position of the ancient continental margin is given

approximately by the western limit of Precambrian rocks, a line which trends nearly N-S through western Idaho, east-central Nevada and into southern California (King, 1977). The upper Proterozoic of northern Idaho is recorded by the Belt Series, a thick, monotonous sequence predominantly consisting of siltstone and argillite which accumulated between 1600$\pm$ 100 and 850 $\pm$ 100 m.y. before present (Obradovich and Peterman, 1968, 1973; Reid et al, 1973). The greatest thickness (to 20 km) of these sediments was deposited in an E-W trending trough, perpendicular to the continental margin (aulocogen?) located immediately north of what is now the Bitterroot lobe of the Idaho batholith (Harrison et al, 1974). Several authors have likened this "Belt basin", and also similar areas in the Uinta region of Utah and in the Apache Basin of western Arizona, to former aulocogens, but Harrison et al (1974) are not in complete agreement.

The great period of time represented by the Belt Series was not devoid of magmatism and tectonism. Significant events include possible high temperature-high pressure metamorphism and associated folding of Beltian rocks at ~ 1500 m.y. (Reid et al, 1970, 1973), intrusion of the granodioritic Hellroaring Creek stock in British Columbia at ~ 1260 m.y. (Ryan and Blenkinsop, 1971), formation of the Coeur d'Alene uraninite ores (Hobbs and Fryklund, 1968), formation of the Purcell sills and flows along with synkinematic metamorphism of Belt sediments at ~ 1100 m.y. (Hunt, 1962; Bishop, 1973), and possibly other episodes of deformation, block faulting, uplift and intrusion of mafic sills (c.f. Harrison et al, 1972; Reid et al 1973).

The relation of Paleozoic sediments to the ancient continental margin

was first outlined by Roberts et al (1958), based on mapping in the northern Great Basin of Nevada. These authors deduced a westward thickening of Cambrian through Devonian sediments and a concomitant change from shallow water to deep water facies, which they thought represented a miogeoclinal-eugeoclinal couplet. Thus, far to the east, in the Colorado Plateau and in central Wyoming, a thickness of a few kilometers of shallow water shelf carbonates and other sediments were deposited - with considerable interruption - on an older Precambrian basement (King, 1977). Further west, in the eastern Great Basin, several kilometers of correlative carbonate and quartzite were deposited, apparently in somewhat deeper water (pelagic fauna common) and with shorter hiatuses (King, 1977; Roberts et al, 1958). Still further west, and presumably outboard of the ancient continental margin, an even thicker (~ 50,000') sequence of pelagic carbonates, chert, shale, and siliceous volcanic rocks were deposited during this time (Roberts et al, 1958; King, 1969, 1977).

Rocks of this age in south-central Idaho have been discussed by Ross (1962a) and more recently by Armstrong (1975b). Ross (1962a) did not believe that the Paleozoic geocline extended into the region, largely because he thought that the strata were deposited in shallow water and that eugeosynclinal sediments were "completely lacking". However, Ross (1962a) did note a definite westward increase in the thickness of the sediments - from a few kilometers in southeast Idaho to several kilometers just east of the Idaho batholith. Armstrong (1975b) proposed that the geocline was present in south central Idaho, but was interrupted immediately to the north, in the region now occupied by the southern Bitterroot lobe, by a persistent, positive, NW trending arch of pre-Belt rocks. Harrison et al

(1972) had previously proposed that the Bitterroot lobe now occupies the site of "Belt Island", which was a positive structural element just south of the Belt basin in Beltian time.

Regardless of the lower Paleozoic relations in Idaho, it is generally agreed that an intense period of folding and faulting occurred during upper Devonian and lower Mississippian time in both central Nevada and south central Idaho (Roberts et al, 1958; Roberts and Thomasson, 1964). This event is known as the Antler Orogeny and is characterized by (1) uplift followed by clastic wedge sedimentation developed both to the east and west (Roberts et al, 1958; Roberts and Thomasson, 1964), a pattern which contrasts with the almost exclusively eastern source in earlier times; (2) by thrusting, which juxtaposed the eugeoclinal and miogeoclinal strata in Nevada (Roberts et al, 1958) and possibly in Idaho (Roberts and Thomasson, 1964); and also (3) by its lack of plutonism (Gilluly, 1965). The clastic wedge sediments subsequently deposited in Idaho are the argillite, chert and limestone of the Milligen and Wood River Formations in the west, and the conglomerate, greywacke, and shale of the Muldoon Formation in the east (Roberts and Thomasson, 1964). These sequences were in turn juxtaposed by another, post early Permian period of thrusting, and now lie partly superimposed immediately east of the Idaho batholith region (Roberts and Thomasson, 1964). The area of uplift, then, was probably that occupied now by the Atlanta lobe of the batholith (c.f. Armstrong, 1975b), also near the position of the ancient continental margin.

A significant new structural element appeared in the region immediately west of the batholith in Permian and Triassic time. The associated rocks are known as the Seven Devils Series, which consists predominantly of

basalt, andesite, spilite, keratophyre, volcaniclastic sediments, and rare limestone, and which probably represents an ancient volcanic arc deposited on oceanic crust (Hamilton, 1963; Vallier, 1977); this terrane may be an allocthonous microplate (D. Jones, pers. comm.). In places the Seven Devils Series is overlain by Jurassic "flyschlike" sandstone, black shale and mudstone deposits (Vallier, 1977). Rocks of Permian to Jurassic age are generally absent in the region immediately east of the batholith; much further east on the continental platform occur marine Permian strata and predominantly continental Triassic and Jurassic strata.

The Seven Devils Series and the overlapping Jurassic rocks were affected by low grade metamorphism and west-directed thrusting during the Jurassic or lower Cretaceous, immediately followed by intrusion of quartz diorite gneiss and trondjhemite (Hamilton, 1960, 1963a,b). These events were followed by intrusion of the main phases of the batholith, probably during a protracted interval encompassing much of Cretaceous time (see Sec. 2.4.2). Intrusion of the batholith approximately coincided in time with relative submergence and renewed marine sedimentation in the Cretaceous "seaway" to the east, which extended from the Gulf Coast to the Arctic Ocean (McGookey et al, 1972). Intrusion of the batholith was also associated with large-scale high-grade metamorphism along its western margin (Hamilton, 1963a) and northern margin (Hietanen, 1962, 1963), but the metamorphism on the eastern side is in general of restricted extent (c.f. Newhouse, in Ross, 1934) probably indicating that these rocks comprise part of the superstructure. Note that although the isograds mapped by Hamilton and Hietanen generally increase toward the batholith, they are in detail truncated by the intrusives (c.f. Chase and Johnson, 1977). This

proves that the metamorphism at least partly predates the emplacement of the batholith, at least at the crustal levels now exposed, as was also found in the Peninsular Ranges batholith of southern California (c.f. Todd and Shaw, 1979). Reid et al (1973) in fact argue that the high temperature-high pressure (e.g. kyanite, sillimanite) metamorphism in the northern region of the batholith is actually Precambrian in age.

Ryder and Ames (1970), and Ryder and Scholton, (1973), have described the relations of the thick (to 5 km) Beaverhead Formation which occurs over a broad area immediately east of the batholith. The Beaverhead Formation is a continental deposit of conglomerate and sandstone which ranges in age from Albian or Cenomanian to the lower Eocene (Ryder and Ames, 1970; Ryder and Scholten, 1973). Approximately correlative rocks deposited in the epicontinental sea further east (in Wyoming) include the Frontier sandstone, Cody Shale, Fort Union Formation, Meeteetse Formation, etc. (Ryder and Scholten, 1973). Ryder and Scholten (1973) view the Beaverhead as a syntectonic formation derived from the rapidly uplifting, positive batholithic terrane.

The Albian to Eocene uplift of the batholith was also accompanied by the development of folds and thrust faults in the superjacent rocks, possibly caused by gravitational gliding off the highland (Scholten, 1968; Scholten and Onasch, 1977). Most of the thrust faults are directed eastward, and some cut the Beaverhead Conglomerate (Ryder and Scholten, 1973). Oveturned and recumbent folds which probably formed at the same time are also found in these sediments (Scholten and Onasch, 1977). It is possible that the tectonism progressed eastward in time, as suggested by Armstrong and Oriel (1965) in the Sevier belt of southeast Idaho, and by

Bally et al (1966) in the Cordillera of British Columbia. The few thrust faults west of the batholith are west-directed and at least in part postdate the folds (Scholten and Onasch, 1977).

The batholith region remained positive and mountainous through the Eocene, and the eastern epicontinental seaway was infilled and tectonically disrupted into a terrane of mountain blocks and large lakes (Axelrod, 1968). Then, following a brief period of relative igneous quiescence, the Eocene Challis volcanic-plutonic episode began (Armstrong, 1974). The Challis episode was characterized by shallow-level, predominantly granitic plutonism associated with andesite, latite and rhyolite volcanism, widespread meteoric hydrothermal activity, ore deposition, and probably also by block faulting, ring faulting and regional uplift (Armstrong, 1974; Taylor and Magaritz, 1976, 1978; Criss and Taylor, 1978). After several millions of years of activity, the magmatism apparently shifted southward and out of the area of immediate interest (Armstrong, 1978).

Renewed igneous activity was widespread in Miocene time, as evidenced by the voluminous flows of Columbia River Basalt which occur immediately west of the batholith (Armstrong, 1978). Furthermore, during the Oligocene the Snake River Plain immediately south of the batholith was downdropped (Axelrod, 1968), and was subsequently filled with bimodal volcanic rocks and intercalated sediments, of Miocene to Holocene age (Armstrong, 1978). Concurrent with the eruption of these latter flows was the development of widespread, N-S trending, Basin and Range faults, most extensively developed in the Great Basin of Nevada but apparently with minor expression in the Idaho batholith region (c.f. Stewart, 1978). Continuing uplift has also characterized much of the Cordilleran region (Stewart, 1978), and in

particular Axelrod (1968) has proposed that at least 1.5 km of post-Eocene vertical uplift occurred in the Idaho batholith region. As already described, some ranges attained high elevations and were affected by Pleistocene glaciation.

Table 2.1 depicts the major Mesozoic and Cenozoic events in the Idaho batholith region, as described above and also in section 2.4.2. Original references should be consulted for details; the best overall syntheses are by King (1969, 1977). No attempt will be made to relate the various aspects of this history to plate tectonic models, but the reader is directed to provocative essays by Atwater (1970), Burchfiel and Davis (1972, 1975) and Coney (1978).

2.2 Mesozoic Plutonic Rocks

2.2.1 General Statement

The purpose of this section is to broadly describe the distribution of igneous rock types within the Atlanta lobe of the batholith, and to direct the reader to more detailed petrographic descriptions of individual units. A brief chemical characterization of the batholith is given in Sec. 2.4.1.

Early studies of the Idaho batholith described it as an integral unit made up of two zones: 1) A giant core-zone of a massive, rather uniform type of quartz monzonite and granodiorite, termed the "inner facies", enclosed within; 2) A slightly older, commonly foliated, and more mafic "marginal facies" consisting predominantly of quartz diorite (Ross, 1936, Anderson, 1942). Although this still constitutes a valid first-order description, it is becoming increasingly recognized that the

TABLE 2.1

MESOZOIC AND CENOZOIC HISTORY OF IDAHO AND SURROUNDING AREAS

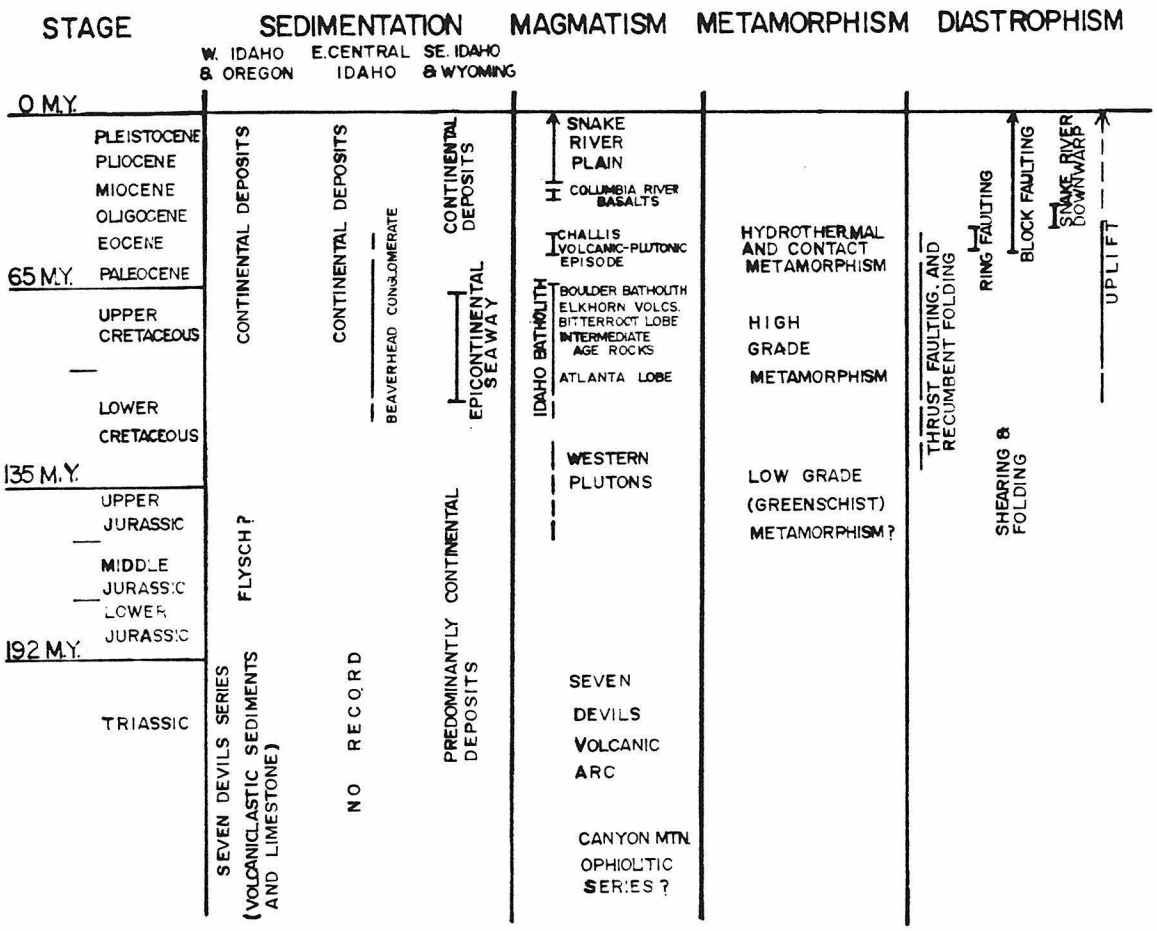

batholith is composed of rocks formed during several different plutonic episodes (Ross, 1928, 1934; Anderson, 1952; Reid, 1963; Swanberg and Blackwell, 1973). Furthermore, recent contributions do not recognize a mafic zone surrounding the interior, but rather that rocks of the western margin are predominantly quartz diorite and generally more mafic than rocks to the east. This west to east transition has been termed the "Quartz Diorite Line" by Moore (1959).

Part of the original descriptive confusion arose because several of the individual plutons are of enormous areal extent (Larson and Schmidt, 1958; Swanberg and Blackwell, 1973) and some may have gradational contacts (Schmidt, 1964). The largest individual plutonic units underlie several thousands of square kilometers, and comprise what Swanberg and Blackwell (1973) have termed the "Main Group" of plutons. These are the oldest intrusions in the Atlanta lobe proper, and constitute almost three-quarters of the entire batholith (Swanberg and Blackwell, 1973); they are described below in an ordered sequence from west to east. Smaller bodies of somewhat younger ("intermediate age") rocks are then described, and finally, the Eocene suite will be discussed in some detail. Note that Bitterroot lobe rocks, including the "Western Border Group" of Swanberg and Blackwell (1973), and also the predominantly Triassic to lower Cretaceous rocks which occur west of the Atlanta lobe in Oregon and westernmost Idaho, will not be described, because they lie outside the study area. The major plutonic units of interest are shown on the generalized geologic map in Fig 2.3.

Figure 2.3 Rock units within the Atlanta lobe, after Schmidt (1964), Swanberg and Blackwell (1973), Reid (1963), Bond (1978), Bennett (1980), and this study.

Eocene Plutons

T_C	Crags Pluton
T_{CB}	Casto Pluton
T_{RB}	Twin Springs - Dismal Swamp - Steel Mtn. - Trinity Mtn. complex
T_{SB}	Sawtooth Batholith
T_{SM}	Soldier Mts. Pluton
T	Tertiary plutons, undifferentiated

Intermediate Age Plutons

4?	Cascade Granodiorite and the Quartz Dioritic Gneiss of Little Valley
7?	Landmark Granodiorite
10	Leucocratic (white) Quartz Monzonite

Main Group Plutons - Western Margin

1	Gneiss of Council Mtn.
2	Migmatite of McCall
3	Quartz Diorite Gneiss of Donnelly
5	Granodiorite of Gold Fork

Main Group Plutons - Batholith Interior and Eastern Margin

6	Quartz Monzonite of Warm Lake
8	Bear Valley Quartz Monzonite and undifferentiated quartz monzonites and granodiorites
9a,b,c	Garnetiferous, Biotite - Muscovite Quartz Monzonites
11?	Atlanta Granodiorite
12	Eastern Quartz Monzonites, undifferentiated

Prebatholithic Metamorphic Rocks

MET

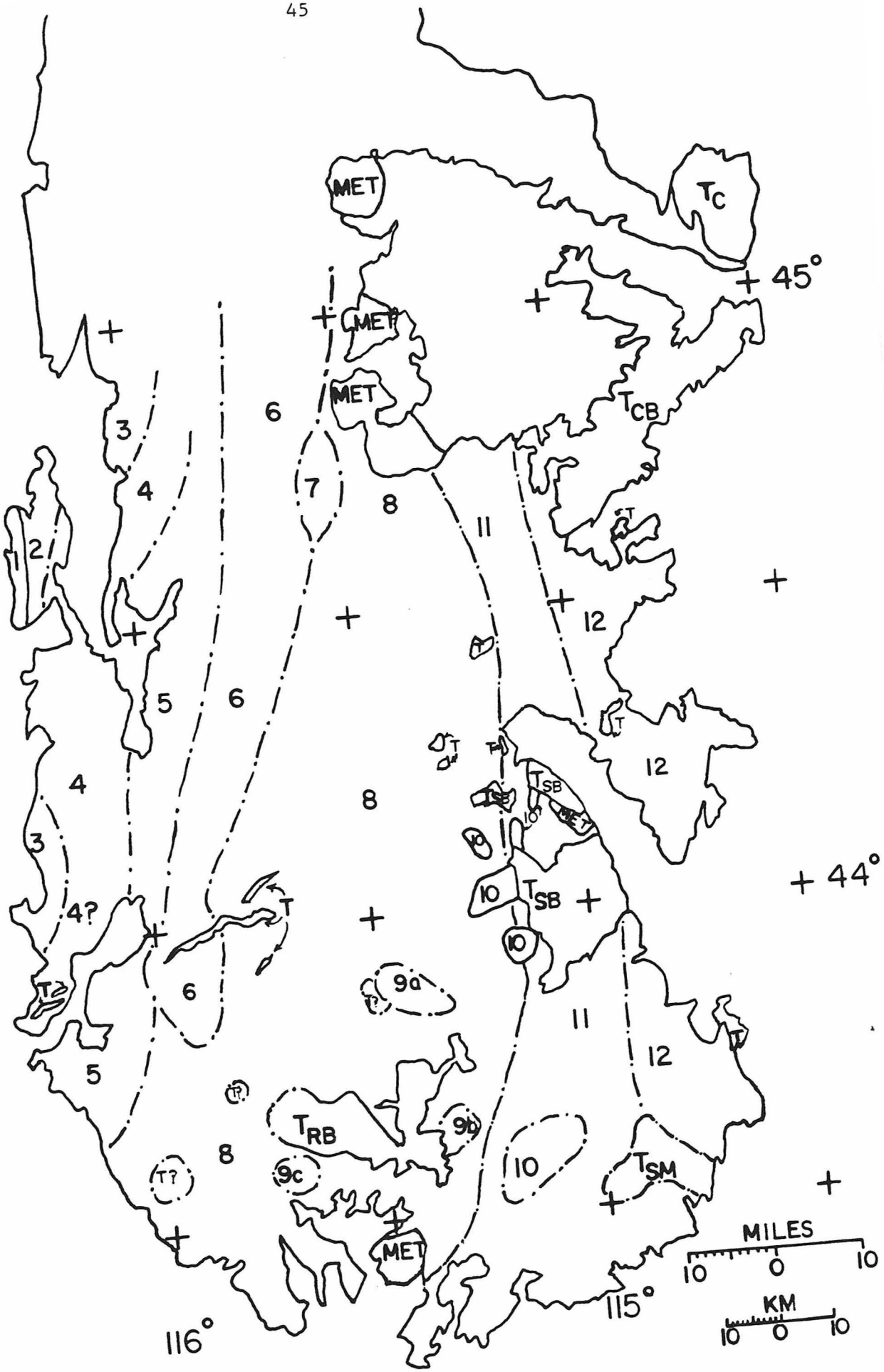
MET
MET
MET
MET
T_C
T_{CB}
T_{SB}
T_{SB}
T_{SB}
T_{RB}
T_{SM}
+ 45°
+ 44°
116°
115°
1
2
3
4
4?
5
6
7
8
9a
9b
9c
10
11
12
T
T?
MILES
10 0 10
KM
10 0 10

2.2.2 Western Margin

Schmidt (1964) has described the rocks of the western margin of the Atlanta lobe noting that the units are generally elongate in a N-S direction and exhibit eastward gradations in both composition and structure (Fig. 2.3). The westernmost rocks are strongly foliated and include a variety of metasedimentary rocks, the "gneiss of Council Mountain", and more importantly the "Migmatite of McCall". The latter unit varies from banded-gneiss to augen-and flaser-gneiss and is compositionally a leucocratic quartz diorite (Schmidt, 1964). It grades eastward into the "quartz dioritic gneiss of Donnelly", which is commonly a medium-grained biotite-hornblende flaser-gneiss that makes up a zone about 10 km wide. East of this unit is the "leucocratic quartz diorite of Little Valley", also occupying a zone about 10 km wide; the latter is typically unfoliated and rarely contains megacrysts of K-feldspar or hornblende. Still further east is the 12 km wide body of the "granodiorite of Gold Fork", an unfoliated, leucocratic, medium-grained rock which also contains K-feldspar megacrysts (Schmidt, 1964). Continuing to the east, the most important unit of the Atlanta lobe is encountered - this is the light-grey, coarse-grained "quartz monzonite of Warm Lake", described below.

It should be mentioned here that Schmidt's (1964) description of gradational contact relationships suggested to him that the rocks described above were intruded during the same plutonic episode. However, Swanberg and Blackwell (1973) concluded that while the Migmatite of McCall, the quartz dioritic gneiss of Donnelly, the Gold Fork granodiorite, and the quartz monzonite of Warm Lake all belong to the "Main Group" of plutons, the leucocratic quartz diorite of Little Valley and its southern

equivalent, the "Cascade Granodiorite", have higher heat generation values which probably indicate a younger age of emplacement. Taubeneck (1971) has also objected to Schmidt's (1964) conclusions, noting that intrusive contacts are observable in several locations in the region and that individual plutons are commonly foliated near contacts. Taubeneck (1971) specifically states that the quartz diorite of Donnelly intrudes the east side of the zone of mixed igneous and metamorphic rocks, and that rock similar to the Donnelly pluton in T19N, R4E is intruded by an "interior-type granodiorite". Taubeneck (1971) also noted that within 50 km of the Snake River Plain, south of the area mapped by Schmidt (1964), a west-to-east traverse passes through porphyritic granodiorite, then through several kilometers of more mafic hornblende-bearing nonporphyritic granodiorite and quartz diorite, then into hornblende-free, porphyritic granodiorite, and then presumably into the more uniform interior of the batholith. Taubeneck (1971) concluded that modal data show no systematic mafic to felsic change across such E-W traverses. The present writer's opinion, however, is that rocks of the western border are indeed more mafic (tonalitic) and more commonly foliated than the interior rocks, but that the exceptions discussed by Taubeneck (1971) indicate that local reversals in this sequence do occur.

2.2.3 "Main Group" Plutons of the Interior

The quartz monzonite of Warm Lake is the largest pluton delineated to date in the Idaho batholith. It extends for about 200 km in a N-S direction and is more than 50 km wide (Fig. 2.3), occupying the entire west-central portion of the Atlanta lobe (Swanberg and Blackwell, 1973). This distinctive rock is light-grey, coarse-grained, contains large

(several cm) K-feldspar megacrysts and typically contains muscovite (Larsen and Schmidt, 1958; Schmidt, 1964).

Lithologies east of the Warm Lake quartz monzonite are diverse and poorly understood. Much more field mapping is required in this region. The Warm Lake pluton appears to grade eastward into a porphyritic, muscovite-free rock termed the "Bear Valley Quartz Monzonite" (Swanberg and Blackwell, 1973). This unit is comparable in size to the giant Warm Lake pluton, and has similar heat generation values (Swanberg and Blackwell, 1973), but modal data show that it is partly granodiorite in composition (Anderson and Rasor, 1934a; Ross, 1963). The unit as defined by Swanberg and Blackwell (1973) includes much of the rock originally termed "Atlanta Granodiorite" by Larsen and Schmidt (1958). Heat generation data (Swanberg and Blackwell, 1973), geologic mapping (Rember and Bennett, 1979) and K-Ar ages (this study) definitely show that the "Atlanta Granodiorite" as originally defined by Larsen and Schmidt (1958) is a composite unit, and the Bear Valley quartz monzonite merely represents one of these sub-units.

For the purposes of the present study the term "Atlanta Granodiorite" will be used in a much more restricted way than used by Larsen and Schmidt (1958), namely it will be applied to the N-trending belt of tonalite and subordinate granodiorite in the Sawtooth Range immediately east of Atlanta, first noted by Reid (1963). Traverses made by the present author several kilometers north and south of the area discussed by Reid (1963) also intersected predominantly tonalite and granodiorite. This belt is definitely composite because some rocks (e.g. tonalite near Grandjean, T10N, R11E, sec. 34) have Pb-α (Jaffe et al, 1959) and K-Ar ages (sample RC 39e) similar to nearby "Main Group" rocks, and other tonalites (e.g within the Soldier Mts. pluton, Tsm) are texturally similar to the

Eocene tonalites and granodiorites, as well as giving Eocene K-Ar ages (e.g. sample RH 85d; see below). Furthermore, heat generation data suggest that rocks along the southernmost traverse (units Tsm and 10 on Fig. 2.3, as well as nearby samples from unit 11 along the S. Fork of the Boise River) are much younger than the nearby "Main Group" rocks; Swanberg and Blackwell (1973) termed these rocks "Atlanta Granodiorite east" and tentatively assigned them all to the Tertiary age grouping. However, the data are compatible with all of these rocks, except Tsm, having "intermediate" ages, or even being altered older rocks. Besides the complexities outlined above, the N-S belt of "Atlanta Granodiorite" also contains several of the characteristic pink granite plutons which are now widely recognized to be Eocene in age (Ross, 1934; Reid, 1963; Bennett, 1980).

Lastly, a belt along the eastern border of the batholith also contains several rock types, and is certainly composed of several distinct plutons, predominantly some "fine-grained quartz monzonite" bodies that are locally porphyritic (Larsen and Schmidt, 1958; Ross, 1963). Tschanz et al (1974) state that dikes of porphyritic quartz monzonite cut hornblende quartz monzonite and quartz diorite in the area.

Before this overview of the "Main Group" rocks of the batholith is concluded, a number of exceptions must be noted to the simple concept that all units are elongate in a N-S direction. For example, traverses made during the present study intersected several small areas (plutons?) within the muscovite-free Bear Valley quartz monzonite zone (unit 8 on Fig. 2.3); in each of these localized areas several nearby outcrops contained significant muscovite, and these zones have been delineated on Fig. 2.3 as: Area 9a, a fairly large muscovite-biotite pluton in

T6N, R8 and 9E (samples RH 44, RH 52a), area 9b (sample RB 21) and area 9c (sample RB 49). Each of these 3 areas is more than 30 km from the nearest exposure of the only large muscovite-bearing pluton in the batholith, namely the "muscovite quartz monzonite of Warm Lake", as approximately mapped by Swanberg and Blackwell (1973). It is logical to delineate these 3 areas (9abc) as separate plutons, which are conceivably related chronologically to the Warm Lake pluton. Similarly, the fine-grained, relatively mafic porphyritic quartz monzonite (unit 13) in the vicinity of Bear Valley Mountain (e.g. RK 72) appears to be a separate pluton not previously described in the literature. Last, the gneiss and schist along the south-central margin of the batholith (indicated by the symbol "Met" on Fig. 2.3; Howard and Shervais, 1973; Rember and Bennett, 1979) are not similar to any rocks further north, and their temporal (prebatholithic?) relationship to the other rocks is unknown, except that they are crosscut by pegmatite dikes. In summary, the map in Fig. 2.3 summarizes the present state of knowledge of the major lithologies in the Atlanta lobe, but a much more detailed petrographic study of the "Main Group" of plutons is needed, especially in the southeast portion of the batholith.

2.2.4 Intermediate Group

An entirely different class of rocks exists in the same geographic region occupied by the plutons of the "Main Group". This "intermediate" age group is younger than the "Main Group" of intrusives described above, yet older than the Eocene granite plutons. Rocks assigned to this intermediate age interval by Swanberg and Blackwell (1973), however,

probably comprise only about 10% of the batholith. Detailed petrographic descriptions are in general not available, and these rocks have in some instances been described along with unrelated rocks. Furthermore, the length of time represented by the "intermediate" interval may be rather large, so that some of these rocks may eventually be shown to be older than others. The following paragraphs attempt to summarize, criticize, and reevaluate the status of these little understood rocks.

Ross (1934) first recognized rocks of "intermediate" age in the Casto Quadrangle, noting that a pluton of "white quartz monzonite" (Unit 10) as well as several small bodies of diorite and quartz diorite, cut the typical rock of the Idaho batholith, but are in turn intruded by Tertiary granite. Similarly, Reid (1963) mapped several plutons of "leucocratic quartz monzonite" in the Sawtooth Mountains, all of which apparently have temporal relationships identical to those described for this unit from the Casto Quadrangle; these rocks are distinguished from the older batholithic rocks by their lighter color and the slightly higher Na contents of their plagioclase (An 4-An 28). Both Ross (1934) and Reid (1963) interpreted these Unit 10 quartz monzonites to be late-stage differentiates of the Idaho batholith, rather than an early phase of the Tertiary igneous activity; Reid (1963) in fact stated that the plutons in the Sawtooth area "are certainly....pre Challis", but without substantiating his claim. Average heat generation values for these Unit 10 quartz monzonites are intermediate between those of the "Main Group" and the "Tertiary epizonal group", in agreement with the field relations (Swanberg and Blackwell, 1973).

As mentioned previously, heat generation values of Unit 4, made

up of the "Cascade granodiorite" and the "leucocratic quartz diorite of Little Valley" are also higher than typical "Main Group" rocks, and Swanberg and Blackwell (1973) tentatively assigned them to the "Intermediate Group". Smaller bodies of "Cascade granodiorite", which have pink K-feldspar megacrysts and occur north of Stanley (Larsen and Schmidt, 1958) were assigned by Swanberg and Blackwell (1973) to the "Tertiary epizonal group" on the basis of even higher heat generation values. It seems that no solid evidence links these various rock-types to a common intrusive epoch. I therefore propose that Larsen and Schmidt's (1958) original "Cascade granodiorite" should be restricted to rocks that crop out along the western border of the batholith (near Cascade), and suggest that the similar (?) rocks farther east (i.e. Unit 7) are better compared to the "Atlanta granodiorite". It is extremely unlikely that any of these rocks are related to the Eocene plutonic suite because none of the known Eocene rocks contain the K-feldspar megacrysts that are common in Unit 7. Incidentally, K-Ar ages of the western "Cascade granodiorite" also preclude an Eocene age for that unit, but the ages are broadly similar to those of the Warm Lake and Bear Valley quartz monzonite and to the "quartz dioritic gneiss of Donnelly". My interpretation is that available K-Ar ages, including the more recent data in this thesis (see below), in no way support an "Intermediate" age for the "Cascade granodiorite", contrary to statements by Swanberg and Blackwell (1973).

Last to be discussed are several small but distinctive bodies of "quartz-bearing, hypersthene-augite-hornblende-biotite diorite" which occur in the western (Horseshoe Bend), west-central (Boise Basin) and southeastern (Hailey-Bellevue) portions of the Atlanta lobe

(Anderson, 1952). Anderson (1952) thought that these plutons constitute a good time marker; he further noted that although the western and west-central diorite bodies cut the Idaho batholith proper, the south-eastern diorite pluton is intruded by a quartz monzonite which must be younger than the batholith (Main Group). In contrast, Swanberg and Blackwell (1973) concluded that the Horseshoe Bend diorite belongs in the "Intermediate group", but assigned the Boise Basin and Hailey-Bellevue diorites to the "Tertiary epizonal group". This cannot be correct. Lead-alpha ages of these diorites are 114, 94, and 115 m.y. respectively (Jaffe et al, 1959). Regardless of the well known uncertainties of the Pb-α techniques, these measurements are significantly older than Pb-α determinations of plutons and dikes known to be of Eocene age (c.f. Armstrong, 1975a). Furthermore, the quartz monzonite cutting the Hailey-Bellevue diorite has been dated by the K-Ar method at 82 m.y. (Berry et al, 1976; Hall et al, 1978). These dioritic intrusives thus should probably all be assigned to the Late Cretaceous "Intermediate Group". The age of a similar, quartz-bearing pyroxene-hornblende-biotite diorite in T13N, R11E, sec. 33 (e.g. RK 31) is more problematical; Armstrong (1975a) reports K-Ar apparent ages of 45.9 m.y. for biotite and 54.3 m.y. for hornblende from this stock.

2.3 Eocene Igneous Rocks

2.3.1 General Statement

A significant part (about 20%) of the Idaho batholith region is composed of a suite of distinctive granitic rocks that is clearly younger than the Mesozoic plutonic complex. The largest plutons are themselves

of batholithic dimensions (Fig. 2.4) and are typically located along a N-trending belt in the east-central part of the Idaho batholith (Armstrong, 1974; Bennett, 1980). These plutons were apparently intruded at relatively shallow crustal levels (Swanberg and Blackwell, 1973) and are of prime interest because the associated heat pulse generated the gigantic meteoric-hydrothermal systems on which this study focuses (Taylor and Magaritz, 1976, 1978).

An early Tertiary stratigraphic age for these intrusions is clearly established by the Casto Pluton, which intrudes the older rocks of the Idaho batholith as well as the Challis Volcanic sequence (Ross, 1934; Cater et al, 1973). The Challis volcanic rocks are a widespread, thick series of dominantly rhyolitic to quartz latitic volcanic flows and tuffs that are in places intercalated with lake beds and other fossiliferous sediments whose flora have variously been regarded to be Eocene, Oligocene and Miocene (see Ross, 1961; Axelrod, 1966). Axelrod (1966) reports that K-Ar determinations of Challis volcanic rocks associated with two fossil plant localities indicate an Eocene age; he suggests that younger age assignments are incorrect and cites Gardner's (1879) observation that high latitude (and altitude) Tertiary forests have a young aspect because they migrated south (and down in elevation) during the progressive cooling of the period, replacing forests that are apparently, but not actually, older. In a more extensive study, Armstrong (1974) confirmed that Challis rocks generally give Eocene K-Ar ages, and attributed a few younger (Oligocene) ages to Ar loss. Armstrong (1974) also reported an Eocene K-Ar age for the Casto Pluton, in agreement with the concept (Hamilton and Myers, 1967) that the intrusives are at least broadly comagmatic and

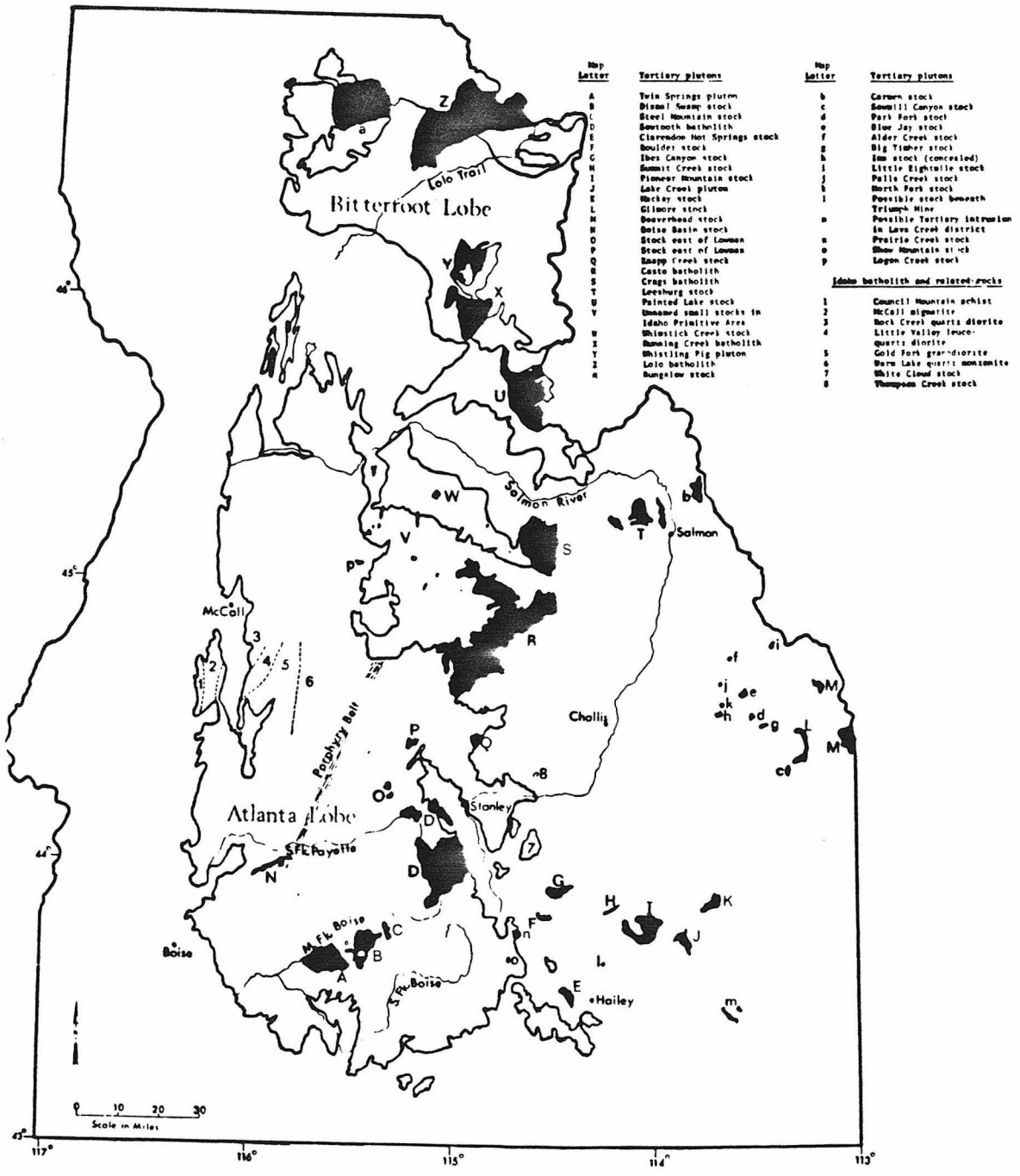

Figure 2.4 Map of Idaho batholith, showing locations and names of Eocene plutons. From Bennett (1980).

contemporaneous with their associated volcanic rocks. The epizonal Eocene plutons thus apparently locally intrude their coeval volcanic cover rocks.

Many other plutons which obviously crosscut the Idaho batholith proper are inferred to be Eocene on the basis of lithologic (Reid, 1963; Bennett, 1980), geochemical (Swanberg and Blackwell, 1973; this study), or geophysical (Tschanz et al, 1974; Bennett, 1980) similarity to the Casto Pluton, or on the basis of K-Ar and Rb-Sr determinations. In addition, a few small plutons east of the batholith also cut Challis volcanic rocks (Tschanz et al, 1974). In this report all of these plutons are collectively termed "Eocene" plutons, but an Oligocene age for a few of them cannot yet be disproved.

2.3.2 The Epizonal Plutons

This section describes the petrographic, geochemical, geophysical and geologic characteristics of the Eocene plutons. Descriptions of the Casto and Sawtooth batholiths and the Twin Springs - Dismal Swamp - Steel Mountain bodies (here termed the Rocky Bar plutonic complex) are emphasized, because these plutons have been most extensively studied and also are of special importance to this isotopic and age study.

Most of the large Eocene intrusives consist of medium-to coarse-grained, equigranular granite which varies in color from light grey to a distinctive pink (Ross, 1934; Reid, 1963, Bennett, 1980). "Granite" is here used in the sense of Streckeisen (1973); modal data have been reported for the Casto (Ross, 1934) and the Sawtooth (Reid, 1963) batholiths and also for several Eocene plutons in the Bitterroot lobe (Williams, 1979). Note that under several older classification schemes (e.g. Williams,

Turner and Gilbert, 1954; Compton, 1962) these plutons would be considered to consist of granite with subordinate quartz monzonite.

Ross (1934) describes a sample of pink granite from the Casto pluton that contains quartz (28%), microcline-microperthite (48%; with greater than 10% Ab component), oligoclase-andesine (13%), biotite (7%), hornblende (3%), and accessory magnetite and apatite. Ross (1934) states that this particular rock is atypically mafic; the "average" Casto granite would contain a little more quartz and less hornblende and biotite. Variants within the Casto pluton contain as little as 10% quartz and others almost 50% quartz (Ross, 1934).

Similar pink rocks of the Sawtooth batholith are described by Reid (1963); they contain quartz, mesoperthitic orthoclase (about 2/3 of total feldspar), plagioclase (An 2-32), minor hornblende, biotite and muscovite, and accessory zircon, apatite, sphene, allanite, ilmenite, magnetite, fluorite and rarely beryl. Several samples of perthite from these rocks (Kuellmer, 1960), at least some of which are from the Sawtooth batholith (Reid, 1963), had an average composition of about Or_{60} Ab_{38} An_2 as compared to a sample of older "Idaho batholith" that had Or_{80} Ab_{17} An_3. Although the Eocene granites contain two feldspars and thus are not of the hypersolvus type, the high Ab content of the perthite suggests that the rocks formed at relatively low pressure (c.f. Bowen and Tuttle, 1950). Alternatively, the pluton could have initially crystallized oligoclase albite at higher pressures, cracked its roof and completed crystallization as a low pressure hypersolvus granite (R. Gregory, pers. comm.).

Swanberg and Blackwell (1973) first emphasized that many of the features of the Eocene plutons can be attributed to their shallow level

of emplacement, and thus contrast sharply with complementary characteristics of the more deep-seated Mesozoic plutonic rocks. A clear-cut example is the widespread occurrence of miarolitic cavities (Williams, 1979; Bennett, 1980) and micrographic textures (Table 4.1) in the Eocene granites, which indicates the presence of a free fluid phase during the late stages of consolidation of the rock (Buddington, 1959). The absence of primary muscovite in the Eocene plutons, and its widespread occurrence in the Mesozoic granitoids, is also compatible with this concept, because muscovite (+ quartz) is not stable at magmatic temperatures if the pressure is low (Yoder and Eugster, 1955; Evans, 1965). The muscovite occasionally reported in the Tertiary rocks is in the writer's opinion probably sericite produced during hydrothermal alteration or, alternatively, primary muscovite in misidentified Mesozoic igneous rocks.

A semiquantitative estimate of the level of emplacement of plutons is provided by the heat generation of the rocks, which reflects the concentrations U, Th and K; the concentrations of these heat producing elements apparently decrease exponentially downward in the continental crust (Lachenbruch, 1968). Swanberg and Blackwell (1973) have applied this concept to the Idaho batholith region and have unequivocally shown that the Tertiary plutons have higher heat-generation valves, and higher values of the "(A-AK)/K" parameter, than the typical Mesozoic plutonic rocks. They interpreted these data directly in terms of emplacement level, suggesting (see their Fig. 5) that the Tertiary plutons were probably emplaced within 6 km of the surface, compared to 12 $\pm$ 3 km for the "Main Group" batholithic rocks; intermediate depths were suggested for the "intermediate group" rocks. Bennett (1980) has compiled gamma-ray

activity data for most of the recognized Eocene plutons, showing that the average U, Th and K contents of these plutons are about 3 times higher than those of the older rocks of the batholith. This observation is in general agreement with the data of Swanberg and Blackwell (1973), but the results cannot be directly compared because Bennett's gamma-ray activity data are unnormalized.

Bennett (1980) has also observed that relatively dark-colored smoky quartz crystals occur in most of the Teritary granite plutons, and suggested that the distinctive color derives from radiation damage. Quartz in the Mesozoic plutonic rocks is typically light grey.

Another conspicuous difference between the Eocene and Mesozoic rocks is that the former do not contain the large (commonly 2 cm, often much larger) alkali feldspar megacrysts that are common in most of the Idaho batholith proper (Williams, 1979). This condition may indicate that the growth of the megacrysts largely occurs under subsolidus (deuteric) conditions, and is thus enhanced when slow cooling takes place and high temperatures are maintained for long periods of time. Because of their shallow level of emplacement (and associated meteoric-hydrothermal activity), the Eocene plutonic rocks cooled off too quickly to allow for significant megacryst growth. It is of interest to note that the megacrysts often have turned from light grey to pink in the vicinity of their contacts with the Eocene plutons (Bennett, pers. comm.). Taylor (1974a) noted that such a color change in feldspars is commonly associated with ^{18}O exchange and that both effects could be attributed to low-temperature hydrothermal alteration within the hematite stability field. These "brick-red" alteration effects in feldspars are particularly common and much

more intense in Precambrian terranes affected by low-temperature aqueous fluids over long periods of time. Boone (1969) suggested that a similar color change in plagioclase of a hypabyssal granitic porphyry from the Gaspé Peninsula, Canada, reflects transfer of iron to feldspar from mafic minerals undergoing chloritization. Chloritization is one of the salient characteristics of the hydrothermally altered rocks in Idaho (see sec. 5.1.3), but a clearcut change in the Fe/Mg ratio of the mafic minerals has not been established. Note that the intensity of the pink coloration of alkali feldspars in the Eocene plutons appears to increase with ^{18}O depletion (see below).

Williams (1979) outlined several differences in the microscopic characteristics of the Eocene and Mesozoic plutonic rocks. Whereas subhedral grains are common in the Eocene rocks, lobate and sutured grain boundaries predominate in the older granitoids. Quartz grains are usually less deformed, and subsolidus reaction effects such as myrmekite less common, in the younger rocks as compared to the Mesozoic units. Furthermore, plagioclase zoning is stronger, and twinning more distinct, in the Tertiary rocks (Williams, 1979). It should also be pointed out that orthoclase is common in the Eocene rocks, whereas Mesozoic rocks contain microcline except where strongly reheated.

The field relations of the Eocene rocks are also distinctive. Dikes of pink granite with chilled contacts intrude the grey rocks of the Idaho batholith (Kiilsgaard et al, 1970), and xenoliths of the older rocks are common in the marginal zones of the Eocene plutons (Reid, 1963). Strong vertical jointing in the Sawtooth (Reid, 1963) and Casto (Cater et al, 1973) batholiths results in rugged "sawtooth" topography, but in the

Eocene plutons that are just being uproofed a relatively subdued topography is observed (Bennett, 1980). Foliation, where present, is confined to the Mesozoic rocks (Reid, 1963; Williams, 1979).

Positive aeromagnetic anomalies are associated with several of the Eocene rocks, notably the Sawtooth (Kiilsgaard et al, 1970), Casto, and Crags batholiths (Cater et al, 1973). Furthermore, a new aeromagnetic map of the state of Idaho (see Figs. 6.3, 6.5) after Zietz et al 1978) clearly shows positive anomalies associated with the Rocky Bar (Twin Springs - Dismal Swamp - Steel Mtn.) complex, the Boise Basin intrusive, and also the Pioneer Mountains and Leesburg stocks east of the batholith. However, the correlation between positive magnetic anomalies and Eocene plutonic rocks is much less pronounced in the Bitterroot lobe. The Painted Lake and Running Creek plutons are probably, but not definitely, related to a large nearby anomaly, the Whistling Pig pluton is even less clearly related, and the Lolo and Bungalow plutons show no relationship whatsoever to the magnetic contours. It remains to be proven that magnetic anomalies by themselves are definitive discriminants of Eocene rocks, contrary to preliminary findings by Tschanz et al (1974). Other aspects of the magnetic anomalies are discussed below in Sec. 6.2.

Several geochemical features characterize the Eocene plutons. The high U, Th and K contents have already been mentioned. Kiilsgaard et al (1970) noted abnormally high U, Mo, Be, Sn and Nb, and low CaO contents, in the Sawtooth batholith. A more detailed discussion of the major element pattern is given in Sec. 2.4.1.

Several lithologies other than pink granite belong to the Eocene group, but are of subordinate areal extent and are geologically poorly

understood. Ross (1934) mapped several bodies of hornblende quartz diorite, granophyre, and other rocks which generally occur near the margin of the main granitic mass of the Casto pluton. Ross interpreted these latter rocks simply as lithologic variants of the main mass. Furthermore, a variety of dike rocks are also concentrated near the margin of the Casto pluton (Ross, 1934; see Sec. 2.3.4). This matter clearly needs further study.

Last, several plutons of apparent Tertiary age occur in the south-central portion of the batholith (hornblende quartz diorite and granodiorite). One large pluton of this type near Trinity Mountain (RH 12) has been mapped by Rember and Bennett (1979), and similar rocks have been found nearby (e.g. I 22, RH 85d, RB 217, RB 64). These rocks are petrographically distinct from nearby Mesozoic rocks in that they are slightly finer-grained, lack K-feldspar megacrysts, usually contain hornblende and sphene, have zoned andesine rather than oligoclase, and have orthoclase rather than microcline. These rocks are considered to be Eocene because of these petrographic differences and because: (1) All analyzed samples (RH 12, RH 85d, I 22) give Eocene K-Ar ages (see Table 4.5); (2) Several of these stocks appear to be surrounded by low-^{18}O aureoles (see Sec. 6.1); (3) A porphyritic variety has been collected (RH 11). It is possible that some of the tonalites within the Sawtooth Mts. (e.g. RK 40) are also Eocene, but additional study is needed.

2.3.3 Challis Volcanic Rocks

A thick and widespread assemblage of dominantly volcanic flows and tuffs occurs immediately east of the Idaho batholith and also in small

isolated bodies within the batholith (Ross, 1962b). Fully 8,000 km^2 of territory in south central Idaho is presently covered by these rocks, and indications are that the unit was formerly much more widespread than this (Ross, 1962b). The thickness is generally unknown and without question variable, but in several places is about 1500 m (Ross, 1962b; Tschanz et al, 1974); just west of the Casto pluton the thickness may exceed 3000 m (Cater et al , 1973). As discussed in Sec. 2.3.1, the unit is at least broadly correlative with the Tertiary plutons in the region and is predominantly Eocene in age, although in part may also be Oligocene.

Ross (1962b) has summarized the characteristics of this unit which he originally defined (Ross, 1934) and subsequently mapped in many quadrangles. The following discussion of the stratigraphy and petrology is largely derived from his detailed summary, but is augmented by recent revisions.

In many places the Challis volcanic rocks overlie a conglomerate unit often referred to as the Beaverhead Conglomerate (Ross, 1962b), deposited immediately above a great regional unconformity (Tschanz et al, 1974). The thick volcanic assemblage above this base can be divided into three members, which are in approximate ascending order: (1) the latite-andesite member, (2) the Germer tuffaceous member and its probable correlatives, and lastly (3) the Yankee Fork rhyolite (Ross, 1962b). Ross (1962b) suggested that these units are partly interlayered, vary in character from place to place, and that many correlations will eventually prove unjustified. This point is to be emphasized, as Tschanz et al (1974) have succinctly stated: "These units are actually interfingering lithologic facies that reflect eruption from several volcanic centers

rather than well-defined superimposed time-stratigraphic units". Brief descriptions of these units follow.

The lowest and dominant member of the Challis volcanic sequence is the latite-andesite member. The unit consists of several thousands of feet of flows, tuffs and flow breccias, which in composition are primarily quartz latite, latite, dacite and andesite with minor rhyolite tuff, augite andesite and basalt (Ross, 1962b). The latite and quartz latite are commonly porphyritic, are green or lavender in color, and largely consist of oligoclase, K-feldspar, quartz, biotite and hornblende (Ross, 1962b). Flows of andesitic composition are mostly fine-grained, but coarser varieties contain phenocrysts of andesine or labradorite, hornblende, augite and rarely biotite and hypersthene in a groundmass of quartz and feldspar (Ross, 1962b). A few spherulitic rhyolite flows and minor obsidian occur within the upper portion of the unit (Ross 1962b). Siems and Jones (1977) suggested that these rocks were erupted from stratovolcanoes within a NE-trending zone centered in the Salmon River Mountains.

The "Germer Tuffaceous member and related strata" of Ross and Forrester (1947) consists of light colored tuff, welded tuff and intercalated sediments which in places exceed 300 m in thickness. Most of the tuff contains fragments of oligoclase, quartz, altered feldspar, biotite and hornblende crystals, volcanic rock fragments, and rare glass shards in a fine-grained, commonly silicified matrix (Ross, 1962b). Some of the material was water sorted, and beds of conglomerate, silt, clay and lignite may be intercalated with the tuff (Ross, 1962b).

The uppermost member (Yankee Fork Rhyolite) consists of brownish

rhyolite and rhyolite welded tuff (Ross, 1962b). Much of the rock contains dark, rounded phenocrysts of quartz in a devitrified matrix of quartz, orthoclase and sodic plagioclase (Ross, 1962b). The thickness of this unit locally exceeds 300 m, especially near the type locality.

Ross (1934) also mapped a large body of altered volcanic flows and tuffs in the Casto quadrangle, which he called the "Casto volcanics". Ross thought they were Permian because they were similar in appearance to the Seven Devils series and because he concluded that they were intruded by the Mesozoic granitoids (Ross, 1927, 1934). However, Cater et al (1973) have shown that these rocks are simply part of the Challis volcanic sequence which are close to, and altered by, the Tertiary Casto pluton.

2.3.4 Dike Rocks

In addition to intrusive stocks and batholiths, several types of dike rocks occur throughout the Idaho batholith region. Firstly, pegmatite and aplite dikes are associated with each major phase of plutonism; the mineralogy of each of these phases of dikes is similar to that of the enclosing Mesozoic, "Intermediate" and Tertiary intrusives (Reid, 1963). This is well shown by the comparable feldspar compositions and also by the presence of distinctive accessory minerals, for example the common presence of fluorite and beryl in the Sawtooth batholith and its pegmatites (Reid, 1963). Note that the sequence of intrusion of the pegmatite and aplite dikes accompanying each plutonic phase is very complex. In many cases pegmatite dikes cut and are cut by associated aplite dikes (Reid, 1963).

The other dikes in the region are fine-grained to porphyritic

rocks of varied compositions that in the main seem to be associated with the Challis volcanic-plutonic episode. Fig. 2.5 shows that these dikes are concentrated near the Eocene plutons and also within a NE trending "porphyry belt" north of Lowman. Reid (1963) has described the dikes in the Sawtooth region and determined their temporal sequence from contact and xenolith relationships; these rock types are indicated in Table 2.2 from oldest to youngest.

Field evidence establishes that dikes of Group 1 predate, and Groups 2-7 postdate, the emplacement of the Sawtooth batholith (Reid, 1963; see Table 2.2). Mineralization in the Sawtooth Mts. postdates dike Group 5 and predates Group 6 (Reid, 1963). Diabase dikes constituting Group 7 are youngest, trend predominantly NW compared to the predominant NE trends of the older dikes, and are probably related to the Miocene Columbia River basalt rather than to the Challis episode (Reid, 1963).

The above relationships are broadly consistent with observations by Anderson (1934, 1947) and Ross (1934) in nearby areas, although the lamprophyres are commonly reported to be closely associated with Au-Ag mineralization and in some cases cut ore veins (Anderson, 1934). Furthermore, not all the dikes in Group 1 need be "Challis related"; some of these may be related to the pyroxene-hornblende-biotite quartz diorite dikes and stocks in the Boise Basin and Pearl-Horseshoe Bend areas which are probably "Intermediate age" rocks (see Sec. 2.2.4). For comparison, the intrusion sequence in the latter area, as outlined by Anderson (1934) follows:

Idaho batholith plutons → px-hbl-bio quartz diorite → dacite porphyry → granite porphyry → syenite porphyry → rhyolite porphyry → basic dikes

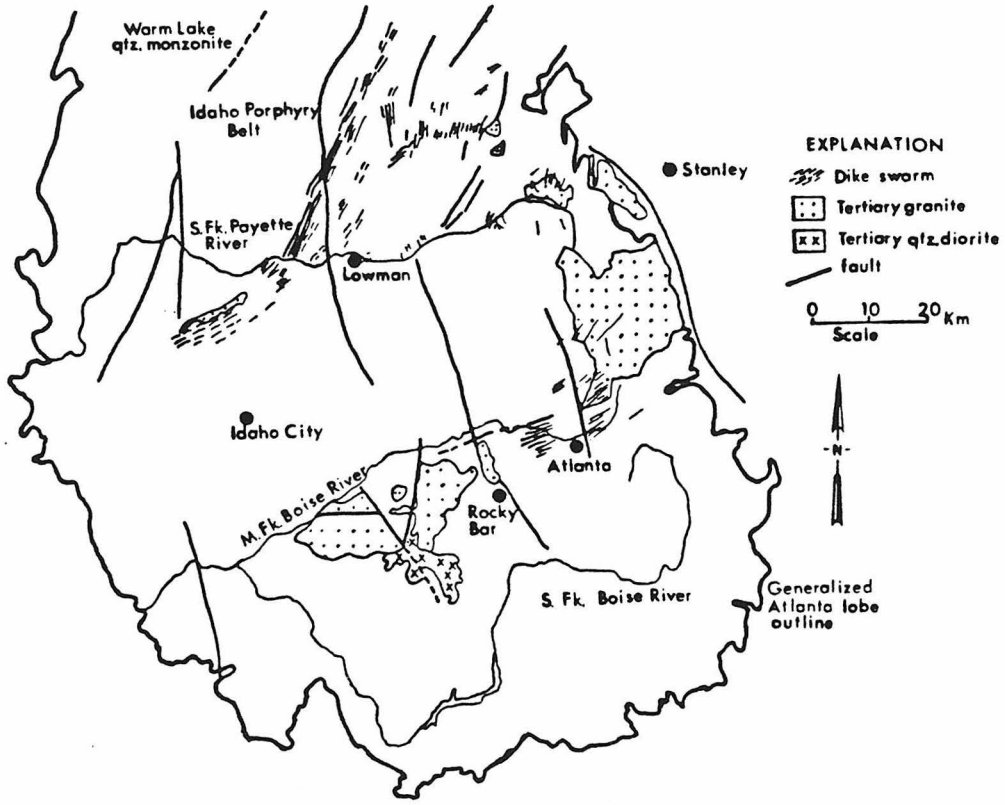

Figure 2.5 Map of a portion of the Atlanta lobe, showing Tertiary plutons and dike swarms. Unpublished map provided by Earl H. Bennett.

Table 2.2 Tertiary dike types in the Sawtooth Mts. region, tabulated in terms of their intrusive sequence, after Reid (1963).

Youngest

Dike Group 7: Diabase

Dike Group 6: Hornblende trachyandesite

- Period of Mineralization -

Dike Group 5: Hornblende andesite, biotite andesite, hornblende-biotite quartz latite, hornblende-biotite andesite, biotite trachyandesite, pyroxene andesite

Dike Group 4: Spessartite*

Dike Group 3: Rhyolite

Dike Group 2: Altered andesite, altered trachyandesite

- Emplacement of the Sawtooth Batholith -

Dike Group 1: Biotite andesite, hornblende-biotite trachyandesite, hornblende quartz latite, quartz latite, quartz monzonite porphyry, augite trachyandesite, micro-diorite hornfels, hornblende quartz monzonite, biotite quartz latite

Oldest

* Lamprophyre; Anderson (1951) reports that these dikes are commonly closely associated in time with ore deposits.

→ (?) andesite dikes.

Detailed descriptions of some of the common dike types can be found in Anderson (1934, 1947) and Ross (1934).

2.4 Summary

2.4.1 Chemical Comparison of Eocene and Mesozoic Igneous Rocks

Preceeding sections have outlined several fundamental petrographic differences between the igneous rocks of the Mesozoic and Eocene suites. This section will demonstrate (1) that a significant chemical contrast exists between the Mesozoic and Eocene rocks, and (2) that the intrusive and extrusive representatives of the Eocene suite are chemically similar. These properties by themselves are often sufficient to allow rocks to be assigned to their appropriate magmatic episode.

Fig. 2.6 is a Peacock diagram showing the variation of CaO and $Na_2O + K_2O$ vs. SiO_2 for Mesozoic rocks of the Idaho batholith (data from Larsen and Schmidt, 1958; Hietanen, 1962, 1963; Hamilton, 1963a). The analyses define nearly continuous, approximately linear arrays ranging from hornblendite (~ 46% SiO_2) through gabbro (ca 46-53% SiO_2), tonalite (primarily 57-65 % SiO_2), granodiorite (ca 65-70% SiO_2), quartz monzonite (ca 70-75% SiO_2) and granite (~ 76% SiO_2), as pointed out by Larsen and Schmidt (1958). The only outstanding exceptions to the trends are the sole olivine gabbro (46.6% SiO_2) and an unusual quartz-rich tonalite (75.5% SiO_2), both collected from the Bitterroot lobe and reported by Hietanen (1962, 1963). Note that SiO_2-poor (< 53% SiO_2) gabbroic rocks, which occur only near the northwest margin of the batholith, are greatly overrepresented on this plot; Larsen and Schmidt (1958) in fact

Figure 2.6 Peacock diagram of the Mesozoic rocks of the Idaho batholith, showing the variation of total alkalis ($Na_2O + K_2O$; diamonds) and CaO (crosses) against the SiO_2 content, in weight percent. Note the crossover of the trend lines at about 63% SiO_2, which defines the suite as "calcic". Most samples are from the western portion of the batholith. Analyses from Hietanen (1962, 1963), Larsen and Schmidt (1958), and Hamilton (1963a).

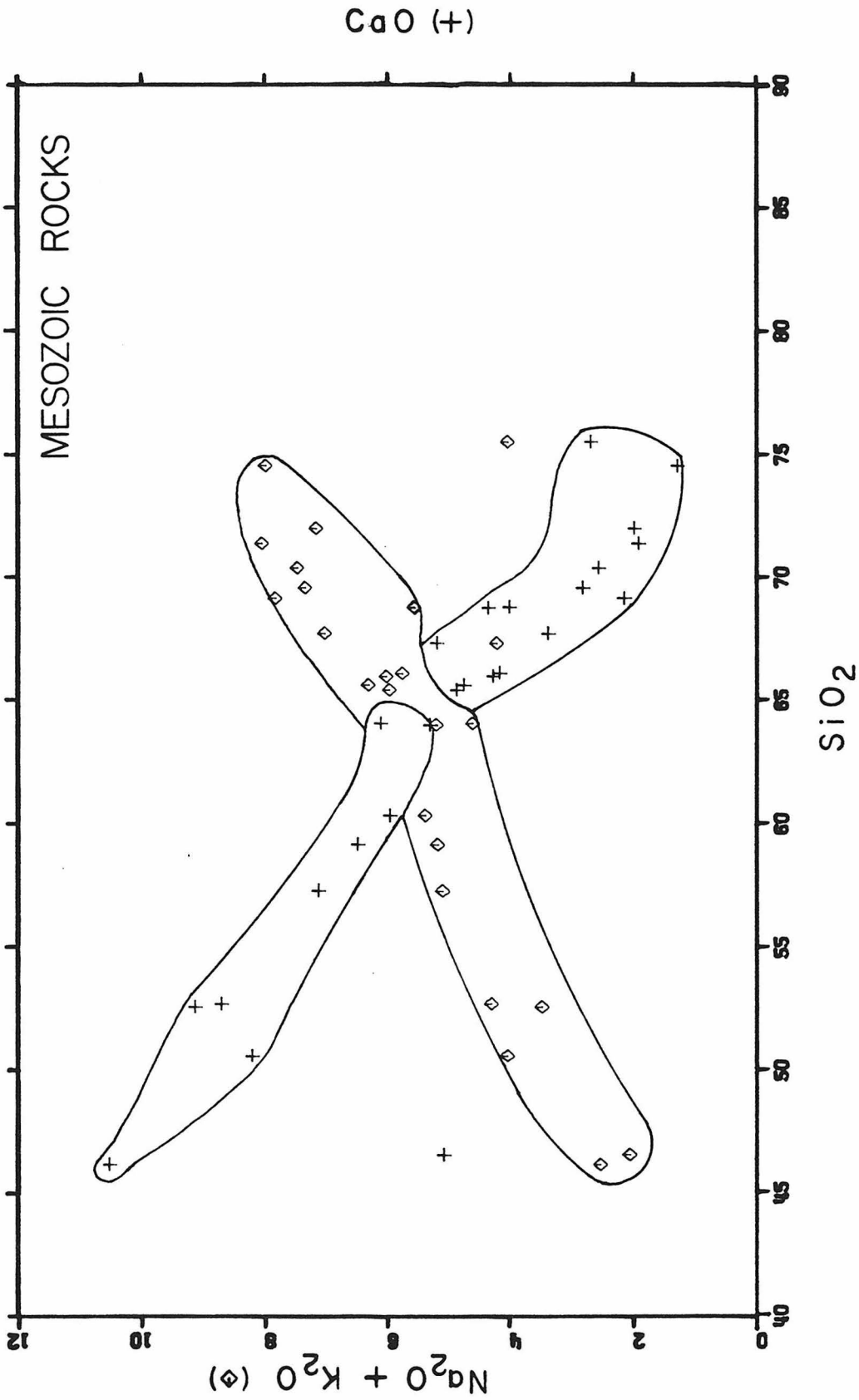
MESOZOIC ROCKS
CaO (+)
$Na_2O + K_2O$ (◇)
SiO_2
0
2
4
6
8
10
12
40
45
50
55
60
65
70
75
80
85
90

estimate that the average SiO_2 content of the batholith is about 70.5%. Furthermore, note that many of the northwestern rocks are actually members of the "west border group" (Swanberg and Blackwell, 1973) and are somewhat older than the interior rocks; however, all these Mesozoic rocks appear to define a common trend.

The intersection of the CaO and $Na_2O + K_2O$ trend lines on the figure defines an SiO_2 content, termed the alkali-lime index, of approximately 63 ± 2 %. Peacock (1931) defines suites of rocks with such high indices to be "calcic" because of their relatively high CaO, and low alkali, contents for a given silica content. Trend lines for the southern California batholith are similar despite the lower average SiO_2 content (64.6%) of this batholith (Larsen and Schmidt, 1958), and so the latter rocks would also be classified as a calcic suite.

Fig. 2.7 is a similar diagram for Challis volcanic and intrusive rocks (data from Ross, 1962b; Fairchild, 1937, Hietanen, 1963). The data again define linear, nearly continuous trends, the principal exceptions being two samples of Germer tuff reported by Ross (1962). Note that the Casto Pluton, and samples of rhyolite, quartz latite porphyry, "quartz diorite" and lamprophyre dikes (Fairchild, 1937; Shenon and Ross, 1936) plot on the same trend lines, which is strong evidence for their coeval character. The Bungalow granite probably also belongs to this suite, but the chemical data do not preclude a Mesozoic age; Bennett (1980) regards this pluton as Eocene on the basis of its miarolitic cavities and its high gamma-ray activity.

Note that the alkali-lime index for the Eocene rocks is about 57% (Fig. 2.7), which indicates that these rocks are much more alkali-rich

Figure 2.7 Peacock diagram of the Eocene rocks of the Idaho batholith and surrounding region. Explanation as in Fig. 2.6, except that Eocene intrusive rocks (mostly dikes) are circled, and points representing the Casto and Bungalow granitic plutons are labeled with a "C" and "B". Other analyses represent Challis volcanic rocks. Note the compositional similarity of the intrusive and extrusive rocks, and also the distinct difference of the trend lines from those of the Mesozoic rocks in Fig. 2.6 (e.g. crossover at ~ 57% SiO_2). Data from Fairchild (1937), Ross (1962b), and Hietanen (1963).

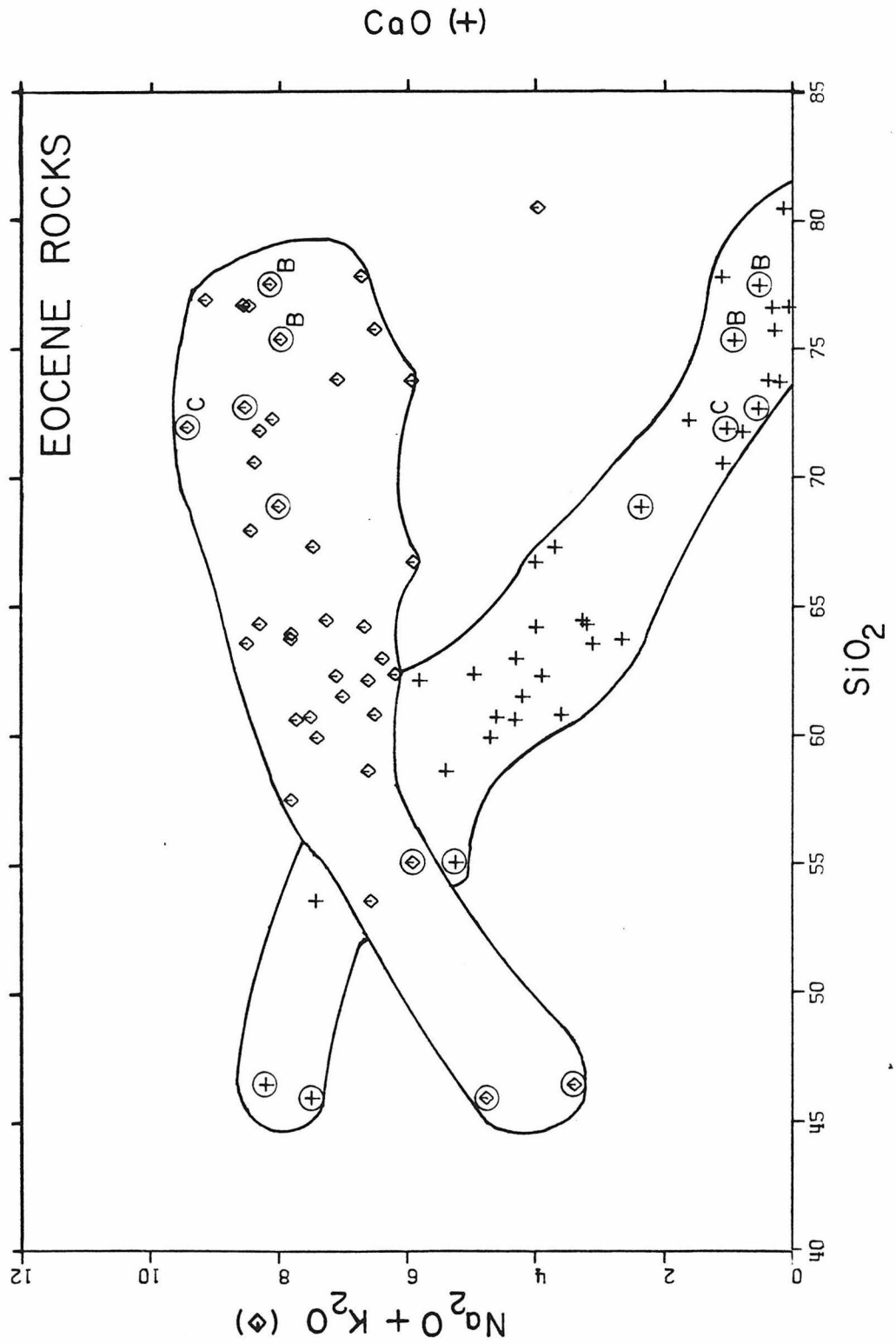
EOCENE ROCKS
CaO (+)
$Na_2O + K_2O$ (◇)
SiO_2
40
45
50
55
60
65
70
75
80
85
0
2
4
6
8
10
12
B
C

than the Mesozoic rocks, comprising a "calc-alkalic" suite (Peacock, 1931). The trend lines are thus significantly different than those of the Mesozoic suite.

The variation diagrams may in some instances by used to determine the magmatic affinity of rocks with unknown or questionable relations. As an example, Fairchild (1937) reports analyses of a granodiorite and a quartz diorite from the complicated Profile Gap area, north of Yellow Pine. Straightforward comparison with the plots shows that these rocks probably belong to the Mesozoic suite, even though Shenon and Ross (1936) tentatively assigned the granodiorite sample to the Tertiary. Similarly, several analyses of dike rocks from the northwest portion of the batholith (Hietanen, 1963) exhibit Mesozoic trends, with one exception which may then be Tertiary. Last, the Challis trend lines contrast sharply with those of the bimodal, Pliocene to Recent volcanic rocks of the Snake River Plain, which are even more alkalic. Chemical analyses therefore could probably be used to distinguish Challis rocks from those of the Snake River Plain in cases where field relations are obscure.

2.4.2 Geochronologic Summary of the Idaho Batholith

The Idaho batholith proper is Mesozoic in age (Larsen et al, 1958), probably dominantly Early to middle Cretaceous. The granitic rocks near the southeast margin of the batholith intrude upper Paleozoic (Pennsylvanian and Permian) sedimentary rocks (Ross, 1928; Hall et al, 1978). Granitic plutons along the western margin intrude the Seven Devils Series, which is a Permian to late Triassic complex comprised mainly of volcanic and volcaniclastic rocks (Cook, 1954; Vallier, 1977). Some of the

outlying plutons in east-central Oregon cut Triassic and Jurassic sedimentary rocks (e.g. near Ironside Mtn.), while others are overlain by fossiliferous mid-Cretaceous rocks (Thayer and Brown, 1964).

Thayer and Brown (1964) suggest that the batholith was largely emplaced between late Jurassic (Kimmeridgian) and late early Cretaceous (Albian) times, additionally observing that sedimentary strata within this age interval are absent from the region. Similarly Taubeneck (1959) observed that middle Jurassic (Callovian) sedimentary rocks in eastern Oregon are strongly deformed and hence are probably prebatholithic; he also noted that granitic cobbles are common in relatively undeformed Albian sediments.

The above stratigraphic age assignments are consistent with the K-Ar and Rb-Sr age determinations of Armstrong et al (1977) for the Bald Mountain (147 to 158 m.y.) and Wallowa (probably 143 to 160 m.y.) batholiths in Oregon. However, they are slightly older than the Albian bentonites of Wyoming, which were shown by Slaughter and Earley (1965) to have a source in the Idaho batholith region. Note that "batholith-related" rocks in east-central Oregon must be distinguished from the earlier Canyon Mountain ophiolitic series of peridotite and related gabbro, quartz diorite, and albite granite; this series was definitely emplaced between the lower Permian (Wolfcampian) and the upper Triassic (Thayer and Brown, 1964). Furthermore, rocks along the NW margin of the Bitterroot lobe, termed the "West Border Group" by Swanberg and Blackwell (1973), are somewhat older than the bulk of the Idaho batholith and are probably Jurassic in age.

A well defined upper age limit for the batholith is provided by

the widespread Eocene rocks produced during the Challis volcanic-plutonic episode. Challis volcanic rocks unconformably overlie the plutonic rocks of the batholith in several localities, and are related in time to several crosscutting epizonal plutons and numerous dikes (Armstrong, 1974). Additional geologic and petrographic characteristics of the Challis rocks are described by Ross (1934, 1962b), Reid (1963), and others.

The above-described field relationships definitely restrict the age of the Idaho batholith proper to the interval between the latest Triassic (~ 180 m.y.) and the Eocene (~ 45 m.y.); this indicates that the rocks are at least broadly correlative with the other great Cordilleran batholithic masses, as first shown by Larsen et al (1958). The detailed age relations of the Mesozoic plutons have not been fully established, however, and indications are that these relationships will be complicated. Anderson (1952) favored multiple emplacement of the batholith. He noted that quartz diorite of the western margin ("Marginal facies") is intruded by quartz monzonite of the interior of the batholith ("Inner facies"), which is in turn cut by a small but distinctive pluton of quartz-bearing pyroxene-hornblende-biotite diorite. A petrographically identical and presumably correlative diorite pluton near the southeast margin of the batholith is in turn cut by another quartz monzonite body, and in Montana another diorite pluton is cut by rocks of the Boulder batholith (Anderson, 1952), which has been well documented to have a late Cretaceous age (~ 70 m.y.; Tilling et al 1968). All available geochronologic and field evidence is thus consistent with a pre-Tertiary age for the bulk of these plutonic rocks, so that the entire Eocene suite represents yet another cycle of plutonism that followed a 20-30 m.y. "quiet" period in which

there was little or no plutonic igneous activity.

Available U-Pb determinations of the Idaho batholith also bear on this subject. Reid et al (1973) studied quartz diorite and granodiorite samples collected near the northwest and west-central margins of the batholith, respectively. The results were very discordant, which they thought reflected contamination with ancient lead, as well as recent lead loss. Grauert and Hofmann (1973) studied four samples of quartz diorite from the northwest portion of the batholith. These analyses were also discordant, which the authors thought reflected "memory" of Precambrian parent rocks, but the data form a linear array on the concordia diagram and extrapolate to a lower intercept age of about 70 m.y. Chase et al (1978) obtained similar results for granodiorite and quartz monzonite samples collected near the northeast border of the batholith. These samples gave a lower intercept age of 66 $\pm$ 10 m.y. and an upper intercept age of 1900 to 2250 m.y. on the concordia diagram. Chase et al (1978) concluded that the 66 $\pm$ 10 my age is close to the true age of the rocks, and emphasized the similarity of this result to the intrusive age of the Boulder batholith (see Fig. 1.1); they also thought that the upper intercept age reflects contamination with Precambrian zircons.

It is possible that most Bitterroot lobe rocks are generally younger than most Atlanta lobe plutons, as suggested by Armstrong et al (1977), although Swanberg and Blackwell (1973) would disagree. It is also probable that the Bitterroot lobe rocks have experienced greater uplift than those in the Atlanta lobe (c.f. Ferguson, 1975, Talbot, 1977), and this would influence the heat generation results on which Swanberg and Blackwell's (1973) interpretation rests (c.f. Lachenbruch, 1968).

Although much more work is required, the available evidence is consistent with the following generalized geochronologic framework for the Idaho batholith:

(1) Emplacement of the Canyon Mountain ophiolite series in the Permian or Triassic; (2) Emplacement of most of the western granitic rocks within the Late Jurassic or Early Cretaceous; (3) Emplacement of much of the batholith, especially the Main Series of the Atlanta lobe, within the Early to Middle Cretaceous, although some plutons could be Jurassic and some could be late Cretaceous; (4) Intrusion of the small cross-cutting diorite plutons and possibly some other "intermediate age" rocks in the Late Cretaceous; (5) Intrusion of the Boulder batholith (Fig. 1.1) and many other younger more easterly plutons, possibly including many in the Bitterroot lobe, in latest Cretaceous ("Larimide") time; and finally (6) Intrusion of the Challis epizonal plutons and related rocks in Eocene time about 38-45 m.y. ago.

CHAPTER 3

GEOTHERMAL SYSTEMS AND CALDERAS

3.1 Geologic Settings of Geothermal Systems

Geothermal systems and hot springs are concentrated in regions of high heat flow where hot rock occurs near the earths's surface, especially along active rifts, plate margins, and other areas of recent vulcanism (White, 1973). A principal requirement is that the permeability of the hot rock be sufficient to allow penetration of water and consequent transfer of heat. Most large geothermal systems also have insulating cap rocks above the premeable zone, which tends to inhibit discharge and conserve heat, but others, such as the impressive Geysers area in California, do not.

Modern geothermal systems thus occur in a wide variety of geologic environments. Areas of hot water and/or steam discharge occur along mid-ocean ridges (e.g. East Pacific Rise; Iceland), in both subaerial (East African rift; Salton Sea) and submarine (Red Sea) areas of recent continental rifting, above active Benioff zones (Matsukawa, Japan; Umnak Island, Alaska), above former Benioff zones (Mt. Lassen, California), along or near active transcurrent faults (Murrieta Hot Springs, California), within complex continent-continent suture zones (Larderello, Italy), and in the interiors of continents (Yellowstone, Wyoming; Steamboat Springs, Nevada). The associated aquifers are most commonly volcanic and pyroclastic rocks (Yellowstone; Valles, New Mexico; Wairakei, New Zealand) but may be relatively young sediments (Salton Sea; Red Sea), older sediments (Larderello), plutonic rocks (Steamboat Springs) or metamorphic rocks (Geysers). Evidence of recent vulcanism is present in all areas where

there is impressive thermal discharge, but is not necessarily found near the vents of the cooler types of thermal springs. With the exception of oceanic areas, the associated vulcanism in most highly active geothermal areas tends to be silicic or at least to have silicic differentiates (Smith and Shaw, 1973). This is apparently because on the continents, silicic magma chambers are often very large and shallow compared to those of basaltic magmas (Smith and Shaw, 1973).

The following discussion is restricted to the geothermal areas on continents. Systems associated with large, shallow-level magma chambers, silicic volcanic rocks, and cauldron subsidence are of particular interest. Such systems (e.g. Yellowstone, Valles, Long Valley, San Juan Mts.) provide probable analogues to the Eocene hydrothermal activity in the Idaho batholith.

3.2 Characteristics and Origin of Silicic Volcanic Plateaus and Associated Calderas

Calderas, craters and other geomorphic depressions related to volcanic activity form in a variety of ways (c.f. Macdonald, 1972). The largest features, known as "calderas of the Valles type" and the genetically similar "volcano-tectonic depressions" are distinguished by their great size (to several thousand km^2), their association with silicic volcanic rocks, and by the absence of a pre-existing volcanic edifice (McBirney and Williams, 1969; Macdonald, 1972). These features are thought to form by subsidence of rock into large underlying batholith-sized magma chambers, during events probably associated with voluminous eruptions of ash-flow tuffs (Macdonald, 1972).

This section reviews the geologic characteristics and historical

development of several rhyolitic plateau regions and their associated calderas. All examples come from the western U.S.A., where Tertiary occurrences are widespread and in many cases well described. The Valles caldera is the type example of this phenomenon, the San Juan volcanic field is of interest since many parallels may be drawn with the Challis rocks of Idaho, and the relatively young Yellowstone and Long Valley calderas have been the subject of extensive geophysical and geological investigation. All of the younger calderas exhibit ongoing geothermal activity.

3.2.1 Valles Caldera, New Mexico

Smith et al (1961) have outlined the historical development of the Valles caldera, located in the Jemez Mts. of New Mexico. The caldera lies within a large (2500 km^2; thickness to 1.5 km) field of late Tertiary alkali-calcic volcanic rocks, which range in composition through basalt, andesite, dacite, rhyodacite, and quartz latite to rhyolite. A short period of quiescence followed the eruption of the volcanic plateau, but in the late Pleistocene there was a voluminous (~ 200 km^3) ash-flow eruption, producing the "Bandelier rhyolite tuff", which was in turn apparently associated with the tectonic collapse that formed the large (19 x 24 km) Valles caldera (Smith et al, 1961). In a more detailed study, Smith and Bailey (1966) divided the Bandelier tuff into upper and lower portions, additionally observing that the lower unit was erupted from the now partly obscured and older Toledo caldera, and that the upper tuff was erupted from the Valles caldera. Doell et al (1968) report K-Ar age determinations of 1.4 and 1.0 m.y. for these two events.

Post-collapse activity in the region included uplift of a large (1 km relief) resurgent dome within the caldera, simultaneous eruption of rhyolite flows along an arcuate fracture zone and also within a graben transecting the dome, then tilting and sedimentation, and finally eruption of an almost complete ring of late rhyolite domes within a complex, ~ 5 km-wide, ring-fracture zone (Smith et al, 1961). This late ring-fracture vulcanism persisted at least until 0.4 m.y. and probably to 0.1 m.y., and was associated with much hydrothermal activity (Doell et al, 1968; also see Lambert, 1976). Smith et al (1961) proposed that ring intrusion may be associated with tensional opening of the ring fractures during resurgent doming, rather than with subsidence of the cauldron block along outward dipping fractures as had been suggested for the Glen Coe complex of Scotland.

3.2.2 San Juan Volcanic Field, Colorado

Lipman et al (1973, 1978) have summarized the geology of the San Juan volcanic field of Colorado, which was developed over the NW trending, late Cretaceous to early Tertiary Brazos-Uncompaghgre uplift. The enormous amount of Oligocene igneous activity is indicated by the field dimensions of ~ 40,000 km^2 and by the average thickness of ~1 km (Lipman et al, 1978). The earliest lavas (30-35 m.y.) comprise a calcalkaline suite of intermediate compositions (primarily andesite, rhyodacite, quartz latite) associated with mudflow deposits and other volcaniclastic sediments (Lipman et al, 1978). These rocks constitute approximately two-thirds of the total volume and are thought to have issued from several large central volcanoes (Lipman et al, 1978).

The remainder of the field was mainly erupted between 26 and 30 m.y. ago, and predominantly consists of at least 16 major (to 3,000 km^3), and many minor, units of ash flow tuffs (Lipman et al, 1978). The various ash flows range in composition from quartz latite to low-silica rhyolite, and some individual sheets are zoned upward toward more mafic compositions (Lipman et al, 1978). Many of the major ash flows have their greatest thickness within the major caldera depressions (Fig. 3.1, Fig. 3.2d), which suggests a close link between the voluminous pyroclastic eruptions and caldera collapse (Lipman et al, 1978).

Post-collapse activity includes resurgent doming of several of the calderas, hydrothermal alteration and mineralization (Taylor, 1974a, Fig. 3.1), and occasional eruption of late lavas of intermediate composition (Lipman et al, 1978). This activity was followed by bimodal volcanism which is probably unrelated to the earlier volcanism. Lipman et al (1978) proposed that the Oligocene ash flows were genetically related to a subjacent, intermediate-composition batholith whose presence is indicated by a major gravity anomaly.

3.2.3 Yellowstone Volcanic Plateau, Wyoming

The geology of the Yellowstone region has been reviewed by Eaton et al (1975). This area comprises the easternmost portion of the Snake River Plain, whose volcanic rocks consist of a bimodal assemblage that generally becomes younger to the east (Armstrong et al, 1975). Following the eruption of tholeiitic basalts and subordinate rhyolite flows, a more important and younger cycle of vulcanism began about 1.2 m.y. ago and was characterized by the construction of a rhyolitic plateau from flows

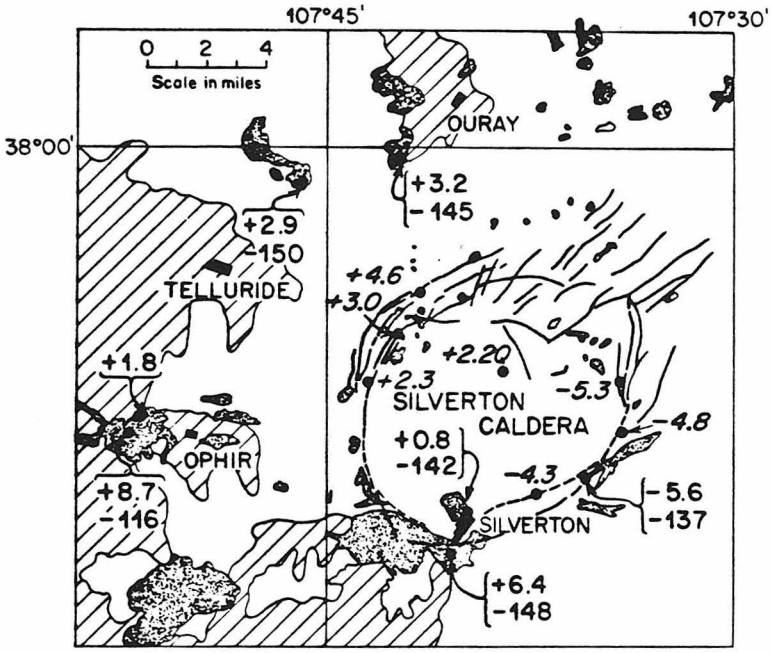

Figure 3.1 Generalized geologic map of the Silverton Caldera and surrounding region, San Juan Mts., Colorado. Tertiary volcanic rocks are shown in blank pattern, intrusions are stippled, and pre-Tertiary country rocks are ruled. Plotted numbers refer to $\delta^{18}O$ analyses of whole rock samples, except large negative numbers (-116 to -150) indicate δD measurements on biotite and chlorite. Note the extremely low $\delta^{18}O$ numbers along the ring fracture zone. From Taylor (1974a).

erupted from a pair of "growing ring fracture zones" (Eaton et al, 1975). This period was followed at 0.6 m.y. by voluminous (~ 900 km^3) eruptions of rhyolitic pyroclastic material from two adjacent ring fracture zones, accompanied by major collapse and the formation of a large (70 x 45 km) caldera (Fig. 3.2a). Shortly thereafter a resurgent dome formed within the foundered block, and a series of post-collapse rhyolitic flows erupted until approximately 0.25 m.y. (Eaton et al, 1975). Another period of magmatism, initiated during resurgent doming of the western portion of the cauldron at ~ 0.15 m.y., was characterized by renewed rhyolitic volcanism and by hydrothermal activity which continues today (Eaton et al, 1975). Most of the present surface hydrothermal activity is confined to the peripheries of the resurgent domes. Fournier et al (1976) estimate that the current heat flux from the 2500 km^2 caldera is an impressive 43 H.F.U.

The region underlying the Yellowstone caldera is characterized by low P-wave velocity, high seismic wave attenuation (especially S waves), a Bouguer gravity low, a negative aeromagnetic anomaly, and is relatively aseismic compared to adjacent areas (Eaton et al, 1975). The large (to 2.2 sec) delays of teleseismic P-waves are consistent with a ~ 55 km wide body of low velocity material which extends almost from the surface to a depth of ~ 100 km; this anomalous body almost certainly consists of hot rock or magma (Eaton et al, 1975). The latter interpretation would explain the other seismic observations, and also the aeromagnetic low, since such material would be above the Curie temperature (Eaton et al, 1975). The gravity anomaly reflects the presence of low density caldera fill and possibly also light rhyolitic magma at deeper levels (Eaton et al, 1975).

Figure 3.2 Comparison of the geology of the Sawtooth Mts. ring zone with relationships in other areas of large scale caldera development, all to the same scale:

A. Yellowstone Caldera, Wyoming, showing caldera rim, areas of resurgent doming, and fracture patterns, after Eaton et al (1975).

B. Sawtooth ring zone, Idaho, showing Sawtooth batholith (T_{SB}), fracture patterns, and the annular low $-^{18}O$ zone ($\delta^{18}O_{feld} < 6$), based on data from the present study and from Reid (1963), Kiilsgaard et al (1970) and Bennett (1980). Small, isolated low $-^{18}O$ zones within the Eocene plutons are not shown (see Fig. 6.4).

C. Long Valley caldera, California, showing the approximate size of the caldera, and some of the fracture zones (after Bailey et al, 1976).

D. Fracture patterns in the Silverton (SC) and Lake City (LC) calderas, separated by the Eureka graben (EG), in the San Juan volcanic field. The figure also shows the topographic wall of the earlier San Juan and Uncompahgre calderas, after Lipman et al (1973) and Steven et al (1974).

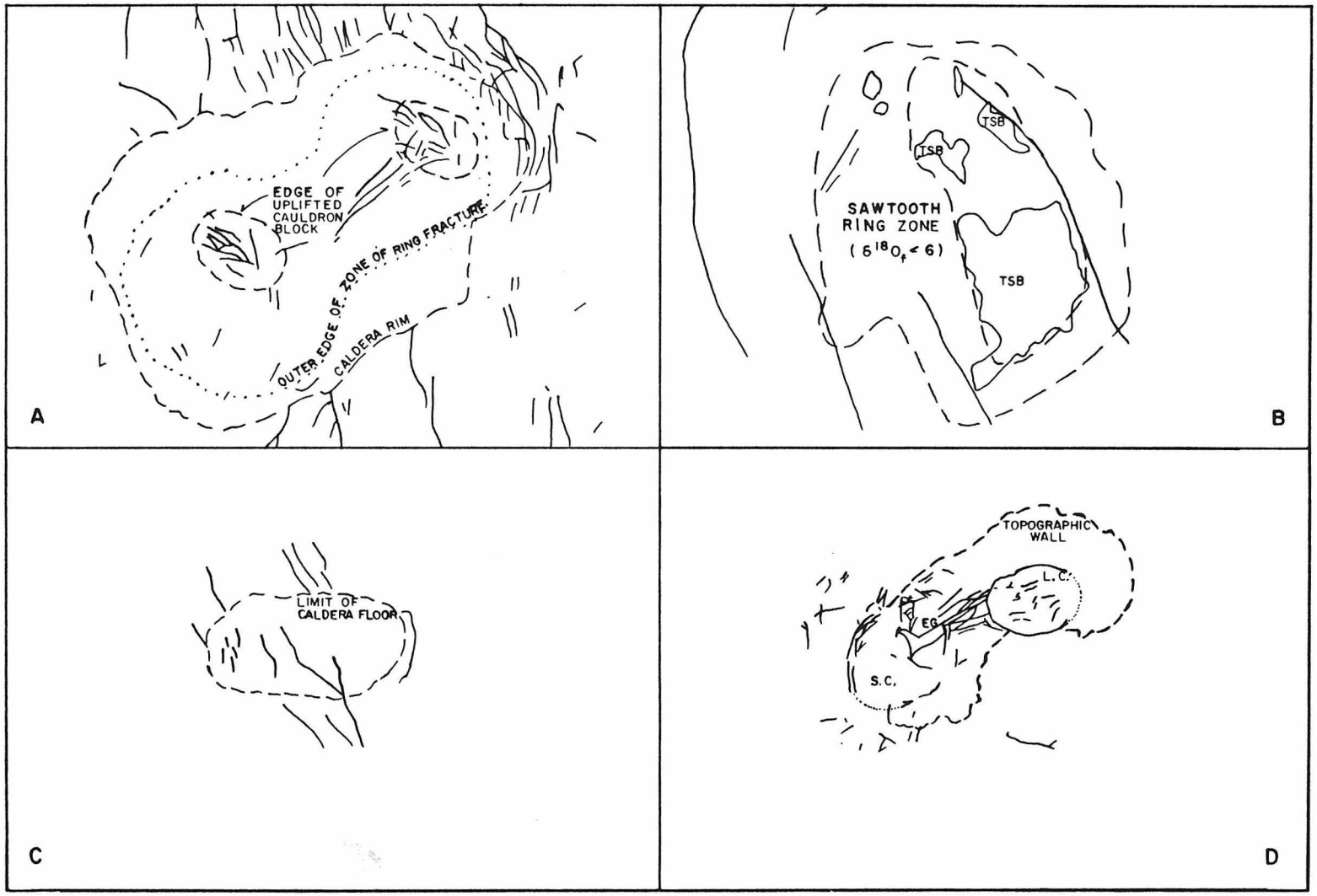
EDGE OF UPLIFTED CAULDRON BLOCK
OUTER EDGE OF ZONE OF RING FRACTURE
CALDERA RIM
A
TSB
TSB
SAWTOOTH RING ZONE
($\delta^{18}O_f < 6$)
TSB
B
LIMIT OF CALDERA FLOOR
C
TOPOGRAPHIC WALL
L.C.
EG
S.C.
D
0 km 20

3.2.4 Long Valley Caldera, California

Bailey et al (1976) have described the geology and geochronology of the large (17 x 32 km) Long Valley caldera in California (Fig. 3.2b). A few hundred meters of pre-caldera (~ 3 m.y.) basalt and andesite flows exists near the west portion of the caldera, but no great accumulation of such rocks exists. The earliest rocks which are clearly related to the Long Valley activity are a group of rhyolite domes and flows immediately NE of the caldera; two K-Ar ages of this material are 0.9 and 1.9 m.y. (Bailey et al, 1976).

The eruption of the voluminous (~ 600 km^3) rhyolitic Bishop tuff occurred about 0.7 m.y. ago, and almost certainly caused collapse along arcuate fractures to form the Long Valley caldera (Bailey et al, 1976). Bailey et al (1976) point out that the volume of subsidence, as calculated from present topography and geophysical data, corresponds closely to the estimated volume of the Bishop tuff. Postcollapse activity (to ~ 0.6 m.y.) began with the eruption of more than 500 m. of intracaldera rhyolite tuffs, domes and flows (early rhyolites), contemporaneous with formation of a ~ 10 km diameter resurgent dome in the west central portion of the caldera (Bailey et al, 1976). This was followed (0.5 to 0.1 m.y.) by eruption of pumiceous "moat rhyolites" along the periphery of the resurgent dome, and also by formation of rhyodacite domes along or near the caldera rim between 0.2 and 0.05 m.y. (Bailey et al, 1976).

Evidence of hydrothermal activity, which Bailey et al (1976) suggest was maximum at about 0.3 m.y., is provided by acid leached, argillized and silicified lacustrine sediments, and by minor hot spring and fumarolic activity today. The youngest volcanic activity includes eruption of basaltic

and trachyandesitic lavas erupted along the east front of the Sierra Nevada, and also the very young (4000 yr.), rhyolitic Mono Craters and Inyo domes which occur between Long Valley and Mono Lake (Bailey et al, 1976).

Recent geophysical investigations also bear on the nature of Long Valley. Seismic refraction profiles show that basement rock, which lies below low-velocity caldera fill, has been downdropped by 1 to 3 km within the caldera (Hill, 1976). The refraction data also suggest that the top of a low velocity (magma?) zone exists about 7-8 km below the valley (Hill, 1976), in general agreement with the probably 7 to 25 km deep low-velocity zone deduced from P wave delays of teleseismic events (Steeples and Iyer, 1976). The location of the caldera coincides with a large (~ 50 milligal) Bouguer gravity low, which primarily reflects the thick low density caldera fill (Pakiser et al, 1964), and probably partly also a deeper (8-16 km) source, possibly a magma chamber (Kane et al, 1976).

Chemical and temperature data on thermal waters allow a minimum subsurface heat flux of 10 H.F.U. to be calculated for the caldera (Sorey and Lewis, 1976). However, direct measurements of surface heat flow are complicated by the hydrologic transport system; low flux occurs along the caldera rim and reflects recharge of meteoric waters, intermediate values (4-8 H.F.U.) characterize much of the interior of the caldera, and extremely high values (to 50 H.F.U.) occur near the vents of the thermal springs (Lachenbruch et al, 1976).

3.2.5 Summary

In summary, the above case histories establish a definite connection between voluminous rhyolitic eruption, major tectonic subsidence, large,

shallow magma chambers, and resultant high heat flow and hydrothermal activity. Associated phenomena commonly include uplift, on both a regional scale preceding the formation of the rhyolitic plateau, and also on a relatively small scale forming postcollapse resurgent domes within the calderas. The major tectonic subsidence commonly occurs along arcuate or crudely circular faults, but grabens are formed in other areas and it is possible that some elliptical calderas are related to deeper tectonic phenomena.

A relationship between calderas and ring intrusions is in cases probable but is not definitely proven. Macdonald (1972) describes several rhyolitic plateaus where no arcuate dikes are known. Figure 3.2 compares the sizes and shapes of some of the above described calderas; also included is the "Sawtooth Ring Zone" of the Idaho batholith that will later be described in detail in Section 6.3.

3.3 Origin and Composition of Geothermal Fluids

3.3.1 Isotopic Relationships

One of the triumphs of stable isotope geochemistry has been the proof that the water of most geothermal areas of the world is dominantly of surficial rather than deep-seated or magmatic origin. This section emphasizes the character and origin of such surface-derived fluids and their compositional modification by interaction and exchange with hot rocks.

Craig et al (1956) studied the stable isotopic composition of several subaerial geothermal waters and proved their surficial origin. The D/H ratios of these waters were in almost all cases identical to those of the local meteoric waters in each geothermal area. In turn, the D/H ratios of these

local meteoric waters have been shown to vary as a well understood and sensitive function of the surface temperature, latitude, and altitude of the locality (Craig, 1961; Dansgaard, 1964; Friedman et al, 1964).

These critical facts establish that essentially all geothermal waters on continents and islands are dominantly of meteoric origin, although a small (~ 5%) component of magmatic water cannot be excluded. Note that since the early work of Craig et al (1956), isotopic evidence for the tentative existence of some connate and metamorphic geothermal waters has been accumulated (Clayton et al, 1966; White et al, 1973), but such waters are clearly of subordinate importance or totally absent in most modern geothermal systems.

Although the $\delta^{18}O$ values of cool, meteoric surface waters are linearly correlated with δD (Fig. 3.3), the $\delta^{18}O$ values of the associated geothermal waters are typically different from the local meteoric waters, often having significantly higher ^{18}O contents (Fig. 3.4, Craig, 1963). This phenomenon has been termed the "^{18}O shift" and reflects oxygen isotopic exchange between the heated meteoric waters and ^{18}O-rich rocks. As a general rule of thumb the hottest, most saline waters in any geothermal area exhibit the largest ^{18}O shift (Craig, 1966). Although similar D/H exchange between water and rocks is known to occur and is in fact typically much faster than ^{18}O exchange, the common lack of a perceptible deuterium shift in the water is a simple consequence of the much lower concentrations of hydrogen in most rocks. Note that oilfield brines, which were for long periods in contact with the hydrogen-rich clay minerals of sediments, do show both deuterium and ^{18}O shifts (e.g. Clayton et al, 1966; Hitchon and Friedman, 1969); however, these waters are complicated by the likelihood

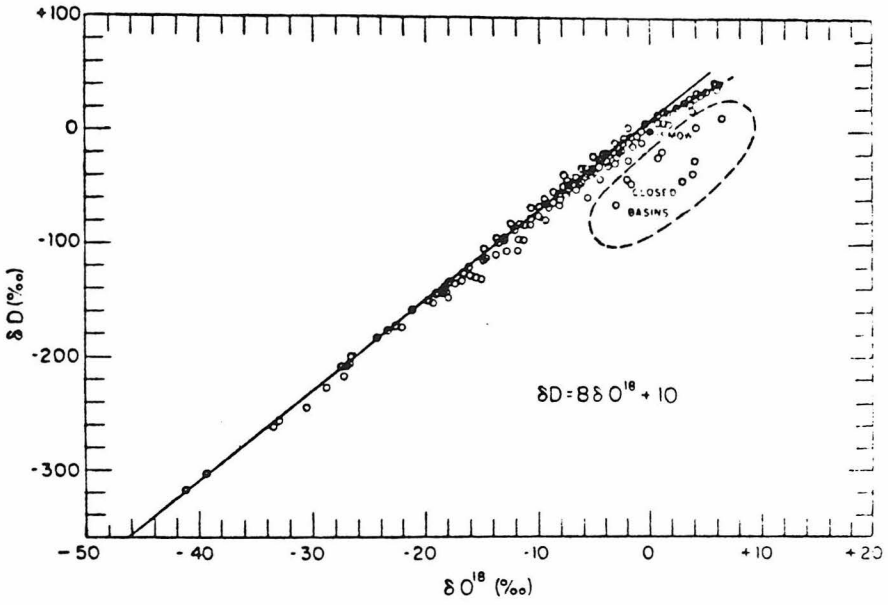

Figure 3.3 Isotopic compositions of meteoric waters (relative to S.M.O.W.). The $\delta^{18}O$ value of most surface waters is linearly correlated with δD, except for samples from closed basins where kinetic fractionations have been caused by evaporation. From Craig (1961).

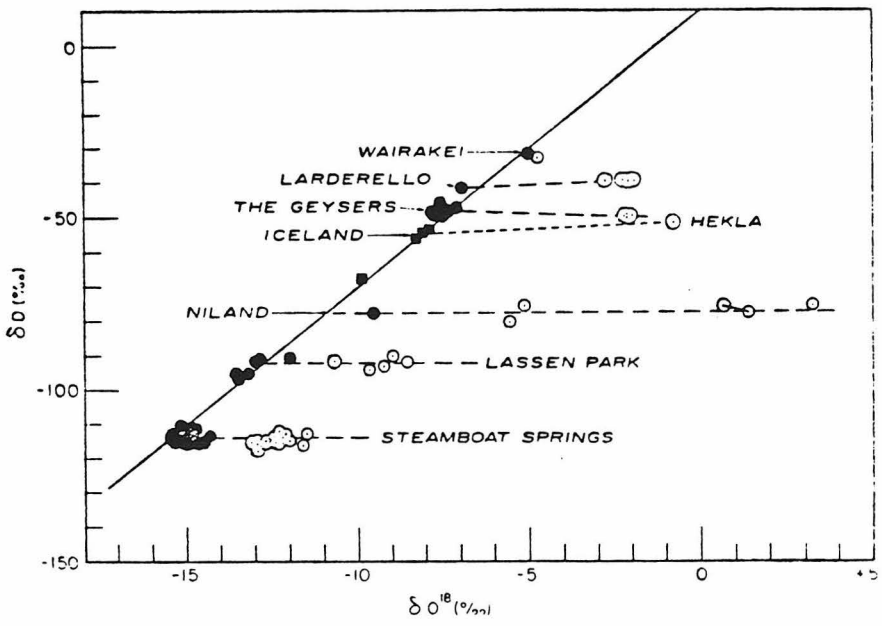

Figure 3.4 Isotope composition of chloride type geothermal waters, compared to local meteoric waters (solid dots) from each locality which fall on the meteoric water line. In each area the δD values of the geothermal waters is identical to local surface waters, but the $\delta^{18}0$ values are shifted to more $^{18}0$ rich compositions. From Craig (1963).

that they also contain a non-meteoric component.

The phenomenon of "^{18}O shift" indicated in Figs. 3.4 and 3.5 is of paramount importance to this thesis, because the ^{18}O enrichment of meteoric waters in geothermal systems requires, by material balance, a corresponding ^{18}O depletion of the affected rocks. Thus ^{18}O analyses of rocks form a basis for the study of ancient geothermal systems and even permit estimation of the former temperatures and water to rock ratios (Taylor, 1974b).

3.3.2 Dissolved Solids

Geothermal waters commonly contain appreciable quantities of solutes. Total concentrations are typically several thousand ppm, but range from essentially fresh water (few ppm) to concentrated brines (25 wt. % solute). The most important waters are neutral to alkaline chloride waters, which have a predominance of alkali and alkaline earth chlorides (NaCl, KCl, $CaCl_2$), are often close to saturation with calcite and amorphous silica, and contain a wide variety of other constituents (Ellis and Mahon, 1964; White et al, 1971). Concentrated waters of this type often occur in near-boiling springs of moderate to high discharge (White et al, 1971).

Another type of water, termed acid sulfate water, is found in gassy springs and fumaroles with relatively low discharge rates (White et al, 1971). Sulfate, rather than chloride, is the dominant anion of these low pH waters, and Fe, Al, Ca and Mg are commonly abundant relative to Na and K (White et al, 1971). These waters probably result from condensed steam boiled from a deeper reservoir of chloride water (Ellis and Mahon, 1964; White et al, 1971). Such waters are also distinguishable from the near-neutral chloride-rich geothermal waters on a δD-$\delta^{18}O$ diagram, because

both the δD and $\delta^{18}O$ values are affected by kinetic processes associated with high-temperature evaporation (boiling ?); the acid sulfate waters plot along linear trends having a slope of about 3 instead of showing the constant δD "^{18}O shift" characteristic of chloride waters (Fig. 3.5). The boiling model is also consistent with the low volatility of the common metal chlorides relative to H_2S, which oxidizes near the surface to form sulfuric acid (White et al, 1971). A few representative analyses of geothermal waters are given in Table 3.1.

It was formerly thought that the dissolved constituents in geothermal fluids were derived along with the water from a magmatic source, but when the meteoric origin of the water was demonstrated it was recognized that a primary magmatic source for all of the solutes was less likely. Subsequently Ellis and Mahon (1964) demonstrated by experiment that the chemistry of these waters could be accounted for by interaction of the hot circulating waters with their host rocks. Ellis and Mahon monitored compositional changes of water reacting with representative volcanic rocks and greywacke at temperatures ranging from 150° to 350°C and water/rock ratios close to 2. Some of their results are discussed below and show that considerable quantities of characteristic solutes were liberated from the rocks on short time scales (<14 days). For example, between 13 and 75 percent of the available chlorine in the various rocks was dissolved by the water at 350°C, which typically gave the solution a chloride concentration of a few hundred ppm. Several hundred pppm of sodium was also obtained from several rocks at this temperature, and the resultant Na/K ratios (3-20) decreased with temperature. The concentration of aqueous SiO_2 was high and temperature dependent, quickly attaining a

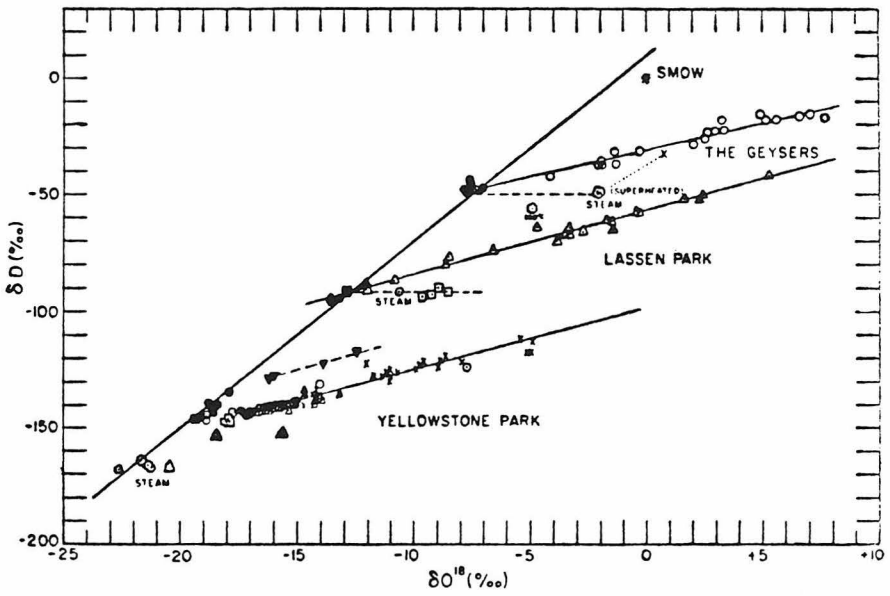

Figure 3.5 Isotopic compositions of acidic hot springs, compared to the meteoric water line. See text. From Craig (1963).

	Geysers, CA Acid Sulfate	Mud Volcano, Yellowstone Wyoming Acid Sulfate	Noris Basin, Yellowstone, Wyoming Cl (HCO_3)	Reykjanes, Reykjavik, Iceland Cl	Wairakei, New Zealand Cl	Boiling Spr, Idaho (HCO_3)	No. 2 IID Salton Sea CA. (Cl Brine)	Ellis Pool Alberta, Canada Oil Field Brine
SiO_2	225	540	529	97	386	81	400	13
Al	14	146		.7		0.1		0.85
Fe	63	17		.3		0.4	2000	0.04
Mn	1.4			0.05		0.004	1370	.00
As			3.1	.12		<0.1		0.23
Ca	47	14	5.8	2200	26	2.2	28,800	9.6
Mg	281	11	0.2	45	<0.1	0	10	15
Na	12	16	439	13,800	1130	74	53,000	1740
K	5	17	74	1920	146	(1.9)	16,500	20
Li			84	7.4	12	0.2	210	1.2
NH_4	1400	26	0.1	1.4	0.9			2.6
HCO_3	0		27	5	35	79	($500\Sigma CO_2$)	2650
CO_3	-		-	0	-	27		84
SO_4	5710	3150	38	128	35	12		223
Cl	0.5	-	744	27,400	1930	14	155,000	830
F		1	4.9	0.7	6.2	11		5.8
Br			0.1	98				3.5
NO_3			-	0.9		0.5		0-
B	3.1		12	13	26		390	1.4
H_2S	-	0	0	0.2	1.1	<.1	($30\Sigma S$)	-
Total	7770	3980	1890	45,700	3750	304	259,000	5600
pH	1.8	Strong Acid	7.5	6.7	8.6	9.1	-	8.6
Temp°C	Boiling?	65	84.5	100	Boiling	88	~ 320	37

Table 3.1 Solute composition of some geothermal waters (in ppm). From White et al (1963,1971), except Salton Sea Brine from Helgeson (1968)

value intermediate between quartz-saturation and amorphous silica-saturation. Magnesium concentrations were low (<1 ppm) and indicated strong incorporation into alteration minerals.

As a general rule the concentrations of most constituents in the waters (e.g. F^-, $SO_4^=$, Ca^{++}, NH_4^-, SiO_2, Na^+, K^+) were governed by equilibrium with the various minerals in the rocks (Ellis and Mahon, 1964). The principal exceptions were the halogens (except F^-), boron, and cesium, all of which strongly favor the water phase (Ellis and Mahon, 1964). All of the above properties have been noted in natural geothermal waters, and it is clear that hydrothermal alteration of solidified volcanic rock is sufficient to explain the chemical characteristics of the waters. No primary magmatic source is required. Incidentally, trace elements in geothermal waters are probably complexed with the chloride or sulfide, and may also in large part be derived from altered rock. The pressure (~ 350 bars) and temperature range (150°-350°C) of the above experiments are realistic in comparison with natural systems, as discussed below.

3.3.3. Physical State of Geothermal Fluids

Most geothermal systems are characterized by hot water under a hydrostatic pressure gradient. The temperature gradient in the main reservoir of large, hot (>100°C) systems is often very gentle because of convective heat transport (Helgeson, 1968; White, 1973). At shallow depths above this zone the temperature gradients are very steep, and in open channelways are controlled by the boiling curve of water under the hydrostatic head (White, 1973). A steep temperature gradient also obtains in the adjacent surface rocks, where the heat transfer mechanism is conduction. The overall effect of the hot circulating water, of course, is to bring high

temperatures close to the surface of the earth (Fig. 3.6).

An economically important but uncommon variant called a "vapor dominated system" has been discussed in detail by White et al (1971) and Truesdell and White (1973). These are typically found in areas of very high heat flow and relatively low permeability. At shallow depths the pressures are hydrostatic and temperatures are again controlled by the boiling curve, but below about 350 m the pore pressure (~ 32 bars) and temperature (~ 240°C) are nearly constant (White et al, 1971). These conditions are uniquely characteristic of steam with the maximum possible enthalpy under saturated conditions (James, 1968). Note that the low, virtually depth-independent pressure indicates that steam is the "continuous, pressure controlling phase", which in turn implies that the coexisting liquid must be present in unconnected pores in the rock (White et al, 1971).

James (1968) suggested that the maximum enthalpy condition is a consequence of boiling at an underlying water table. If the temperature and pressure at the water table were higher than 240°C and 32 bars, the steam produced would on cooling increase in enthalpy and the remainder would condense to liquid and return. This process would lower the temperature of the water table until eventually the conditions of maximum enthalpy steam obtained. Lower temperatures are not realized because the steam would on further isoenthalpic cooling become superheated, and would not produce any condensate. This condition stabilizes the unique pressure and temperature of the reservoir (James, 1968).

White et al (1971) outlined several differences in the geologic characteristics of hot-water and vapor-dominated systems. Hot water

Figure 3.6 Temperature-depth profiles in some geothermal areas, compared to a normal conductive geothermal gradient (curve A; ~30° C/km), and to the boiling curve of pure water under a hydrostatic head. Curves B and D represent two hot water systems with different reservoir temperatures (140°; 265°); the steep portions of these curves illustrate rapid heat transfer by convection. Ascending waters in such systems will boil when the boiling curve is intersected. Curve C illustrates a vapor-dominated system with a reservoir of 240° C steam, overlying a deeper pool of brine. Simplified after White (1973).

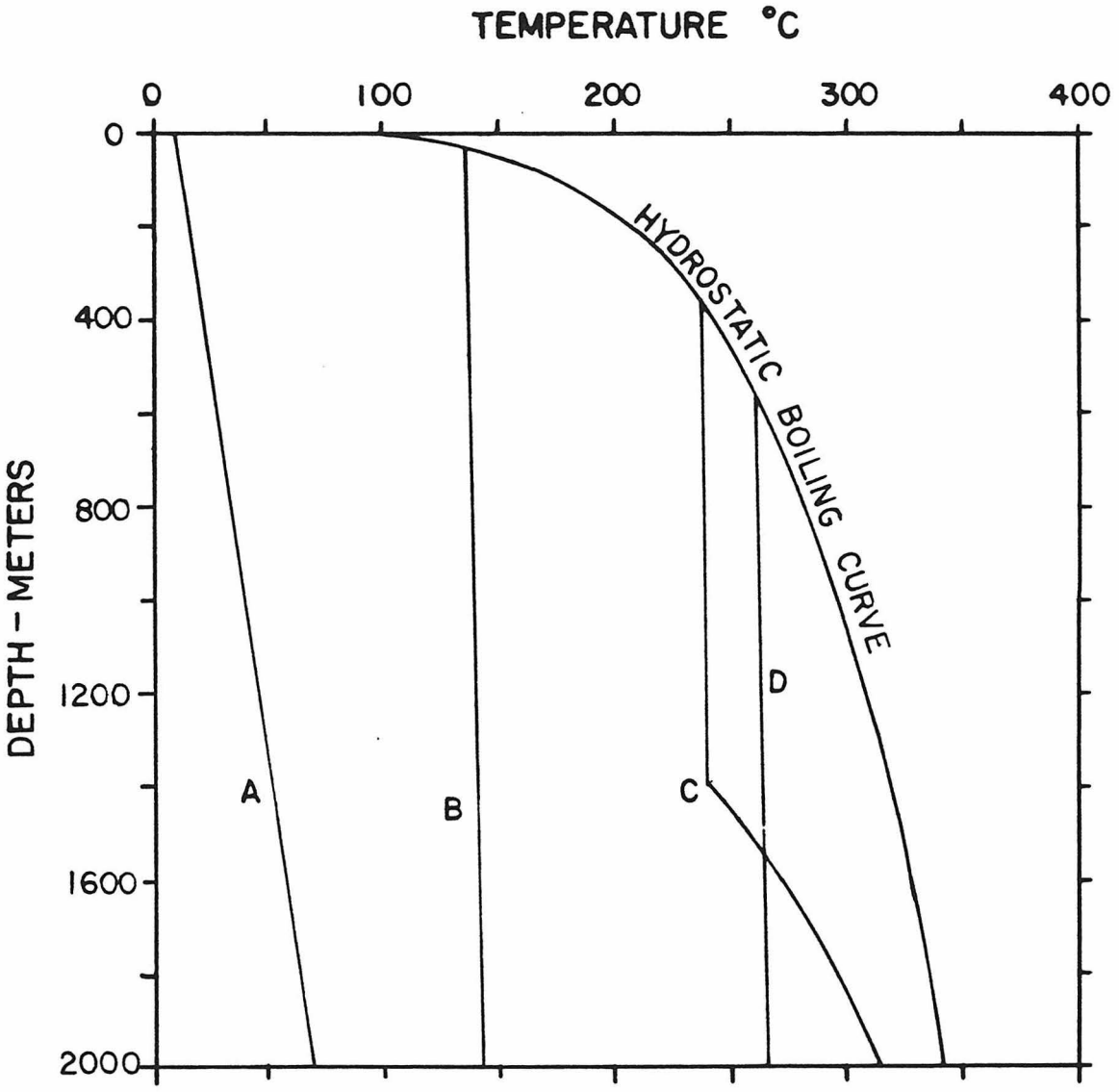
TEMPERATURE °C
0
100
200
300
400
0
400
800
1200
1600
2000
DEPTH - METERS
HYDROSTATIC BOILING CURVE
A
B
C
D

systems are found in relatively permeable sedimentary and volcanic rocks and in highly fractured, competent rocks, and are often characterized by high discharge of chloride waters (White et al, 1971). High-temperature systems are often associated with siliceous sinter and natural geyser activity, whereas travertine deposits imply lower temperatures (White et al, 1971). In contrast, vapor-dominated systems are characterized by lower-permeability host rocks, and by low discharge of acid sulfate water; mud pots, fumaroles and acid leached ground are found in areas of intense activity (White et al, 1971).

White et al (1971) suggest that vapor dominated systems develop from hot water systems where the heat supply is sufficient to vaporize all recharge. This condition could obtain by precipitation of minerals (esp $CaCO_3$ and $CaSO_4$) at the margins of the system, which would decrease the permeability (White et al, 1971). Note that a vapor dominated cap was artifically created over the hot water system at Wairakei when the fluid production rate from wells exceeded the natural recharge (Truesdell and White, 1973).

3.3.4 Circulation Dynamics of the Geothermal Fluids

It is now clearly established that circulation of hydrothermal fluids occurs around shallow level heat sources in the crust. This section will briefly summarize the theoretical cause of this circulation and the nature of the governing geologic variables. Model calculations (Norton and Knight, 1977) of heat and fluid transport around a pertinent pluton geometry will then be discussed.

Fluid motion in permeable rocks occurs in response to lateral, thermal or solute-induced perturbation of the fluid density (Norton and

Knight, 1977). The magnitude of flow is given by Darcy's equation:

$$\overline{q} = \frac{-K}{\nu} (\rho\overline{g} + \overline{\nabla P})$$

where $\overline{q}$ is the fluid flux vector (g cm^{-2} sec^{-1}), K is the rock permeability, $\overline{g}$ is the gravitational acceleration, $\overline{\nabla P}$ is the pressure gradient, and ν and ρ refer to the viscosity and density of the fluid. The condition of no flow requires that $(-\rho\overline{g})$ equals the pressure gradient, i.e. that $\partial P/\partial x$ and $\partial P/\partial y$ are zero and that the vertical gradient $\partial P/\partial z$ equals negative $(\rho\overline{g})$. Any horizontal variation in pressure or density will thus require fluid flow (Norton and Knight, 1977). Thermal density perturbations, of course, naturally arise around shallow level magma chambers and other geothermal anomalies.

The Darcy equation defines the fluid and rock properties pertinent to fluid motion. The rock permeability is of paramount importance and principally relates to continuous open fractions in the rock (Norton and Knapp, 1977). Norton and Knapp (1977) theoretically argue that the permeability is given by:

$$K = nd^3/12$$

where (n) is the fracture abundance (number per cm) and d is the fracture aperture. Aperture widths are estimated to range from 5×10^{-5} to 2×10^{-2} cm, and fracture abundances range from 0.5 per cm in some ore deposits to 10^{-3} per cm in unaltered igneous rocks (Norton and Knapp, 1977). An unexpected feature of this analysis is that porosity associated with these fractures constitutes only a small fraction of the total porosity of the rock (Norton and Knapp, 1977). Note that model calculations

of cooling plutons show that convective heat transport predominates over conduction when host rock permeability exceeds 10^{-14} cm^2 (i.e. 10^{-3} millidarcies, Norton and Knight, 1977). Most rocks of the upper crust have permeabilities greater than or equal to this number (Norton and Knapp, 1977).

The viscosity and density of the fluid also dictate the nature of flow. The first-order dependence of fluid motion on the viscosity is obvious, but the detailed circulation patterns depend on the change of viscosity with temperature and pressure. The density dependence principally relates to the coefficient of thermal expansion of the fluid, which also is a function of temperature and pressure, and also to solute concentration effects which will not be considered (Norton and Knight, 1977). Norton and Knight (1977) concluded that the circulation and heat transport properties are strongly influenced by the approximate coincidence of a maximum in the isobaric thermal coefficient of expansion and heat capacity, together with a minimum in the viscosity, in supercritical H_2O ($350° < T < 550°C$; $200 < P < 800$ bars). In this range the buoyancy and heat transport properties of the fluid are maximized and drag forces minimized (Norton and Knight, 1977).

A model calculation of fluid circulation around a pluton, computed by Norton and Knight (1977), will now be discussed. The model is based on the Darcy equation and parameters just mentioned, and also on conservation relations for mass, energy and momentum which they derive and justify in detail. The two dimensional numerical calculations are assumed to represent a cross section through the crust (Norton and Knight, 1977).

The initial and boundary conditions of the model (P5) are shown in

Fig. 3.7a. A slightly permeable ($K = 10^{-14}$ cm^2) pluton with an initial temperature of 920°C is instantaneously emplaced into more permeable (10^{-12}cm^2) host rocks, in which the initial temperature gradient is 20°C per km. Emplacement of the pluton is considered to cause fracturing of the overlying rocks, whose permeability is increased to 10^{-10}cm^2. Heat and fluid may pass through all boundaries except the lower.

The various Figs. 3.7bcd represent the heat and fluid transport after 50, 100, and 160 thousand years. The right hand side of the figures shows the isotherms. The "streamfunctions" given on the left hand side are defined by:

$$\bar{q}_y = \frac{-\partial \Psi}{\partial z} \qquad \bar{q}_z = \frac{\partial \Psi}{\partial y}$$

where $\bar{q}_y$ and $\bar{q}_z$ are the fluid flux vectors in the y and z directions, respectively, and Ψ is the streamfunction. Note that the gradient of the streamfunction is proportional to, and orthogonal to, the fluid flux vectors. Thus the "streamlines" shown in the figure are everywhere tangent to the instantaneous fluid flux vectors. Furthermore, since the gradient of the streamfunction is proportional to the magnitude of the fluid flux, the total mass flow between any two streamlines is constant.

The calculations show that fluid circulation is induced at <u>great</u> distances from the causal pluton (note that these long-distance effects on fluid motion are critical to much of the discussion in later portions of this thesis). The circulation, however, is strongly concentrated in the channels above the pluton, where transport rates are probably on the order of a few gcm^{-2} yr^{-1}. Heat transport is dominated by convection in this region, as shown by the narrow thermal dome and the steep, near-

Figure 3.7 Calculated model (P5) of the evolution of a convective circulation system developed around a hot, ~ 3 km wide epizonal intrusion. Figure 3.7a shows the geologic and initial conditions, where K is the permeability, Tp = 920° C is the initial temperature of the stock, and To = 20° C/km is the geothermal gradient in the country rocks. Heat and fluid may pass through all boundaries except the lower. Figs. 3.7b, c, and d show the isotherms (right side) and fluid streamlines (S, left side) at 50000, 100000, and 160000 years. Note the extensive lateral migration of the fluid. See text. From Norton and Knight (1977).

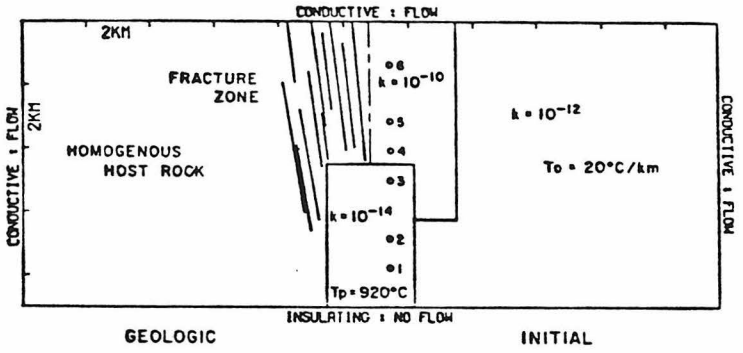

GEOLOGIC INITIAL

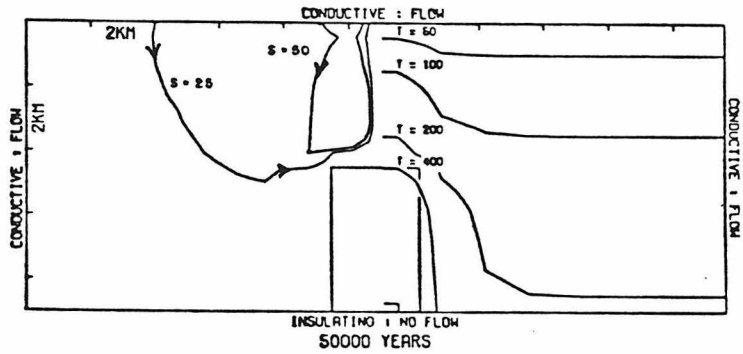

50000 YEARS

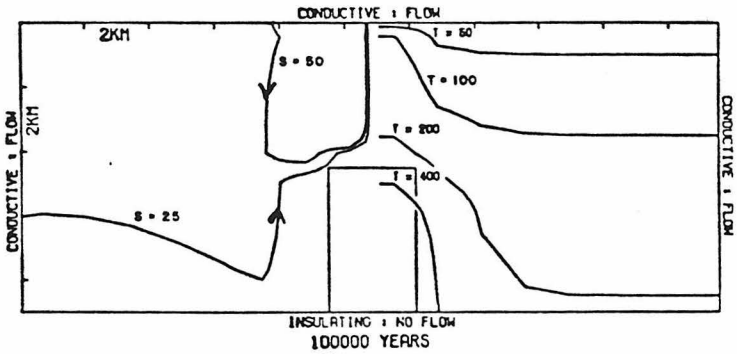

100000 YEARS

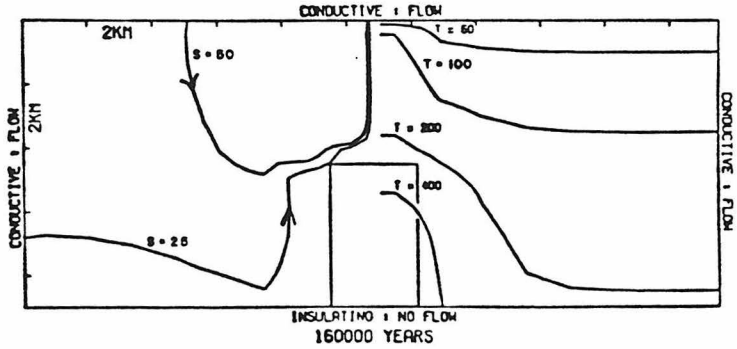

160000 YEARS

surface temperature gradient. At lower levels, and within the pluton, conductive heat transport is considerably more important. A surprising feature of the model is that even though large amounts of H_2O are involved, the cooling rate of the pluton is not shortened as much as one might imagine, as compared to the purely conductive rates (Norton and Knight, 1977). The primary effect of the fluid, then, is to redistribute heat from the sides toward the surface, (Norton and Knight, 1977). Note, however, that in another model in which the pluton was shattered after consolidation, and was thus much more permeable, the pluton rapidly cooled to low temperatures (200°- 400°C; Norton and Knight, 1977).

Other models of Norton and Knight (1977) show the effects of increased pluton width. The fluid flux is for short times concentrated along the margins of a batholith sized (54 km wide) pluton. Although these zones of concentrated fluid flux are very large, they are proportionately small and narrow compared to those developed around smaller stocks. Secondary circulation later develops above the pluton and eventually dominates the circulation style (Norton and Knight, 1977). If the top of the batholith were conical rather than flat, these secondary effects would not be as strongly developed. Small stocks or protrusions on top of the batholith would develop their own secondary convective circulation systems.

CHAPTER 4

METHODS AND DATA

4.1 Fluorine Method for $^{18}O/^{16}O$ Determination of Silicates

The technique used for $^{18}O/^{16}O$ determination of silicate minerals in this work is essentially the same as that outlined by Taylor and Epstein (1962a), and involves reaction of the silicate with excess fluorine gas in a vacuum line, purification of the released oxygen, conversion of the oxygen to carbon dioxide, and analysis on a mass spectrometer. Five purified mineral separates and one standard, each between 20 to 25 mg. and weighed to $\pm$ 0.1 mg, were placed along with a detachable manifold of six nickel reaction vessels in a dry box for 24+ hours. The samples were then sealed into the nickel cells, the manifold was removed from the dry box and bolted to the fluorine extraction line with a vacuum tight teflon seal, and the dry air was evacuated with a mechanical pump. About 1/6 atm. of fluorine gas was flushed into all metal portions of the line except the nickel vessels to react any atmosphere water which may be present; this "waste" fluorine was then reacted with solid KBr granules at about 120°C, the resultant bromine gas frozen into a liquid nitrogen trap (ℓN_2), and then the line was repumped to vacuum (~ 10 microns pressure). About 5/6 atm. of high purity fluorine gas with a negligible oxygen blank was then introduced into each nickel reaction vessel; each vessel was resealed with teflon vacuum-tight valves and then heated to ~ 525°C overnight. The next day, following removal of any unwanted fluorine gas in the line, the first nickel vessel was opened to the extraction line, allowing expansion of the released gas sample; the latter consisted primarily of oxygen and silicon tetrafluoride (from the sample) and unreacted fluorine. The SiF_4 and any other condensable gasses were

frozen into a ℓN_2 trap, the remainder was introduced into a hot (~ 180°C) KBr trap to react unwanted fluorine, and the sample was then passed through several additional ℓN_2 traps to remove bromine. The now essentially pure oxygen gas was quantitatively combusted to CO_2 with a resistance heated, spectrographic grade carbon rod with platinum leads, care being taken to keep the temperature low enough to prevent production of carbon monoxide, and the resultant CO_2 simultaneously frozen into a ℓN_2 trap. At the end of the combustion process an aliquot of sample oxygen which had been "saved" in a closed side arm was introduced into the combustion chamber and burned to react any (minor) CO which may have been produced. Then the CO_2 gas was transferred into a calibrated manometer to allow measurement of the amount of gas. The CO_2 gas was then placed in contact with hot mercury vapor to react any remaining bromine or fluorides, and frozen into a sample tube- ready for mass spectrometer determination. The extraction line was pumped to high vacuum, and the next sample was then treated in the same fashion. After all six samples had been purified, combusted and collected, about 1/6 atm. of fluorine was reintroduced into each nickel cell and heated several hours at >525°C to react any (small) amount of remaining silicate and ready the manifold for another set of samples.

Mass spectrometer analyses were made with a McKinney-Nier, 60° sector double-collecting mass spectrometer, with a working standard of Harding Iceland Spar which measures +21.62 on the SMOW scale. The analyses were corrected to SMOW measurements with a straightforward procedure which utilized the running average of the Rose quartz standards run with each manifold. The latter typically has a "raw machine number" of about

-13.3 ± 0.5 permil relative to HIS, or +8.45 permil relative to SMOW (NBS-20 has $\delta^{18}O = +9.60$ on this scale). The correction formula is *

$$\delta_{SMOW}\ \text{Sample} = (\delta_{HIS}\ \text{Sample} + 13.3 \pm 0.5) \times (1.02162) \times (1 + \text{Bkg}/2520) + 8.45$$

The first multiplicative factor refers to the "standard conversion formula" of Craig (1957), and the second factor to the background and leakage correction which was usually measured for each sample and is typically about 1.025. This correction method minimizes systematic errors resulting from the extraction procedure and from machine drift over time. Precision is normally $\pm$ 0.2 permil.

*(Note: R.H. Becker has pointed out that the true correction formula should have an additional multiplicative factor of 1.0014; i.e. 1.02162 should become 1.02305. This was not used but will not affect any of the reported numbers by more than 0.02 permil).

4.2 D/H Determination of Hydrous Minerals

Hydrogen extractions were performed both at Caltech and in the stable isotope laboratory of the U.S.G.S. at Menlo Park, in a manner similar to that outlined by Friedman (1953) and Godfrey (1962). The technique involves thermal decomposition of the mineral in a vacuum line, reaction of the released water to H_2 with hot uranium, and mass spectrometer analyses. About 100 mg of purified "biotite" was loosely crimped in an envelope of molybdenum foil, placed in a platinum crucible, and either: 1) loaded into a pyrex-quartz vacuum vessel in a drybox, pumped down to high vacuum (~ 10 microns pressure) and heated to 200°C for at least 1 hr

(CIT), or (2) placed in a pyrex-quartz reaction vessel, pumped down and heated overnight at ~ 150°C (USGS). The platinum crucible was then heated with the working coil of an RF generator to ~ 1400°C to fuse the mineral sample, allowing complete release of hydrogen gas and water into the vacuum line. During this stage, plasma discharge at CIT was prevented by allowing rapid pressure buildup in the reaction vessel (Sheppard and Taylor, 1974); at the USGS there was no ionization problem and all water was frozen into a cold ℓN_2 trap, while hydrogen was converted to water with a hot (~ 550°C) Cu-CuO furnace and then frozen. The sample gas was then passed several times through a hot (~ 700°C) uranium furnace allowing complete conversion of the sample to H_2 gas. Following manometric measurements most H_2 samples were frozen onto activated charcoal within a sample tube, but a few of the samples analyzed at CIT were pushed into a sample tube with a mercury Toepler pump. The samples were always analyzed on the mass spectrometer within 36 hours, and usually immediately, to prevent diffusive loss of hydrogen which can fractionate the sample.

The mass spectrometer analyses were made with either a 60° (CIT) or 180° (USGS) double-collecting mass spectrometer. Raw numbers were corrected for the contribution of H_3^+ to the HD beam, which was determined by analyzing the working gas at different pressures and extrapolating the results to zero pressure. The correction formula used at CIT is

$$\delta \underset{\text{SMOW}}{\text{Sample}} = \left\{ \delta \underset{\text{MS}}{H_3^{+\,\text{corr}}} \times \left(1 + \text{Bkg}/2500 \right) - 74 \right\} \div 1.074$$

where M.S. refers to the machine standard which measures +74 permil relative to SMOW. Analyses at the USGS were not made by the traditional method of a balance (resistance) panel, but rather by direct current

measurement of the mass 2 and mass 3 beams. Corrections to SMOW were made with a computer program which utilized analyses of several standard waters which were extracted each day on the same hydrogen line. All but four samples in Table 4.5 were extracted and analyzed at the USGS: most other samples in Table 4.1 and all samples in Table 4.2 were analyzed at CIT. Precision for most analyses is considerably better than ±3 permil.

4.3 K-Ar Age Measurement of Minerals

The methods used for K-Ar age measurement of minerals are identical to those described by Dalrymple and Lanphere (1969). All determinations are of the conventional type and were made in the geochronologic laboratories of the USGS at Menlo Park.

About 1 to 3 grams of "biotite" was obtained from the rocks and purified by standard mineral separation techniques. Approximately one gram was carefully divided into four fractions with a sample splitter - two for potassium measurement, one for Ar extraction, and one as a backup.

Potassium measurements were made by flame-photometry. A precisely weighed, ~ 100 mg sample of "biotite" was mixed with 0.700 $\pm$ .005 g of lithium metaborate, placed in a pre-ignited graphite crucible, and fused at ~ 950°C in a furnace. The hot bead was quenched by dissolving it in 100 ml of 4% nitric acid, and then the solution was stirred to homogenization. A 1 ml aliquot of the solution was diluted with 10 ml of triply distilled water, and the resultant solution was analyzed on a flame photometer which utilized the lithium as an internal standard. Several (generally four) rock and mineral standards with different K_2O contents were run with each set of samples, and the sample concentrations were

computed from the results. All samples and standards were analyzed in duplicate; precision was generally better than ±0.04%.

Argon was extracted from the samples in an "off line" ultrahigh vacuum system. A precisely weighed, ~ 250 mg sample of "biotite" was crimped in a small molybdenum foil envelope, placed in a molybdenum crucible, and placed in the extraction "bottle" of the extraction line. An essentially pure Ar-38 spike in a breakseal tube, and a sample "takeoff" tube, were blown onto the glass line, which was baked out at ~ 300° C and pumped on overnight. Following cooldown, the line pressure was checked with an ionization gauge and the extraction was made if the pressure was less than 5×10^{-7} torr. The sample was heated by induction with an RF generator, the Ar spike was added, and all released gas was frozen onto an activated charcoal finger cooled by liquid nitrogen. After the fusion was completed the charcoal finger was warmed and gas components other than argon were removed by an artificial molecular sieve at room temperature, by a Cu-CuO mixture at ~ 550° C, then with titanium metal at ~ 800° C. After cooling the titanium furnace to room temperature, the remaining argon and small amounts of other noble gasses were collected on activated charcoal in the "take-off" tube cooled with liquid nitrogen. The "take-off" tube was then sealed with a torch and removed from the line.

Ar isotope ratios were measured on a computer controlled, 5 collector mass spectrometer run in the static mode. This instrument permits simultaneous measurement of the mass 36, 38 and 40 ion currents. The amounts of radiogenic and atmospheric argon were determined by isotope dilution from the isotope ratios and the precisely known quantity of the Ar-38 spike. Machine discrimination effects are determined in the U.S.G.S.

laboratory by periodic measurements of air argon. These data, the sample size, and the K_2O measurements permit calculation of the K-Ar age (see formulas in Dalrymple and Lanphere, 1969). Estimated error is generally less than $\pm$ 1% but may be as large as $\pm$ 3.0% for the youngest rocks.

DATA TABLES

Table 4.1 Complete Listing of all Plutonic Mineral and Rock Samples Analyzed for $\delta^{18}O$ and δD in this Work

Note that the data for each sample are given on two lines. The following explanatory notes refer to the various columns, as are enumerated on the first page of the table:

1) T-R-S (above): Township (North, unless indicated S), Range (E) and section. U.S. Forest Service extrapolations were used in unsurveyed areas.
Field# (below): Prefix RM, RH, RC (1976 field season); RB (1977); RK (1978); RJ (1979): RSR (1978, collected by J. Given).

2) Rock Type (above): Field name only. Gdr (grandiorite), QM (Quartz Monzonite, actually a Streckeisen granodiorite), Grt(granite), Ton (tonalite), Q Dio (quartz diorite), Gph (granophyric), Porph (porphyry)
Alt. (below): Alteration intensity estimated from visual abundance of alteration minerals in thin section. W(weak), M(moderate), S(strong), E(extreme).

3) Mineralogy: Primary phases above, alteration phases below in brackets. Q(quartz), P(plagioclase), M(Microcline), Or(orthoclase), B(biotite), Mu(muscovite), H(hornblende), Px(pyroxene), Sp(sphene), Ap(apatite), Al(allanite), O(opaque), G(garnet), Z(zircon), S(sericite), C(chlorite), Cc(calcite), Ox("oxybiotite"), E(epidote), L(leucoxene), py(pyrite), Act(actinolite). The single and double asterisk superscripts indicate strongly and very strongly sericitized feldspar.

4) $\delta^{18}O$ and δD columns: F(feldspar), Q(quartz), B(biotite), Mu(muscovite), WR(whole rock), K(potassium feldspar)

5) Remarks: Above abbreviations often used. Also, V(veinlets), def(deformed), rexlized(recrystallized), MXL (K-feldspar megacrysts, generally >2 cm), L.Z. (low 18_O zone), Cr(creek), R(route, or river), alt.(altered), peg(pegmatite), Mtn.(mountain), Res(reservoir), Mgt(magnetite), SRZ(Sawtooth Ring Zone), Do.(ditto). Samples which were also analyzed for K-Ar are noted as being listed in Table 4.5.

6) Latitude north (above), longitude west (below), both in degrees, minutes and decimal minutes.

(1) T-R-S, Field#	(2) Rock, Alt.	(3) Mineralogy	$\delta_F{}^{18}O$	$\delta_Q{}^{18}O$	(4) $\delta^{18}O$ other	δD	(5) Remarks	(6) Location
6-1-17 RM 2	Gdr		8.7				West margin of batholith Gold Fork Gdr	43°51.38' 116°21.28'
6-1-23 RM 6a	Gdr (M)	Q,P,M,S,Sp,Ap [S,C,E,Cc,O,L]	7.2	10.7			Prospect pit near Aspen mine; few V. Gold Fork Gdr	43°50.98' 116°18.32'
6-2-29 RM 8a	Gdr		9.6				Roadcut, R15, Gold Fork Gdr	43°49.57' 116°15.17'
5-2-19 RM 10	Gdr (W)	Q,P,M,B,Mu,O,Z,Al [S,C,O,E,]	9.7	11.4			Roadcut, R15, MXL, Gold Fork Gdr	43°45.54 116°16.15'
1S-8-12 RH 2b	Ton (E)	Q,P‡*B,Ap,Al,O,Or? [S,C,E,Ox,O,Cc]	-5.5	5.3			Nr. Anderson Ranch Dam, 2m from 2m mafic dike; minor def, V	43°21.3' 115°26.95'
1-9-20 RH 3c	Grt?		2.4				Complicated outcrop-several faults, 2m from small dike	43°24.0' 115°24.7'
1-9-21 RH 5a	QM		7.0				Roadcut, MXL	43°24.7' 115°23.7'
2-8-25 RH 7a	Gdr (M)	Q,P,M,B,Mu,Sp,O,Ap [S,Ox,O,Sp]	7.3				Roadcut, 3m from >3m mafic dike; some def	43°29.2' 115°26.5'
2-9-6 RH 8	QM (M)	Q,P,M,B,Mu,G,Z [S,Ox,O]	8.4				Roadcut, beneath lava flow,MXL	43°32.39' 115°26.10'
3-9-31 RH 9	QM		6.0				Roadcut, Trinity Mtn. L.Z.	43°33.24' 115°25.93'
3-9-19 RH 10	Gdr (E)	Q,P‡*M,B,Sp,Z,O,Al [S,C,E,O,Sp]	-2.5				Roadcut, Trinity Mtn. L.Z.; V	43°34.52' 115°26.32'

T-R-S, Field#	Rock, Alt.	Mineralogy	$\delta_F{}^{18}O$	$\delta_Q{}^{18}O$	$\delta^{18}O$ other	SD	Remarks	Location
3-8-13 RH 11	Gdr Porph (M)	Q,P*,Or,B,H,Sp? [S,C,Ox,O,Sp,E]	10.3				Fine grained phase of Trinity Mtn Pluton	43°36.02' 115°26.76'
3-8-12 RH 12	Gdr (W)	Q,P,Or,B,H,Sp,O,Ap [S,C,Ox,O,E]	9.7	11.3	5.4_B	-108_B	Trinity Mtn Pluton (Table 4.5)	43°36.74' 115°26.55'
4-9-15 RH 14a	Gdr (M)	Q,P,Or,B,Mu,G [S,B,E]	1.2	6.8	-0.2_B	-161_B	Scotch Peak, near Dismal Swamp Pluton, rexlized (Table 4.5)	43°41.21' 115°22.80'
5-9-25 RH 16a	Gph Porph (S)	Q,P,Or*,M,B,O [S,C,O,E]	8.8	10.3			Cliff, margin of Dismal Swamp Pluton	43°44.12' 115°19.78'
5-9-25 RH 16b	Grt		7.4				Do.	Do.
4-9-1 RH 17	Grt		7.3				Eocene rock?	43°42.68' 115°19.74'
4-9-1 RH 18	QM (E)	Q,P*,M,B,O [S,C,E,O,Py]	-8.2				Rocky Bar L.Z., V, minor def	43°42.52' 115°19.86'
4-9-12 RH 19	Gdr (E)	Q,P*,M,B [S,O,E,C]	-1.8				Do.	43°41.92' 115°19.64'
4-10-7 RH 20	QM		8.3				near Rocky Bar	43°41.56' 115°18.47'
4-10-17 RH 23a	QM (M)	Q,P*,M,B,Z,Ap [S,C,O,Ox]	10.0			-120_B	near Rocky Bar, few V	43°41.19' 115°17.03'
4-10-5 RH 25b	Gdr (E)	Q,P*,M,B [S,C,E,O]	-6.9				Rocky Bar L.Z., strongly V, def	43°42.97' 115°16.94'

T-R-S, Field#	Rock, Alt.	Mineralogy	$\delta_F{}^{18}O$	$\delta_Q{}^{18}O$	$\delta^{18}O$ other	δD	Remarks	Location
5-10-28 RH 27a	QM (S)	Q,P*,M,B,Z [S,C,O,Ox,E?]	0.2	9.9			Do.	43°44.12' 115°15.67'
5-10-27 RH 28	Gdr		-2.6				~1 m from 2m mafic dike	43°44.49' 115°15.21'
5-10-23 RH 29	QM (M)	Q,P,M,B,Mu,Al,O,Ap,Z [S,Ox,O,E]	8.2		3.1_B	-130_B	Roadcut, few V (Table 4.5)	43°45.5' 115°14.1'
5-11-7 RH 31	QM (M)	Q,P,M,B,O [S,C,O,Ox]	7.0				Roadcut	43°46.8' 115°11.9'
5-11-4 RH 33	Gdr (S)	Q,P*,M,B [S,O,E]	2.1	10.5			SRZ, near Yuba R. bridge, few V	43°47.99' 115°9.42'
6-11-32 RH 35	QM (S)	Q,P*,M,B,G,O,Al [S,C,O,Cc]	3.2				SRZ, V, def	43°48.5' 115°10.7'
6-10-27 RH 39	Gdr		8.9				SRZ	43°49.45' 115°15.4'
6-10-32 RH 41a	Gdr (M)	Q,P*,M,B [S,Ox,C,O,E]	7.7	10.6			Roadcut at Black Warrior Cr., SRZ, V, minor def, 3m from 3 m mafic dike	43°49.12' 115°17.40'
6-9-35 RH 43a	Gdr (S)	Q,P*,M,B [S,C,O,Cc]	3.5	11.4	-0.1_B 7.1_K	-132_B	Roadcut near Swanholm Cr, 40 m west of 4 m mafic dikes, V, (Table 4.5).	43°49.15' 115°21.20'
6-9-26 RH 44a	QM (M)	Q,P*,M,B,Mu,G,Z [S,C,Ox,O]	8.2				Roadcut, along Swanholm Cr	43°50.0' 115°21.5'
6-9-23 RH 45	QM		7.9				Do	43°50.9' 115°22.0'

T-R-S, Field#	Rock, Alt.	Mineralogy	$\delta_F{}^{18}O$	$\delta_Q{}^{18}O$	$\delta^{18}O$ other	δD	Remarks	Location
6-9-3 RH 46	QM (S)	Q,P*,M,B,Mu,Z [S,C,O]	7.2				Do, with few V	43°53.3' 115°22.9'
7-9-29 RH 48	QM (S)	Q,P*,M,B,O,Ap,Z [S,C,O,Cc,E]	-0.4				SRZ, several V	43°54.7' 115°24.6'
7-9-31 RH 50a	QM (M)	Q,P*,M,B,Mu [S,C,O,E?]	8.5				Roadcut	43°54.2' 115°26.7'
7-8-35 RH 52a	QM (M)	Q,P*,M,B,Mu,G,Z [S,C,O,Ox]	8.6	10.5		-108_B -62_{Mu}	Roadcut at Bear R/Boise R confluence, 1 m above small peg dike	43°53.55' 115°29.3'
7-8-22 RH 54	QM (W)	Q,P,M,B,O,Ap [S,Ox,O]	8.6				Roadcut, few V	43°55.9' 115°29.3'
7-8-8 RH 57	QM (M)	Q,P,M,B,O,Ap,Z [S,C,Ox,O,E?]	8.5		4.6_B	-104_B	Roadcut, near Crooked R bridge, few V, (Table 4.5)	43°57.5' 115°31.7'
7-7-1 RH 58	QM (M)	Q,P,M,B,O,Z,Ap? [S,C,O,E?]	8.7				Roadcut	43°58.2' 115°34.05'
7-7-10 RH 60	QM (W)	Q,P,M,B,O,Z [S,O,C?]	8.9				Roadcut, several V	43°57.4' 115°36.7'
7-4-11 RH 66	QM		10.2				MXL, Warm Lake Pluton	43°57.13' 115°56.68'
7-4-26 RH 68	QM		10.1				Do	43°55.17' 115°56.77'
6-4-1 RH 70	QM		10.1				Warm Lake Pluton	43°53.41' 115°55.24'

T-R-S, Field#	Rock, Alt.	Mineralogy	$\delta_F{}^{18}O$	$\delta_Q{}^{18}O$	$\delta^{18}O$ other	δD	Remarks	Location
7-5-10 RH 72	QM		10.0				Do, Mu on joints	43°57.23' 115°51.54'
1-16-13 RH 79	QM (M)	Q,P*,M*,B,O,Z [S,Ox,O,C]	8.3	10.4			Cliff, near Hailey Gold Belt, moderate def.	44°25.4' 114°29.26'
2-14-9 RH 83	QM		-0.5				Eocene?, Soldier Mts. L.Z.	43°31.39' 114°47.90'
3-14-29 RH 85b			2.3				Alt. rock, within 1 m of 25 m porphyry dike	43°33.70' 114°49.53'
3-14-29 RH 85d	Gdr (S)	Q,P⅓Or⅓H,B,O,Sp,Ap, Al,Z? [S,C,O,E,Sp]	-0.8		-2.3_B	-166_B	Eocene rock?, 35 m from 25 m porphyry dike, V, minor def, (Table 4.5)	43°33.68' 114°49.52'
3-13-12 RH 86	QM		8.8				Roadcut, MXL	43°36.22' 114°51.56'
3-13-9 RH 88	Gdr (E)	Q,P⅓Or⅓B,H,Sp,O,Al [S,C,O,Sp,E]	-1.1	9.8			Soldier Mts L.Z., near Big Smokey Cr/Boise R confluence, V	43°36.26' 114°54.82'
3-12-15 RH 92a	Gdr		2.6				Soldier Mts. L.Z.	43°35.44' 115°0.82'
3-11-9 RH 95	QM (M)	Q,P⅓M,B,Sp?,O,Z? [S,C,Sp,O,E]	8.0	10.0	3.6_B	-133_B	White Q.M., moderate def., (Table 4.5)	43°36.60' 115° 8.93'
3-10-12 RH 97	Gneissic QM				9.0_{WR}		Roadcut, sheared rock	43°36.53' 115°13.00'

T-R-S, Field#	Rock, Alt.	Mineralogy	$\delta_F{}^{18}O$	$\delta_Q{}^{18}O$	$\delta^{18}O$ other	δD	Remarks	Location
3-10-3 RH 99	QM (M)	Q,P≫M,B,O,Sp,Ap,Al? [S,C,O,Ox,E]	7.7	9.8	1.3_B	-147_B	Roadcut at Cow Cr., (Table 4.5)	43°37.36' 115°15.34'
4-10-29 RH 101	Gdr		8.3				Roadcut	43°39.58' 115°17.13'
4-10-16 RH 103	QM		7.4				Roadcut	43°40.69' 115°16.20'
5-9-23 RH 104	Gph Porph (M)	Q,P,Or≫M,B,O,Z [S?,C,Ox,O,Sp,E]	8.8				Steel Mtn Pluton; miarolitic	43°45.7' 115°20.5'
6-9-34 RH 105	Gdr		5.9				Roadcut, "Rocky Bar" L.Z.	43°48.45' 115°22.6'
5-9-6 RH 109	Gdr (M)	Q,P≫Or,B,O,Z,Ap,Al? [S,C,O,Ox,E]	5.6	9.3			Do	43°47.55' 115°25.3'
5-8-11 RH 111	Gdr		0.2				Do	43°46.9' 115°28.4'
5-8-17 RH 113a	QM		-3.7				Roadcut, Rocky Bar L.Z., Alt. rock 2 m above 1 m mafic dike, C on joints	43°46.5' 115°32.05'
5-7-26 RH 115	QM (M)	Q,P,Or≫B,Al,Ap [S,C,O,Sp?]	7.1	9.8	2.4_B	-173_B	Roadcut, minor def. (Table 4.5)	43°44.66' 115°34.88'
5-7-34 RH 115.5	Gdr		9.2				Roadcut	43°43.56' 115°36.07'

T-R-S, Field#	Rock, Alt.	Mineralogy	$\delta_F{}^{18}O$	$\delta_Q{}^{18}O$	$\delta^{18}O$ other	δD	Remarks	Location
4-7-4 RH 117	QM		7.6				Roadcut	43°42.63' 115°38.05'
4-7-8 RH 118b	Grt (M)	Q,P⁋M,B,Al,Z,Sp [S,C,Ox,O,E]	7.9	10.3			Eocene granite, Twin Springs Pluton	43°41.98' 115°38.71'
4-7-18 RH 120	Grt (S)	Q,P⁋M⁋B,O,Sp,Al? [S,C,Ox,O,E]	6.2	10.1	0.2_B	-150_B	Pinnacles, Twin Springs Pluton, (Table 4.5)	43°41.29' 115°40.40'
4-6-22 RH 123	Grt (S)	Q,P⁋M⁋B,O [S,C,O,E,Sp]	8.4	10.3			Twin Springs Pluton; 15 m from 35 m porphyry dike	43°40.11' 115°43.47'
9-7-32 RC 3a	QM (M)	Q,P⁋M,B,Mu,Al,Z,O [S,C,Ox,O,E]	9.2	10.7	4.2_B	-126_B	Roadcut, Deadwood R/Payette R confluence, MXL, 30 m from 1 m mafic dike (Table 4.5)	44°4.76' 115°39.50'
8-6-1 RC 4a	QM (S)	Q,P⁋M,B,Al [S,C,O,E,Sp?]	8.6	10.6			Roadcut, 40 m from 8 m mafic dike	44°3.8' 115°41.4'
9-6-35 RC 7a	QM (S)	Q,P⁋Or,B,O,Ap,Z [S,C,O,E,Sp?]	1.3	8.7			Roadcut, Boise Basin L.Z., 7 m from 40 m porphyry dike, V	44°4.1' 115°42.5'
9-6-34 RC 8c	Q Dio (S)	Q,P⁋Or,B,H,O,Sp,Ap [S,C,O,E,Sp,Cc]	1.1			-133_B	Diorite intrusive, ~ 35 m from large porphyry intrusive	44°4.2' 115°43.7'
9-6-33 RC 10b	QM		6.8				Roadcut, near Big Pine Cr./Payette R confluence, 8 m from large aplite dike	44°4.28' 115°45.48'
8-5-10 RC 13	QM (M)	Q,P⁋M⁋B,Al,Ap [S,C,O,Cc,Ox,E?]	9.0	10.9	4.5_B	-95_B	Hanks Cr/Payette R confluence (Table 4.5)	44°2.69' 115°51.01'
8-4-22 RC 18	QM (M)	Q,P,M,B,Mu,Ap,Z [S,C,O,E]	9.9	12.0	6.1_B	-87_B -55_{Mu}	Warm Lake Pluton, MXL, few V, (Table 4.5)	44°0.82' 115°57.80'

T-R-S, Field#	Rock, Alt.	Mineralogy	$\delta_F{}^{18}O$	$\delta_Q{}^{18}O$	$\delta^{18}O$ other	δD	Remarks	Location
8-5-22 RC 21	QM?		7.6	10.0			Roadcut, Grimes Pass, alt. rock near Boise Basin intrusive, B destroyed	44°1.26' 115°50.56'
8-5-15 RC 22	QM (M)	Q,P⁑M,B,O,Ap [S,C,Ox,O,E?]	8.2	10.5			Roadcut, ~ 1 km from Boise Basin intrusive, strongly V	44°1.65' 115°50.85'
11-12-28 RC 35a	QM		9.5				Outcrop with several peg dikes, near Stanley Lake	44°14.95' 115°4.35'
10-10-27 RC 36a	QM		5.9				Roadcut, White QM	44°10.35' 115°14.64'
10-11-34 RC 38	QM (M)	Q,P⁑M⁑B,O,Sp,G [S,C,O,E]			7.8_{WR}		Cliff, Grandjean Creek, Sawtooth Pluton	44°9.77' 115°10.02'
10-11-34 RC 39e	Gdr (S)	Q,P⁑M,B,H,E,Sp,O,Ap [S,C,O,E,Cc,L]	5.5	9.7	1.7_B	-160_B	Cliff, near contact with Sawtooth Pluton, minor def. (Table 4.5)	44°9.65' 115°10.5'
9-14-18 RC 45	QM (S)	Q,P⁑M,B,O [S,C,Ox,O,E]	2.1	10.2			SRZ, near U.S. 93, V	44°6.67' 114°51.53'
7-13-26 RC 46a	QM (M)	Q,P⁑M,B,Al,O,Ap [S,C,Ox,O,E,Sp]	5.0				SRZ, V	43°54.07' 114°54.54'
1S-9-36 RB 2a	Gdr		8.4				Roadcut, R. 68	43°17.8' 115°19.6'
1S-10-19 RB 5b	Gdr		8.6				Castle Rocks	43°19.6' 115°18.5'
1-10-16 RB 10a	Gdr (M)	Q,P,Or,B,H,Sp,O,Z,Ap [S,C,O,Sp,E]	0.3				Eocene Rock?, 8 m from mafic dikes	43°25.1' 115°16.65'

T-R-S, Field#	Rock, Alt.	Mineralogy	$\delta_F{}^{18}O$	$\delta_Q{}^{18}O$	$\delta^{18}O_{other}$	δD	Remarks	Location
2-10-19 RB 13a	Gdr		8.0				Cliff, Gdr with pink MXL, 1 m from 10 cm peg dike	43°29.45' 115°18.6'
3-10-33 RB 15a	QM		5.3				Cliff, Eocene Rock?	43°32.88' 115°16.72'
3-10-8 RB 17	Gdr		8.4				Roadcut, MXL	43°36.72' 115°17.00'
3-9-1 RB 21	QM (M)	Q,P‡M,B,Mu,G [S,C,Ox,O,E]	3.1			-160_B -149_{Mu}	Rocky Bar L.Z.	43°37.83' 115°20.30'
4-9-35 RB 22	QM		6.2				Do	43°38.26' 115°21.36'
3-10-25 RB 26a	QM		8.2				Along road, outcrop cut by several small peg dikes	43°33.60' 115°12.63'
1S-8-12 RB 34a	Gdr				0.3_{WR}		Near Anderson Ranch Dam, 2 m from 1 m light granitic dike	43°21.2' 115°27.0'
1S-8-16 RB 40	Gneiss		0.1				Roadcut, 2 m above mafic dike, Anderson Ranch L.Z.	43°19.8' 115°31.1'
3-7-33 RB 45c	Gdr (M)	Q,P,M,B,G,Z [S,C,O]	9.2		5.1_B	-125_B	Roadcut, rexlized rock, (Table 4.5)	43°33.53' 115°37.23'
3-6-23 RB 49	QM (M)	Q,P,M,B,Mu,G [S,Ox,O,Sp]	8.6			-150_B -161_{Mu}	Roadcut, similar to Warm Lake Pluton, several V, minor def	43°35.17' 115°41.84'
3-6-2 RB 50a	QM		5.1		4.7_{WR}		Roadcut, 7 m from 5 m basic dike, Rocky Bar L.Z.	43°37.12' 115°42.76'

T-R-S, Field#	Rock, Alt.	Mineralogy	$\delta_F{}^{18}O$	$\delta_Q{}^{18}O$	$\delta^{18}O_{other}$	δD	Remarks	Location
4-6-34 RB 51	Grt		4.9				Eocene granite, Twin Springs Pluton	43°38.15' 115°43.55'
4-5-35 RB 60a	QM		9.6				Roadcut	43°38.16' 115°49.56'
4-5-10 RB 62	Gdr		-4.7				Roadcut, Eocene rock?, alt. B+H Gdr with C along joints	43°42.31' 115°50.99'
5-5-34 RB 64	Gdr (M)	Q,P,Or,B,H,O,Ap [S,C,O,Sp?]	9.3			-117_B	Eocene rock?	43°43.89' 115°50.82'
5-5-29 RB 65a	Gdr (M)	Q,P,M,B,Al,Z,Ap [S,C,O,Cc,E?]	8.8			-97_B	Roadcut, MXL	43°44.76' 115°53.39'
5-4-35 RB 68	QM (M)	Q,P,M,B,Al [S,C,O,Sp?]	8.9		4.4_B	-89_B	Roadcut, MXL, R. 21 at Grimes Cr., (Table 4.5)	43°43.55' 115°57.00'
7-6-25 RB 70	QM (S)	Q,P‡M,B,Z,Al,Ap [S,C,O,Ox,Cc]	8.5		3.3_B	-133_B	Roadcut, R. 21, 30 m from 1 m mafic dike, (Table 4.5)	43°54.56' 115°41.82'
7-7-19 RB 71	QM (S)	Q,P‡M,B [S,C,O,Cc]	8.0				Roadcut, R. 21, MXL	43°55.83' 115°40.72'
7-7-32 RB 72a	QM		9.3				Sunset Mtn.	43°53.95' 115°38.73'
7-7-17 RB 73	QM		9.2				Roadcut, R. 21	43°56.19' 115°39.80'
8-7-27 RB 75d	QM				7.4_{WR}		Roadcut, R. 21	44°0.01' 115°36.36'

T-R-S, Field#	Rock, Alt.	Mineralogy	$\delta_F{}^{18}O$	$\delta_Q{}^{18}O$	$\delta^{18}O$ other	δD	Remarks	Location
9-7-13 RB 79a	QM (M)	Q,P,M,B,O,Al,Ap,Z [S,C,O,Cc,E]	9.0			-115_B	Roadcut, MXL	44°7.28' 115°34.95'
10-7-25 RB 81	QM		7.6				Roadcut, margin of SRZ	44°10.05' 115°33.6'
11-8-22 RB 83a	QM		6.6				Do., 8 m from > 4 m mafic dike	44°16.43' 115°28.76'
12-8-35 RB 84	QM		5.8				Roadcut, SRZ	44°19.82' 115°27.58'
14-7-23 RB 89f	QM (M)	Q,P,M,B,Al,Ap?,Sp? [S,C,O,E]	9.0		3.8_B	-120_B	Roadcut, 180 m from 8 m porphyry dike, few V, (Table 4.5)	44°32.6' 115°33.9'
16-8-36 RB 90	Gdr		-1.3				L.Z. north of Landmark	44°41.1' 115°32.7'
16-8-13 RB 92	QM		8.1				Roadcut, Do.	44°43.7' 115°33.5'
17-8-30 RB 94	Gdr		6.9				Roadcut, rock with pink MXL, 5 m from 0.5 m felsic dike	44°47.0' 115°32.4'
18-8-16 RB 96	QM		9.9				Roadcut, MXL	44°54.02' 115°29.28'
19-8-26 RB 98	QM		8.2				Roadcut, few MXL	44°57.67' 115°26.98'
18-9-3 RB 101a	Gdr (E)	Q,P,M,B,Ap,Z [S,Cc,O]	8.6				Yellow Pine Mine, V	44°55.70' 115°20.00'

T-R-S, Field#	Rock, Alt.	Mineralogy	$\delta_F{}^{18}O$	$\delta_Q{}^{18}O$	$\delta^{18}O$ other	δD	Remarks	Location
18-9-3 RB 101b	QM				9.6_{WR}		Yellow Pine Mine	Do
18-9-3 RB 102a	Ton (M)	Q,P,M,B,O,Ap [S,Ox,O]	8.6				Roadcut near Yellow Pine Mine, several V, MXL	44°55.59' 115°20.24'
19-8-30 RB 105a	QM (M)	Q,P,M,B,Mu?,Z [S,C,O,E]	9.6			-77_B	Roadcut, few MXL, Warm Lake Pluton?	44°57.53' 115°31.4'
19-7-34 RB 107	QM		9.7				Roadcut, near Caton Cr/Salmon R. confluence, Warm Lake Pluton, MXL	44°56.87' 115°35.30'
19-6-16 RB 117	QM (M)	Q,P,M,B,Mu,Z [S,C,O,L]	10.6				Roadcut, MXL, Warm Lake Pluton	44°58.67' 115°43.7'
18-6-23 RB 122	Gdr		10.3				Do.	44°52.8' 115°41.5'
16-6-11 RB 125a	QM		10.5				Do., 30 m from 25 cm felsic dike	44°44.5' 115°41.2'
13-7-11 RB 130a	QM		9.6				Deadwood Mine, MXL, 2 m from 15 cm peg dike	44°28.31' 115°34.80'
11-7-17 RB 134	QM (W)	Q,P,M,B,Mu,O,Z? [S,Ox,O]	9.4	10.9	5.1_B	-101_B -51_{Mu}	Near Deadwood Res. Dam, few MXL, few V, (Table 4.5)	44°17.55' 115°38.45'
10-6-2 RB 137	QM		9.1				Roadcut	44°13.3' 115°42.0'
10-5-7 RB 142	QM (M)	Q,P,M,B,Mu,O,Z [S,Ox,C?]	9.2				Roadcut, Warm Lake Pluton, MXL, few peg dikes nearby	44°13.24' 115°54.85'

T-R-S, Field#	Rock, Alt.	Mineralogy	$\delta_F{}^{18}O$	$\delta_Q{}^{18}O$	$\delta^{18}O_{other}$	δD	Remarks	Location
11-5-10 RB 148	QM (W)	Q,P,M,B,Mu?,Z [S,O]	9.9	11.4	6.1_B	-88_B	Roadcut near summit, MXL, Warm Lake Pluton, (Table 4.5)	44°18.2' 115°50.5'
9-5-18 RB 151	QM		9.8				Roadcut, Warm Lake Pluton, 8 m from 0.5 m peg dike, MXL	44°6.63' 115°54.88'
9-4-20 RB 152a	QM (W)	Q,P,M,B,H,Sp,E,Ap [S,C,L,Cc,O]	9.4			-81_B	Roadcut, MXL, relatively dark rock	44°6.0' 116°0.37'
8-3-8 RB 158	Gdr		8.8				Roadcut, R.15, B+H Gdr	44°2.25' 116°7.95'
7-2-11 RB 159a	Px Gdr (M)	Q,P,M,B,H,Px,Sp,Z,Ap,O [S,C,E,Cc]	8.9			-68_B	Roadcut, R.15	43°57.69' 116°11.51'
7-2-33 RB 161f	Gdr (M)	Q,P‡Or?,B,H,O,Ap,Z [S,C,E,Cc]	9.0			-100_B	Roadcut, 40 m from contact with Pearl-Horseshoe Bend diorite stock, rexlized	43°54.36' 116°13.85'
2-13-1 RB 163	QM (E)	Q,P‡*Or?,B,Sp,O,Ap [S?,C,E,O]	-5.8				Eocene rock, Soldier Mts, several V, minor def.	43°32.21' 114°50.72'
3-14-32 RB 167	Px Gdr (M)	Q,P,M,B,H,Px,Sp,O,Ap [S,C,O,E,Sp,L]	6.0				Unusual rock, few V, minor def, Mgt-Px symplectic intergrowth	43°32.80' 114°49.01'
3-14-27 RB 169a	Gdr		8.7			-102_B	Roadcut, 1 m from 10 cm felsic dike	43°33.68' 114°46.33'
3-13-1 RB 173	Gdr		-0.2				Alt. rock, C along joints	43°37.75' 114°51.52'
4-13-22 RB 178c	Gdr		6.7				Cliff, 15 m from 10 m porphyry dikes	43°40.23' 114°53.35'

T-R-S, Field#	Rock, Alt.	Mineralogy	$\delta_F{}^{18}O$	$\delta_Q{}^{18}O$	$\delta^{18}O$ other	δD	Remarks	Location
3-12-24 RB 180a	Gdr		-3.8				Cliff, 2 m from 1 m mafic dike, numerous felsic dikes at this outcrop	43°35.12' 114°58.14'
3-10-11 RB 186a	Gdr		8.4				Roadcut	43°36.68' 115°14.28'
4-10-26 RB 189	QM		8.2				Roadcut,~ 40 m from porphyry dike	43°39.13' 115°13.58'
4-9-4 RB 190	Grt		5.7				Roadcut, Dismal Swamp Pluton	43°42.4' 115°22.9'
4-9-5 RB 191	Fine Grt (M)	Q,P,Or,B,O,Z [S,Ox,O,E?,C]			8.4_{WR}		Do., minor micrographic texture	43°42.79' 115°24.62'
5-9-31 RB 193c	Gdr (M)	Q,P‡Or,B,O,Al,Z,Ap [S,O,E,C]	6.4				Roadcut, minor def, Dismal Swamp Pluton?	43°43.91' 115°25.97'
5-8-26 RB 195	Gdr (S)	Q,P‡Or,B,Z,Al,Ap [S,C,O,E,Sp]			5.3_{WR}		Roadcut, near contact with Dismal Swamp Pluton, few V, MXL	43°44.18' 115°27.65'
6-11-31 RB 205a	Gdr		7.4				Roadcut, SRZ	43°48.93' 115°12.11'
5-11-4 RB 207a	Gdr		4.8				Roadcut, MXL, SRZ near Atlanta	43°47.79' 115°9.52'
5-11-9 RB 209	Gdr (M)	Q,P,Or,B,Sp,O,Al,Ap [S,C,O,Sp,L,E,Cc]	8.8				Do., several V, pink MXL	43°46.83' 115°8.95'

T-R-S, Field#	Rock, Alt.	Mineralogy	$\delta_F{}^{18}O$	$\delta_Q{}^{18}O$	$\delta^{18}O$ other	δD	Remarks	Location
5-11-15 RB 210a	Gdr		8.2				Roadcut, MXL, Mu along joint	43°46.16' 115°8.36'
6-10-30 RB 211c	QM?				1.4_{WR}		Roadcut, Alt. rock, 10 m from > 15 m porphyry dike	43°49.81' 115°18.80'
6-8-17 RB 217	Gdr (M)	Q,P,Or,B,H,Sp,Z [S,C,O,Sp]			9.7_{WR}		Eocene rock?	43°51.47' 115°31.77'
6-8-17 RB 218	QM		8.0				Roadcut, ~ 300 m from contact with above pluton	43°51.24' 115°32.20'
6-8-20 RB 219	QM (S)	Q,P‡M,B [S,C,Ox,O,E,Cc]	0.3		5.6_{WR}		Roadcut, 25 m from 1 m mafic dike, C along joints	43°50.43' 115°32.18'
5-7-1 RB 223	QM		8.6				Roadcut, MXL, B-Mu rock	43°47.67' 115°33.55'
5-7-3 RB 226	QM (M)	Q,P,M,B,Z,Ap [S,C,O,Ox,E?]	8.8			-103_B	Roadcut, few MXL, few V, minor def.	43°48.38' 115°36.75'
6-7-32 RB 228a	QM		8.9				Roadcut, 1 m from 1 cm Q vein	43°48.83' 115°39.02'
6-6-29 RB 232	QM (M)	Q,P,M,B,Ap [S,Ox,C,O]	9.3				Roadcut, 3 m from 29/30 sec. boundary, few MXL	43°49.76' 115°47.00'
9-9-15 RB 233b	Gdr		-1.0				Roadcut, R. 21, alt. rock with C along joints, SRZ	44°7.15' 115°22.23'
9-9-12 RB 235	QM? (E)	Q,P‡*M,Z,B? [S,C,Cc,O]			0.6_{WR}	-156_B	Roadcut, R. 21, SRZ, several V, moderate def.	44°7.82' 115°19.77'

T-R-S, Field#	Rock, Alt.	Mineralogy	$\delta_F{}^{18}O$	$\delta_Q{}^{18}O$	$\delta^{18}O_{other}$	δD	Remarks	Location
9-10-5 RB 237a	QM (S)	Q,P‡*M,B,Sp,Al? [S,Ox,E,C,O]	4.3	10.1	-1.2_B	-139_B	Roadcut, R. 21 near Warm Springs bridge, (Table 4.5)	44°8.70' 115°18.18'
10-11-33 RB 239a	QM		3.1				Along trail, Sawtooth Pluton, 2 m from 5 cm Q vein	44°9.07' 115°8.77'
10-11-34 RB 240	Gdr		7.1				Cliff above trail, 100 m from mafic dike, near contact with Sawtooth Pluton	44°9.56' 115°7.65'
10-10-32 RB 241	QM (E)	Q,P*,M [S,Cc,C,O]	0.6				Roadcut, R. 21, leucocratic rock with C along joints	44°9.28' 115°17.41'
10-10-15 RB 243a	QM		5.0				Roadcut, R. 21, alt. along joints, outcrop cut by several small peg dikes	44°11.78' 115°14.97'
11-10-36 RB 245	QM		7.0				Roadcut, R. 21, MXL	44°14.15' 115°12.92'
5-3-21 RK 5	Gdr		10.0				Roadcut, near Shafer Butte, few MXL	43°45.02' 116°6.36'
2-3-12 RK 6	Gdr		9.2				Roadcut near Lucky Peak Dam; Eocene? rock with xenoliths	43°31.83' 116°3.05'
3-4-9 RK 8	QM		9.7				Roadcut, R. 21, friable rock, few MXL	43°36.97' 115°59.42'
8-8-32 RK 10	QM		7.6				Roadcut, alt. rock, B destroyed, MXL, sulfide smell	43°59.16' 115°32.20'

T-R-S, Field#	Rock, Alt.	Mineralogy	$\delta_F{}^{18}O$	$\delta_Q{}^{18}O$	$\delta^{18}O_{other}$	SD	Remarks	Location
8-8-27 RK 12a	QM				-0.4_{WR}		Roadcut, alt. rock, 20 m from 7 m rhyolite dike, 3 m from 30 cm Q vein.	44°0.23' 115°29.76'
8-8-14 RK 14	QM		8.1				Cliff, MXL	44°1.58' 115°28.11'
8-9-6 RK 15a	QM		8.8				Roadcut, 1 m from 10 cm aplite dike, MXL	44°3.19' 115°26.33'
8-9-5 RK 16	QM		3.3				Roadcut, Eocene rock?, 40 m from >3 m porphyry dike, SRZ	44°3.15' 115°24.97'
8-9-13 RK 17a	QM		0.1				Cliff, 5 m from 7 m porphyry dike, SRZ	44°2.03' 115°20.72'
8-8-20 RK 19	QM		8.9				Roadcut, MXL	44°0.56' 115°32.52'
8-8-17 RK 21a	QM		3.2				Roadcut, alt. rock with MXL, several small Q veins nearby, Banner District	44°1.67' 115°31.83'
9-7-36 RK 24	QM		8.0				Roadcut, R. 21, MXL	44°4.30' 115°34.04'
9-8-32 RK 25	QM		1.9				Roadcut, R. 21 near Kirkham Hot Springs	44°4.40' 115°32.69'
9-8-33 RK 26a	QM		3.5				Roadcut, R. 21, MXL, 8 m from 1 m aplite dike	44°4.25' 115°31.29'

T-R-S, Field#	Rock, Alt.	Mineralogy	$\delta_F{}^{18}O$	$\delta_Q{}^{18}O$	$\delta^{18}O$ other	δD	Remarks	Location
9-8-26 RK 27a	QM		8.2				Roadcut, R. 21, MXL, 40 m from 20 m aplite dike	44°5.44' 115°28.98'
9-8-24 RK 28a	QM (M)	Q,P,M,B,Al,Ap [S,C,Ox,Cc,E]	8.7	10.2	3.3_B	-122_B -95_{MU} (S?)	Roadcut, R. 21, MXL, 50 m from 10 m mafic dike (Table 4.5)	44°6.32' 115°26.98'
9-9-16 RK 29a	QM (S)	Q,P*,M,B,Al,Ap [S,C,Ox,O,E]	5.6	9.9	-1.8_B	-150_B	Roadcut, R. 21, SRZ, MXL, between and 35 m from two >15 m porphyry dikes (Table 4.5)	44°7.15' 115°23.66'
13-11-28 RK 31	Q Dio (M)	Q,P,K feld?,Px,B,H [S,C,Sp,E?,O]			6.1_{WR}		Diorite stock, along trail	44°25.52' 115°11.51'
12-12-33 RK 33a	QM		8.2				Cliff, 10 m from 1 m mafic dike	44°19.88' 115°3.77'
12-12-27 RK 34	QM?		7.6				Alt rock, Valley Creek Mine	44°20.16' 115°2.99'
10-12-15 RK 35	Grt		7.7				H Grt, Sawtooth pluton, above trail	44°11.60' 115°2.37'
10-12-22 RK 36	Grt (E)	Q,P**,M,B,H,Al [S,C,Sp,O,E]	-7.9				Sawtooth pluton, above trail, V, moderate def.	44°11.28' 115°3.24'
10-12-22 RK 37	Grt (M)	Q,P**,M*,B,Z [S,C,O]	-4.3				Sawtooth pluton, V	44°11.02' 115°3.19'
10-12-21 RK 40	Ton (M)	Q,P,M?,B,H,Px,Sp?, Al,Ap [S,Act,E,Sp,Ox]	7.9	10.0	4.6_B	-111_B	Near contact with Sawtooth pluton, above trail (Table 4.5)	44°10.73' 115°3.58'

T-R-S, Field#	Rock, Alt.	Mineralogy	$\delta_F{}^{18}O$	$\delta_Q{}^{18}O$	$\delta^{18}O$ other	δD	Remarks	Location
10-12-15 RK 41a	Grt		-3.0				Sawtooth pluton, 25 m from 5 m mafic dike, 5 m from Q vein	44°11.54' 115°2.83'
6-14-6 RK 42a	QM		8.5				Cliff, MXL, 10 m from 2 m aplite dike	43°53.02' 114°51.81'
6-13-24 RK 43a	QM		8.4				Pilgrim Mine	43°50.91' 114°53.38'
6-13-13 RK 44a	QM		8.0				Cliff, MXL, 5 m from pyritiferous rock	43°51.72' 114°52.59'
8-14-3 RK 45	QM		9.3				Along road, Fisher Creek, MXL	44°3.13' 114°48.73'
8-14-2 RK 46	QM		9.3				Cliff, Do	44°3.32' 114°47.46'
9-13-20 RK 52	Grt		7.4				Sawtooth batholith, near contact	44°5.70' 114°58.16'
9-12-36 RK 53a	Grt (M)	Q,P⁑M*,Or,B,O,Sp,Ap, Al,Z [S,C,O,Sp]	3.7	8.6			Sawtooth batholith, along trail, miarolitic rock	44°4.30' 115°0.38'
9-12-36 RK 54	Grt (S)	Q,P,Or**⁑B,O,Al,Z [S,C,O,Sp,E]	1.3				Do, with few V	44°4.05' 115°0.84'
8-13-35 RK 55	QM		-2.3				Cliff above trail, alt. rock near contact with Sawtooth batholith	43°58.61' 114°54.32'
10-13-25 RK 56	QM (S)	Q,P*,M,B,O [S,C,O,E,Cc]	7.8				Cliff, near U.S. 93., alt. rock, SRZ	44°9.69' 114°52.78'

T-R-S, Field#	Rock, Alt.	Mineralogy	$\delta_F{}^{18}O$	$\delta_Q{}^{18}O$	$\delta^{18}O$ other	δD	Remarks	Location
13-12-5 RK 58	Gdr		-2.6				Roadcut, alt. rock, Casto L.Z., cavities with drusy quartz	44°29.36' 115°5.23'
14-11-12 RK 60a	Gdr		0.0				Roadcut, alt. rock, Casto L.Z., 1 m from >15 m dike	44°33.68' 115°4.13'
14-11-21 RK 62a	Gdr		0.6				Cliff, vicinity of Seafoam Mine	44°32.56' 115°7.34'
13-12-21 RK 63b	Gdr		8.5			-160_B	Cliff	44°26.56' 115°4.22'
12-10-21 RK 69a	Gdr		6.2				Roadcut	44°21.92' 115°16.12'
13-10-32 RK 71a	QM		8.5				Roadcut, MXL, 7 m from >3 m mafic dike	44°24.96' 115°17.11'
13-9-21 RK 72	Gdr		8.9				Roadcut, Bear Valley Mtn.	44°26.65' 115°23.74'
13-9-13 RK 74	Gdr		9.5				Roadcut, pink MXL	44°27.58' 115°19.05'
13-10-6 RK 75	QM?		-0.5				Roadcut, alt. rock, Casto L.Z.	44°29.92' 115°18.76'
14-10-19 RK 76a	Gdr		6.5				Cliff near Dagger Falls, Casto L.Z.	44°31.68' 115°17.08'
8-4-35 RK 77a	QM		9.4				Roadcut, near contact with Boise Basin intrusive, MXL	43°59.13' 115°56.65'

T-R-S, Field#	Rock, Alt.	Mineralogy	$\delta_F{}^{18}O$	$\delta_Q{}^{18}O$	$\delta^{18}O$ other	δD	Remarks	Location
6-3-11 RK 83	QM		9.7				Roadcut, Warm Lake Pluton, MXL	43°52.68' 116°4.32'
6-3-8 RK 84	Gdr		8.7				Roadcut, MXL	43°52.07' 116°8.01'
2-5-8 RK 87	QM		7.9				Roadcut	43°31.54' 115°52.52'
2-5-1 RK 88	QM		8.9				Roadcut, MXL	43°32.15' 115°48.85'
5-4-10 RJ 2	QM		9.2				Roadcut along Grimes Cr., MXL	43°47.08' 115°57.90'
7-11-2 RJ 5b	Gdr (M)	Q,P,Or,B,Sp,O,Al [S,C,O,E,Sp]	3.9				Cliff along trail, SRZ, few km from Sawtooth batholith, few small peg dikes	43°58.33' 115°7.72'
7-11-4 RJ 7a	QM		0.4				Along trail, SRZ, outcrop cut by several small peg dikes	43°58.33' 115°9.50'
7-11-6 RJ 8a	QM (M)	Q,P,M,B,O,Al,Ap [S,C,Ox,Sp,O,E?]	5.6				Do., 1 m from 6 cm aplite dike	43°58.62' 115°12.05'
7-10-11 RJ 9a	Grt (E)	Q,P,M* [S,Cc,C]	-0.6				Along trail, SRZ, several V, def.	43°57.86' 115°13.88'
7-10-22 RJ 10a	QM				2.5_{WR}		Along trail, SRZ, alt. rock 25 m from 10 m columnar jointed dike	43°56.05' 115°15.17'
7-10-16 RJ 12a	QM		8.6				Cliff near Johnson Cr. camp, MXL	43°56.47' 115°17.01'

T-R-S, Field#	Rock, Alt.	Mineralogy	$\delta_F{}^{18}O$	$\delta_Q{}^{18}O$	$\delta^{18}O_{other}$	SD	Remarks	Location
7-10-16 RJ 12b	QM		-2.5				Alt. shear zone, 3 m from RJ 12a	Do.
8-10-35 RJ 13a	QM (M)	Q,P*,Or,B,O,Z [S,Ox,O,E,Sp]	2.8				Cliff along trail, Eocene rock?, SRZ,	43°59.27' 115°14.27'
8-10-29 RJ 14a	QM				-1.2_{WR}		Cliff, SRZ, leucocratic QM, 8 m from 2 m dike	43°59.93' 115°17.38'
8-10-31 RJ 15	QM (S)	Q,P*,M,B,O,Z? [S,C,O,Ox,E]	-1.9				Roadcut, SRZ, many V, MXL	43°59.11' 115°19.09'
8-9-24 RJ 17a	QM (S)	Q,P*,M,B,Ap [S,C,O,Cc]	-0.4				Roadcut, SRZ, 15 m from intrusive leucocratic rock	44°0.87' 115°19.98'
10-8-10 RJ 21	QM		6.9				Roadcut	43°13.00' 115°28.72'
12-10-35 RJ 24a	Grt	Q,P,Or*,B,Al,Z [S,C,O,E?Sp?]	7.2				Cliff near R. 21, Eocene rock, 5 m from 2 m mafic dike	44°19.99' 115°13.52'
11-10-17 RJ 26a	Grt		2.8				Along trail, Eocene Grt, 5 m from 2 m mafic dike	44°17.07' 115°17.30'
12-12-32 RJ 27a	QM		7.3				Roadcut, SRZ, alt. rock, 5 m from 15 cm Q vein, Eocene?	44°19.72' 115°5.45'
12-12-30 RJ 28a	Gdr		8.7				Roadcut, few MXL	44°20.23' 115°5.93'
11-13-30 RJ 30a	QM		-3.5				Roadcut, alt. rock, SRZ	44°15.50' 114°59.72'

T-R-S, Field#	Rock, Alt.	Mineralogy	$\delta_F{}^{18}O$	$\delta_Q{}^{18}O$	$\delta^{18}O$ other	SD	Remarks	Location
11-13-18 RJ 31a	Gdr		6.8				Roadcut, SRZ, MXL	44°16.83' 114°58.68'
12-13-31 RJ 32	Gdr		9.8				Roadcut, few MXL	44°19.38' 114°59.06'
10-13-4 RJ 33a	QM		5.8				Cliff, Sawtooth Valley, SRZ, alt. rock, MXL	44°13.25' 114°56.41'
10-13-4 RJ 33b	QM		1.7				Do.	44°13.22' 114°56.36'
16-11-17 RSR 2	Grd		7.9				Along Salmon R., Casto L.Z., (RSR samples collected by J. Given)	44°43.3' 115°8.6'
17-14-5 RSR 3	Grt Porph (S)	Q,P*,Or*,B,Al,O [S,C,O]	-3.8				Tertiary porphyry, Hospital Hot Springs, Salmon R.	44°50.2' 114°47.3'
18-14-21 RSR 4	Grt (S)	Q,P*,Or*,B,O,Z [S,C,O,E?]	-1.7	8.4			Casto pluton, several V	44°52.8' 114°44.7'
18-14-10 RSR 5	Gph Porph (S)	Q,P*,Or*,B [S?,C,O,Cc,E?]	-2.4				Tertiary granophyric porphyry, along Salmon R., several V	44°54.9' 114°44.0'
20-14-15 RSR 6	QM (M)	Q,P*,M*,B,Sp [S,C,O,E,Ox,Sp,L]	0.9				Casto L.Z., along Salmon R. near Veil Falls	45°5.55' 114°43.7'

T-R-S, Field#	Rock, Alt.	Mineralogy	$\delta_F{}^{18}O$	$\delta_Q{}^{18}O$	$\delta^{18}O_{other}$	SD	Remarks	Location
6-1 RM 4a	Gdr		6.1				Cliff by defunct Gem State Mill, Gold Fork Gdr?	43°51.39' 116°19.42'
8-5-5 RC 14	QM		9.1				Roadcut, MXL	44°3.2' 115°53.1'
8-5-26 RC 20a	Q Dio				-4.1_{WR}		Roadcut	44°0.5' 115°50.1'
7-13-26 RC 46d	Gdr		6.0				Cliff, 15 m from large porphyry dike, SRZ, pink MXL	43°54.4' 114°54.5'
9-6-15 RB 139a	QM		5.3				Roadcut, alt. rock 3 m from 25 m porphyry dike	44°6.7' 115°44.0'
6-11-30 RB 204c	QM		6.6				Roadcut, C on joints, SRZ	43°49.8' 115°11.6'
4-2-14 RK 1	Gdr		10.5				Roadcut, MXL, Gold Fork Gdr.	43°41.3' 116°10.8'
7-4-32 RK 81	QM		9.7				Roadcut, MXL, Warm Lake Pluton	43°53.8' 116°0.95'

Table 4.2

$\delta^{18}O$ and δD Determinations of Granitic Rocks from the Atlanta Lobe: Data of Taylor and Magaritz (1976, 1978). Abbreviations are identical to those in Table 4.1. Samples also analyzed for K-Ar are noted as being listed in Table 4.5.

(1) T-R-S Field #	(2) Rock, Alt.	(3) Mineralogy	$\delta^{18}O$ F	(4) $\delta^{18}O$ Q	$\delta^{18}O$ other	δD	(5) Remarks
12-12-32 I 6	QM		0.7	9.8		-153_B	altered rock
11-10-11 I 7	QM (M)	Q,P,M,B,D,Mu? [S,C,E,O,Ox]	5.0	11.1	2.6_B	-168_B -156_{Mu}	Mu on joint, v, (Table 4.5)
10-10-2 I 9	Gdr (M)	Q,P,Or,B,Sp,Al,O [S,C,E,O,Ox,Sp?)	7.6	9.0	3.5_B	-135_B	MXL, moderate def (Table 4.5)
9-8-32 I 14	QM (M)	Q,P,M,B,Al,O [S,C,O,E]	8.1	10.4	3.2_B	-139_B	few MXL, Mu on joint, (Table 4.5)
8-7-3 I 16	QM		8.3	11.0		-138_B	MXL, minor pyrite
7-7-19 I 18	QM					-149_B	few MXL
6-6-20 I 19	Gdr		8.9	10.6		-105_B	MXL
3-4-16 I 22	Gdr (M)	Q,P,Or,B,Ap,O [S,C,O,Sp,E]	9.5	11.7	5.4_B	-115_B	Eocene? (Table 4.5)
7-2-14 I 23	Gdr					-70_B	
9-3-28 I 24a	Gdr (W)	Q,P,M,Or,B,Sp,Al O,Ap [S,C,Sp]	9.5	11.7	5.7_B	-69_B	(Table 4.5)
9-3-22 I 25	Gdr		8.8	10.4		-76_B	
9-3-22 I 31	Q Dio		8.7			-69_B	Slightly foliated
21-1-35 I 32	Q Dio (W)	Q,P,B,Px,H,O, Ap [E,C]	7.8	10.6	5.0_B	-66_B	Slightly foliated (Table 4.5)
19-4-10 I 202	Ton		10.7			-67_B	Slightly foliated Donnelly pluton
18-4-8 I 205	Ton (W)	Q,P,Or,B,D,Ap, Z [S,C,O,Cc,Sp]	10.3	12.1	6.6_B	-66_B -48_{Mu}	Mu on joint, (Table 4.5), probably Donnelly pluton
18-4-6 I 206	Ton					-74_B	

T-R-S, Field #	Rock, Alt.	Mineralogy	$\delta^{18}O$ F	$\delta^{18}O$ Q	$\delta^{18}O$ other	δD	Remarks
14-4-27 I 207	Gdr		10.3				Gold Fork Gdr, MXL
15-5-32 I 208	Gdr					-73_B	Do
15-6-18 I 210	QM (M)	Q,P,M,B,Ap,O [S,C,E,O]	10.2	12.1	5.9_B	-73_B -52_{Mu}	Warm Lake Pluton, MXL, (Table 4.5)
15-7-17 I 214						-93_B	Warm Lake Pluton, MXL
15-7-15 I 215	QM		10.0	11.7		-74_B	Warm Lake Pluton few MXL, Mu on joint
14-7-23 I 216	QM		9.3	11.4		-95_B	MXL
13-7-35 I 217	Gdr		10.0	11.2		-97_B	MXL
12-8-5 I 220	QM		8.9	9.6		-72_B	few MXL
11-5-19 I 222	QM		8.8	11.1		-87_B	
11-5-19 I 223	Gdr		9.2			-85_B	MXL
11-14-23 I 224	QM (M)	Q,P,M,B,H,Sp,O, AP [S,C,O,E,L]	8.9	11.2		-142_B	MXL
11-14-21 I 225	Gdr		8.8	10.8		-116_B	few MXL
11-14-20 I 226	QM (M)	Q,P,Or,B,H,Sp,O, Ap,Al [S,C,O,E,Cc,L]	8.6	10.9		-121_B	relatively mafic rock, MXL
11-13-36 I 227A	QM (S)	Q,P,M,B,H,Sp,O, Ap,Al [S,C,O,Cc,L]	6.3	10.8	0.8_B	-166_B	several, light pink MXL, (Table 4.5)
11-13-36 I 227B	QM				0.8_{WR}		

T-R-S, Field #	Rock, Alt.	Mineralogy	$\delta^{18}O_F$	$\delta^{18}O_Q$	$\delta^{18}O$ other	δD	Remarks
10-13-3 I 228	QM		-6.8	7.9		-152_B	
10-13-3 I 228A	QM (S)	Q,P$\frac{1}{2}$M,B,O,Ap [S,C,O,Cc,E]	1.1	10.5			altered rock, many v
12-12-32 I 230	QM		5.1	10.5			altered rock
12-10-24 I 232	QM		8.6	10.6		-158_B	MXL
11-10-11 I 233	Gdr		7.4	10.9			few MXL
9-9-15 I 234	QM?		-6.7	6.3		-158_B	alt rock, prob. Eocene, C on joints
4-4-2 I 235	QM					-110_B	MXL
4-6-22 I 236	Grt Porph (S)	Q,P$\frac{1}{2}$Or,B,O [S,C,O,E,Sp,Cc]	5.0	9.8			Twin Springs Pluton
4-6-22 I 237	Grt		0.1	8.2		-145_B	Twin Springs Pluton
4-6-29 I 239	QM		0.8	9.8		-142_B	alt. rock
3-5-9 I 241	Gdr		9.6	11.2		-148_B	Eocene?
3-4-11 I 242	Gdr		6.0	11.5		-123	Eocene?
8-13-27 YAG-1023	Grt		5.6	9.0	3.5_B 7.0_{WR}	-163_B	Sawtooth batholith; Table 4.6
YAG-1033	QM		6.9	9.2	0.5_B 6.7_{WR}	-176	Crags Pluton, Table 4.6
YAG-1034	QM		8.1	9.4	4.3_B 8.9_{WR}	-120	Do; Table 4.6

Table 4.3 $\delta^{18}O$ Determinations of Dike Rocks from the Idaho Batholith

Field #	T-R-S	Rock	Phenocrysts	$\delta^{18}O_{WR}$ Dike	$\delta^{18}O_{feld}$ in Host Rock
RH 43c	6-9-35	Diabase		4.7	3.5
85a	3-14-29	Rhy Porph	Q,P,H	-0.9	-0.8
93a	3-12-17	And Porph	P,B,H	7.8	-
113b	5-8-17	Lamp		-3.1	-3.7
123b	4-6-22	Rhy Porph	Q,F,B	-6.2	8.4
RC 7b	9-6-35	Rhy Porph	Q,F,B	1.8	1.3
8a	9-6-34	Rhy Porph	Q,F,B	1.6	1.1
9c	9-6-34	Lamp		-5.9	-
46c	7-13-26	Rhy Porph	Q,F,H?	-1.6	6.0
RB 89c	4-7-23	Rhy Porph	Q,F	6.3	9.0
89d	4-7-23	QMP?	Q,P,Or,B,H?	7.8	9.0
177	5-13-34	QMP	Q,P,Or,H	4.6	-
178f	4-13-22	QMP	P,B,Q?	2.2	6.7
RK 17c	8-9-13	QMP	P,H,B?	-6.0	0.1
17d	8-9-13	QMP	Q,F,B	-4.5	0.1
29b	9-9-16	QMP	P,H,B?	0.1_{feld}	5.6
41c	10-12-15	And	F,H	-4.0	-3.0
68	5-4-35	Rhy	-	5.4	-
78	7-4-2	QMP	P,H,B	1.4	-
I 229	11-12-14	And Porph?	F,H	-0.5	-
231	12-10-13	QMP	F,H	3.1	-

Table 4.4 $\delta^{18}O$ Analyses of Vein Quartz from the Idaho Batholith

Field #	T-R-S	$\delta^{18}O$ Vein	$\delta^{18}O$ Host Rock
RK 12b	8-8-27	0.7_Q	0.4_{WR}
RK 20e	8-8-20	4.1_Q	-
RK 41b	10-12-15	-6.2_Q	-3.0_{feld}
RK 43d	6-13-24	14.6_Q	8.4_{feld}

Table 4.5 K-Ar Age Determinations of the Idaho Batholith: This Study

Field #	T-R-S	Age m.y.	% Rad	$\frac{^{40}Ar^*}{g} \times 10^{10}$	K_2O%	δD_{bio}	$\delta^{18}O_{bio}$	elev	LAT	LONG
RB 45c	3-7-33	45.0	60.2	5.186	7.90	-125	5.1	4640	43°33.53'	115°37.23'
68	5-4-35	57.5	54.6	6.200	7.37	- 89	4.4	3320	43°43.55'	115°57.00'
70	7-6-25	60.4	68.3	5.438	6.145	-133	3.3	5120	43°54.56'	115°41.82'
89f	14-7-23	68.5	57.4	7.052	7.015	-120	3.8	6800	44°32.6'	115°33.9'
134	11-7-17	65.3	71.8	8.459	8.83	-101	5.1	5200	44°17.55'	115°38.45'
148	11-5-10	68.6	71.5	9.270	9.215	- 88	6.1	5020	44°18.2'	115°50.5'
237a	9-10-5	42.1	13.6	1.145	1.865	-139	-1.2	4640	44°8.70'	115°18.18'
RC 3a	9-7-29	62.4	50.0	7.367	8.06	-126	4.2	3720	44°4.76'	115°39.50'
13	8-5-10	55.1	35.3	6.699	8.322	- 95	4.5	3200	44°2.69'	115°51.01'
18	8-4-22	68.0	70.4	8.838	8.863	- 87	6.1	3820	44°0.82'	115°57.80'
39e	10-11-33	61.5	63.4	7.289	8.095	-160	1.7	5400	44°9.65'	115°10.5'
RH 12*	3-8-12	44.2	41.4	5.389	8.368	-108	5.4	8440	43°36.74'	115°26.55'
14a	4-9-15	40.5	37.0	5.393	9.14	-161	-0.2	8120	43°41.21'	115°22.80'
29	5-10-23	63.2	29.0	6.356	6.86	-130	3.1	7640	43°45.5'	115°14.1'
43a	6-9-35	60.1	62.6	4.330	4.92	-132	-0.1	4440	43°49.15'	115°21.20'
57	7-8-9	65.6	65.2	8.336	8.665	-104	4.6	5400	43°57.5'	115°31.7'
85d*	3-14-29	46.1	41.5	4.580	6.81	-166	-2.3	5760	43°33.68'	114°49.52'
95	3-11-9	53.4	61.3	5.862	7.515	-133	3.6	4800	43°36.60'	115°8.93'
99	3-10-3	53.9	56.8	3.653	4.635	-147	1.3	4680	43°37.36'	115°15.34'
115	5-7-26	37.2	24.5	3.829	7.08	-173	2.4	3680	43°44.66'	115°34.88'
120*	4-7-18	38.0	26.3	1.954	3.535	-150	0.2	3440	43°41.29'	115°40.40'
RK 28a	9-8-24	63.4	59.8	6.769	7.29	-122	3.3	4240	44°6.32'	115°26.98'
29a	9-9-16	58.0	37.1	2.821	3.325	-150	-1.8	4400	44°7.15'	115°23.66'
40	10-12-21	44.9	59.3	5.771	8.81	-111	4.6	8760	44°10.73'	115°3.58'
I 7	11-10-11	62.6	73.6	7.962	8.685	-168	2.6	6900	44°21'	115°14'
9	10-10-2	58.6	40.9	6.314	7.365	-135	3.5	5800	44°14'	115°13'
14a	9-8-32	62.0	61.8	5.778	6.363	-139	3.2	4000	44°4.5'	115°32.5'
22*	3-4-16	38.7	75.5	4.864	8.646	-114	5.4		43°36'	115°59'
24a	9-3-28	71.8	42.0	9.500	9.005	- 69	5.7	2820	44°5'	116°7'
32	21-1-35	92.9	70.0	12.86	9.369	-66	5.0	3800	44°9'	116°17'
205	18-4-8	74.4	66.7	9.855	9.009	-66	6.6	5400	44°56'	115°57'
210	15-6-18	69.4	41.9	9.018	8.85	-73	5.9	6300	44°38.2'	115°46.8'
227	11-13-36	72.5	55.5	5.784	5.43	-166	0.8	6200	44°14.8'	114°53.1'

Table 4.6 K-Ar Age Determinations of the Idaho Batholith: Previous Studies

Field #	T-R-S	Rock	Age	$\%K_2O$	Elev[1]	LAT	LONG	Source
				MESOZOIC ROCKS				
L-957	11-3-23	Gdr	73.1	8.72	4800	44°16.08'	116°4.42'	McDowell and Kulp, 1969
L-1028	18-3-1	Ton	77.0	8.57	5100	44°55.67'	116°1.5'	Do
R-130		QM/Gdr	95.5	8.85	8700	44°23.5'	114°22.0'	Armstrong, 1975a
SWH-45-72	11-16-2	QM	88.4	8.94	6900	44°18.5'	114°32.5'	Do
YU-876	19-3-23	Ton	65.2	8.97	5000	44°58.5'	116°3.3'	Do
YU-877		QD Gneiss	77.0	6.71	7100	45°0.00'	116°7.67'	Do
YU-925	13-9-20	Gdr/QM	69.6	8.66	7400	44°27.0'	115°23.8'	Do
YU-926	13-9-29	Gdr/QM	71.2	8.77	6700	44°26.2'	115°23.9'	Do
YU-1040	11-10-21	Gdr	95	7.39	6200	44°15.8'	114°42.5'	Do
YU-1041	11-15-20	Gdr	79	8.62	6050	44°16.00'	114°43.42'	Do
YU-1042	11-15-19	Gdr	82	8.53	6200	44°16.2'	114°14.7'	Do
YU-1043	11-14-29	Gdr	79	8.46	6200	44°15.58'	114°50.2'	Do
YU-871	13-11-33	Gdr	62.6	9.29	6700	44°24.7'	115°11.2'	Do
YU-WT-160	14-2-2	QD	76	8.23	6700	44°34.33'	116°10.52'	Do
YU-WT-258	14-3-25	Gdr	75	8.92	4800	44°31.52'	116°3.00'	Do
YU-WT-133	15-2-6	QD	82.0	8.68	5300	44°40.38'	116°8.13'	Do
YU-WT-151	16-1-1	QD	84.0	9.24	6800	44°44.9'	116°16.37'	Do
YU-WT-242	6-1-14	Gdr	64	8.38	4400	43°51.18'	116°18.23'	Do
YU-WT-236	5-2-19	QM	69	9.27	3100	43°45.67'	116°16.23'	Do
L-1029	15-10-20	Gdr	43.1	8.05	5200	43°10.5'	115°17'	McDowell and Kulp, 1969
L-1123	5-9-7	Gdr	43.7	7.58	4200	43°47.58'	115°25.25'	Do
HJO-6-65	8-6-1	Gdr	44.8	7.80	3960	44°3.8'	115°41.5'	Percious et al, 1967
A-230	2-18-31	QM	81.7	6.91		43°27.6'	114°21.5'	Berry et al, 1976
H-198		-	76.7	8.57	6200	43°31.8'	114°31.8'	Hall, unpub.
				EOCENE PLUTONS				
YU-872	13-11-33	Dio[2]	45.9	7.68		44°25.5'	115°11.5'	Armstrong, 1974, 1975a
YU-1033		QM [3]	47.5	6.93		45°3.92'	114°33.00'	Do
YU-1034		QM [3]	44.2	7.05		45°3.92'	114°33.50'	Do
YU-1035		Aplite[3]	47.4	6.84		45°3.92'	114°33.50'	Do
YU-802	7-13-6	Grt[4]	44.4	9.85		43°57.83'	114°58.42'	Do
YU-1023	8-13-27	Grt[4]	44.1	6.77		43°59.25'	114°55.17'	Do
YU-1022	8-13-34	Grt[4]	43.7	5.37		43°59.00'	114°55.75'	Do
YU-FWC 6-67	18-14-3	Grt[5]	42.7	3.91		44°55.25'	114°43.83'	Do
HJO-1-65	9-6-34	Mz Porph[6]	48.0	8.63		44°4.25	115°44.00'	Percious et al, 1967
HJO-2-65	9-6-35	Mz Porph[6]	44.0	8.64		44°4.17	115°42.92	Do

1 Elevation determined by plotting coordinates on U.S.G.S. 7.5' and 15' topographic maps
2 Cape Horn Quartz Diorite
3 Crags Pluton
4 Sawtooth batholith
5 Casto Pluton
6 Stocks near Boise Basin

CHAPTER 5

OXYGEN AND HYDROGEN ISOTOPE RELATIONS IN THE IDAHO BATHOLITH

5.1 Alteration Effects vs. Primary Magmatic Values

5.1.1 $^{18}O/^{16}O$ Variations

This section discusses the first order $^{18}O/^{16}O$ variations in the granitic rocks of the Idaho batholith, and attempts to distinguish between isotopic signatures due to primary magmatic effects and those due to hydrothermal alteration. These relationships form the basis for mapping the "fossil" hydrothermal systems. Many such $^{18}O/^{16}O$ maps will be described in Chapter 6.

Figure 5.1 shows two histograms of $\delta^{18}O$ values, one for quartz and one for feldspar, from plutonic igneous rocks in the Atlanta lobe of the batholith. The data points in the figure represent measurements on individual rock samples and are not weighted for areal significance.

The quartz $\delta^{18}O$ values vary from 5.3 to 12.1, have a mean of 10.2, and a standard deviation of 1.3. The analyses nearly conform to a gaussian distribution but are slightly skewed toward low values. This distribution is quite narrow, considering that the measurements represent samples covering an area of about 25,000 km^2. Most of the quartz $\delta^{18}O$ values are similar to, or slightly higher than, those of average granitic rocks elsewhere in the world (Taylor, 1968); therefore most of them are believed to be close to the original primary igneous values. If all of these quartz $\delta^{18}O$ values were "primary" (which is not true; several have undergone some ^{18}O depletion) the $\delta^{18}O$ values of the original whole-rock samples would have been about 1 to 2 permil lower than the $\delta^{18}O$ of the quartz. This suggests that some of the original whole-rock $\delta^{18}O$ values

Figure 5.1 Histograms illustrating the distribution of $\delta^{18}O$ measurements of quartz and feldspar from granitic rocks of the Atlanta lobe of the Idaho batholith. The strongly skewed feldspar $\delta^{18}O$ distribution is due to meteoric-hydrothermal alteration effects.

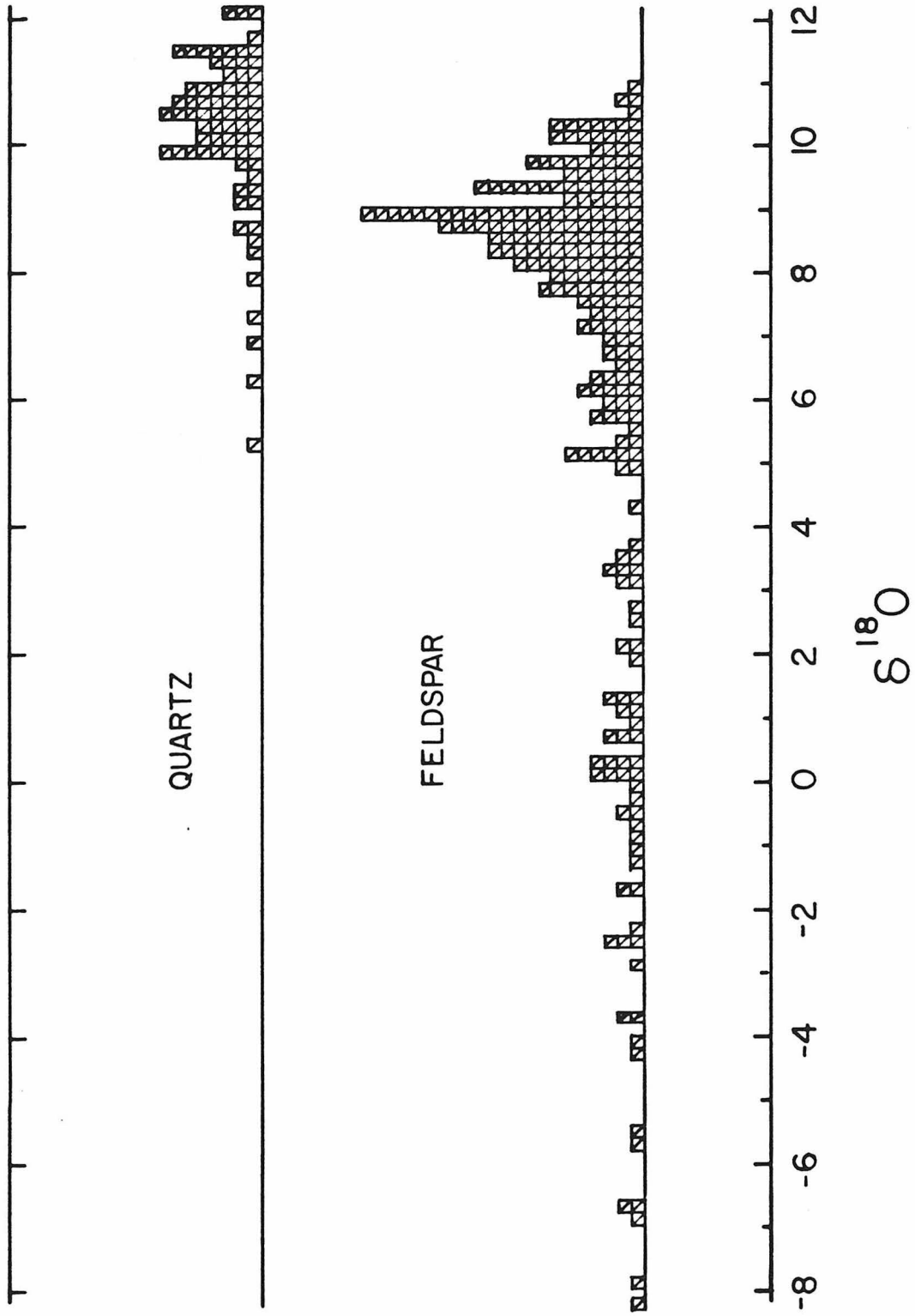
QUARTZ
FELDSPAR
-8
-6
-4
-2
0
2
4
6
8
10
12
$\delta^{18}O$

of the granitic rocks in the Idaho batholith were as high as +11, and many were higher than +10. These relatively high primary $\delta^{18}O$ values are consistent with the batholith magmas having been derived from, or having exchanged with, moderately high - ^{18}O metasedimentary or metavolcanic rocks at depth.

The other histogram in Fig. 5.1 shows the $\delta^{18}O$ values of feldspars from the granitic plutons of the batholith, as well as a few whole-rock measurements, which typically will crudely approximate the feldspar $\delta^{18}O$ value (e.g. Taylor, 1968). The feldspar $\delta^{18}O$ values vary between -8.2 and + 10.7, have a mean of about + 6.0, a standard deviation of 4.0, and are strongly skewed toward low values, such that the mean is significantly lower than the most commonly observed value of +8.9. The $\delta^{18}O$ distribution for feldspar is thus dramatically different than that for quartz, even though analyses of both minerals are in most cases from exactly the same rock samples.

It is known from a variety of previous studies (Taylor, 1967; Bottinga and Javoy, 1975; see Sec. 1.2.3) that the "normal" oxygen isotopic fractionation (Δ-value = $\delta^{18}O_{qtz} - \delta^{18}O_{feld}$) between quartz and alkali feldspar in plutonic granitic rocks is about 0.8 - 1.5, and between quartz and plagioclase is 1.0 - 2.5. These are thought to be close to the actual equilibrium values at temperatures slightly below the solidus of the magmas. Comparison of these "normal" Δ -values in plutonic igneous rocks with the histograms in Figure 5.1 shows that most rocks in the Idaho batholith are similar to ordinary primary magmatic granitoids; that is, they display small (<2 permil) quartz-feldspar Δ-values which reflect their high temperature origin. However, the rocks with low $\delta^{18}O$ feldspar (<8 permil) are all characterized by abnormally large Δ_{QF} - values, in some cases

exceeding 14 permil. If these large fractionations were to be interpreted as equilibrium features they would require formation of the rock, or subsequent recrystallization, at extremely low temperatures (down to 20°C or lower, see Sec. 1.2.3). However, the $\delta^{18}O$ of quartz in these "abnormal" rocks is usually similar to, or only slightly lower than, that of the normal rocks. Note that simple closed system reequilibration of a granitic rock under subsolidus conditions would produce a significant ^{18}O enrichment in the quartz; in fact the quartz would show a greater permil ^{18}O shift than the corresponding ^{18}O depletion in coexisting feldspar because of the lower modal abundance of quartz (20-30%) compared to feldspar (60-65%).

The above considerations strongly suggest that : (1) most of the Idaho batholith rocks originally had relatively similar initial whole-rock $\delta^{18}O$ values; (2) after formation, the ^{18}O contents of many of the feldspars (hence many of the whole-rock values as well) were markedly lowered; (3) the quartz $\delta^{18}O$ values were either preserved or only slightly lowered; and (4) none of the quartz $\delta^{18}O$ values appear to have been increased during subsolidus cooling, as would be required if closed-system ^{18}O exchange were an important process. These conclusions imply that the rocks with large Δ-values must all have interacted with an external ^{18}O reservoir of oxygen of some type.

A mechanism which is consistent with the above observations is that the "abnormal" granitic rocks were hydrothermally altered at moderate temperatures with low-^{18}O aqueous fluids, sometime after their formation. Such ^{18}O lowering has previously been demonstrated to be a common phenomenon in granitic batholiths (Magaritz and Taylor, 1976 a,b; Taylor and Magaritz,

1976, 1978; Taylor and Silver, 1978) and also in volcanic piles in the vicinity of epizonal stocks (Taylor, 1968, 1971, 1974a; Taylor and Forester, 1971, 1979; O'Neil et al, 1973). The marked ^{18}O depletions in plutonic feldspars relative to the nearly constant ^{18}O content of quartz reflects the much slower rate of isotopic equilibration between quartz and H_2O, consistent with experimental (O'Neil and Clayton, 1964; O'Neil and Taylor, 1967) and natural (Clayton et al, 1968; Taylor and Forester, 1971) observations.

Considerable insight into the nature of the hydrothermal alteration process is provided by a more detailed examination of the differing responses of various minerals to the presence of hydrothermal fluid. Together with plagioclase-pyroxene effects in gabbros (Taylor and Forester, 1979; Gregory and Taylor, 1981), quartz-feldspar effects in granitic rocks are to date the best studied and most clear-cut examples of differential ^{18}O exchange behavior in coexisting mineral systems. However, similar oxygen isotope behavior can be observed in quartz-biotite and feldspar-biotite mineral pairs. The following sections will discuss this type of behavior in more detail, will contrast the ^{18}O exchange effects with deuterium exchange effects, and will also discuss relative deuterium exchange rates in biotite and muscovite.

The differential quartz-feldspar ^{18}O exchange systematics discovered in the Idaho batholith provide the most complete and regular patterns yet found for this mineral pair anywhere in the world. Figure 5.2 compares the $\delta^{18}O$ values of coexisting quartz and feldspar in the granitic rocks of the Atlanta lobe. The tight cluster of points near the 45° line (termed the "primary cluster") represents rocks with quartz-feldspar fractionations

Figure 5.2 $\delta^{18}O$ relations of coexisting quartz and feldspar in granitic rocks of the Atlanta lobe. Rocks which show little or no evidence of hydrothermal alteration plot in the "primary cluster" and have quartz-feldspar fractionations of about 2 permil (the Δ_{QF}= 2 line). Hydrothermally altered rocks show large nonequilibrium quartz-feldspar fractionations, and plot below the primary clusters. Data from Tables 4.1 and 4.2.

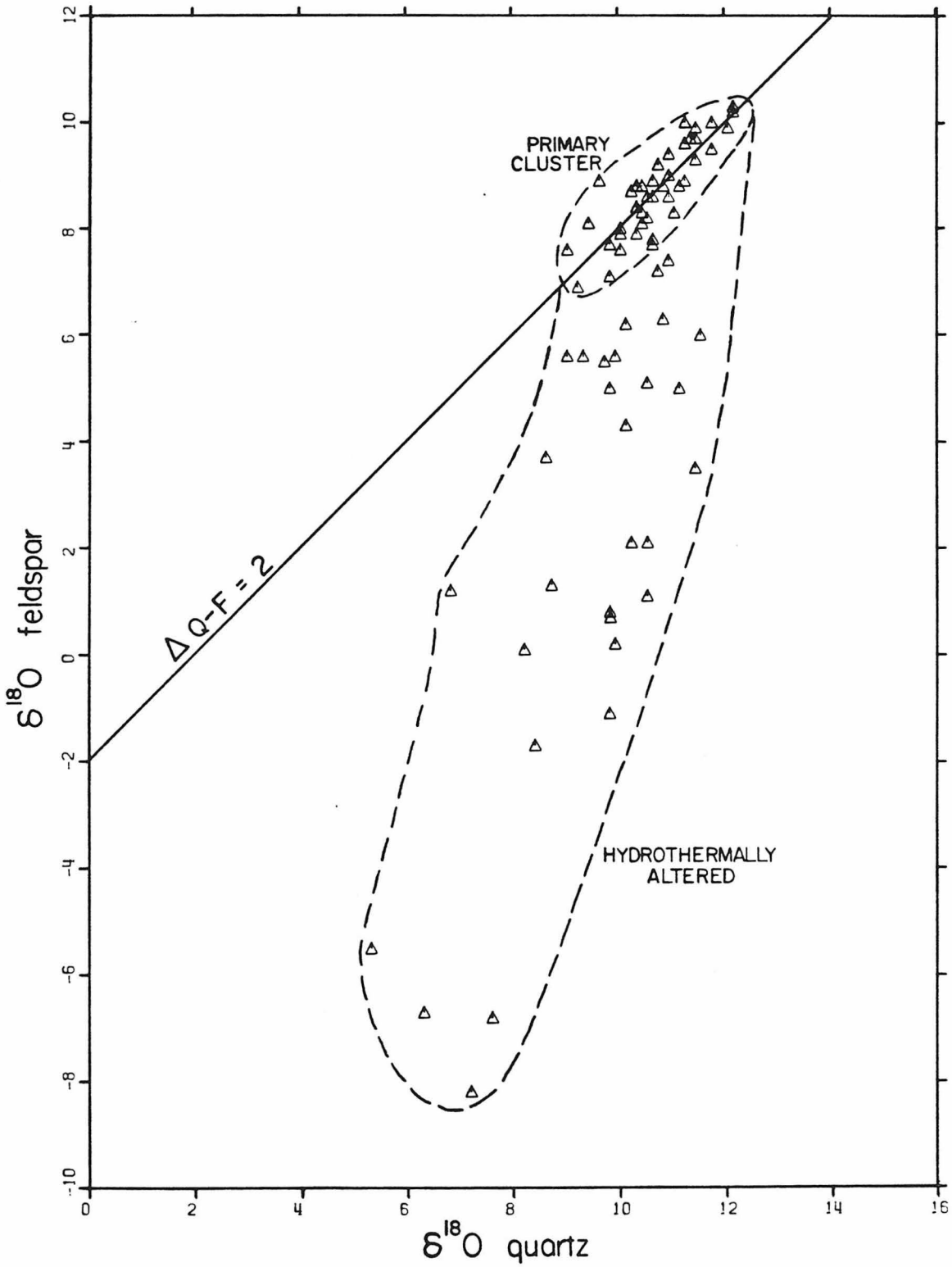
PRIMARY
CLUSTER
HYDROTHERMALLY
ALTERED
ΔQ-F=2
δ18O feldspar
δ18O quartz
12
10
8
6
4
2
0
-2
-4
-6
-8
-10
0
2
4
6
8
10
12
14
16

of about 2 permil; hence, these are essentially "normal" igneous rocks in terms of the $\Delta^{18}O_{Q-F}$ relationships. The total $\delta^{18}O$ variation of quartz and feldspar along this line is about 3 permil, and probably closely represents the primary $\delta^{18}O$ variation within the batholith. Inasmuch as quartz and feldspar together constitute more than 90% of most of these rocks, the primary whole-rock $\delta^{18}O$ values of the samples can be fairly accurately calculated. Thus the whole-rock $\delta^{18}O$ values are constrained to range from about +8.0 to +11.0, with the highest values occurring in the west-central portion of the Atlanta lobe.

The points lying below the "primary cluster" on Fig. 5.2 all have large quartz-feldspar fractionations clearly indicative of hydrothermal alteration. The slope of the dashed envelope that encompasses the altered samples suggests that the feldspar exchange rate is about 4 times faster than that of quartz; a more elaborate calculation is given in Criss et al (in prep). Thus, despite its relative inertness, it is clear that in the hydrothermally altered rocks the quartz has undergone <u>some</u> ^{18}O depletion. Note that all of the rocks with low $\delta^{18}O$ quartz values ($< +9$) also have extremely large (> 6) quartz-feldspar fractionations, indicating that strong <u>subsolidus</u> hydrothermal alteration is probably responsible for all of the low $\delta^{18}O$ quartz values in the Idaho batholith.

The quartz-biotite relationships shown on Fig. 5.3 have the same general form and explanation as the quartz-feldspar relations just discussed. The most important difference is that the "normal" points constituting the "primary cluster" are concentrated about a 45° line represented by a quartz-biotite fractionation of 6 permil, significantly different than the quartz-feldspar Δ-value of about 2. The length of

Figure 5.3 Graph of $\delta^{18}O$ values of coexisting biotite (+ chlorite, see text) and quartz for granitic rocks from the Atlanta lobe. Most samples have typical igneous quartz-biotite fractionations of about 6 permil and thus plot within the "primary cluster", but hydrothermally altered (typically chloritized) samples show large nonequilibrium ^{18}O fractionations.

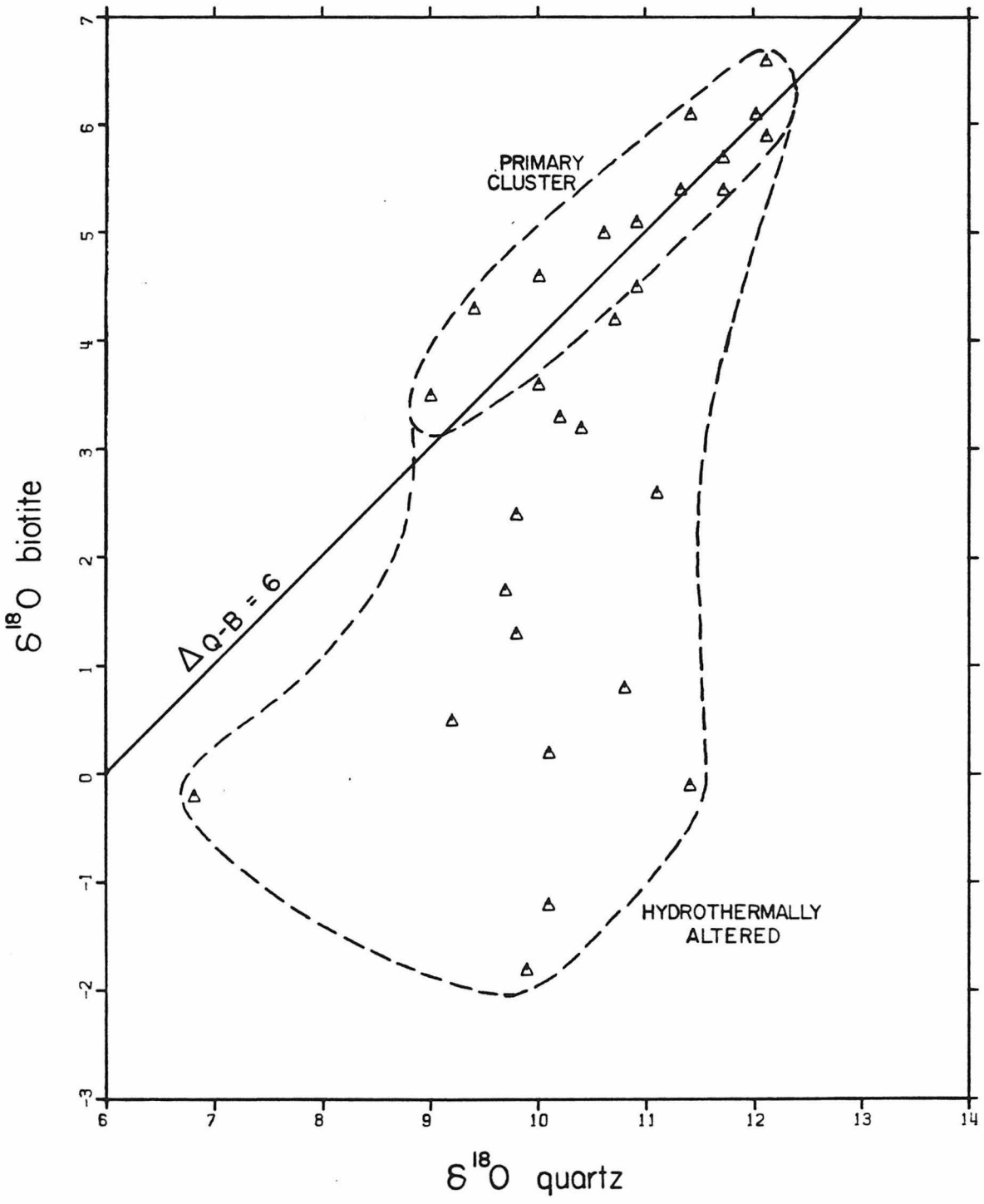
PRIMARY
CLUSTER
HYDROTHERMALLY
ALTERED
ΔQ-B = 6
δ18O biotite
δ18O quartz
7
6
5
4
3
2
1
0
-1
-2
-3
6
7
8
9
10
11
12
13
14

this line segment is again about 3 permil, and points which fall significantly below the line have been ^{18}O-shifted by the hydrothermal fluids. Note that although these biotite concentrates were made as pure as possible, many of these "biotites" contain finely interlayered chlorite (see below).

The $\delta^{18}O$ values of coexisting biotite and feldspar are compared on Fig. 5.4. The line in the figure represents a 4 permil feldspar-biotite fractionation, which of course is the difference between the positions of the "primary clusters" at 6 on the quartz-biotite diagram and at 2 on the quartz-feldspar diagram (Fig. 5.2 and 5.3). Only the points along the uppermost 3 permil segment of this line can represent primary, unaltered rocks. Note that beyond this line-segment the data points markedly diverge from the line. Surprisingly, the "biotite" and feldspar appear to have similar exchange rates, with biotite perhaps exchanging slightly faster. However, it should be made clear that in most samples a significant amount, if not all, of the apparent $\delta^{18}O$ change of the "biotite" actually represents chlorite formation, as will be discussed below in Section 5.1.3. Thus the biotite itself may not undergo significant $^{18}O/^{16}O$ exchange with the fluid, but instead may simply be transformed layer by layer to a chlorite mineral that is in approximate isotopic equilibrium with the fluid.

5.1.2 D/H Variations

D/H exchange between hydroxyl minerals and the hydrothermal fluids occurs concurrently with the $^{18}O/^{16}O$ exchange effects described above. This section describes the D/H variations of biotite in the batholith and

Figure 5.4 $\delta^{18}O$ values of coexisting biotite (+ chlorite, see text) and feldspar from Atlanta lobe granitic rocks. Compare with Figs. 5.2 and 5.3.

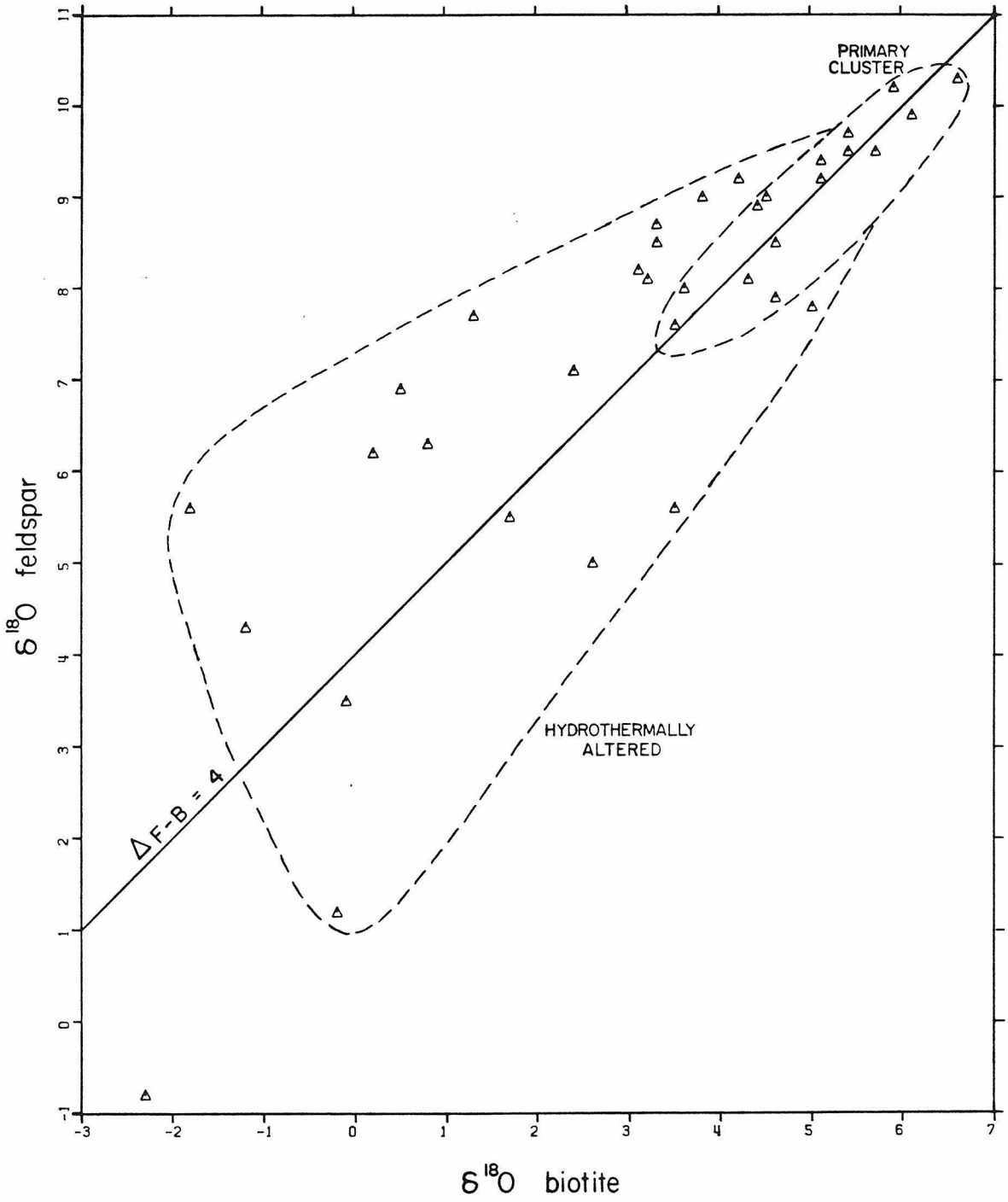
PRIMARY
CLUSTER
HYDROTHERMALLY
ALTERED
ΔF-B = 4
δ18O feldspar
δ18O biotite
-3
-2
-1
0
1
2
3
4
5
6
7
-1
0
1
2
3
4
5
6
7
8
9
10
11

relates the measurements to $\delta^{18}O$ determinations in the same rocks. It will be shown below that the δD values provide a very sensitive indicator of small water/rock ratios and/or low intensities of hydrothermal alteration.

Figure 5.5 is a histogram showing D/H analyses of biotite in the southern half of the Idaho batholith. Although the points represent individual analyses, the graph to a first approximation also represents the weighted areal distribution of δD in the Atlanta lobe. Note that in many instances the "biotite" is partly converted to chlorite, expecially in the low δD examples. Inasmuch as it was not possible to separate this chlorite from the analyzed biotite concentrates, the chlorite contributes significantly to the D/H ratios of some of the mineral separates, especially considering that chlorite contains about 4 times more stoichiometric hydrogen than biotite. The relative proportions of these two minerals in the concentrates are discussed in Sec. 7.2, but the analytical data described in this section are not corrected for this effect and hence all refer to biotite-chlorite mixtures (here termed "biotite").

The histogram (Fig. 5.5) shows that the δD values of the "biotites" range from -66 to -176 permil and are more or less continuously distributed between these limits. As discussed below, a δD value of about -70 characterizes all of the petrographically fresh, unaltered rocks from the western and northwestern part of the Atlanta lobe. The δD values of about -150 represent highly altered rocks, many of which are also strongly depleted in ^{18}O. The intermediate values characterize rocks which have also been hydrothermally exchanged, but with relatively small amounts of water; the latter typically show only minor ^{18}O depletions.

Figure 5.6 compares the $\delta^{18}O$ values of feldspar with the δD values

Figure 5.5 Histogram of δD contents of biotite (+ chlorite) for Atlanta lobe granitic rocks. Note the almost continuous, nearly uniform distribution between "unaltered, primary" values (δD ≈-65) and highly altered values (δD ≈-150 to -176).

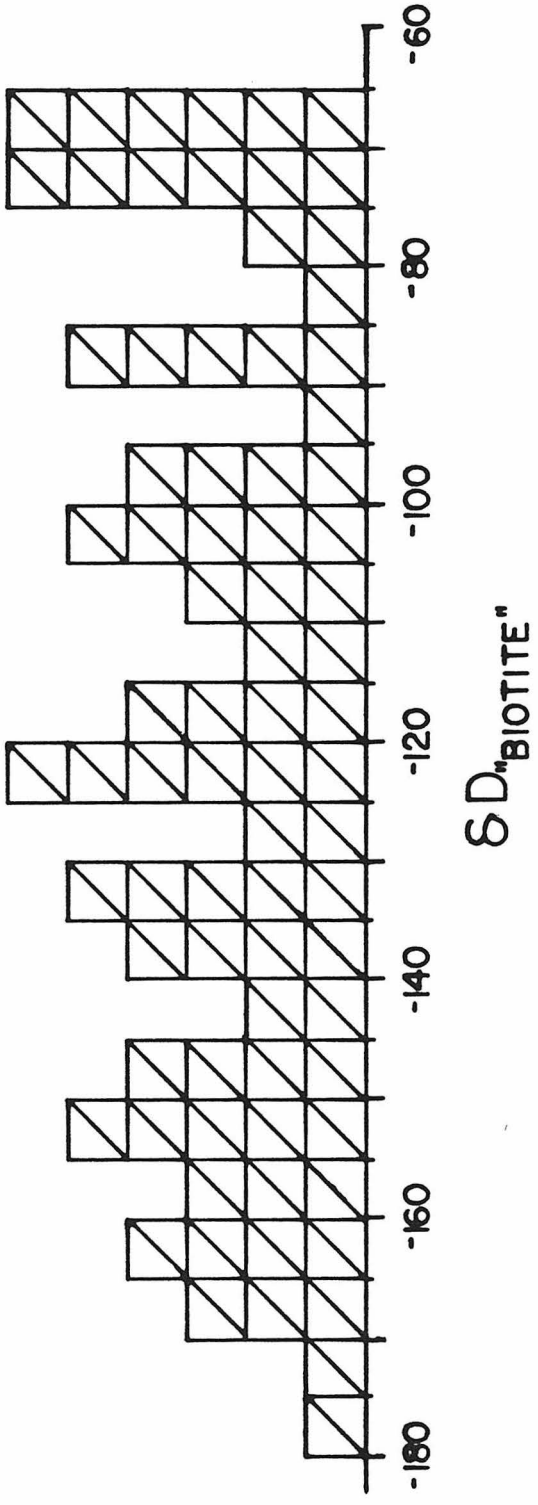
-60
-80
-100
-120
-140
-160
-180
δD"BIOTITE"

of "biotite" from the same rock. Rocks with normal feldspar $\delta^{18}O$ values ($\sim$ + 9) are generally characterized by heavy δD values ($\sim$ -70). This appears to be a typical primary δD value for the Idaho batholith, and is consistent with the δD range of about -40 to -80 previously established for most igneous and metamorphic rocks that are known to be of deep seated origin (Sheppard and Epstein, 1970; Taylor, 1974b). The figure also shows that rocks with abnormally low $\delta^{18}O$ values (<+ 8) are without exception strongly depleted in deuterium ($\delta D < -120$); this was, a priori, an expected consequence of hydrothermal alteration by low $-^{18}O$ meteoric waters, because such waters must also have low δD values (Fig. 3.3) and because the hydrogen/oxygen ratio of rocks is small. Similar relations are exhibited in a plot of the δD of "biotite" vs. the $\delta^{18}O$ of "biotite" (see Fig. 5.11).

A complementary plot (Fig. 5.7) shows that the δD values of "biotite" systematically decrease as the quartz-feldspar fractionations increase, which is clearly indicative of progressive alteration and increasing water/rock ratios. Note that the δD value is much more sensitive to low degrees of alteration than either the feldspar $\delta^{18}O$ value or the quartz-feldspar ^{18}O fractionation, but that the opposite is true for strong alteration; in the latter case the δD values remain almost constant at -150 to -175. This relationship was first described by Taylor (1977) as the "L-shaped plot", and is effectively a result of the low hydrogen contents of rocks as compared to their total oxygen contents, as is exactly the reverse of the situation in the coexisting water. Thus, small amounts of low δD water can drastically modify the δD value of the rock without the water undergoing any appreciable deuterium-shift,

Figure 5.6 Graph of δD values of biotite (+ chlorite) vs. the $\delta^{18}O$ value of coexisting feldspar in Atlanta lobe granitic rocks. Most samples show signs of isotopic exchange, from an original composition of about $\delta D = -65$, $\delta^{18}O_{feld} = +8$ to $+10.5$, to lower values. The "inverted L-shaped" distribution of the data is discussed in the text. This plot includes the earlier data of Taylor and Magaritz (1976, 1978).

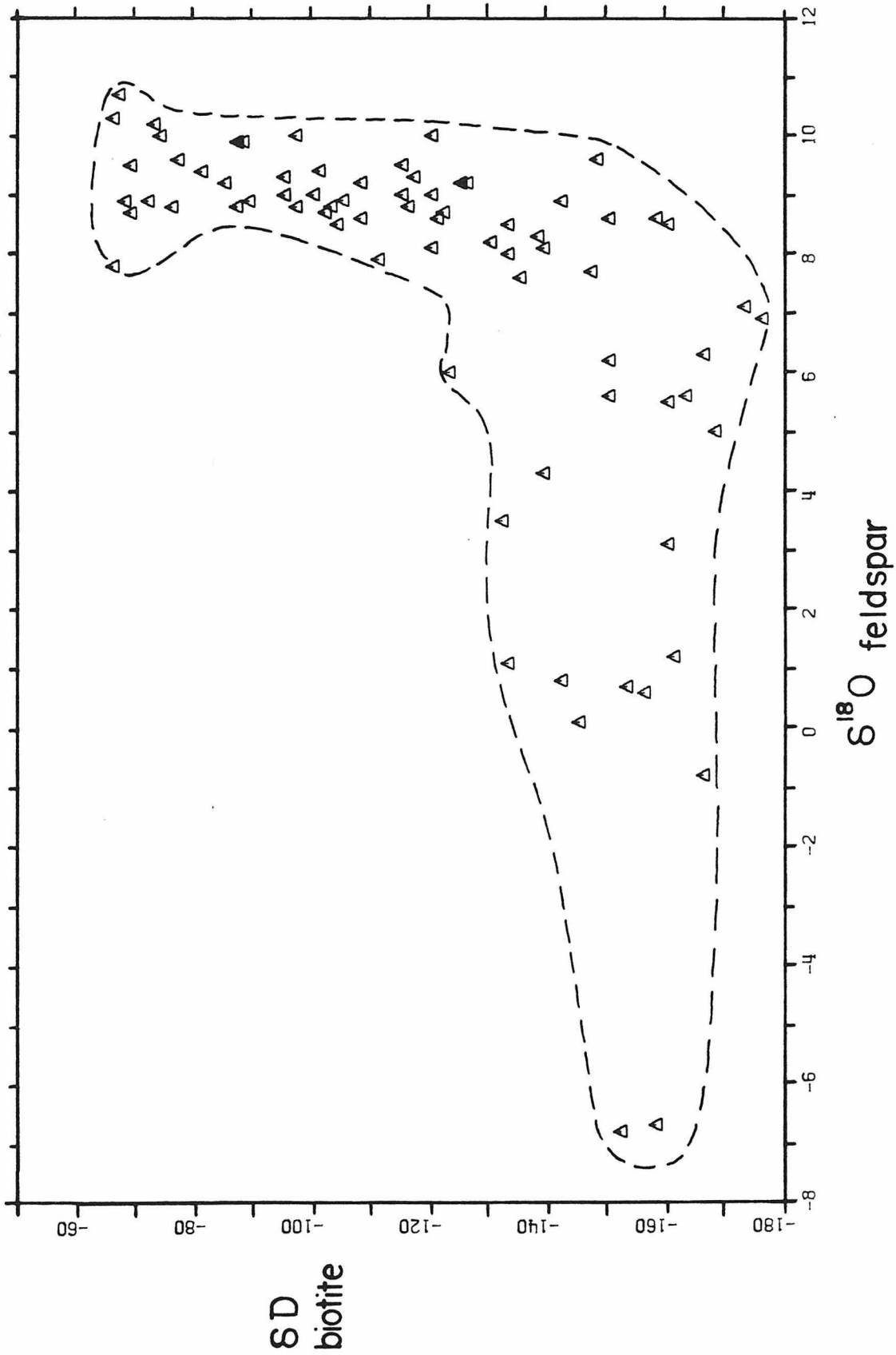
δD biotite
-60
-80
-100
-120
-140
-160
-180
δ18O feldspar
12
10
8
6
4
2
0
-2
-4
-6
-8

Figure 5.7 Graph of the δD value of biotite (+ chlorite) versus the $\Delta^{18}O$ value of coexisting quartz and feldspar for Atlanta lobe granitic rocks. The isotopic compositions of most samples have been modified from their primary isotopic values of δD ≈−65 and $\Delta_{Q-F} \approx 1.0$ to 2.5; some samples have extremely large Δ-values indicative of gross nonequilibrium produced by exchange with low-^{18}O hydrothermal fluids.

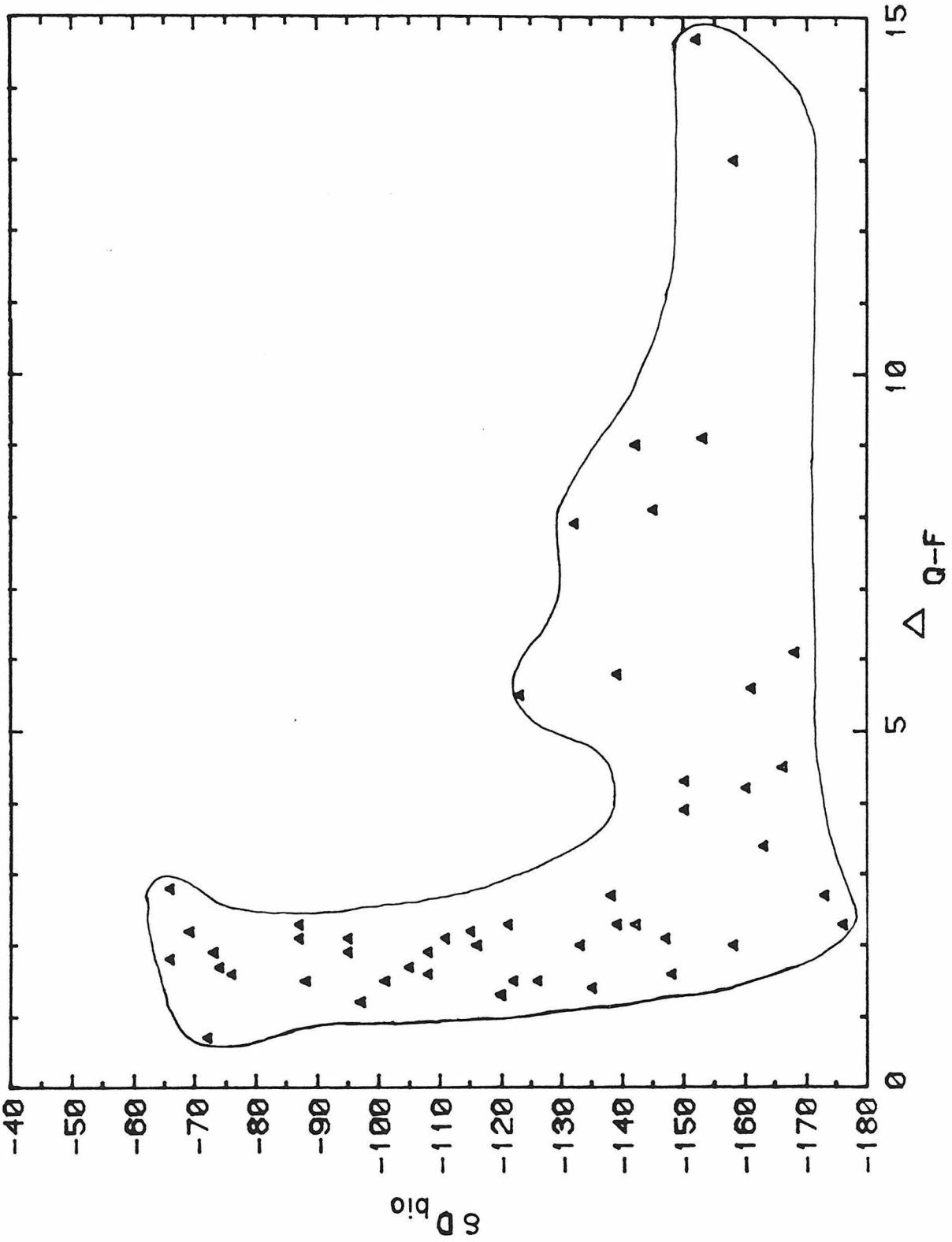
-40
-50
-60
-70
-80
-90
-100
-110
-120
-130
-140
-150
-160
-170
-180
δ D bio
0
5
10
15
Δ Q-F

whereas high water/rock ratios are required to significantly lower the $\delta^{18}O$ contents of the minerals. Note in this connection that the points do not define a perfect "L" but actually conform to a continuous curve in which there is a very sharp change in curvature at the "elbow", showing that minor $\delta^{18}O$ lowering does occur when water/rock ratios are small (Taylor, 1977; c.f. Sec. 5.4.1).

Figure 5.8 contrasts the δD contents of coexisting biotite and muscovite. The shaded band in the figure represents the "normal" 10-20 permil fractionation between muscovite and biotite, which appears to be relatively insensitive to temperature (Taylor and Epstein, 1966; Suzuoki and Epstein, 1976). The numbers in parentheses represent the $\delta^{18}O$ values of coexisting feldspar, and show that two of the data-points (3.1; 5.0) represent samples that have exchanged with large amounts of low-^{18}O hydrothermal fluids. Note that both the least ^{18}O-shifted and most strongly ^{18}O-shifted points all lie near the"equilibrium" band. Points showing weak to moderate alteration or ^{18}O exchange lie along a crude (curved?) reaction path which suggests that the D/H exchange rate of "biotite" with H_2O is much faster than that of coexisting muscovite.

Although the above conclusion is accepted, several factors complicate the interpretation. It has already been mentioned that chlorite is intimately interlayered with individual biotite grains in the altered rocks, and this chlorite contributes to the observed D/H ratio of many of the "biotite" separates. However, it will be shown below in Sec. 7.2 that the biotite itself does in fact undergo significant D/H exchange.

The graph in Fig. 5.8 is also possibly complicated by the formation of sericite, which would be concentrated along with the primary muscovite

Figure 5.8 δD values of coexisting biotite (+ chlorite) and muscovite (or sericite) for Atlanta lobe granitic rocks. The numbers in parentheses represent the $\delta^{18}O$ values of coexisting feldspar. Note that both unaltered and strongly altered samples plot close to or within the Δ_{Mu-bio} = 10 to 20 permil "equilibrium band" (ruled pattern), but that samples showing the effects of moderate hydrothermal alteration plot far from this band and have large, nonequilibrium Δ_{Mu-bio} values. It is clear that the rate of D/H exchange of muscovite with hydrothermal fluid is much slower than that of coexisting "biotite". In most samples the muscovite is primary and relatively abundant; the most significant exception is sample RK 28a, which contains coarse sericite (i.e. hydrothermal white mica that grew in the presence of the aqueous fluids).

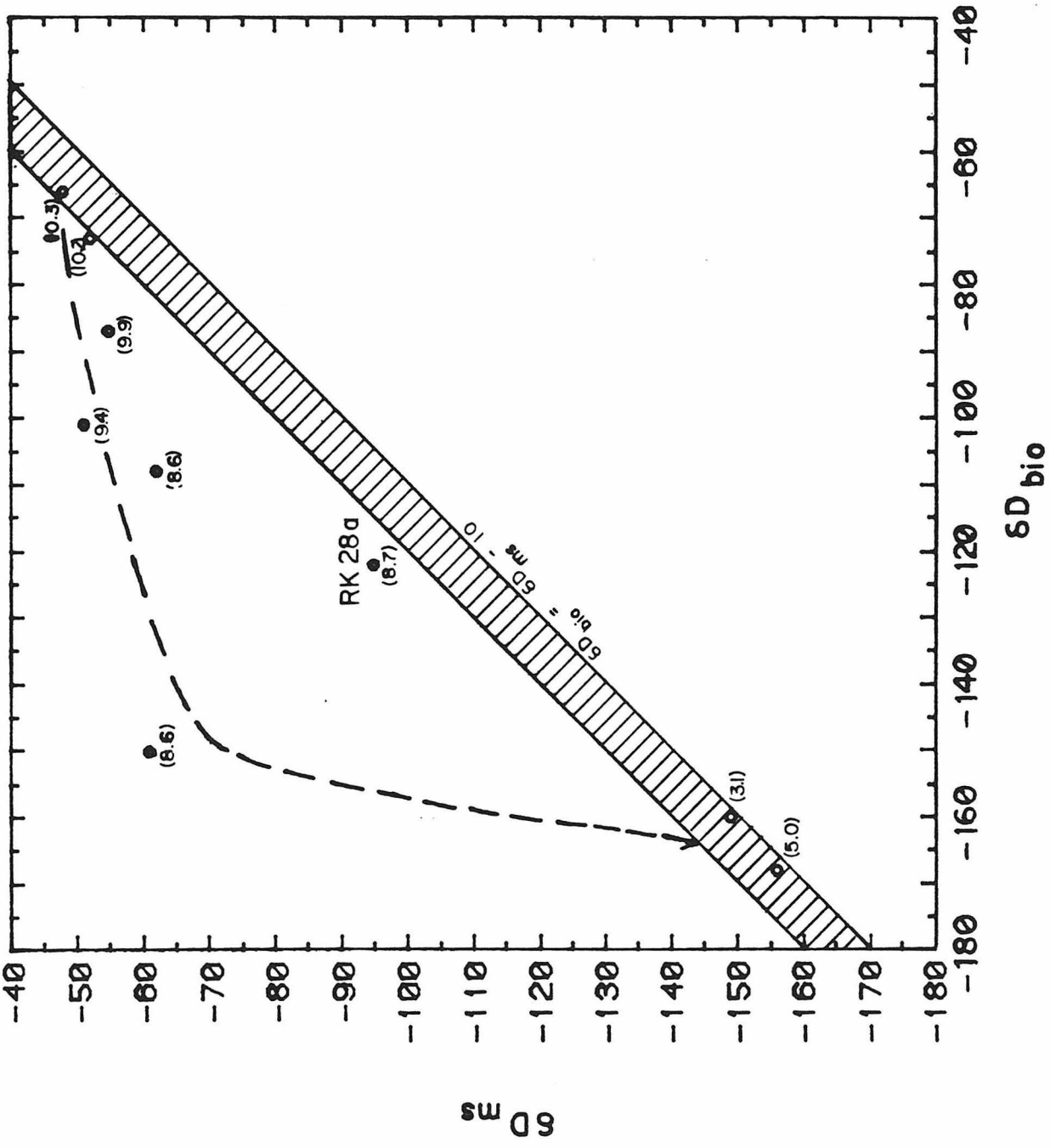
δD ms
δD bio
-40
-50
-60
-70
-80
-90
-100
-110
-120
-130
-140
-150
-160
-170
-180
-40
-60
-80
-100
-120
-140
-160
-180
δD bio = δD ms - 10
RK 28a
(8.7)
(10.3)
(9.9)
(9.4)
(8.6)
(8.6)
(3.1)
(5.0)

in each mineral separate; the sericite would probably have grown in approximate D/H equilibrium with the hydrothermal fluid and thus would have a very low δD value. However, this factor is thought to be minor except for sample RK 28a (see Fig. 5.8). There is unambiguous petrographic evidence for the existence of considerable primary muscovite in most of the analyzed rocks, including at least one strongly altered rock (-160_{bio}, -149_{musc}, 3.1_{feld}); this observation implies that the isotopic data in Fig. 5.8 cannot wholly represent formation of new minerals. Actual D/H exchange is required between the primary muscovite and the hydrothermal fluid. Another minor complication is produced by variations in the modal muscovite/biotite ratios in the rocks. The most extreme data-point (-150_{bio}, -62_{musc}, 8.6_{feld}) is from a sample with a great deal of muscovite and very little biotite, so that the effective amount of water "seen" by the biotite was unusually enhanced relative to that seen by the muscovite. Lastly, although a small amount of interlayering between biotite and muscovite made mineral separation difficult, this mixing effect does not significantly complicate any of the measurements.

5.1.3 Relationship between $\delta^{18}O$ and δD Values and Petrographic Changes

5.1.3.1 General petrographic features

Several mineralogic and petrographic changes attend the hydrothermal alteration of the granitic rocks. Most of the alteration assemblages are of the propylitic type, which includes, in addition to several textural changes, the development of abundant chlorite and sericite, and smaller amounts of calcite, epidote, sphene, opaques and/or other secondary minerals. These changes are described below and are related to the

isotopic effects.

One of the most informative and widespread features in the altered granitic rocks is the presence of alteration minerals along small cracks, voids, and grain boundaries. These are filled with fine opaque minerals, together with fine chlorite, sericite, calcite, epidote, quartz, and some amorphous material. Small amounts of these minerals are even observed in rocks that have been only slightly depleted in deuterium (e.g. $\delta D \sim -80$); this either implies the existence of another type of hydrothermal fluid, or more likely testifies to the extended path length followed by some of the meteoric-hydrothermal fluids. Some rocks also show signs of cataclastic deformation, for example bent plagioclase twins and biotite cleavage planes, multidomain quartz grains, and evidence of granulation. These rocks are usually lower in $\delta^{18}O$ than nearby undeformed rocks, but it is important to point out that most of the low-^{18}O rocks are essentially undeformed. Most of the hydrothermal alteration has probably proceeded in a static environment; except for fracturing and faulting there was little or no accompanying deformation.

Another important and commonly observed feature is the clouding of feldspar. This process commonly selectively affects plagioclase relative to potassium feldspar, especially the calcic centers of normally zoned grains. Much of this turbidity reflects the growth of fine sericite crystals within the host, but calcite, saussurite, chlorite, and perhaps clay minerals are also formed. Some of the clouding may also represent fluid inclusions (c.f. Martin and Lalonde, 1979). In some extremely ^{18}O-depleted rocks the alteration is so intense that it can be seen in hand specimen, and the feldspars have a dull, almost chalky appearance.

In such cases the K-feldspar is also strongly clouded, and albite twinning in plagioclase may be absent. In at least some altered rocks, large single crystals of sericite have grown within the plagioclase grains.

5.1.3.2 Chloritization of biotite

The most conspicuous and quantifiable petrographic change observed in the altered rocks is chloritization of mafic minerals, principally the biotite. This change is easily seen with the petrographic microscope, which additionally shows that the conversion to chlorite first proceeds along cleavage planes and grain boundaries of the biotites. In hand specimen this conversion is marked by a distinct decrease in the luster of the "biotite" grains (i.e. the biotite-chlorite mixtures) and in extreme cases by the unmistakable green color of chlorite.

Definitive evidence for the chlorite mineralogy is provided by both chemical and X-ray diffraction methods. Figure 5.9 shows the relation between the K_2O and H_2O contents of the "biotite" separates used in the K-Ar study (see Sec. 7.2; Table 4.5). Note that on this diagram all samples appear to conform closely to a simple mixture of an annite-phlogopite solid solution (biotite) with a Fe-Mg chlorite. The consistent shift of the points below the theoretical biotite-chlorite mixing band probably results from the substitution of F^- and Cl^- for OH^-, and also from partial oxidation, both of which would lower the concentration of structural water in the "biotite". The figure also suggests that no clearcut change in the Fe/Mg ratio occurs during chloritization, but rather that the chlorite inherits the Fe-rich composition of the biotite. A relatively Fe-rich composition for the primary biotite is appropriate

Figure 5.9 Relationship between K_2O (wt. %) and H_2O (μmoles H_2O/mg sample) of the "biotite" separates analyzed in this study. The linear relationship is thought to represent alteration of part of the biotite, which originally had $K_2O \approx 9.0$ and $H_2O \approx 1.6$, to chlorite group minerals with a much higher H_2O content (~ 5 μmoles/mg) and no potassium. All water contents are slightly lower than predicted for stoichiometric (pure OH) biotite-chlorite mixtures.

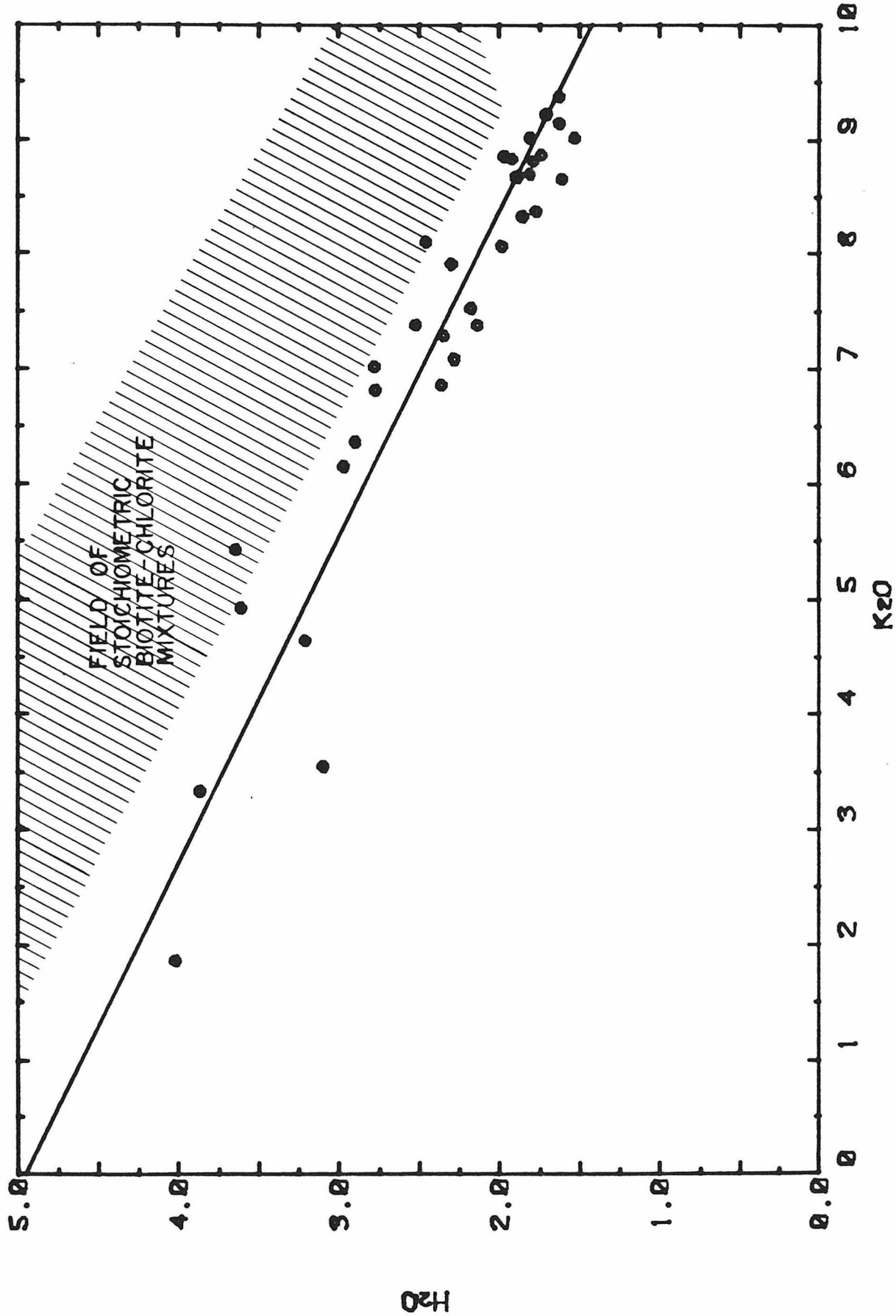
FIELD OF
STOICHIOMETRIC
BIOTITE-CHLORITE
MIXTURES
H2O
K2O
0.0
1.0
2.0
3.0
4.0
5.0
0
1
2
3
4
5
6
7
8
9
10

for these rocks, which are predominantly quartz monzonites (e.g. see Deer, Howie and Zussman, 1966), and this is confirmed by a few biotite analyses from the Idaho batholith (Larsen and Schmidt, 1958; Fe/Mg atom ratio = 2.2 and 0.96 for quartz monzonite and tonalite, respectively).

An X-ray diffractometer study has been made on several of the "biotite" separates. The proportion of chlorite, crudely indicated by the relative intensity of its peaks compared to those of biotite, increases with decrease in the K_2O content. Furthermore, the low intensity ratios of the chlorite peaks (14.5 Å: 7.3Å) indicate that the chlorite is an iron-rich variety.

The relation between chloritization and hydrothermal alteration is dramatically shown on Fig. 5.10. Whereas primary, unaltered biotite with about 9 wt. % K_2O has a normal $\delta^{18}O$ value of 4.5 to 6.6, the low-potassium chlorites formed in the presence of the low $-^{18}O$ hydrothermal fluids have extrapolated $\delta^{18}O$ values ranging from about -3.5 to -6.0, with a maximum possible range of -2 to -8. All intermediate points on the diagram represent biotite-chlorite mixtures and lie on a linear mixing line (actually a band) between these extreme compositions. Note that this result indicates that, like quartz, the biotite itself does not exchange $^{18}O/^{16}O$ readily with the fluid. The ^{18}O changes in the "biotites" that lie within the mixing band seem to be produced almost completely by transformation of the primary biotite to an alteration product (chlorite) that crystallizes in approximate isotopic equilibrium with the fluid.

The four low - ^{18}O points with relatively high K_2O contents (RH 14a, RH 85d, RC 39e, I 7) represent clear-cut exceptions to the above conclusion. These relatively pure biotite samples may represent rocks altered at

Figure 5.10 Relationship between $\delta^{18}O$ and K_2O for the analyzed "biotite" separates. Most samples lie within a narrow band representing mixtures between a high (~9 wt.%) K_2O, "normal" (4.5 to 6 permil) $\delta^{18}O$ biotite and a potassium-free, low $-^{18}O$ (-3.5 to -6 permil) chlorite that formed in the presence of meteoric-hydrothermal fluids. Four samples show anomalous relationships; these may have been mainly altered at high temperatures above the stability field of chlorite. The latter roughly straddle the dashed reference line that extrapolates to $\delta^{18}O \approx -25$ at $K_2O = 0$; inasmuch as this is an impossibly low $\delta^{18}O$ value for chlorite, these four samples cannot represent mixing between a normal $-^{18}O$ biotite and any type of hydrothermal chlorite.

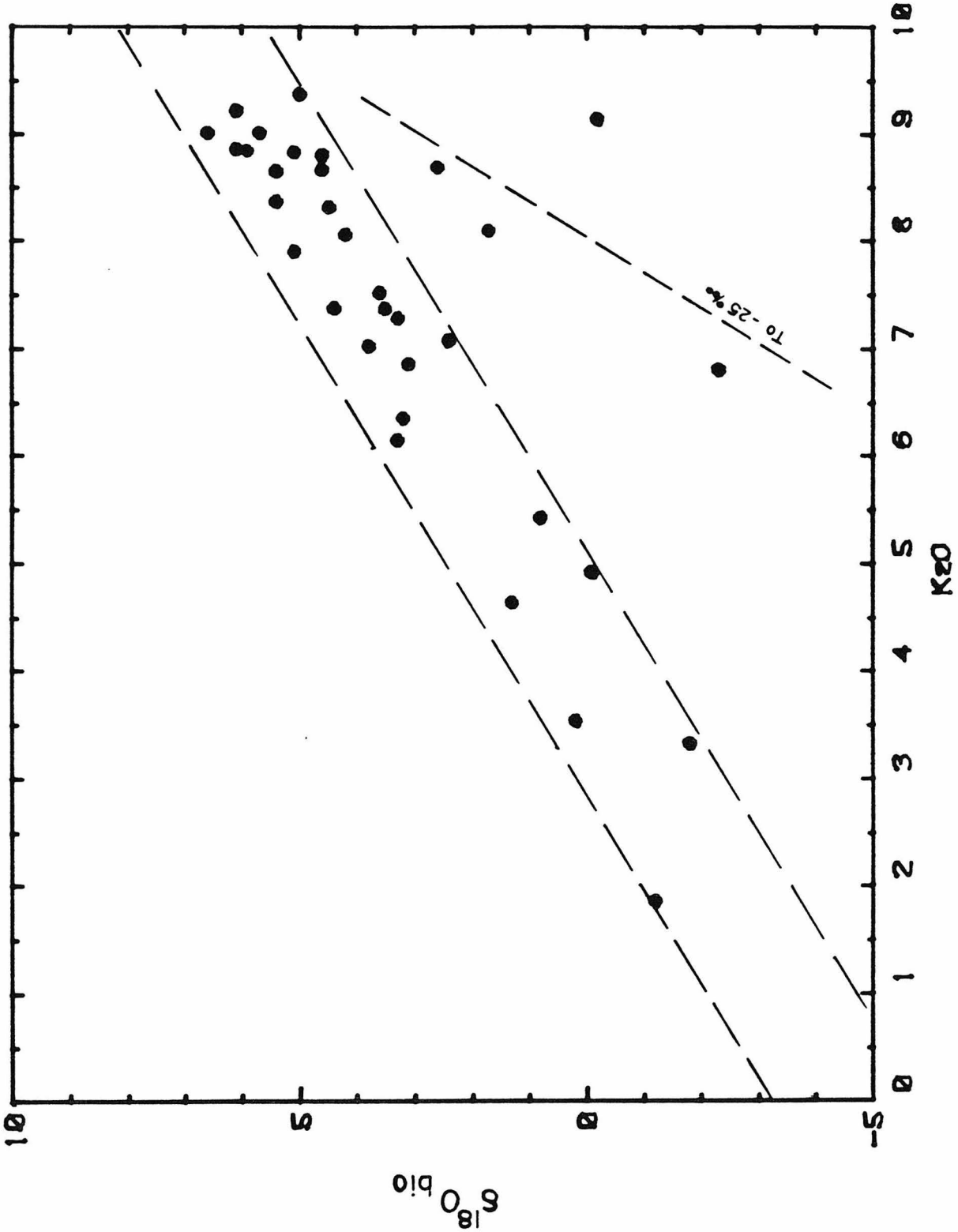
$\delta^{18}O_{bio}$
10
5
0
-5
0
1
2
3
4
5
6
7
8
9
10
K2O
To -25‰

higher temperatures, mostly within the stability field of biotite; this is plausible, because two of these rocks (RH 14a, RC 39e) lie within a few hundred meters of mapped contacts with large Eocene plutons, and thus must have been heated to fairly high temperatures.

It should be mentioned that the relatively restricted range of $\delta^{18}O$ values of most of the endmember chlorites (-2 to -8) is somewhat surprising in the light of the very low calculated $\delta^{18}O$ values of unshifted Eocene meteoric waters in this area (about -16; see Sec. 5.4.4), and the relatively small (-3 ± 2) chlorite-water $^{18}O/^{16}O$ fractionations estimated for moderate temperatures ($250 \pm 100°C$) by Wenner and Taylor (1971). This indicates that most of the hydrothermal fluids probably were ^{18}O-shifted upward to $\delta^{18}O$ values of about -5 to +1 in essentially all of the analyzed localities in the batholith. The consistency of this ^{18}O shift is remarkable. These data clearly imply that overall water/rock ratios could not have been large, and that pristine meteoric water with $\delta^{18}O \approx -16$ was not an important hydrothermal fluid in the Idaho batholith. This result contrasts markedly with the situation in the Tertiary volcanic Au-Ag districts of western Nevada (see Taylor, 1973; O'Neil et al, 1973; O'Neil and Silberman, 1974); these differences are probably explicable in terms of the lower permeability and much greater depths of circulation in the Idaho batholith (see below).

The δD vs. $\delta^{18}O$ relations of the "biotites" (biotite-chlorite mixtures) are shown on Fig. 5.11, which indicates that whereas the unaltered, high-^{18}O biotites have normal δD values of -60 to -70 and $\delta^{18}O \approx +4.5$ to +6 (Fig. 5.3), the low-^{18}O chlorite endmember has a δD value of approximately -150 to -160 and $\delta^{18}O \approx -3$ to -6 (Fig. 5.10). As shown on

Figure 5.11 Graph showing δD vs. $\delta^{18}O$ values for "biotite" (i.e. biotite + chlorite) separates from Atlanta lobe granitic rocks. Assuming the δD of chlorite is approximately -150 to -160, a mixing "band" was calculated for the end-member biotites and chlorites from Fig. 5.10 and Fig. 5.3 and is shown for comparison. However, this mixing "band" is only approximate because this is not a simple two end-member mixing process (see text). Note that the four anomalous points (solid dots) from Fig. 5.10 lie outside the mixing band.

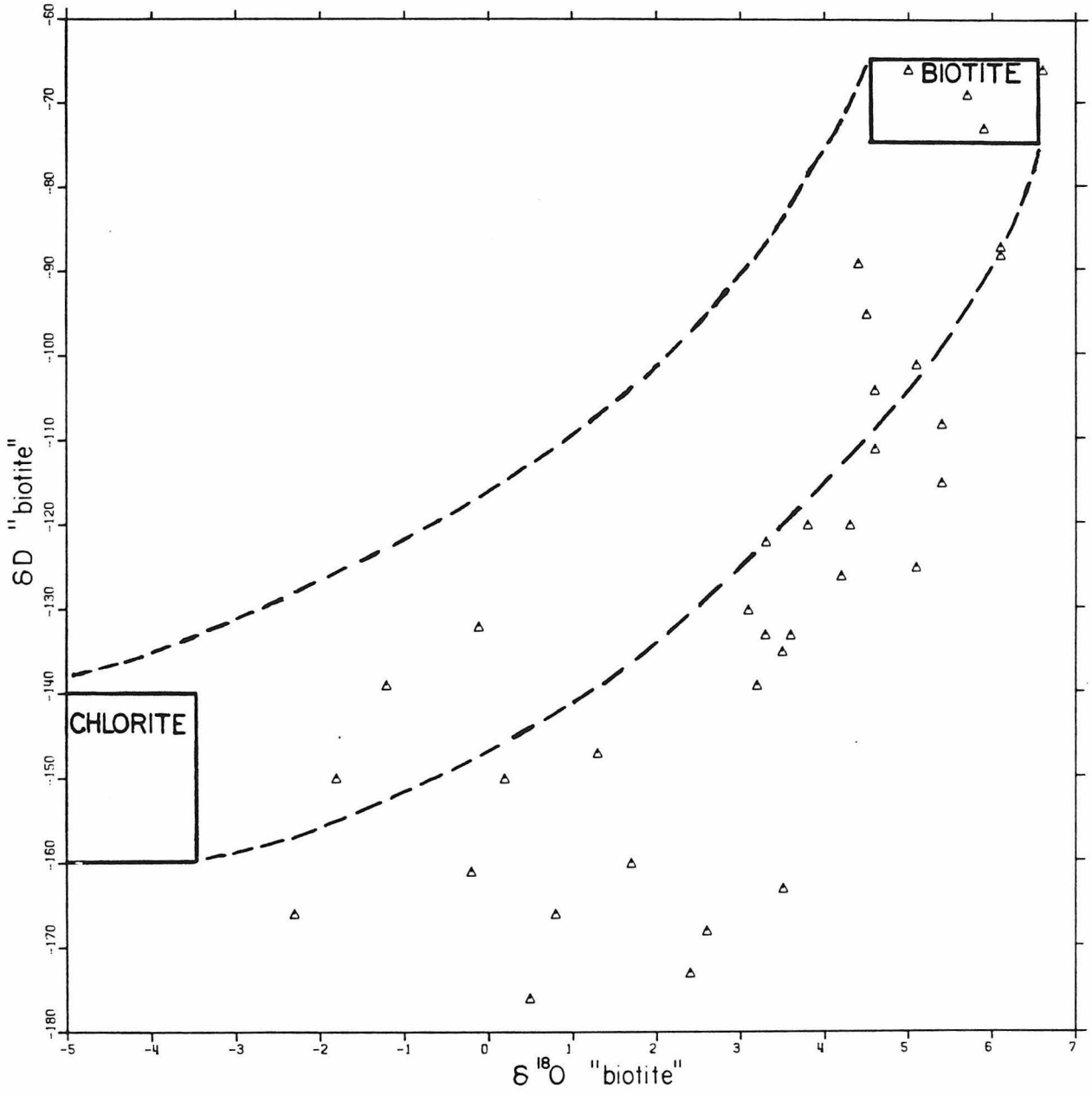
BIOTITE
CHLORITE
δD "biotite"
δ 18O "biotite"
-60
-70
-80
-90
-100
-110
-120
-130
-140
-150
-160
-170
-180
-5
-4
-3
-2
-1
0
1
2
3
4
5
6
7

Fig. 5.11, theoretical mixing lines are not straight on this figure, owing to the high H_2O content of chlorite; an added complication is that this is not a simple two-endmember mixing process because the biotite itself undergoes D/H exchange, but discussion of this critical aspect is deferred to Sec. 7.2. However, note that O'Neil and Kharaka (1976) have demonstrated in hydrothermal experiments that D/H exchange in clay minerals progresses at a much faster rate than $^{18}O/^{16}O$ exchange, similar to most of the Idaho samples.

Fig. 5.11 also shows that all four of the data points which depart from the $\delta^{18}O/K_2O$ mixing band on Fig. 5.10 have unusually low δD values (< -160) and fall outside the approximate mixing band on Fig. 5.11 as well. This is compatible with the biotite itself having been depleted in deuterium, and with the fact that biotite typically has a lower δD value than coexisting chlorite at equilibrium (Taylor and Epstein, 1966; Suzuoki and Epstein, 1976).

Before concluding this aspect of the rock alteration phenomenon, it should be noted that biotite in these rocks also alters to opaque minerals, sericite, sphene, epidote, and other fine-grained alteration products in addition to chlorite. However, chlorite is by far the most common alteration mineral, and none of these other alteration minerals are present in the specially purified mineral separates used for the K-Ar work; finely intergrown chlorite is the only impurity in these separates.

5.1.3.3 Correlation between $\delta^{18}O$ and degree of alteration

Figure 5.12 is a series of histograms showing the feldspar $\delta^{18}O$ distributions in rocks having different degrees of petrographic alteration

Figure 5.12 Histograms of feldspar $\delta^{18}O$ analyses (including a few whole-rock measurements) for rocks assigned to different alteration categories based solely on petrographic inspection (see text). The $\delta^{18}O$ values tend to decrease with increase in the development of hydrous phases and feldspar turbidity, but many reversals and irregularities occur.

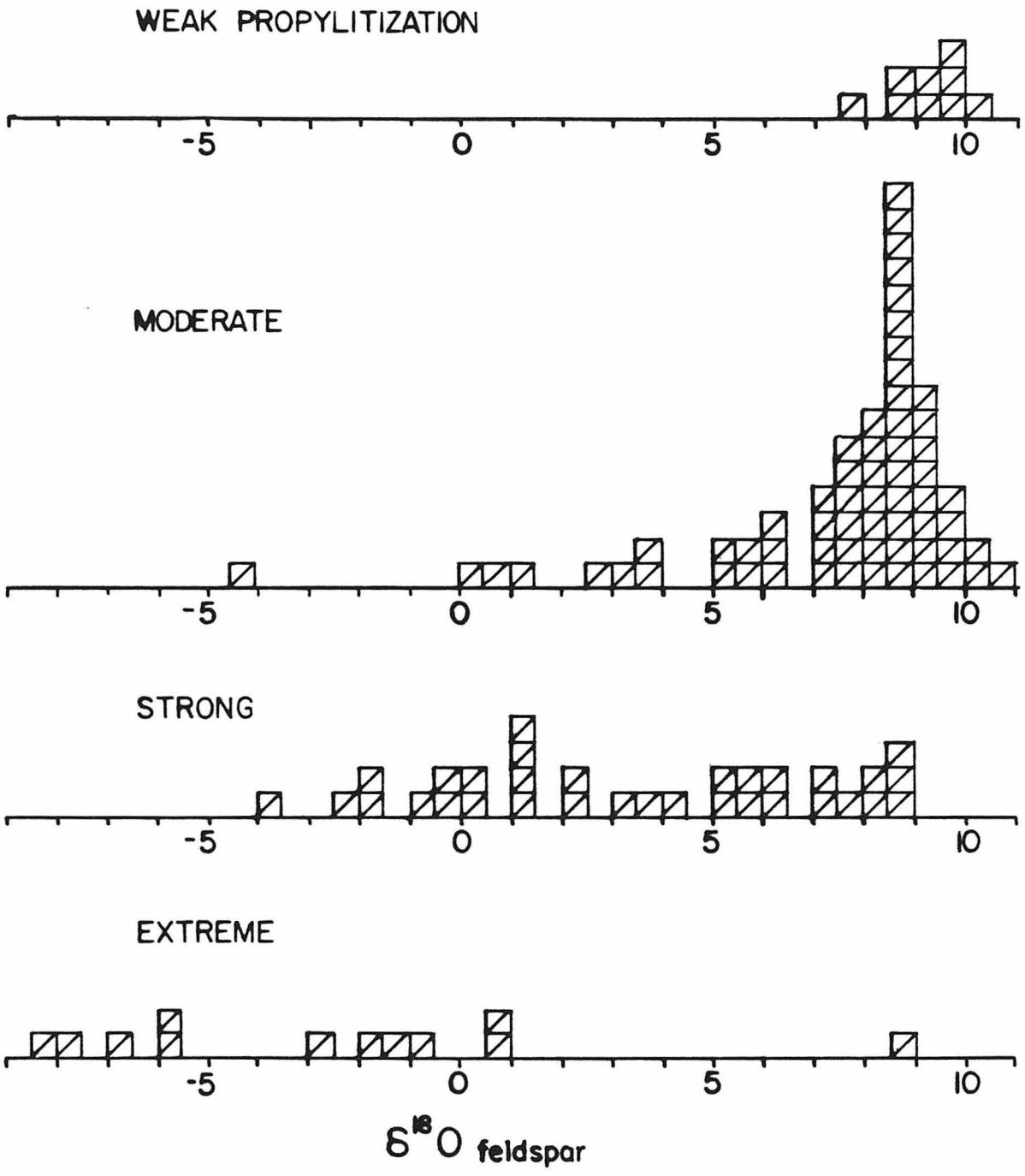
WEAK PROPYLITIZATION
-5
0
5
10
MODERATE
-5
0
5
10
STRONG
-5
0
5
10
EXTREME
-5
0
5
10
δ18O feldspar

(see Tables 4.1, 4.2). The "intensity of alteration" was visually estimated from the appearance of the biotite and feldspar in thin section; the boundaries between the categories are arbitrary, but care was taken to maximize consistency. In terms of this classification, fresh or "weakly" propylitized rocks are uncommon in the region, occurring only along the west and northwest margins of the Atlanta lobe, where there is insignificant development of chlorite, sericite, and turbid feldspar. The most intensely altered rocks, namely those assigned to the "extremely propylitized" category, are fairly common in the east-central portion of the batholith; these all have highly turbid feldspar, considerable sericite and other hydrous secondary minerals, and these rocks generally have no remaining biotite but rather aggregates of chlorite, sericite, opaques and sphene. Rocks assigned to the "moderately" and "strongly" propylitized categories are the most common rocks of the batholith and they exhibit less extreme development of the same petrographic features described above.

Overall, the histograms in Fig. 5.12 show that ^{18}O depletions correlate very well with mineralogical evidence for progressive hydration and alteration of the rocks. The mean $\delta^{18}O$ value of rocks within each category becomes progressively lower as the "alteration intensity" increases. The range of $\delta^{18}O$ variation within the "moderate", "strong" and "extreme" categories is very broad, however, and this proves that the oxygen isotopic exchange and mineralogic hydration effects do not proceed at constant relative rates in all rocks. In particular, it is possible for rocks to exchange ^{18}O with fluids at high temperatures ($\geq$ 400° C), beyond the stability range of many hydrous phases; many of the low - ^{18}O rocks assigned to the "moderate" class may have been altered primarily

under these higher temperature conditions. In particular, two of the four anomalous, low δD rocks on Figs. 5.10 and 5.11 (RH 14a, I 7) have relatively low feldspar $\delta^{18}O$ values (+ 1.2 and + 5.0) but show only "moderate" propylitization. In this connection, note that although this type of feature is relatively uncommon in granitic rocks, it has been shown that development of OH-bearing alteration minerals commonly does not accompany ^{18}O exchange in gabbroic rocks, implying that hydrothermal alteration occurred at consistently higher temperatures than in the case of the granitic rocks (c.f. Taylor and Forester, 1979; Gregory and Taylor, 1981).

5.2 Primary Magmatic Isotopic Composition of the Atlanta Lobe

5.2.1 Primary $^{18}O/^{16}O$ Variations

There is surprisingly little variation in the primary ^{18}O contents of igneous rocks from the Atlanta lobe. The magnitude of this variation is partially obscured by all the hydrothermal activity, but it can be approximately deduced from the $\delta^{18}O$ values of quartz, which is the mineral least affected by this subsolidus process. Inferred primary $\delta^{18}O$ values of the Mesozoic rocks are described from west to east below, followed by discussion of some remarkable relationships in the Eocene rocks.

The $\delta^{18}O$ value of quartz from a single tonalite (I 32) from the western margin of the batholith is +10.6 (whole rock = +8.5). Immediately to the east, granodiorites and tonalites (e.g. RM 6a, 10; I 24a, 25, 205) have slightly higher $\delta^{18}O$ quartz (+10.4 to +12.1) and whole-rock values (generally 10 $\pm$ 0.7). Somewhat further east the highest $\delta^{18}O$ quartz (11.7 to 12.1) and whole-rock (~ + 11) values in the batholith

are found in the Warm Lake Quartz Monzonite (e.g. RC 18; I 210, 215), which is also distinguished by its high muscovite content; one sample of this unit that is atypical in its lack of abundant muscovite (RB 148) has a somewhat lower quartz $\delta^{18}O$ value of + 11.4. This sequence of increasing $\delta^{18}O$, going from the hornblende-bearing tonalites to the muscovite-rich Warm Lake pluton, is reminiscent of the increase in ^{18}O that typically accompanies a change from I-type to S-type character in plutonic granitic rocks (Taylor, 1977; O'Neil and Chappell, 1977).

Proceeding still further east, the Mesozoic rocks from the large interior zone of the batholith have somewhat lower $\delta^{18}O$ quartz (+10.6 $\pm$ 0.8; 30 samples) and estimated primary whole rock values (+ 9.5 $\pm$ 1.0), with no clearcut spatial variations. The principal exceptions to this are from rocks whose feldspars have experienced extreme ^{18}O depletion (e.g. RH 2b, RH 14a, RC 7a, I 228), and it is evident that the strong hydrothermal activity also caused some ^{18}O depletion in coexisting quartz. Finally, several relatively mafic rocks from the eastern margin of the batholith (I 222, 224, 225, 226) have slightly higher quartz $\delta^{18}O$ values of +11.0 $\pm$ 0.2 (est. primary whole-rock = + 9 to + 9.5); although one unusual leucocratic rock (RH 79) from an outlying pluton has $\delta^{18}O$ quartz = + 10.4. In conclusion, the average unaltered igneous quartz from the batholith is about 11.0, with a range of slightly more than about $\pm$ 1 permil, which indicates that almost all of these rocks belong in the high $-^{18}O$ (H_2 and HH) groups of Taylor (1968).

Several analyses have also been made of quartz from the Eocene plutons. Inasmuch as these plutons are intimately connected with the Eocene hydrothermal activity, their primary magmatic composition cannot

be deduced from simple inspection of the quartz $\delta^{18}O$ values. However, the alteration effects may be assessed from relationships on a quartz-feldspar $\delta^{18}O$ plot with the primary $\delta^{18}O$ values detrmined by extrapolation to the primary magmatic fractionation line. These relationships are shown for all analyzed samples of Tertiary granites on Fig. 5.13. Note that although the hydrothermal activity has produced large variations in $\delta^{18}O$ of the quartz and feldspar, the analyses from each pluton plot on linear, remarkably consistent trends with slopes of about 4:1. The primary $\delta^{18}O$ compositions of quartz are seen to be approximately 9.2 for the Crags and Sawtooth plutons, 10.3 for the Twin Springs and Dismal Swamp plutons from the Rocky Bar Complex, and probably about 10.9 for the Casto pluton. With the exception of the poorly defined value for the Casto Pluton, these values are all slightly lower than those of the typical Mesozoic plutonic rocks of the batholith. This suggests that these Eocene rocks probably are not simply remelted portions of the Idaho batholith proper, because, if anything, such a process would tend to slightly <u>increase</u> the $\delta^{18}O$ value of the granitic melt relative to the parent material. The depletion in ^{18}O in the Eocene magmas conceivably could have been brought about by some involvement of deeply circulating meteoric water in the melting process (c.f. Hildreth et al, 1980), or possibly through assimilation of low-^{18}O hydrothermally altered roof rocks. It is equally plausible that these Eocene rocks were derived by differentiation from source materials that are totally unrelated to the Mesozoic plutonic rocks.

Last, several samples of relatively unaltered Eocene (?) granodiorite were also analyzed. The quartz from these samples (RH 12; I 22, 241, 242)

Figure 5.13 $\delta^{18}O$ values of coexisting quartz and feldspar from several Eocene granite plutons of the Idaho batholith region. Even though the $\delta^{18}O$ values of most samples have been disturbed by exchange with low ^{-18}O hydrothermal fluids, with feldspar having a much higher exchange rate than quartz, the primary isotopic composition of these plutons can be estimated by extrapolating the nearly linear arrays back to the primary magmatic line (Δ = 1.4). SB (Sawtooth batholith), CRAGS (Crags pluton), CASTO (Casto pluton), RB ("Rocky Bar", i.e. Twin Springs - Dismal Swamp pluton).

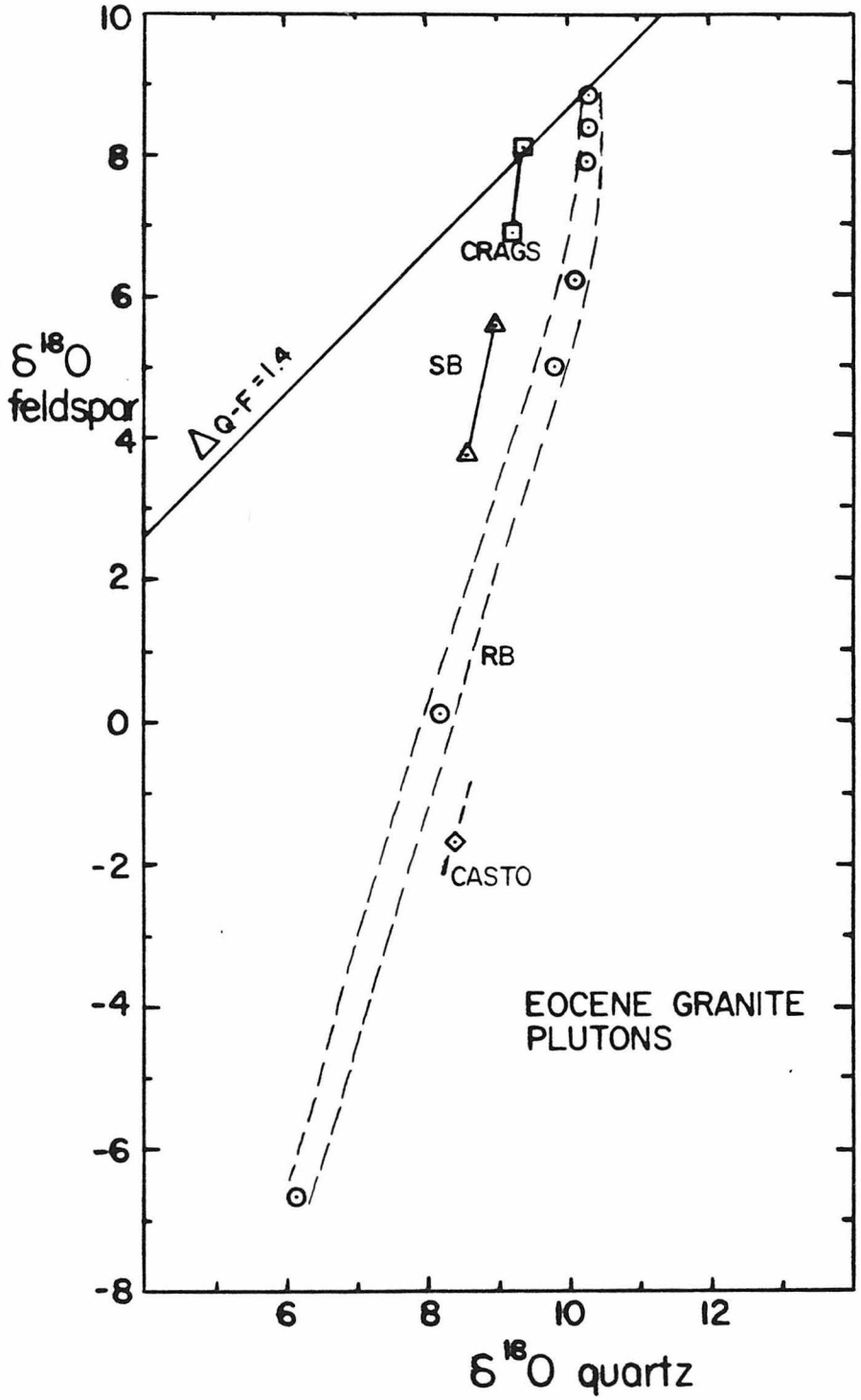
10
8
6
4
2
0
-2
-4
-6
-8
6
8
10
12
δ18O feldspar
δ18O quartz
ΔQ-F=1.4
CRAGS
SB
RB
CASTO
EOCENE GRANITE
PLUTONS

ranges from 11.2 to 11.7 permil, which is slightly higher than nearby Mesozoic rocks. Thus, based solely on the ^{18}O data, these granodiorites do not appear to be genetically related to the suite of Eocene granites, and they could indeed be derived by melting of the older batholithic rocks. Note that there is no definite evidence that these granodiorites actually have an Eocene age.

5.2.2 Primary D/H Variations

As a result of the widespread hydrothermal activity and the high susceptibility of biotite to exchange, little can be said about primary D/H variations in the Idaho batholith. The least altered rocks, which occur only in the western portion of the batholith, have biotite δD values of -66 to -74; these are interpreted to be very close to the primary magmatic values (e.g. RB 159a; I 23, 24a, 25, 31, 32, 202, 205, 206, 208, 210). These values lie within the range (-58 ± 18) of phlogopites from rocks of deep-seated origin (Sheppard and Epstein, 1970), particularly when it is remembered that their slightly lower δD values can in part be attributed to the ~ 25 permil equilibrium enrichment of deuterium in phlogopite relative to Fe-rich biotite at magmatic temperatures (Suzuoki and Epstein, 1976).

The δD values of coexisting muscovite (-50 ± 2) in two of these western rocks (I 205, 210) also probably represent primary values, and the indicated muscovite-biotite fractionations of 20 ± 2 permil in these rocks are compatible with equilibrium at high temperatures (Suzuoki and Epstein, 1976). Three samples from the central portion of the batholith which have been only moderately affected by the hydrothermal activity (RC 18, RB 134, RH 52a; δD_{bio} = -87, -101, -108) also have essentially unaltered muscovite with values of -55, -51 and -62 permil; one remarkable

muscovite-rich, more strongly altered sample (RB 49; $\delta D_{bio} = -150$) still retains muscovite with $\delta D = -61$. These δD values of -51 to -62 are very similar to those of the rocks further west, especially considering that the hydrothermal activity which lowered the δD values of all central zone biotite samples should have produced minor δD lowering of these muscovites.

All of the other analyzed muscovite-bearing samples have been very strongly altered by the low-D hydrothermal fluids, and it is unfortunate that rocks with primary muscovite were not found in the eastern portion of the batholith. Thus, all that can be said from the combined muscovite and biotite δD data is that none of the available analyses are in any way incompatible with the primary δD variation in the batholith being any greater than about 15 permil prior to the Eocene hydrothermal event. The actual range in the primary δD composition of the Mesozoic plutonic rocks is probably even less than this (i.e. primary biotite $\delta D \approx -65$ to -75 and primary muscovite $\delta D \approx -48$ to -58). This conclusion is made much more firm when comparisons are made with other batholiths that have suffered much less meteoric-hydrothermal alteration than the Idaho batholith (see Sec. 5.3.2).

5.3 Comparison with Isotopic Data from Other Cordilleran Batholiths

5.3.1 Mineral-Mineral Isotopic Relationships

This section compares some of the isotopic relationships between coexisting minerals in the Idaho batholith with those of the other Cordilleran batholiths shown on Fig. 5.14 . In a few cases, analyses from other areas are also included. The mineral pairs discussed below are quartz-feldspar ($\delta^{18}O/\delta^{18}O$), quartz-biotite ($\delta^{18}O/\delta^{18}O$),

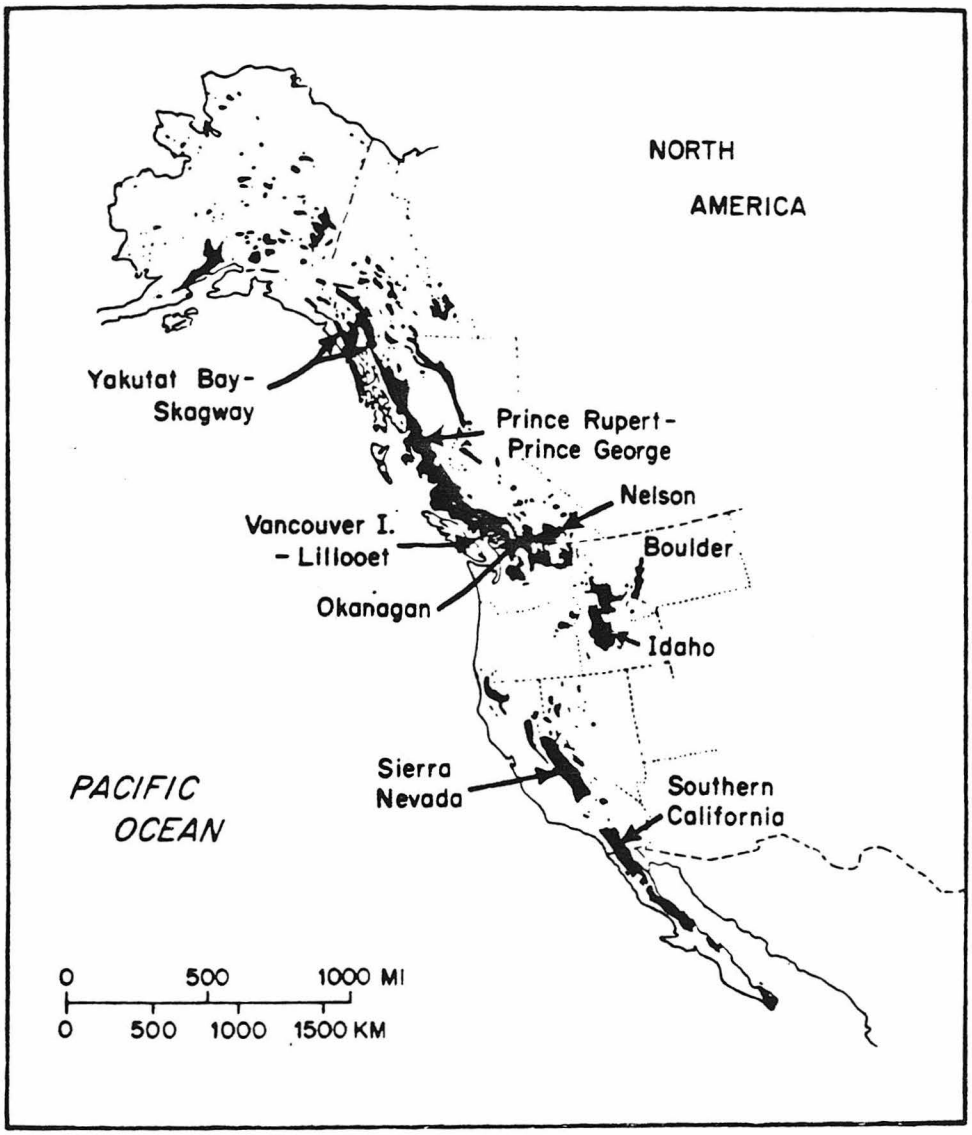

Figure 5.14 Locations of Cordilleran batholiths in western North America. Note that "Southern California batholith" is another name for the Peninsular Ranges batholith (PRB). From Taylor and Magaritz (1978).

feldspar-biotite ($\delta^{18}O/\delta D$), and muscovite-biotite ($\delta D/\delta D$); pyroxene-plagioclase relationships in gabbroic plutons are described in Criss et al (1981).

As pointed out by Taylor (1977), ^{18}O depletions due to meteoric-hydrothermal activity are most pronounced in the northern batholiths, where meteoric waters tend to be isotopically "light", and where intrusive histories are complex and include Tertiary epizonal plutonism. This is especially true for the Coast Range batholith of Alaska and British Columbia, which is the largest and the northernmost of the Cordilleran batholiths, and has a complicated intrusive history ranging from the late Paleozoic into the later Tertiary (Hudson et al, 1977). Meteoric-hydrothermal events of Jurassic (?), Eocene and Miocene age have all been identified in this complex set of plutons (Magaritz and Taylor, 1976 a,b); the mineral-mineral isotopic effects produced by these events are discussed in Sec. 5.3.1.1. In contrast, meteoric-hydrothermal events are much less common in the Peninsular Ranges and Sierra Nevada batholiths, and it will be shown in Sec. 5.3.1.2 that the mineral-mineral isotopic relationships of these rocks are comparatively straightforward.

5.3.1.1 Coast Range batholith

Figure 5.15 contrasts the $\delta^{18}O$ values of quartz and feldspar of granitic rocks from the Coast Range batholith, Alaska and British Columbia (data of Magaritz and Taylor, 1976 a,b). Many of the points exhibit "normal" ($\leq$ 2 permil) primary magmatic quartz-feldspar fractionations, including all of the rocks from the deep-seated "gneissic core complex" of the Prince Rupert-Prince George traverse. The points which fall below the line have large quartz-feldspar Δ-values, indicating that exchange

Figure 5.15 $\delta^{18}O$ values of coexisting quartz and feldspar from the Coast Range batholith, Alaska and British Columbia (data of Taylor and Magaritz, 1976 a,b). Most samples have "normal" Δ - values of 1 to 2 permil, but samples which plot below the 2 permil fractionation line have been affected by exchange with meteoric-hydrothermal fluids. The field of data-points from the Atlanta lobe (Fig. 5.2) is shown for comparison.

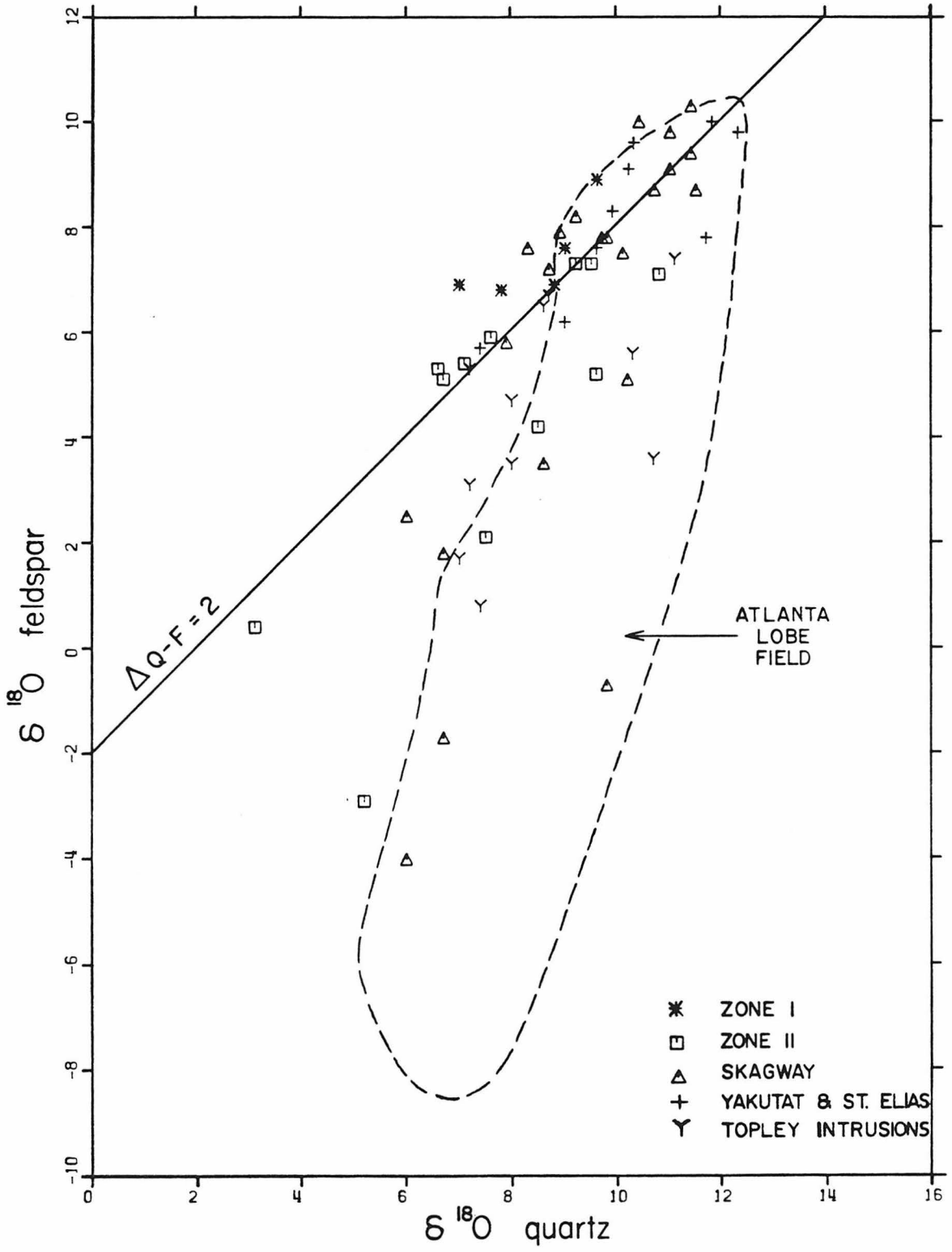
δ 18O feldspar
δ 18O quartz
ΔQ-F=2
ATLANTA
LOBE
FIELD
ZONE I
ZONE II
SKAGWAY
YAKUTAT & ST. ELIAS
TOPLEY INTRUSIONS
12
10
8
6
4
2
0
-2
-4
-6
-8
-10
0
2
4
6
8
10
12
14
16

with low $-^{18}O$ meteoric-hydrothermal water has lowered the $\delta^{18}O$ values of feldspar more than those of coexisting quartz (Magaritz and Taylor, 1976b).

The data in Fig. 5.15 are generally similar to those presented in Fig. 5.2 for the Idaho batholith, but the relationships in the Atlanta lobe are better constrained because more low $-^{18}O$ rocks have been analyzed. The data-points that lie to the left of the Atlanta lobe "field" on Fig. 5.15 thus can all be explained by the same 4:1 feldspar-quartz exchange process described above, the only important difference being that many of the Coast Range rocks originally had primary $\delta^{18}O$ values somewhat lower than those in the Atlanta lobe. Note also that a few of the quartz-feldspar fractionations reported by Magaritz and Taylor (1976 a,b) are very small (~ 0), either reflecting very low-temperature alteration or interactions with high ^{18}O fluid.

Figure 5.16, taken from Taylor and Magaritz (1978), compares the feldspar-biotite ($\pm$ hornblende and chlorite) $\delta^{18}O/\delta D$ relationships of the Idaho batholith with those of the Prince Rupert and Skagway traverses of the Coast Range batholith; also included are two low $-^{18}O$ rocks from the Boulder batholith of Montana (Sheppard and Taylor, 1974). The new isotopic data from the present work are not included in Fig. 5.16, but they do not change the basic pattern. The general similarity of the isotopic relationships in all of these northerly Cordilleran batholiths is clear. This further emphasizes that during late Mesozoic and Tertiary plutonism, most of the rocks in these regions have interacted to varying degrees with hot meteoric waters that had a δD value of about -120 ± 10.

Figure 5.17 shows the same type of data for the granitic rocks of southernmost Canada (Taylor and Magaritz, 1978). These data show that

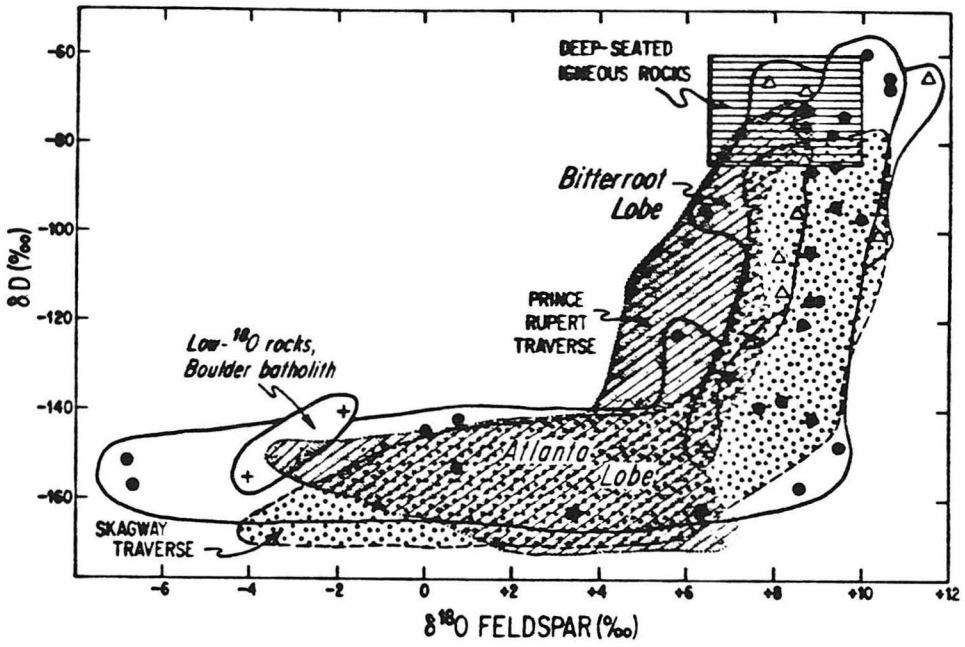

Figure 5.16 Plot of biotite (± chlorite and hornblende) δD vs. feldspar $\delta^{18}O$ for samples of granitic rocks from the Atlanta lobe (dots) and Bitterroot lobe (triangles) of the Idaho batholith, two low $-^{18}O$ rocks from the Boulder batholith (crosses), along with generalized fields for the Prince Rupert and Skagway traverses across the Coast Range batholith, and the field of most deep-seated normal granitic rocks (from Taylor and Magaritz, 1978). See text. Figure 5.6 contains additional data for Atlanta lobe rocks, but is basically similar.

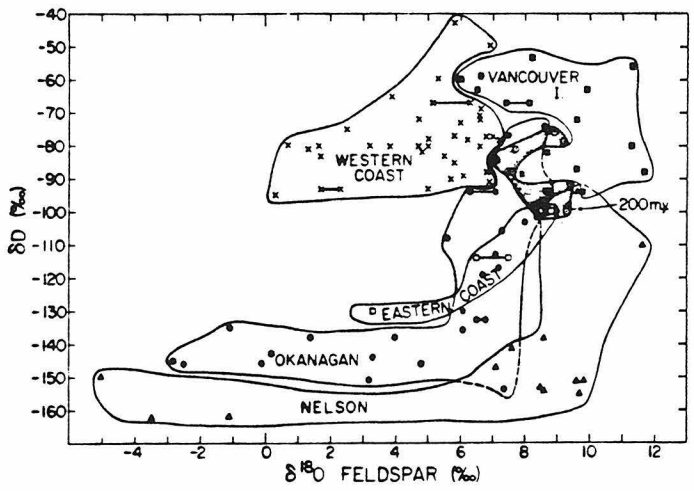

Figure 5.17 Plot of δD vs. feldspar $\delta^{18}O$ for granitic batholiths and plutons of southern British Columbia, from Taylor and Magaritz (1978). Stippled area represents the Guichon and Thuya batholiths. Various "L-shaped" trends are related to the varying δD and $\delta^{18}O$ content of meteoric waters perpendicular to the Pacific coastline. See text.

many of these rocks have also undergone meteoric-hydrothermal interactions, but comparison of the western and eastern coast samples with those of the Okanagan and Nelson batholiths indicates that the fluids became progressively depleted in deuterium and ^{18}O as their distance from the western coastline of North America increased (Taylor and Magaritz, 1978). This type of relationship is expressed by the different positions of the various "L-shaped" plots on Fig. 5.17, and it is entirely compatible with the usual variation of meteoric waters at the edges of continents (c.f. Friedman et al, 1964). On the other hand, the Triassic Guichon and Thuya batholiths show no definite evidence of meteoric-hydrothermal interactions (Taylor and Magaritz, 1978). These batholiths are also the only ones in the region which have apparently preserved their original (200 m.y. old) Triassic K-Ar ages, possibly because these two batholiths for some reason escaped later Tertiary plutonism and associated hydrothermal alteration (Taylor and Magaritz, 1978).

Figure 5.18 shows the δD values of coexisting muscovite and biotite for samples from a small stock in northwest Nevada, from the Monte Rosa granite of the western Alps, from the Yakutat-St. Elias plutons, and for several sericite "biotite" pairs from the Prince Rupert-Prince George traverse in British Columbia (Shieh and Taylor, 1969; Frey et al, 1976; Magaritz and Taylor, 1976 a,b). Most of the muscovite-"biotite" pairs show strong isotopic disequilibrium, indicating that muscovite retains its δD value better than biotite during alteration with meteoric waters (Magaritz and Taylor, 1976b). These relations are similar to those observed in the two-mica plutons of the Atlanta lobe, although the Idaho samples span a considerably greater range of D/H and $^{18}O/^{16}O$ exchange. In

Figure 5.18 δD values of coexisting muscovite and biotite for samples of the Sawtooth stock, Nevada, the Yakutat-St. Elias plutons of Alaska and British Columbia, the Monte Rosa granite of the Alps, along with coexisting sericite - "mafic" δD pairs from the Prince Rupert-Prince George traverse of British Columbia (data from Shieh and Taylor, 1969; Magaritz and Taylor, 1976 a,b; Frey et al, 1976). Most muscovite-biotite pairs show strong isotopic disequilibrium. See text; compare Fig. 5.8.

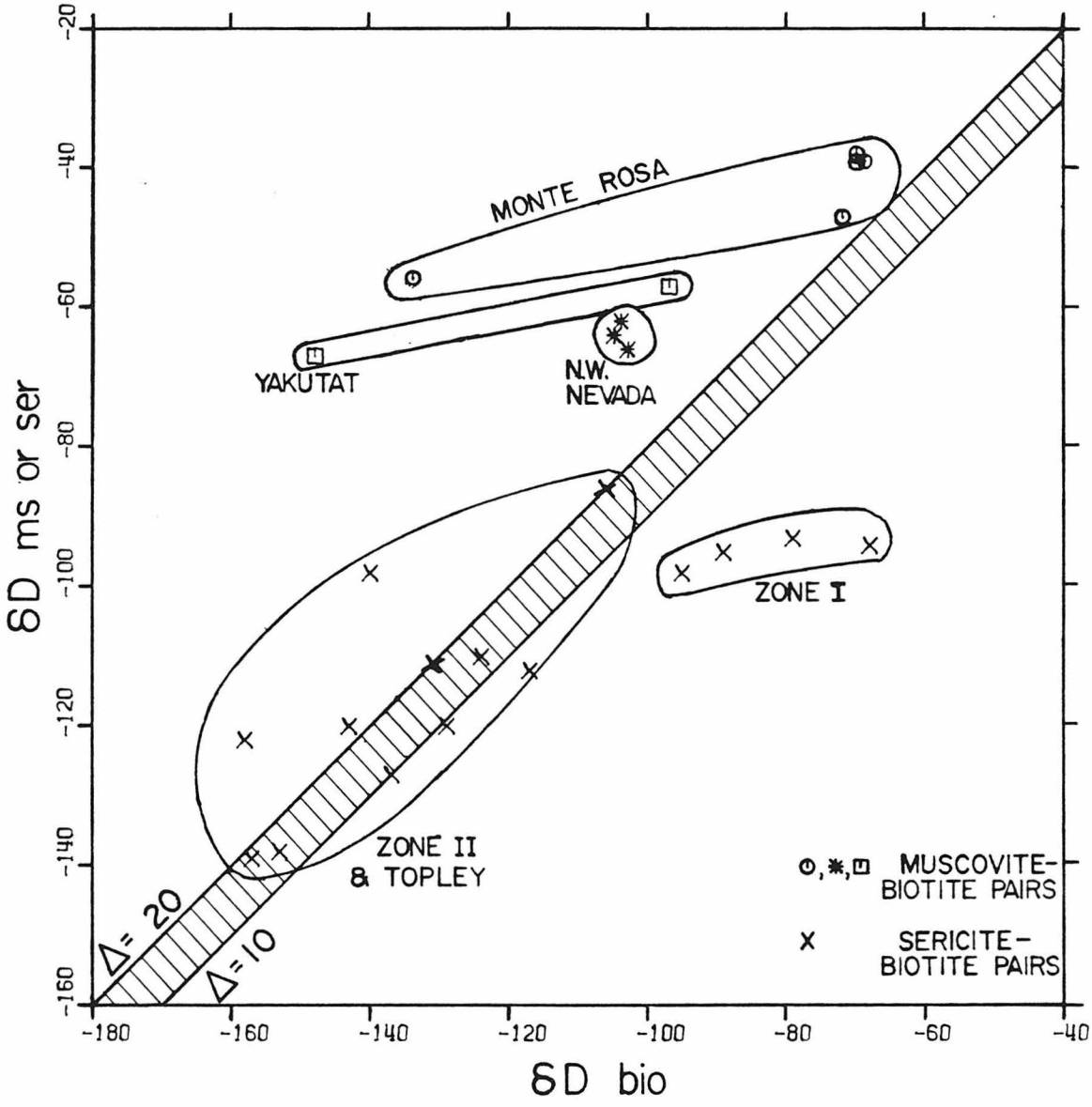
δD ms or ser
δD bio
-20
-40
-60
-80
-100
-120
-140
-160
-180
-160
-140
-120
-100
-80
-60
-40
MONTE ROSA
YAKUTAT
N.W.
NEVADA
ZONE I
ZONE II
& TOPLEY
Δ= 20
Δ=10
MUSCOVITE-
BIOTITE PAIRS
SERICITE-
BIOTITE PAIRS

contrast, the δD values of the sericites from Zone II of the Coast Range batholith and from the epizonal Topley intrusions (Fig. 5.18) are similar to, and could conceivably be in equilibrium with, the chlorite in the coexisting "biotite". This indicates that the sericites form in the presence of the meteoric-hydrothermal fluids which are known to have altered these rocks and caused chloritization of the biotite (Magaritz and Taylor, 1976b). Note that sample RK 28a from the Idaho batholith is very similar to the "Zone II" sericites (see Fig. 5.8). Magaritz and Taylor (1976b) proposed that the unusual "Zone I" samples indicate either that the temperatures of sericitization were very low, or that the water/rock ratios were very low, such that little or no chlorite was formed; it is possible that the meteoric water was totally used up in making the trace amounts of sericite in these rocks.

Figure 5.19 shows the $\delta^{18}O$ values of coexisting quartz and biotite for samples from the Coast Range batholith, the outlying Topley intrusions and the plutons in the Yakutat Bay-St. Elias area of Alaska and British Columbia (Magaritz and Taylor, 1976 a,b); also shown are a few samples from the Peninsular Ranges and Sierra Nevada batholiths (Taylor and Epstein, 1962b; Turi and Taylor, 1971; Masi et al, 1980). Only one data-point (average central zone) is shown for the Domenigoni Valley pluton from the Peninsular Ranges batholith, as the marginal samples from this pluton have all undergone exchange with the high $-^{18}O$ country rocks (Turi and Taylor, 1971). Most of the samples on Fig. 5.19 exhibit "normal" quartz-biotite fractionations of 5 ± 1 permil; the samples with significantly greater Δ-values, all of which are from northern regions, have clearly been affected by exchange with heated low $-^{18}O$ meteoric waters (Magaritz and Taylor, 1976a,b). These latter samples are thus similar to

Figure 5.19 $\delta^{18}O$ values of coexisting quartz and biotite from granitic rocks of the Peninsular Ranges, Sierra Nevada and Coast Range batholiths and some outlying plutons (data from Taylor and Epstein, 1962b; Turi and Taylor, 1971; Magaritz and Taylor, 1976 a,b). Most samples exhibit normal, primary magmatic fractionations of 5 ± 1 permil; samples with larger fractionations have probably been affected by exchange with low $-^{18}O$ heated meteoric waters. Compare Fig. 5.3.

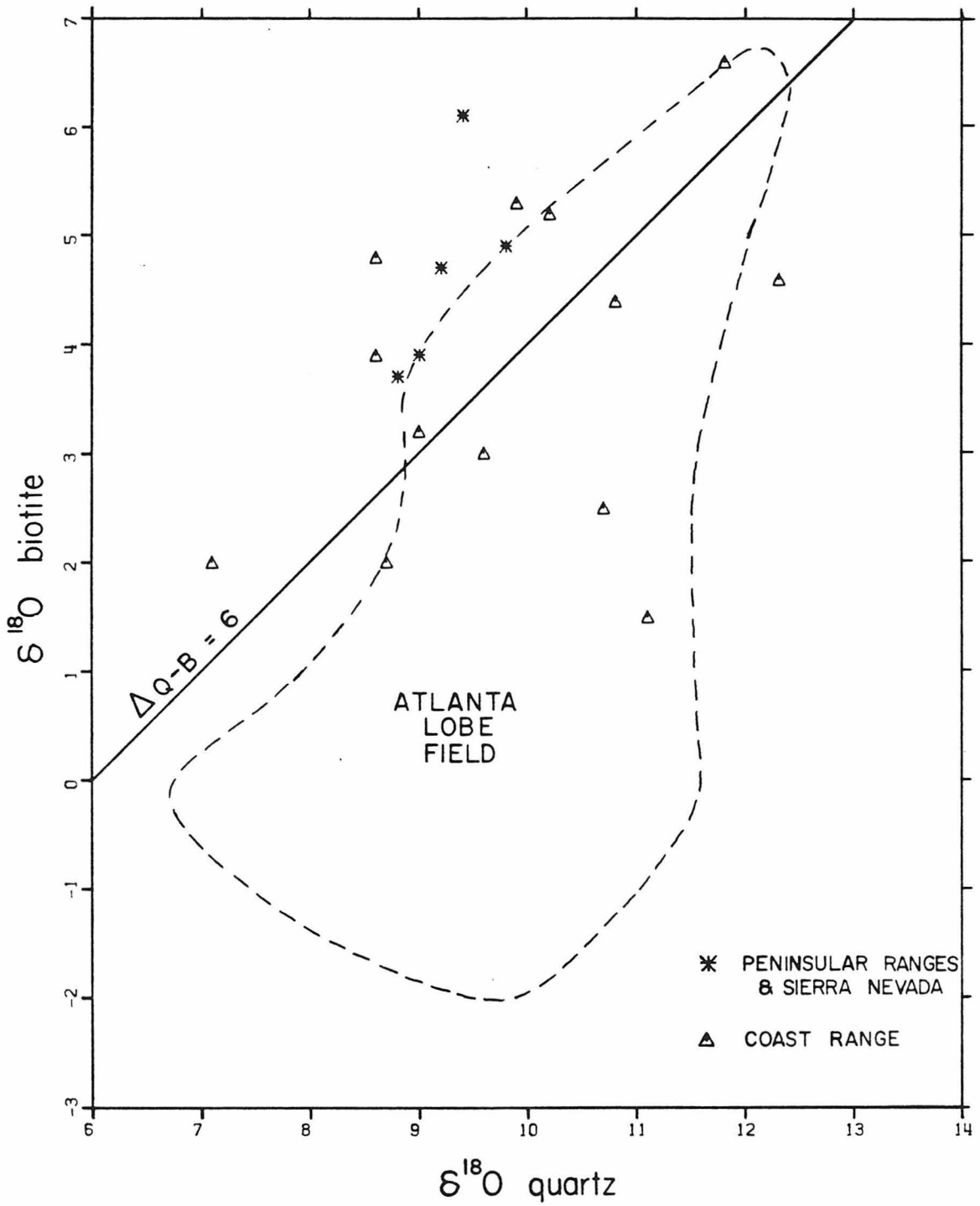
$\delta^{18}O$ biotite
$\delta^{18}O$ quartz
$\Delta Q\text{-}B = 6$
ATLANTA
LOBE
FIELD
PENINSULAR RANGES
& SIERRA NEVADA
COAST RANGE
7
6
5
4
3
2
1
0
-1
-2
-3
6
7
8
9
10
11
12
13
14

the hydrothermally altered rocks of the Idaho batholith.

5.3.1.2 Peninsular Ranges batholith

Of the major Cordilleran batholiths, the Peninsular Ranges batholith (PRB) is the best documented example of primary isotopic variations that are, in the main, unobscured by subsolidus hydrothermal effects. This batholith also has the least complicated intrusive history, having formed entirely in the Cretaceous (Silver et al, 1979).

Figure 5.20 shows quartz-feldspar $\delta^{18}O$ data from the Peninsular Ranges batholith (Taylor and Epstein, 1962b; Turi and Taylor, 1971; Taylor and Silver, 1978), together with a few samples from the Sierra Nevada batholith (Taylor and Epstein, 1962b; Masi et al, 1980). Note that in striking contrast to Figs. 5.2 and 5.15, essentially all the data in Fig. 5.20 exhibit "normal" quartz-feldspar fractionations, demonstrating that pervasive subsolidus exchange with low $-^{18}O$ hydrothermal fluids was much less common in these southerly Cordilleran batholiths. This is in part because the samples plotted in Fig. 5.20 were selected to be as free from secondary alteration effects as possible. However, this effect is mainly due to the fact that, although meteoric-hydrothermal systems are found in the PRB, they are much less abundant and more geographically restricted than in the northerly Cordilleran batholiths. As pointed out by Taylor (1977), this is a result of the total absence of Tertiary epizonal plutonism in the PRB. All of the meteoric-hydrothermal systems in the latter terrane are Cretaceous in age and are confined to a narrow strip along the extreme western edge (roof) of the batholith, where whole-rock $\delta^{18}O$ values go down to -5.0 (Taylor and Silver, 1978). In addition to

Figure 5.20 $\delta^{18}O$ values of coexisting quartz and feldspar from the Peninsular Ranges and Sierra Nevada batholiths (data from Taylor and Epstein, 1962b; Turi and Taylor, 1971; Taylor and Silver, 1978; Masi et al, 1980). In contrast to many northern batholiths, almost all of these samples display "normal, primary" igneous Δ_{Q-F} fractionations of 1.0 to 2.5 permil. The field of Atlanta lobe samples is shown to illustrate this contrast. See text.

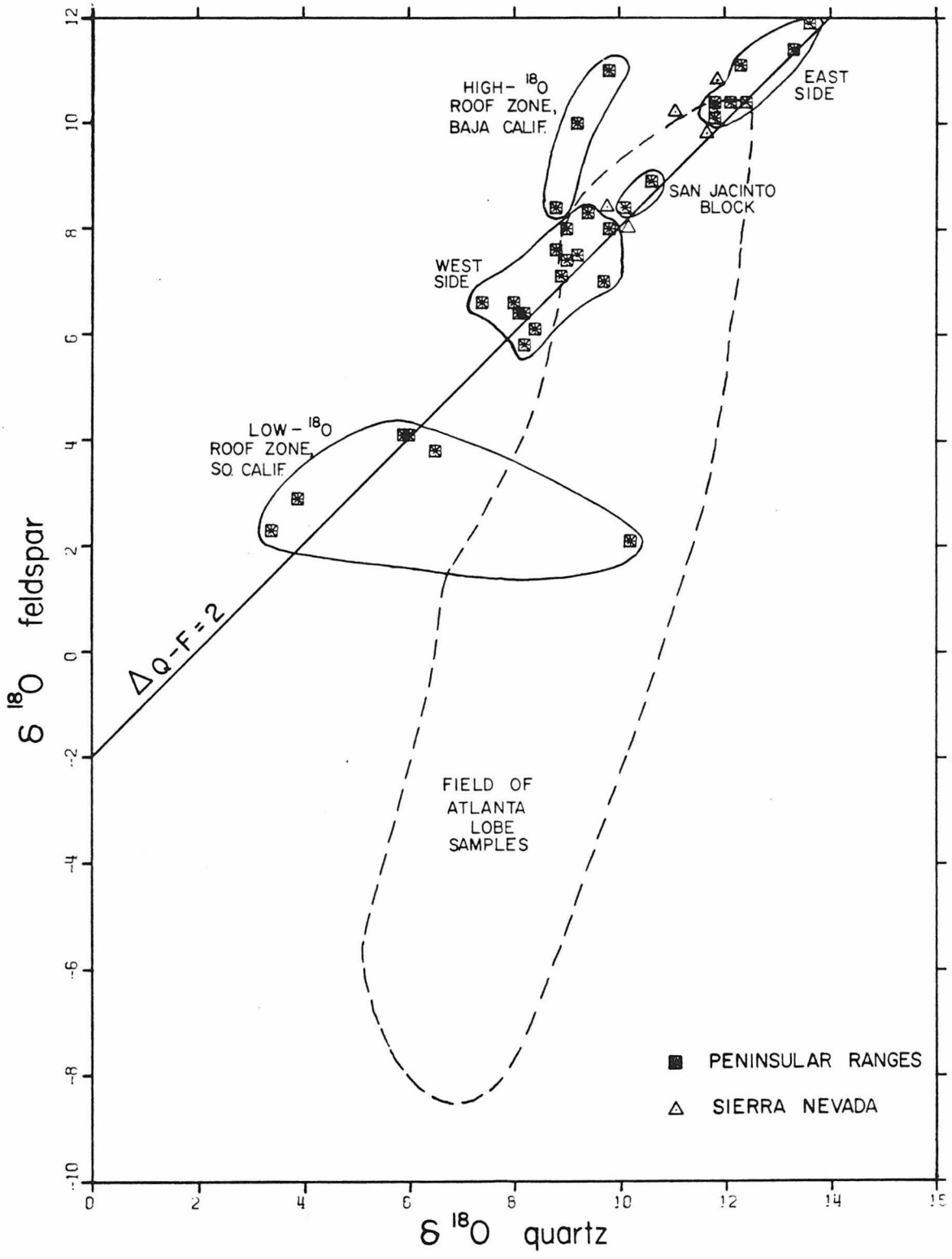
HIGH- ^{18}O ROOF ZONE, BAJA CALIF.
EAST SIDE
SAN JACINTO BLOCK
WEST SIDE
LOW- ^{18}O ROOF ZONE, SO. CALIF.
$\Delta Q-F=2$
FIELD OF ATLANTA LOBE SAMPLES
PENINSULAR RANGES
SIERRA NEVADA
$\delta^{18}O$ feldspar
$\delta^{18}O$ quartz
12
10
8
6
4
2
0
-2
-4
-6
-8
-10
0
2
4
6
8
10
12
14

these interactions with low $-^{18}0$ meteoric waters, some rocks have exchanged with high $-^{18}0$ marine pore fluids (negative Δ_{Q-F} values are found in Baja California; Taylor and Silver, 1978).

Analyses of whole-rock $\delta^{18}0$ in 140 plutons of the Peninsular Ranges batholith shows that the primary isotopic compositions range from 5.3 to 12.8, with a conspicuous, almost complete gap between 8.5 and 9.0 permil (Taylor and Silver, 1978). The whole-rock $\delta^{18}0$ values exhibit a distinct and consistent eastward increase, and except for the gabbros, which have low (<8.3) $\delta^{18}0$ values and are almost wholly restricted to the western half of the batholith, the $\delta^{18}0$ trend is essentially independent of rock type. Furthermore, the 8.5 to 9.0 permil $\delta^{18}0$ gap nearly coincides with a transition from relatively shallow-level gabbro, tonalite and high-SiO_2 granodiorite plutons on the west, with U-Pb zircon ages of 105 to 130 m.y., to deeper-seated sphene-rich tonalite and low-K granodiorite plutons with zircon ages of 80 to 103 m.y. in the east (Silver et al, 1979). Last, most of the samples show a distinct positive correlation of $\delta^{18}0$ with the initial $^{87}Sr/^{86}Sr$ ratios of Early and Silver (1973); Taylor and Silver (1978) suggest that this represents melting, assimilation, or exchange of radiogenic, high $-^{18}0$ rocks with a primitive (mantle ?) source material at depth.

Note that Masi et al (1980) did not observe a clearcut correlation between $\delta^{18}0$ and initial $^{87}Sr/^{86}Sr$ in the Sierra Nevada batholith. This is probably because the Sierra Nevada batholith has a much more complex intrusive history, involving superposition of both Jurassic and Cretaceous plutonic arcs. In addition, it is interesting to note that almost all of the Sierran granites which have δD values greater than -70 do show

Sr isotope - oxygen isotope patterns similar to those of the Peninsular Ranges batholith; this may indicate that weak meteoric-hydrothermal activity has disturbed the $^{87}Sr/^{86}Sr$ ratios in many of the low-D rocks.

Few δD measurements are available from the Peninsular Ranges batholith. Turi and Taylor (1971) report that biotites from the Domenigoni Valley pluton range from -65 to -74, and several biotites analyzed by Mattson and Taylor (unpub.), including a sample from the western low ^{18}O zone, range from -55 to -65 permil. Most of these values are regarded as primary, and the similar analysis from the low ^{18}O zone indicates that the meteoric waters responsible for the alteration were considerably enriched in deuterium compared to those of the northerly batholiths; this is compatible with the southerly and coastal occurrence of this batholith. Also, the southernmost (Baja California) part of the batholith is known to have formed as a true island arc, thus explaining the local interactions with marine pore fluids (Silver et al, 1963; Taylor and Silver, 1978).

5.3.2 Whole Rock Isotopic Comparisons with other Cordilleran Batholiths

In spite of the pervasive hydrothermal activity, the primary $\delta^{18}O$ and δD composition of the Idaho batholith can be shown to be broadly similar to that of other Cordilleran batholiths and to most deep-seated plutonic rocks in the world (see Sec. 5.2; also see Taylor and Magaritz, 1978; Taylor, 1968, 1977). This section will undertake a more detailed examination and comparison of the Idaho data with the primary isotopic variations in other Cordilleran batholiths.

5.3.2.1 $\delta^{18}O$ data

Figure 5.21 summarizes the range of whole-rock $\delta^{18}O$ values of the Cordilleran batholiths of North America, which are approximately arranged according to latitude. Included are analyses from the Coast Range batholith and outlying plutons (Magaritz and Taylor, 1976 a,b; Taylor and Magaritz, 1978), the Boulder batholith of Montana (Garlick and Epstein, 1966; Sheppard and Taylor, 1974), the Idaho batholith (Taylor and Magaritz, 1976, 1978; this study), the Klamath Mts. and Coast Ranges of California (Masi et al, 1980), the Sierra Nevada batholith (Masi et al, 1976, 1980; Taylor and Epstein, 1962b), and the Peninsular Ranges batholith (Taylor and Silver, 1978; Taylor and Epstein, 1962b; Turi and Taylor, 1971).

The whole-rock $\delta^{18}O$ values of these batholiths commonly show a wide range (ca. -5 to + 12.8). This is true for most of the northern batholiths, and also for the Peninsular Ranges batholith (Fig. 5.20). It is clear from these studies that the wide $\delta^{18}O$ range in these regions is in large part the result of subsolidus hydrothermal activity, which typically produces ^{18}O depletions in the rocks. Accordingly, on Fig. 5.21 an attempt has been made to estimate the primary range of whole-rock $\delta^{18}O$ in these batholiths (hatched pattern); this was accomplished either by inspection of available measurments of quartz, or alternatively by inspection of feldspar and whole-rock $\delta^{18}O$ values in rocks which have the highest δD values. Thus, in many cases the "primary" $\delta^{18}O$ range has been estimated rather than directly measured.

Figure 5.21 shows that the primary $\delta^{18}O$ compositions of all the great Cordilleran batholiths are similar and generally restricted to the range $\delta^{18}O$ = + 5 to + 13, with the great majority of rocks lying in the range +7

Figure 5.21 Ranges of whole-rock $\delta^{18}O$ and biotite or whole-rock δD values of major Cordilleran batholiths and isolated plutons, arranged according to latitudes. In many cases the range of whole-rock $\delta^{18}O$ was estimated from measurements of feldspar. The primary magmatic $\delta^{18}O$ compositions are shown by the ruled pattern; in cases where the primary range is less than the total range, primary values were distinguished from those produced by subsolidus alteration effects by inspection either of quartz-feldspar fractionations or δD values. The "primary range" in δD compositions is also shown by a ruled pattern, and was simply assumed to lie between -50 and -75 permil. Note that almost all the major Cordilleran batholiths have primary whole-rock $\delta^{18}O$ values within the range +5 to +13, but that hydrothermal alteration has produced marked ^{18}O depletions in many localities - especially in the northern batholiths. Deuterium depletions are also systematically greater in northern regions.

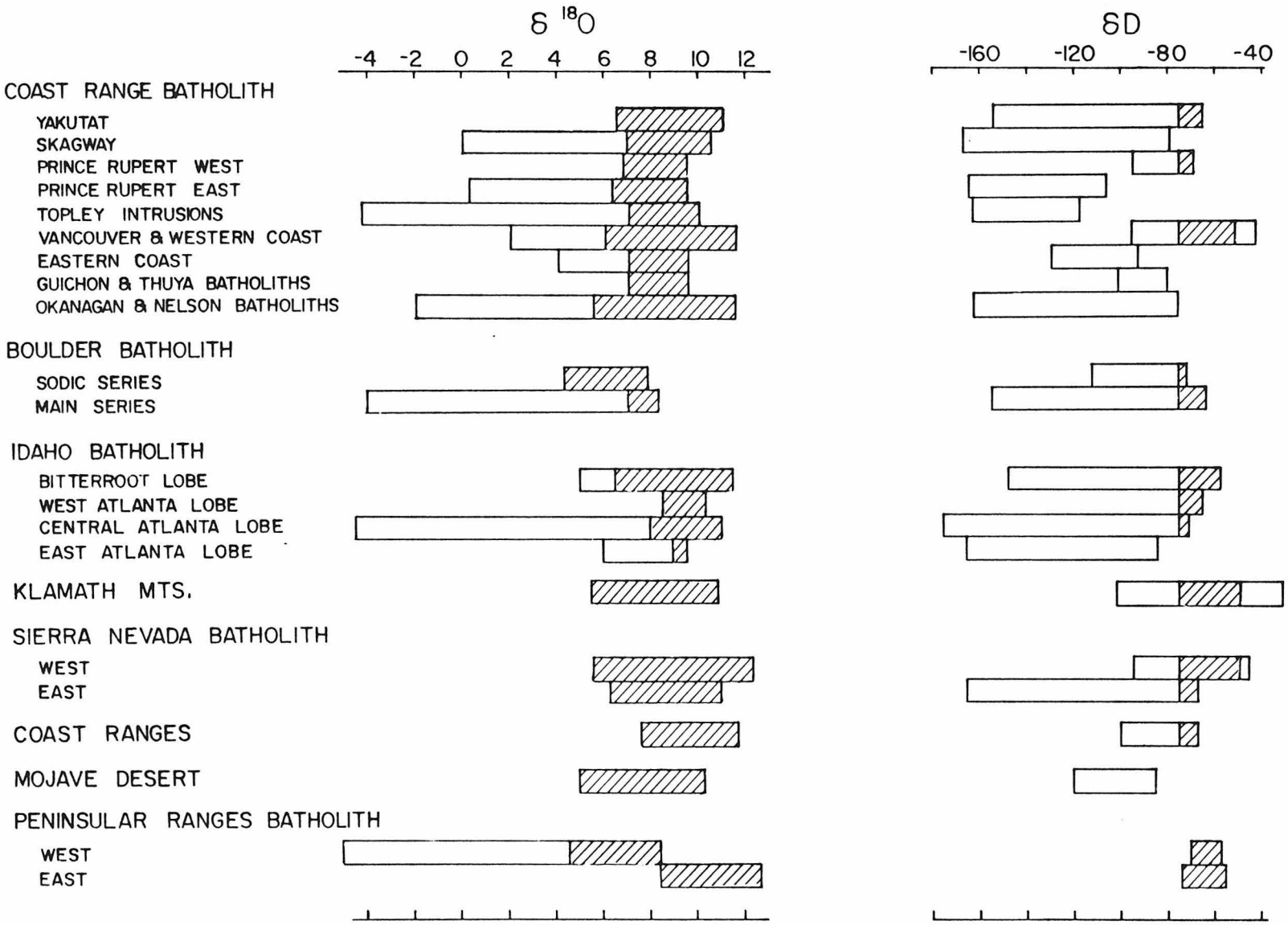
δ 18O
-4 -2 0 2 4 6 8 10 12
δD
-160 -120 -80 -40
COAST RANGE BATHOLITH
YAKUTAT
SKAGWAY
PRINCE RUPERT WEST
PRINCE RUPERT EAST
TOPLEY INTRUSIONS
VANCOUVER & WESTERN COAST
EASTERN COAST
GUICHON & THUYA BATHOLITHS
OKANAGAN & NELSON BATHOLITHS
BOULDER BATHOLITH
SODIC SERIES
MAIN SERIES
IDAHO BATHOLITH
BITTERROOT LOBE
WEST ATLANTA LOBE
CENTRAL ATLANTA LOBE
EAST ATLANTA LOBE
KLAMATH MTS.
SIERRA NEVADA BATHOLITH
WEST
EAST
COAST RANGES
MOJAVE DESERT
PENINSULAR RANGES BATHOLITH
WEST
EAST

to + 11. No obvious geographic or temporal $\delta^{18}O$ relationships appear to be common to all of these batholiths, except that rocks in the low portion of the primary range are most common in the relatively mafic portions of these batholiths (i.e. the portions which lie west of the quartz diorite line). The primary range in $\delta^{18}O$ probably reflects the fact that the magmas that produced these batholiths were derived from both mantle (low ^{18}O) and crustal (high ^{18}O) sources (c.f. Taylor and Silver, 1978). Note that most of the $\delta^{18}O$ and $^{87}Sr/^{86}Sr$ values of these batholiths overlap the isotopic values observed in the hydrous, hydrothermally-altered rocks which comprise the upper portions of ophiolite sequences (Gregory and Taylor, 1980; McCulloch et al, 1980), and such rocks would presumably be easily melted during subduction of ancient oceanic slabs. However, the $\delta^{18}O$ and $^{87}Sr/^{86}Sr$ data, together with available $^{143}Nd/^{144}Nd$, $^{206}Pb/^{204}Pb$, $^{207}Pb/^{204}Pb$ and $^{208}Pb/^{204}Pb$ data, demonstrate that a significant crustal component must also be involved in the generation of many of these magmas (DePaolo, 1979; Jacobsen, pers. comm.).

5.3.2.2 δD variations

Figure 5.21 also shows the range of δD contents of biotite, hornblende and/or whole-rocks of the Coast Range batholith and outlying plutons (Magaritz and Taylor, 1976 a,b; Taylor and Magaritz, 1978), the Boulder batholith (Sheppard and Taylor, 1974), the Idaho batholith (Taylor and Magaritz, 1976, 1978; this study), the Klamath Mts. and Coast Ranges of California (Masi et al, 1980; Godfrey, 1962), and the Peninsular Ranges batholith (Turi and Taylor, 1971; Mattson and Taylor, unpub.). The primary range of δD in these rocks is assumed to be represented by analyses with

δD of -50 to -75, shown by the hatched pattern. Note that all of the analyses from certain regions lie within this "primary" range (e.g. Peninsular Ranges; west Atlanta lobe). Rocks with δD less than -75 have in most or all cases undergone exchange with meteoric-hydrothermal fluids (see below); the heaviest δD values (e.g. -31 for Klamath Mts.; Masi et al, 1980) represent whole-rock measurements, and it is possible that some of these rocks contain sericite and/or epidote, both of which are known to strongly concentrate deuterium relative to biotite and hornblende.

Figure 5.21 shows that deuterium depletions become progressively larger and more common as the latitude increases, as is also shown by Figure 5.22a (Taylor and Magaritz, 1978). In many areas the δD values also become more negative as the distance from the coastline increases, as is shown for the Prince Rupert traverse and also areas in southern British Columbia (Fig. 5.22b; Taylor and Magaritz, 1978), as well as for the Sierra Nevada batholith (Masi et al, 1980). These systematics are probably related to the ordinary geographic variations in δD of meteoric waters, which become progressively depleted in deuterium as latitude increases and as the distance to the ocean increases (e.g. Friedman et al, 1964). Hydrothermal exchange of the rocks with waters of this type could thus account for the observed variations (Taylor and Magaritz, 1978). On the other hand, Masi et al (1980) believe that all the δD values in the Sierra Nevada batholith reflect the fundamental chemistry of the rocks and are thus primary; however, they did not completely rule out the possibility that weak meteoric water effects have influenced the δD values in some of the felsic rocks.

Figure 5.22a Histograms of δD values of the major Cordilleran batholiths. The proportion of low δD values become systematically greater as the latitude increases from southern California to the Coast Range batholith. See text. From Taylor (1977).

Figure 5.22b δD values of granitic rocks from southern British Columbia, plotted according to their distance from the Pacific coastline. The δD values systematically decrease as the distance increases, which is a characteristic shared with δD values of modern meteoric waters. See text. From Magaritz and Taylor (1976b).

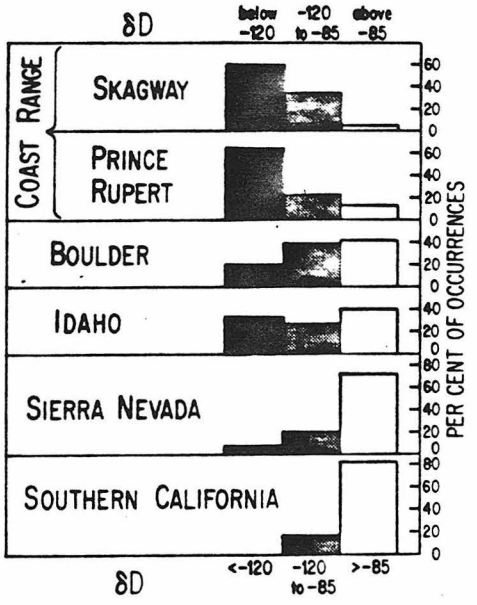

Fig. 5.22a

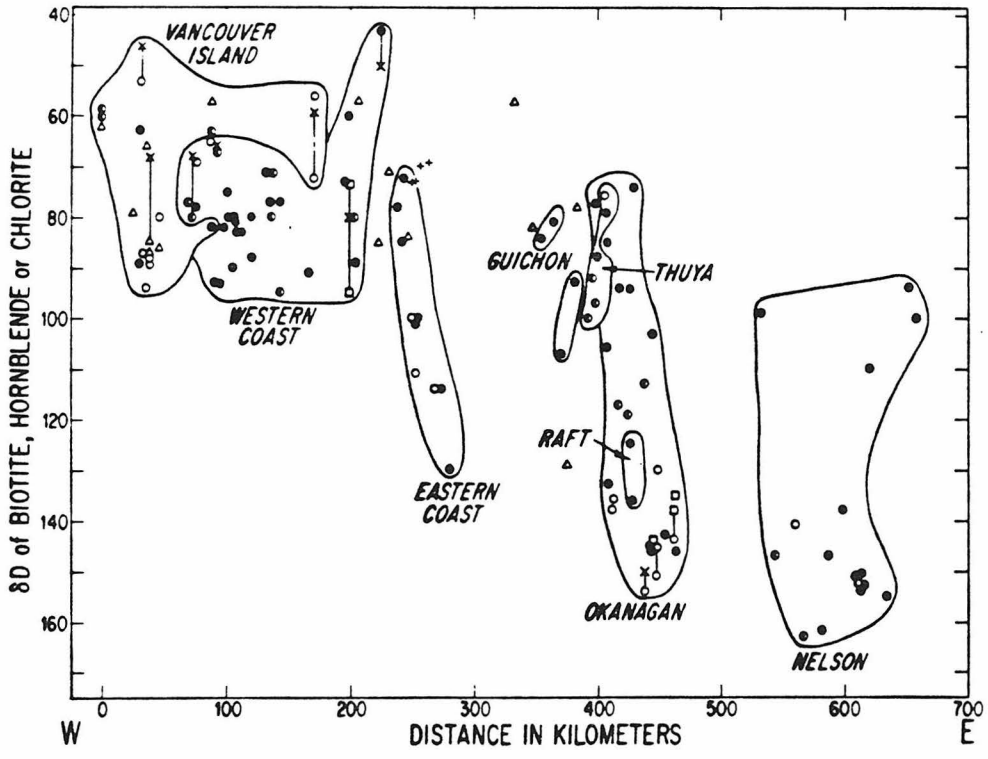

Fig. 5.22b

5.3.2.3 Discussion of the whole-rock $\delta^{18}O$ data

Whole-rock $\delta^{18}O$ data of batholiths provide important information about the source materials from which the granitic magmas were derived. This section discusses the implications of the $\delta^{18}O$ data to the nature of the source materials of the Cordilleran batholiths, and also considers the implications of the Idaho batholith data to the genesis of low $-^{18}O$ magmas.

It is clear from Fig. 5.20 that the primary range of $\delta^{18}O$ in the Mesozoic plutons of the Atlanta lobe is appreciably smaller than in the Peninsular Ranges batholith (PRB). Analogs of both the extreme low $-^{18}O$ endmembers and the extreme high $-^{18}O$ endmembers of the PRB are missing in Idaho. The only large zone in the PRB where the $\delta^{18}O$ values resemble the $\delta^{18}O$ of the Atlanta lobe is the San Jacinto block. This is interesting because the latter zone lies closest to the nearest known outcrops of Precambrian basement, and is the only part of the PRB where the $\delta^{18}O$ and $^{87}Sr/^{86}Sr$ systematics, as well as the presence of some older inherited zircons, indicate the possible involvement of ancient continental craton in the melting process (Taylor and Silver, 1978).

Excluding the San Jacinto block, even the highest $-^{18}O$ rocks from the east side of the PRB all have $^{87}Sr/^{86}Sr$ initial ratios less than 0.707 (Taylor and Silver, 1978). Although the initial $^{87}Sr/^{86}Sr$ values in the Mesozoic plutons of the Atlanta lobe are difficult to determine because of the paucity of precise age dates based on zircon geochronology, it is clear that the bulk of these Idaho plutons have $^{87}Sr/^{86}Sr$ of about 0.707 or higher, suggestive of some type of interaction with the craton (Armstrong et al, 1977). Also, the Precambrian basement is known to

underlie much of the Idaho batholith (Armstrong, 1975b). The bulk chemistry and petrology of the Idaho batholith (quartz monzonite and granodiorite with very little tonalite and virtually no gabbro) is also markedly different from the Peninsular Ranges batholith (dominantly tonalite, with abundant gabbro on the west side). All of the presently available data thus suggest that the source materials of the Idaho batholith magmas were completely different from the bulk of the Peninsular Ranges batholith. Both the low $-^{18}O$ west side of the PRB (mantle component) and the high $-^{18}O$ east side of the PRB (a component derived from altered pillow basalts in subducted oceanic crust, and/or Franciscan-type metasediments) appear to be absent from the Atlanta lobe. The only exceptions to this generalization may be a very narrow strip along the extreme west side of the Atlanta lobe, which bears some resemblance to the highest $-^{18}O$ west-side tonalites (Bonsall-type) in the PRB that are abundant along the central axis of that batholith just west of the ^{18}O step (Taylor and Silver, 1978). The chemical and isotopic differences between the Idaho and Peninsular Ranges batholiths appear to be largely explicable in terms of the types of country rocks found at depth in the two regions. The PRB represents an unroofed island arc (Baja California) transitional onto young continental crust (southern California) marginal to the continental craton, whereas the Idaho batholith was mostly emplaced well inside the craton. The Sierra Nevada batholith contains representatives of all these petrologic zones and may be considered to be somewhat intermediate between the two types; it is also intermediate in its isotopic and chemical characteristics.

The Eocene granitic magmas of the Idaho batholith (see Fig. 5.13) also

have no petrologic counterpart in the Peninsular Ranges batholith. They are much more alkalic than any of the granitic rocks in the PRB (Sec. 2.4.1), even though their estimated whole-rock $\delta^{18}O$ values (about +8.5 to +9.5) are similar to those of plutons in the San Jacinto block of the PRB. Also, the Eocene Idaho plutons were emplaced at much shallower depths than any of the plutons in the San Jacinto block.

$\delta^{18}O$ data of batholiths also bear on the genesis of low $-^{18}O$ granitic magmas, which are typically defined as silicate <u>melts</u> with $\delta\ ^{18}O < 6$. It is extremely difficult to develop clear-cut criteria proving the existence of such low $-^{18}O$ magmas in plutonic environments. This is because of the ubiquitous subsolidus ^{18}O-depletions in essentially all terranes where such low $-^{18}O$ magmas are suspected (see the extensive discussions of Taylor, 1974; Forester and Taylor, 1977). One of the possible lines of evidence for such low $-^{18}O$ magmas is the presence of low $-^{18}O$ quartz or of quartz-feldspar ^{18}O systematics that fall off the types of 4:1 exchange trends shown in Figs. 5.2 and 5.15. For example, some of the PRB samples from the low $-^{18}O$ roof zone shown in Fig. 5.20 also have almost "normal" Δ_{Q-F} values and <u>could</u> represent low $-^{18}O$ magmas. However, this effect in the PRB could also be due to the relatively high $-^{18}O$ meteoric waters involved in the alteration or to the fact that these samples contain extremely fine-grained quartz that is very susceptible to ^{18}O exchange. The above-described difficulties are either much reduced or non existent where fresh, unaltered volcanic rocks are concerned. In fact, Friedman et al (1974) and Lipman and Friedman (1975) have demonstrated the existence of several eruptions of low $-^{18}O$ magmas from large silicic volcanic centers, and Hildreth et al (1980) have found evidence for an eruption of a vast

volume ($\approx$ 80 km^3) of rhyolite with $\delta^{18}O \approx 0$ at Yellowstone.

In spite of the difficulties of proving or disproving the existence of low $-^{18}O$ magmas in plutonic environments, it seems clear from the isotopic systematics shown in Figs. 5.2 and 5.13 that none of these Atlanta lobe rocks crystallized from low $-^{18}O$ magmas. In fact, no Atlanta lobe magma with $\delta^{18}O < 8$ has yet been identified. This is an important conclusion because of the massive evidence for deep circulation of meteoric-hydrothermal fluids in the Idaho batholith and the abundant evidence for eruption of low $-^{18}O$ magmas in several large silicic volcanic centers associated with calderas elsewhere in the world. The discrepancy is tentatively attributed to the likelihood that the low $-^{18}O$ magmas are very volatile-rich because they are formed by stoping and interaction with hydrothermally altered roof rocks (Taylor, 1977). Because these low-^{18}O magmas are so H_2O-rich and because they form the extreme upper parts of zoned magma chambers (McBirney, 1980), they may typically (invariably?) be erupted as gigantic ash-flow tuff deposits rather than being intruded as epizonal plutons. It is very important to continue gathering data in deeply eroded caldera environments and to continue looking for evidence for the existence of the types of low $-^{18}O$ magmas that seem to be very commonly represented in the sequences of ash-flow tuff eruptions associated with rhyolitic volcanic centers and calderas. Nonetheless, at the present time, the Atlanta lobe of the Idaho batholith represents by far the best studied example of the lower portions of such caldera systems, and <u>no</u> evidence for any low $-^{18}O$ magma has yet been forthcoming. The only possible exceptions to this statement are some low $-^{18}O$ porphyry dike rocks described below in Sec. 5.4.2. However, even these samples

are probably best interpreted as resulting from subsolidus ^{18}O depletion during meteoric-hydrothermal alteration.

5.4 Nature of the Hydrothermal Interaction

5.4.1 Water/Rock Ratios

5.4.1.1 $^{18}O/^{16}O$ Relationships

Provided that equilibrium is attained in a closed system involving just rock and hydrothermal fluid, it is possible to calculate the total amounts of water involved in interactions with the volume of rock occupied by the geothermal system. This is determined by the temperature and the initial isotopic compositions of the water ($\delta_i W$) and rock($\delta_i R$). Under these conditions the conservation relation is:

$$\frac{W}{R} = \frac{\delta_f R - \delta_i R}{\delta_i W - (\delta_f R - \Delta)}$$

where W/R is the ratio of oxygen contents of the water and rock involved in the exchange, $\delta_f R$ is the δ-valve of the altered rock, and Δ is the fractionation factor at the appropriate temperature (Taylor, 1977). Alternatively, under open system conditions where each small packet of fluid equilibrates with the rock and then moves out of the system, this becomes by integration (Taylor, 1977):

$$\frac{W}{R} = \ln \left\{ \frac{\delta_i W + \Delta - \delta_i R}{\delta_i W - (\delta_f R - \Delta)} \right\}$$

or

$$\frac{W}{R} = \ln \left\{ (W/R)_{closed} + 1 \right\}$$

These equations allow the interrelationships between the variables to be deduced, as shown in Fig. 5.23, which was designed to be applicable to hydrothermally altered rock of the Idaho batholith. $\delta_i R$ was taken as the $\delta^{18}O$ value of feldspar in normal rock of the region (+8.5), $\delta_f R$ represents the measured $\delta^{18}O$ values of feldspar in altered rock, and Δ indicates alkali feldspar-water fractionation at 150°, 250°, and 350°C (O'Neil and Taylor, 1967). These temperatures and the value of $\delta_i W = -16$ will be justified in section 5.4.4.

The figure shows that overall water to rock ratios of about 0.5 to 10 (closed) or 0.5 to 2.5 (open) characterize the strongly altered rocks shown on the histogram in Fig. 5.1. Note that these crude estimates of the water/rock ratio actually indicate the minimum amount of water required to cause the observed isotopic depletions in the rocks, because they are based on a $\delta_i W$ value of -16. Because any water-rock interactions will increase the $\delta^{18}O$ value of the fluid to values greater than -16, any previous interactions in the convective system will reduce the capacity of the water to lower the ^{18}O content of rock it subsequently encounters. Furthermore, if equilibrium is not achieved the ^{18}O depletion of the rock would not be as large as indicated. Thus these numbers are minimum estimates of the true water/rock ratios in natural systems. Note that, because of the lack of attainment of $^{18}O/^{16}O$ equilibrium between quartz and feldspar, the measured isotopic fractionations in rocks that have undergone hydrothermal exchange cannot be used to calculate the temperature of alteration. For example, in rocks that have encountered very small water to rock ratios, the feldspar ^{18}O content will shift only slightly and the quartz value not at all, so the inferred "temperature" of alteration would be almost magmatic. In rocks altered with large

Figure 5.23 Calculated $\delta^{18}O$ values of feldspar (initially +8.5 permil) altered at different W/R ratios with fluid of $\delta^{18}O$ = -16 at temperatures of 150°, 250°, and 350° C. Feldspar - H_2O fractionations from O'Neil and Taylor (1967). See text.

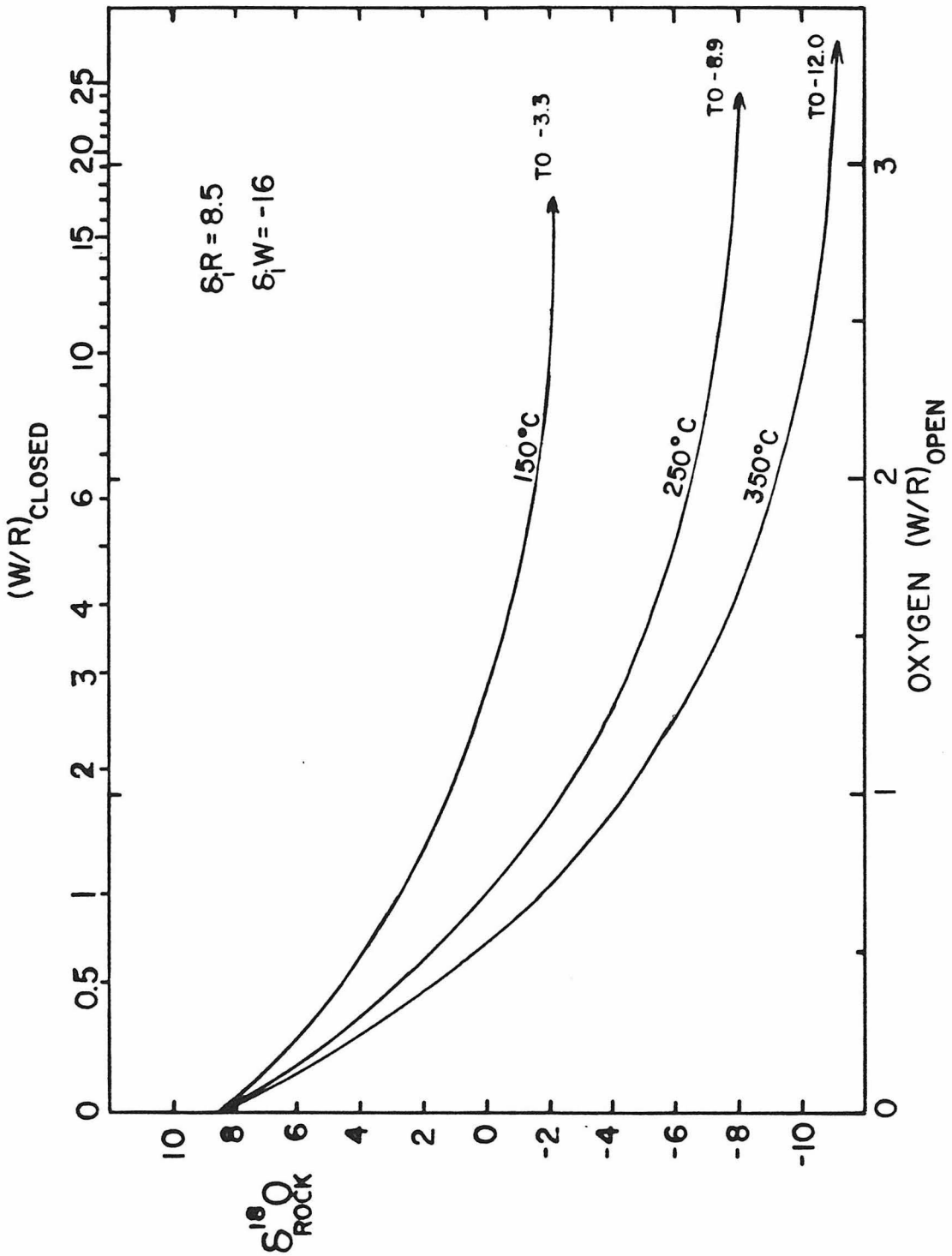
$\delta^{18}O_{ROCK}$
10
8
6
4
2
0
-2
-4
-6
-8
-10
0
0.5
1
2
3
4
6
10
15
20
25
$(W/R)_{CLOSED}$
0
1
2
3
OXYGEN $(W/R)_{OPEN}$
$\delta_1 R = 8.5$
$\delta_1 W = -16$
150°C
250°C
350°C
TO -3.3
TO -8.9
TO -12.0

amounts of water, the sluggish equilibration rate of quartz compared to that of feldspar usually results in measured fractionations that are very large, hence "equilibrium temperature" estimates based on isotope geothermometry will be much too low. Between these extremes, rocks altered with moderate amounts of water may fortuitously display measured quartz-feldspar ^{18}O fractionations appropriate for their alteration temperatures.

5.4.1.2 D/H relationships

Many of the observed D/H relationships are also codified by water-rock calculations. Figure 5.24 shows such calculations modeled to represent hydrothermal alteration in the batholith. The values of $\delta_i R$ and $\delta_i W$ were taken as -65 and -115 respectively, and the water-biotite isotopic fractionations were taken from Suzuoki and Epstein (1976). It is essential to realize that the W/R values shown on the abscissa are calculated on the basis of hydrogen contents, and are much higher (by a factor of ~ 100) than W/R ratios calculated on an oxygen basis. This is because 100g of granite which is 10% biotite by weight contains about 3 moles (48g) of oxygen but only about 0.02 moles (0.04g) of hydrogen (as H_2). Thus a small amount of water reacting with a given quantity of rock will have a very high (W/R) hydrogen ratio, and thus can drastically influence the δD value of the rock. To take a specific example, a (W/R) hydrogen ratio of 3 on Fig. 5.24 would translate approximately to a (W/R) oxygen ratio of 0.02 on Fig. 5.23. If a rock were equilibrated with the water at moderate temperatures under these conditions, the δD value of biotite would be almost completely shifted but the ^{18}O content of feldspar would remain essentially unchanged.

As in the case for (W/R) oxygen ratios, (W/R) hydrogen ratios based

Figure 5.24 Calculated δD values of biotite (initial δD = -65 permil) altered at various W/R ratios with fluid of δD = -115 at temperatures of 150°, 250°, and 350°C. Fractionation factors between biotite and water from Suzuoki and Epstein (1976); chlorite formation is not considered. Note that these hydrogen W/R ratios have a significantly different meaning than the oxygen W/R ratios of Fig. 5.23; see text.

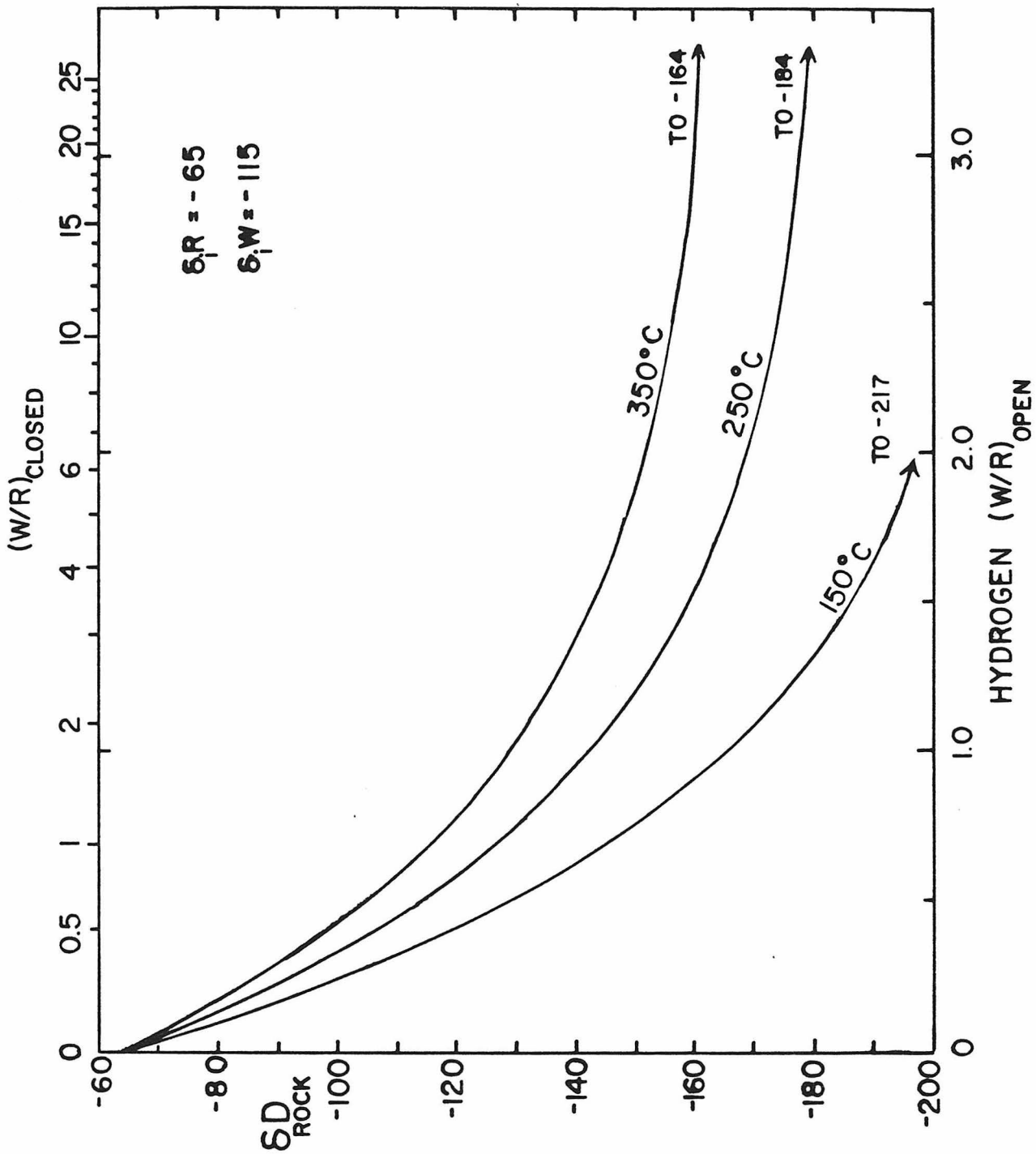
$\delta_i R = -65$
$\delta_i W = -115$
350°C
250°C
150°C
TO -164
TO -184
TO -217
δD_{ROCK}
$(W/R)_{CLOSED}$
HYDROGEN $(W/R)_{OPEN}$
-60
-80
-100
-120
-140
-160
-180
-200
0
0.5
1
2
4
6
10
15
20
25
1.0
2.0
3.0

on δD values of minerals are minimum estimates of the actual W/R ratios. Figures 5.10 and 5.11 show that the $\delta^{18}O$ contents of the analyzed biotite-chlorite mixtures are significantly lowered for all rocks with δD values of less than -100 permil (or $K_2O < 8.5$ %), which indicates that W/R ratios calculated from the δD values are probably lower than the actual ratios by a factor of approximately 5 to 10. This result does not invalidate any of the general concepts outlined above, but illustrates that the accuracy of estimated W/R ratios is influenced by the relative rates at which the different minerals tend toward equilibrium.

The above considerations suggest that in rocks showing strong ^{18}O exchange the hydroxyl minerals are probably completely deuterium-shifted and thus in approximate D/H equilibrium with the fluid, inasmuch as the effective W/R ratio for hydrogen would be extremely large. Furthermore, the fluid would not be expected to exhibit a significant "deuterium shift" in this case. These conditions permit the calculation of the initial isotopic composition of the water from the δD value of the altered biotite provided that the temperature is known. Using the fractionation factors of Suzuoki and Epstein (1976), biotite with a δD value of -175 would be in equilibrium with fluid with a δD value of -68 at 150°C, -106 at 250°C, and -126 at 350°C. The higher temperatures (250-350°C) are probably most realistic for these strongly altered rocks in the Idaho batholith, as will be elaborated on more fully below.

It was mentioned above that the "biotite" in altered rocks actually represents a mixture of biotite and chlorite. It will be shown in Section 7.2 that the δD values of this chlorite and biotite are probably about -150 and -175, respectively, in highly altered rocks, and that coexisting muscovite is about -155. These muscovite δD values could reasonably have

been in equilibrium with fluid of δD -115 at ~ 300°C (Suzuoki and Epstein, 1976); the water-chlorite fractionations are too poorly known to permit a check on this estimated value.

5.4.2 Evidence from Tertiary Dike Rocks

$\delta^{18}O$ analyses of several lamprophyre, rhyolite, and porphyry dikes provide important information about the timing of the hydrothermal activity in the Atlanta lobe. At several localities the $\delta^{18}O$ values of these dikes are either similar to, or less than, the $\delta^{18}O$ values of the host granitic rocks form the same outcrops (Fig. 5.25; Table 4.3), as was observed by Magaritz and Taylor (1976b) for Tertiary dike rocks crosscutting the Coast Range batholith in British Columbia (Fig. 5.26). This result indicates that none of the analyzed dikes completely post-date the hydrothermal activity. The fractures occupied by the dikes were probably the zones of influx of hydrothermal fluids and in general the influx apparently continued even after dike emplacement.

In cases where the $\delta^{18}O$ values of the dikes are significantly lower than the host rock, it is probable that: (1) the fine grain size of the dikes renders them more susceptible to exchange, and (2) there are probably small-scale ^{18}O gradients centered on the dikes and fractures. Similar features have been observed by Magaritz and Taylor (1976b) and Forester and Taylor (1977). However, there are also significant differences in the ages and petrographic characteristics of the Atlanta lobe dikes, and these parameters appear to correlate with the $\delta^{18}O$ data. With one significant exception (RH 123b), most of the dikes which fall well below the line defining the locus of equal host rock and dike $\delta^{18}O$ values are "quartz monzonite porphyry" dikes, a type which Reid (1963) considers to predate the emplacement of the Sawtooth batholith (Dike Group 1 of

Figure 5.25 Graph comparing the $\delta^{18}O$ values of Tertiary dike rocks (mostly whole-rock data) with feldspar from nearby Atlanta lobe granitic host rocks. The oldest dikes (quartz monzonite porphyries, QMP) are typically much lower in $\delta^{18}O$ than the adjacent host rocks, but younger dikes tend to have $\delta^{18}O$ values similar to those of the host granitic rocks and thus plot near the "1:1" line of equal values. See text.

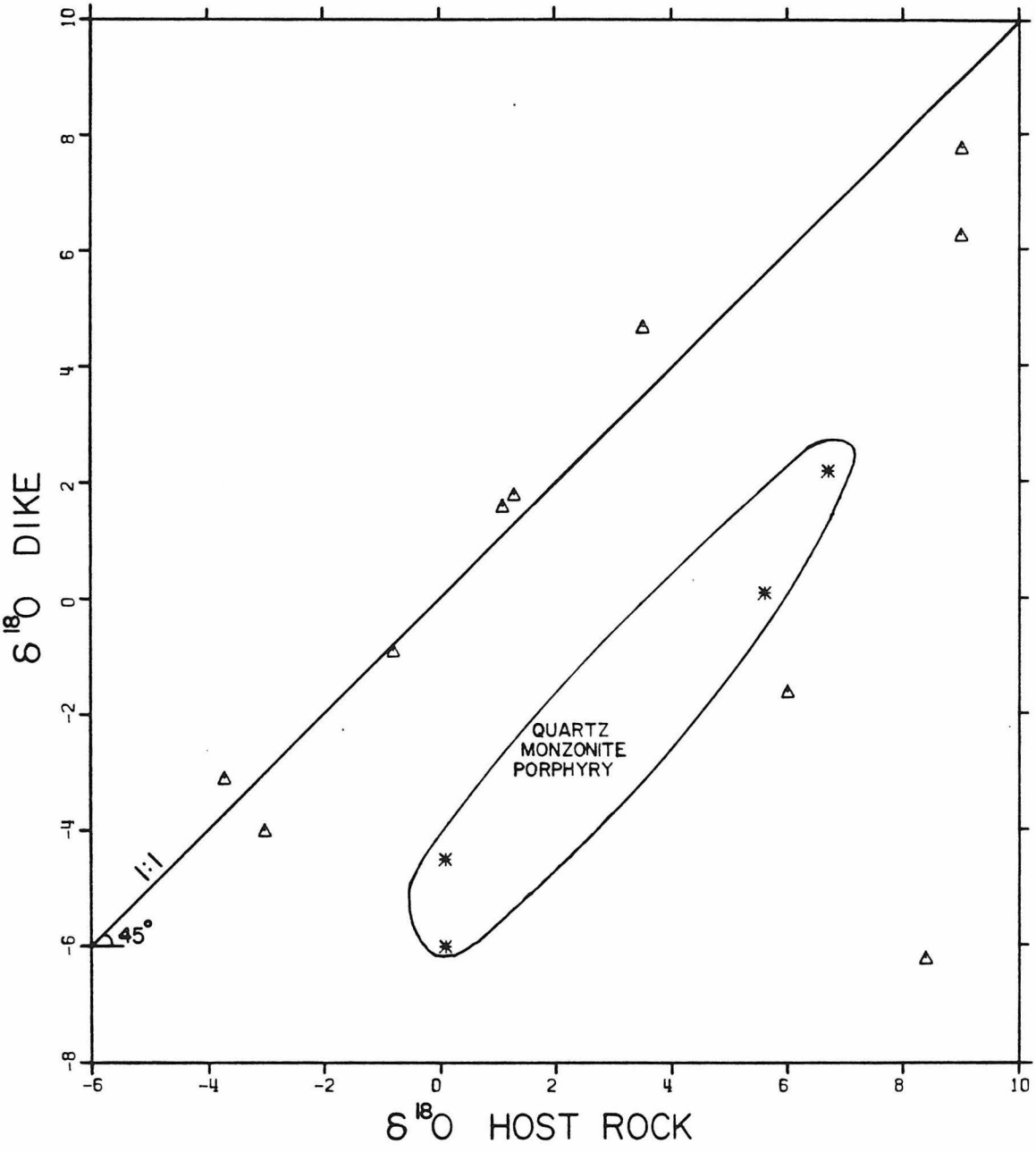
δ18O DIKE
δ18O HOST ROCK
1:1
45°
QUARTZ
MONZONITE
PORPHYRY
10
8
6
4
2
0
-2
-4
-6
-8
-6
-4
-2
0
2
4
6
8
10

Figure 5.26 Graph comparing the $\delta^{18}O$ values of Tertiary dike rocks and host granitic rocks from the Coast Range batholith. Data from Magaritz and Taylor (1976b).

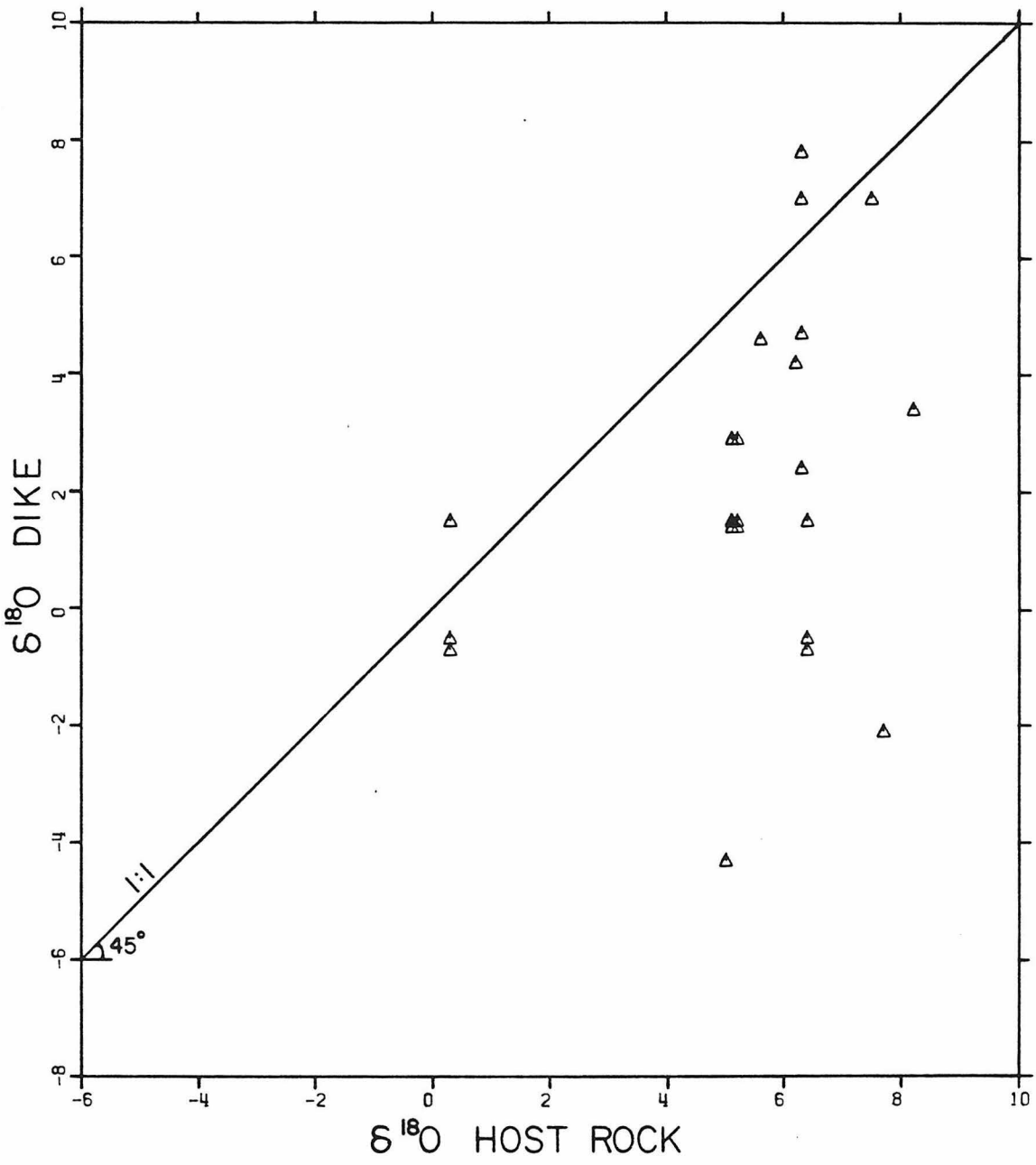
δ18O DIKE
δ18O HOST ROCK
1:1
45°
10
8
6
4
2
0
-2
-4
-6
-8
-6
-4
-2
0
2
4
6
8
10

Table 2.2).

In contrast, almost all dikes which lie near the 1:1 line of Fig. 5.25 are rhyolite and rhyolite porphyry (Dike Group 3), lamprophyre (Dike Group 4), andesite (Dike Group 5) and diabase (Dike Group 7), lithologies which are known to postdate emplacement of the Sawtooth batholith (Reid, 1963; Table 2.2). This observation represents good evidence that the hydrothermal activity was initiated shortly after intrusion of the large Eocene batholiths, such that the older dikes were altered for longer times and initially at higher temperatures than the younger dikes, and secondly, that the duration of the hydrothermal event must have been protracted. Note that even the youngest analyzed dike (diabase RH 43c; 4.6 permil) has undergone minor ^{18}O depletion from its probable initial value of ~ +6. Similar observations in the Tertiary ring-dike complex on the Isle of Mull, Scotland, have been interpreted in the same way by Forester and Taylor (1976). Although it is possible that these dikes were emplaced as low-^{18}O magmas, or that the magmas originally had normal -^{18}O values and then were lowered in ^{18}O by exchange with their previously hydrothermally-altered host-rocks at the time of intrusion (Turi and Taylor, 1971), it is most probable that the low $\delta^{18}O$ values of the dikes were all produced under subsolidus conditions during continuing meteoric-hydrothermal activity along the fracture zones and joints that guided dike emplacement.

5.4.3 Evidence from the Quartz Veins

This section discusses the $\delta^{18}O$ variations in vein quartz in the Idaho batholith, discusses their temperatures of origin, and compares these relations with a few other localities. These samples have a unique

interpretive value inasmuch as they were deposited directly by the hydrothermal fluids.

The $\delta^{18}O$ values of vein quartz in the batholith vary by more than 20 permil (Tables 4.4, 5.1). Most veins are located at the margins of the geographic regions where low ^{18}O host rocks occur (see Sec. 6.1); the vein quartz is generally high in ^{18}O, especially near the Au-Ag mines. This would imply deposition at relatively low temperatures (50°-150° C) if the $\delta^{18}O$ value of the water was -16 (i.e. pristine meteoric water). Somewhat higher temperatures (to ~ 400° C) are more likely, because appreciable ^{18}O enrichment (to values of -2 ± 3; see Sec. 5.1.3) of the water commonly occurred through interaction with the host rocks. The relatively high $\delta^{18}O$ values of the granitic host rocks suggest that the W/R ratios in most cases were low, so appreciable ^{18}O shift of the water probably occurred. If all the vein quartz samples in Table 5.1 were deposited at ~ 250° C, either the waters must have undergone a range of ^{18}O shifts (H_2O attaining values of -15 to + 5.6) or else the fluids were formed by mixing of waters of different origin.

In contrast, a vein from the low ^{18}O zone inside the Sawtooth batholith (RK 41b) is comparatively much lower in $\delta^{18}O$ (-6.2), which implies deposition at a minimum temperature of ~ 240° C, even assuming no oxygen shift whatsoever in the water. The extremely low $\delta^{18}O$ value of the host rock (-3.0) suggests that the W/R ratios at this locality were very high, so this latter condition may have been approximated. Note that O'Neil et al (1973), O'Neil and Silberman (1974) and Taylor (1973) found a similar situation in the Bodie District in California and in other western Nevada Au-Ag districts; the quartz veins in these deposits were commonly formed in equilibrium with unshifted meteoric water of the region.

Table 5.1 Calculated Temperatures of Quartz Veins for Different Fluid $\delta^{18}O$ Values

Field # T-R-S	$\delta^{18}O$ quartz vein	$\delta^{18}O$ host rock	Temperature (°C) for Indicated Fluid $\delta^{18}O$ *					
			-16 (unshifted)	-12	-8	-4	0	+4
RK 12b 8-8-27	0.7	-0.4_{WR}	134°	183°	254°	372°	782°	-
RK 20e 8-8-20	4.1	-	104°	141°	192°	268°	399°	-
RK 41b 10-12-15	-6.2	-3.0	229°	331°	560°	-	-	-
RK 43d 6-13-24	14.6	8.4	41°	61°	86°	118°	160°	219°

* Quartz-Water Fractionation factors from Matsuhisa et al (1979)

On the other hand, quartz gangue in the Wood River District immediately east of the Idaho batholith has a $\delta^{18}O$ value of +16.4 (Hall et al, 1978). This suggests either a non-meteoric water, which is very unlikely considering the fluid inclusion δD values of -110 to -120, or else that the $\delta^{18}O$ value of the water at this locality had completely shifted to be in equilibrium with the fine-grained, high $-^{18}O$ argillite country rock. Fluid inclusion measurements indicate that the deposition temperature of this deposit was high (~ 270°C; Hall et al, 1978).

Garlick and Epstein (1966) noted a wide range (13 permil) in ^{18}O contents of vein quartz in the giant Cu-Zn ore deposit at Butte, Montana, about 300 km northeast of the Atlanta lobe. These veins are probably considerably older (probably ~ 60 m.y.; Woakes, 1959, cited in Meyer et al, 1968) than the quartz veins in the Idaho batholith. The highest $\delta^{18}O$ values, which are in veins associated with the early Cu and Mo mineralization in the center of the Butte District, are almost identical to the values of plutonic quartz in the host quartz monzonite. The Main-Stage veins all show varying degrees of ^{18}O depletion, with the veins in the peripheral region being lowest in ^{18}O; the latter are associated with Zn and Mn ore with less Cu. Sheppard and Taylor (1974) suggest that strongly ^{18}O -shifted meteoric water was predominant in the higher levels of the center of the district and that it became isotopically more like unshifted meteoric water in the deeper, advanced argillic vein assemblages (kaolinite, dickite, topaz), which Meyer et al (1968) believe represent minerals deposited by fluids that have suffered the least exchange with the granitic host rocks and thus the least loss of their ability to alter the rocks. The meteoric-hydrothermal waters that formed the Butte ore bodies were thus isotopically similar to those that affected the rocks of the Atlanta lobe,

but more detailed study is required to determine whether the systematic relationships observed at Butte also apply to some of the Eocene veins in the Idaho batholith.

5.4.4 Temperature, Isotopic Composition and Origin of the Hydrothermal Fluids in the Atlanta Lobe

Many of the data discussed in the previous sections bear on the isotopic composition of the hydrothermal fluid and on the temperature of rock alteration. This section will summarize and amplify the pertinent arguments and will discuss certain implications regarding the origin of these fluids.

Theoretically, both the temperature and isotopic composition of a hydrothermal fluid can be calculated from isotopic measurements of two coexisting minerals in equilibrium with that fluid. Unfortunately, the situation in the batholith is greatly complicated by the different rates of exchange between the fluid and the preexisting plutonic minerals, and also by the variable proportions of water and rock involved in the alteration. Thus, in most cases the minerals are probably not in equilibrium with the fluid, and in many of the cases where equilibrium was attained (such as with feldspar, or in the veins) the $\delta^{18}O$ value of the fluid probably was strongly shifted from its original isotopic composition.

The difficulties mentioned above completely frustrate calculations based on mineral pairs from the rocks studied in this work. The approach used here, which is decidedly inferior to the ideal situation, is to first compute possible $\delta^{18}O$ and δD values of coexisting fluids at different temperatures, based upon the $\delta^{18}O$ and δD values of the most isotopically extreme ^{18}O and D depleted samples, and then to look for some systematics or consistency in the results. Table 5.2 illustrates such calculations

for the lowest- ^{18}O feldspar (-8.2) and vein quartz (-6.2) and for the lowest δD biotite (-176) and muscovite (-156). The lowest ^{18}O plutonic quartz and biotite values were not used for this purpose, because of extremely low exchange rates and interlayering of biotite with chlorite.

Table 5.2 shows that the $\delta^{18}O$ values of fluid calculated from the low- ^{18}O feldspars are in good agreement with those calculated from the vein quartz, and that the δD values of the fluid calculated from biotite are similar to those calculated from muscovite, regardless of temperature. The agreement is encouraging, but all of these values still only represent possible fluid compositions, because the temperature is not known. However, Figure 5.27 shows that the band of calculated waters from Table 5.2 intersects the meteoric water line at a $\delta^{18}O$ value of about -15 and a δD value of about -110. This is the only possible unshifted meteoric water that could have been involved in exchange with these particular minerals. The estimated temperature of about 260°C at the "cross-over" point is a minimum value; if these waters had previously undergone a small ^{18}O-shift, the temperatures would have to be higher (300°-350°C) and δD would then be as low as -115 to -125 (Fig. 5.27). However, the 260° calculated water is reasonable and is isotopically identical to the unshifted meteoric water that was the source of the Main-Stage ore fluids at Butte (Sheppard and Taylor, 1974). This suggests that meteoric ground waters probably were isotopically similar over a broad region in Idaho and western Montana throughout the early Tertiary.

The above calculated δD value is also in substantial agreement with fluid inclusion measurements of -110 to -120 permil in vein minerals from the nearby Wood River District, which incidentally had homogenization temperatures of 244° to 307°C (Hall et al, 1978). This δD value

Table 5.2 Calculated $\delta^{18}O$ Values of Hydrothermal Fluid

			Isotopic Composition of fluid in equilibrium with mineral at indicated temperature *				
Mineral	Field #	δ-Value	150°	200°	250°	300°	350°
Feldspar	RH 18	$\delta^{18}O = -8.2$	-20.9	-17.7	-15.3	-13.6	-12.2
Vein Quartz	RK 41b	$\delta^{18}O = -6.2$	-21.3	-17.7	-15.0	-13.0	-11.4
Biotite	YAG-1033	$\delta D = -176$	-69	-91	-107	-118	-127
Muscovite	I 7	$\delta D = -156$	-63	-86	-102	-114	-123

* Based on Fractionation factors from O'Neil and Taylor (1967), Matsuhisa et al (1979), and Suzuoki and Epstein (1976)

Figure 5.27 $\delta^{18}O$ and δD values of waters in equilibrium with the most ^{18}O and deuterium depleted samples so far obtained from the Idaho batholith, calculated at various plausible temperatures of alteration (150°- 350°C). The calculated band for these highly altered samples intersects the meteoric water line at approximately $\delta^{18}O = -15$, $\delta D = -110$ permil. These represent our best present estimates of the isotopic compositions of Eocene meteoric waters in southern Idaho, but these are clearly minimum values. (see text).

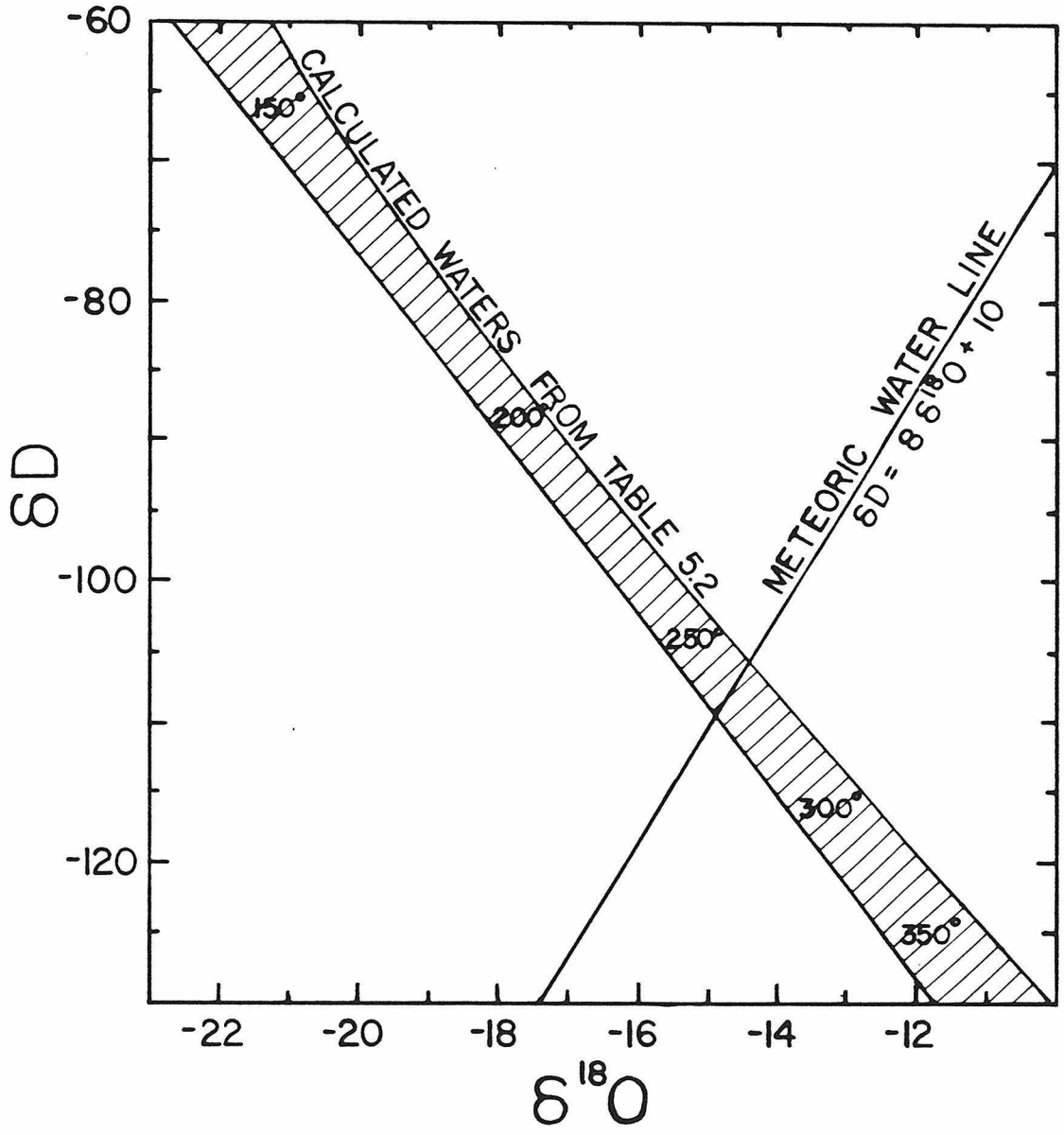
-60
-80
-100
-120
δD
-22
-20
-18
-16
-14
-12
δ18O
CALCULATED WATERS FROM TABLE 5.2
150°
200°
250°
300°
350°
METEORIC WATER LINE
δD = 8 δ18O + 10

is also similar to, but slightly heavier than, modern meteoric water in Idaho (δD = -130 to -155; Hall et al, 1978; Appendix 1). The above data are all consistent with a slightly warmer climate in the region about 40 m.y. ago, compatible with the evidence for warmer world-wide temperatures at intermediate and high latitudes during the Eocene (Savin, 1977). The data are also compatible with the evidence for a somewhat lower elevation of the batholith region at this time (Axelrod, 1966). A meteoric origin for the fluid is, of course, also consistent with the concepts outlined in Chapter 3 regarding modern geothermal systems on continents.

CHAPTER 6

GEOGRAPHIC DISTRIBUTION OF THE HYDROTHERMAL SYSTEMS AND GEOLOGIC IMPLICATIONS OF THE ISOTOPE DATA

6.1 Isotope Contour Maps (1:1,000,000): Relation to Eocene Plutonism

Regional patterns of $\delta^{18}O$ and δD values in the Idaho batholith provide important information on the location, nature, and origin of "fossil" hydrothermal systems. This section considers these isotopic patterns on a scale of 1:1,000,000 (1" ≈ 16 mi.), illustrating several geometrical properties of the hydrothermal systems- most importantly that they are centered on the Eocene plutons in the region, as pointed out by Taylor and Magaritz (1976). More detailed descriptions of individual isotopic anomalies are given in Sections 6.3, 6.4, and 6.5.

Figure 6.1 is a map showing the outline of the Atlanta lobe of the batholith, the Eocene plutons (stippled), $\delta^{18}O$ feldspar measurements (including a few whole-rock analyses), and $\delta^{18}O$ contours. The $\delta^{18}O$ contours are drawn at +10, +8, and +6 permil; for clarity, the more extreme $\delta^{18}O$ depletions are not shown on the diagram, even though some $\delta^{18}O$ values are as low as -8 permil.

Figure 6.1 shows that most of the "normal", high- ^{18}O rocks ($\delta^{18}O > 8$) occur in the west-central portion of the batholith, and in smaller areas far removed from the Eocene plutons. The highest ($\geq$ + 10) $\delta^{18}O$ feldspars in this "normal" zone are also associated with the highest $\delta^{18}O$ values in plutonic quartz (~ +12), which proves that the +10 $\delta^{18}O$ contour reflects a primary $\delta^{18}O$ characteristic of the batholith (c.f. Sec. 5.2.1). In the east-central part of the batholith, immediately east of this extensive "normal" ^{18}O region, are several conspicuous areas of anomalously low $\delta^{18}O$ values. It is clear that the largest anomalies are spatially

Figure 6.1 Contour map of $\delta^{18}O$ values of feldspar (dots; including a few whole-rock analyses) from granitic rocks of the Atlanta lobe. The Eocene plutons are shown in pattern; CP (Crags pluton), CB (Casto batholith), SB (Sawtooth batholith), RB (Rocky Bar complex). The low $-^{18}O$ zones are centered on these intrusives and are designated as: CRZ (Casto Ring Zone), SRZ (Sawtooth Ring Zone), RBA (Rocky Bar Anomaly), SM (Soldier Mts. anomaly), P (Pine anomaly), BF (Barber Flat anomaly), AR (Anderson Ranch anomaly), LP (Lucky Peak anomaly), B (Banner anomaly), BB (Boise Basin anomaly), PHB (Pearl-Horseshoe Bend anomaly). Note that low $-^{18}O$ rocks are not present in the west-central portion of the Atlanta lobe. This figure includes the earlier data of Taylor and Magaritz (1976, 1978). Scale 1:1,000,000; see text.


8
10
10
8
CP
6
45°
8
6
CB
CRZ
6
8
8
6
6
SRZ
6
6
SB
+ 44°
8
8
B
BB
PHB
8
BF
8
8
6
RBA
RB
10
LP
8
SM
P
6
8
AR
8
6
116°
115°
MILES
10 0 10
KM
10 0 10

associated with the Eocene batholiths, notably the Casto Pluton (CB), the Sawtooth batholith and its outliers (SB), and the Twin Springs-Dismal Swamp-Steel Mtn-Trinity Mtn (Rocky Bar) intrusive complex (RB). Smaller anomalies are associated with the Boise Basin (BB) and Pearl-Horseshoe Bend (PHB) diorite stocks.

Several other low- ^{18}O zones were found where no Eocene intrusives had been previously mapped, but where such rocks were conclusively identified during the present study. These will be called the Anderson Ranch (AR), Pine (P), Soldier Mtn (SM), Lucky Peak (LP), Barber Flat (BF) and Banner (B) anomalies.

In addition to the association with the Eocene plutons, the $\delta^{18}O$ anomalies mentioned above display several other significant geometrical features. Practically all of the low- ^{18}O zones have extremely steep isotopic gradients at their peripheries; locally these gradients exceed 10 permil per kilometer of distance. Secondly, the size of the anomaly is crudely proportional to the size of the associated interior pluton. Thus the small diorite stocks are associated with small ^{18}O anomalies, whereas the three large Eocene batholiths are each surrounded by enormous (500-2400 km^2) low- ^{18}O zones. However, although these latter three intrusives are each roughly comparable to one another in area (ca. 300-500 km^2), the Rocky Bar anomaly is proportionately much smaller than the other two; possible reasons for this will be given in section 6.4.

Another surprising feature is that the best studied low- ^{18}O zones appear to occur as annular <u>rings</u> more or less centered on the Eocene plutons. The sharp outer edges of these low- ^{18}O ring zones can be likened in some respects to an isotopic "wall" or "moat" where the $\delta^{18}O$

values change by several permil. The best example is the "Sawtooth Ring Zone" (SRZ) located near the center of Fig. 6.1, but the Rocky Bar Anomaly (RBA) also shows this feature, and with more extensive sampling the Casto Pluton might also show such a clear-cut low- ^{18}O ring zone. Thus, a core zone of higher $\delta^{18}O$ values exists interior to the low- ^{18}O ring zones in each of these areas. This core zone of higher $\delta^{18}O$ values (lower W/R ratios?) includes the wallrocks and the margins of the Eocene Sawtooth plutons, but not the interior portions of these plutons. The geometry is probably similar in the Casto Region, although the data are scanty. In marked contrast, the interior "high"- ^{18}O zone in the Rocky Bar area is almost totally restricted to the center of the Eocene intrusives. Incidentally, +8 and +10 contours exist within these latter intrusives but were not shown on Fig. 6.1 to avoid clutter (see the more detailed Figs. 6.4 and 6.7); similarly, one whole-rock sample in the high- ^{18}O zone interior to the SRZ has a $\delta^{18}O$ value of 9.5, but the +8 contour is omitted from Fig. 6.1 for clarity.

The δD patterns shown on Fig. 6.2 provide several complements as well as contrasts to the $\delta^{18}O$ anomalies. First, there is a good overall spatial correspondence between the $\delta^{18}O$ and δD patterns, which of course was expected from the "L-shaped plot" (Fig. 5.6). Thus, the rocks in the west-central portion of the batholith have essentially "normal" δD values of -66 to -90, but the values decrease markedly (to less than -150 permil) in the vicinity of the Eocene plutons. Note that in both the Rocky Bar and Sawtooth areas a few rocks with δD values higher than -150 exist interior to the most deuterium-depleted rocks of the ring zones; this is analogous to the $\delta^{18}O$ relationships described above for these core zones.

Figure 6.2 δD contour map showing the distribution of δD values in biotite (+ chlorite) for the Atlanta lobe; scale 1:1,000,000. Normal δD values of about -70 permil are found only in the west-central portion of the Atlanta lobe; pronounced D/H alteration effects occur near the Eocene plutons (stippled). This figure includes all the earlier data of Taylor and Magaritz (1976, 1978).

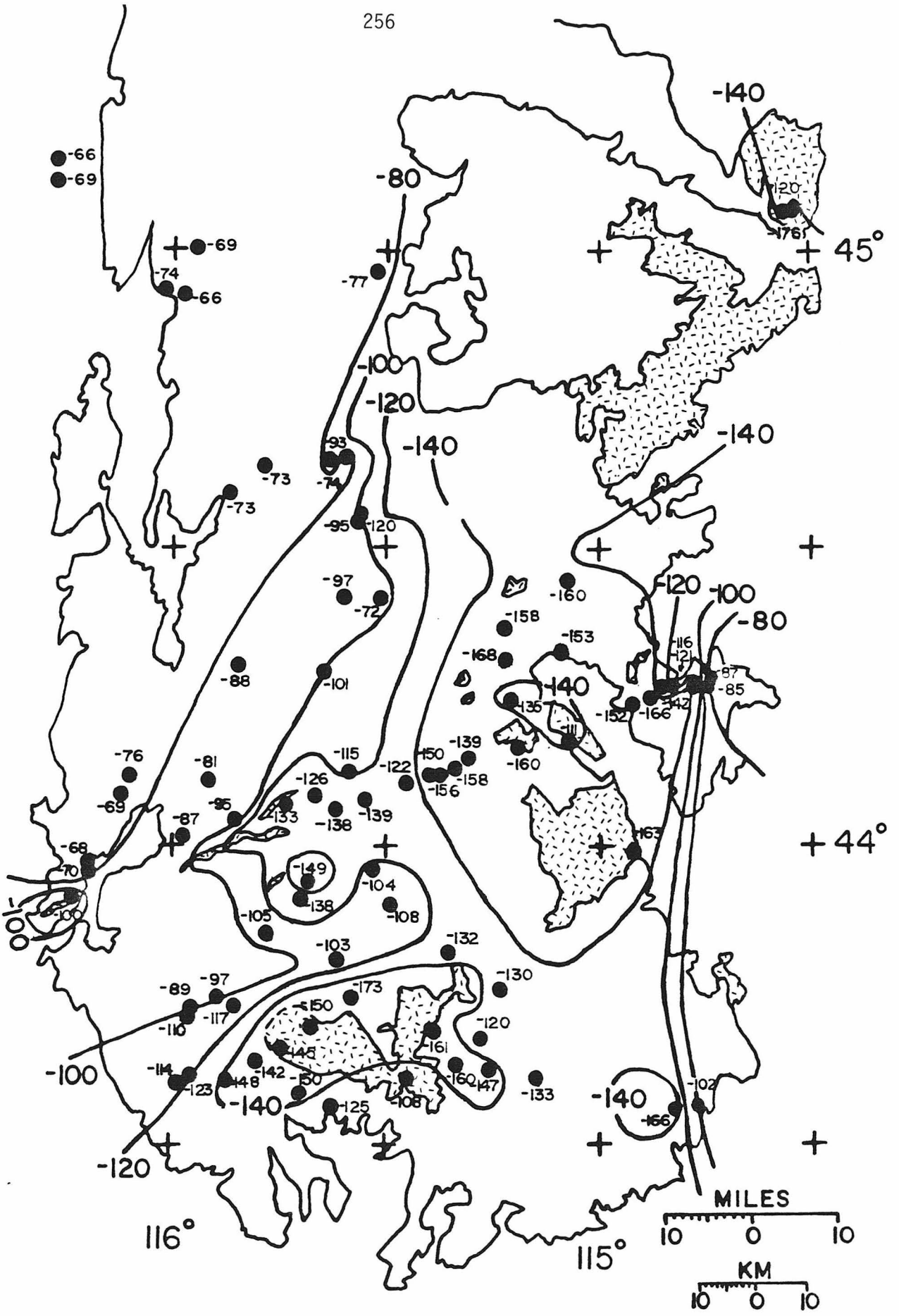
-140
-66
-69
-80
-69
-74
-66
-77
-100
-120
-140
-93
-73
-74
-73
-95
-120
-97
-72
-160
-158
-153
-168
-88
-101
-135
-152
-166
-111
-76
-81
-115
-122
-150
-139
-160
-69
-126
-156
-158
-87
-95
-133
-138
-139
-68
-70
-149
-104
-105
-108
-103
-132
-130
-89
-97
-173
-117
-110
-150
-120
-161
-114
-123
-148
-142
-150
-160
-147
-133
-125
-108
-102
-166
45°
44°
116°
115°
MILES
10 0 10
KM
10 0 10

In contrast to the $\delta^{18}O$ pattern, the δD values show relatively gentle horizontal gradients. Furthermore, discernible D/H alteration effects occur far outboard of the Eocene plutons; in fact most of the Atlanta lobe of the batholith is characterized by "abnormally" low δD rocks, as originally pointed out by Taylor and Magaritz (1976). This feature results because significant D/H changes can occur even when W/R ratios are too low to permit any perceptible oxygen isotope changes, as discussed in Sections 5.1.2 and 5.4.1.2. These peripheral effects probably reflect exchange between the rocks and ground waters which were migrating radially inward to the zones of higher temperatures and high W/R ratios. This large-scale convective system(s) clearly involved extensive lateral migration of the ground waters over distances of at least 25-50 km. As discussed in Sections 5.4 and 7.5, many of these inwardly migrating waters probably would have had temperatures in excess of 200°C, simply as a result of the geothermal gradient that existed in the region prior to the Eocene plutonism.

6.2 Relation of Isotopic Variations to Aeromagnetic Anomalies

Figure 6.3 shows an extremely close correspondence between positive aeromagnetic anomalies (Zietz et al, 1978) and the low- ^{18}O zones. The figure also shows that the highest magnetic anomalies are associated with Eocene granites, particularly pronounced for the Sawtooth (Kiilsgaard et al, 1970), Casto (Cater et al, 1973), and the Rocky Bar plutonic complexes. In interpreting this map it is important to note that the positive anomalies are displaced SSW from the outcrops of their causal body of rock. In addition, a weaker magnetic low usually occurs immediately NNE

Figure 6.3 Aeromagnetic contours of Zietz et al (1978) superimposed on the $\delta^{18}O$ contour map. Only the +8 permil $\delta^{18}O$ contour delineating the periphery of the low $-^{18}O$ zones is shown (heavy solid line). Dotted and dot-dashed aeromagnetic contours divide the batholith into regions of low (L), intermediate (blank pattern), and high positive magnetization (H; crosshatched pattern). The low-^{18}O zones, and especially the large Eocene plutons (dashed pattern), appear to correlate with the positive aeromagnetic anomalies. See text.

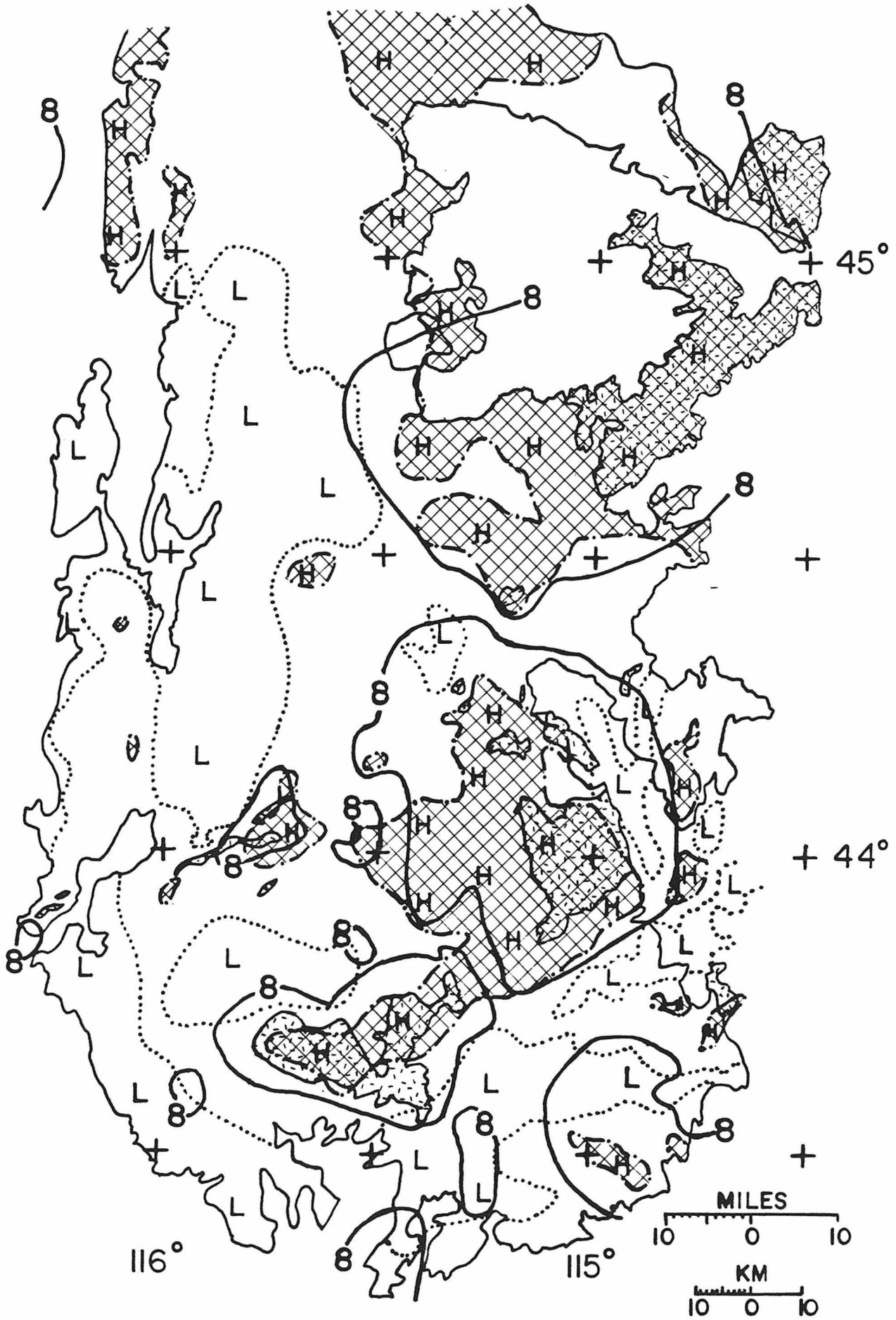
45°
44°
116°
115°
MILES
10 0 10
KM
10 0 10

of each pluton. This relation is especially conspicuous for the Sawtooth batholith, and results because the geomagnetic declination in the region is N 18° E and the inclination is 68° N. The dipoles induced within the magnetic bodies also lie in this orientation, neglecting remanent effects, which results in the observed anomaly pattern (Vacquier et al, 1951). That is, induced magnetic anomalies will be directly centered over such a causal feature only at the geomagnetic north pole where the inclination is 90°.

Note that the positive magnetic anomaly (>11,000 γ) in the Sawtooth region is much larger than the size of the mapped Eocene plutons, and is comparable in size to the low- ^{18}O SRZ area mapped on Fig. 6.1. This strongly suggests that there is considerably more Eocene granitic material in the area than has been mapped, or that such rocks are present in the shallow subsurface. In either case the magnetic anomaly explains the remarkable size of the low- ^{18}O zone and supports the caldera hypothesis of Criss and Taylor (1978), as discussed in more detail in Section 6.3. Positive magnetic anomalies also exist near other low- ^{18}O zones where no Eocene rocks have been mapped, as in the southeast portion of the batholith. This independently suggests that Eocene rocks exist in these areas, confirming the inferences made from the $\delta^{18}O$ data and petrographic studies.

An alternative explanation for the correspondence between positive magnetic anomalies and the low- ^{18}O zones is that the magnetic susceptibility of the rocks increases with hydrothermal alteration. This could presumably result from some recrystallization or oxidation process, or by changes in mineralogy, or by any other process which increases the susceptibility or concentration of magnetic minerals. Changes in magne-

tization accompanying alteration have in fact been suggested to occur in the Boulder batholith (Hanna, 1969), and the aeromagnetic anomaly pattern in this area does crudely correlate with the biotite D/H results of Sheppard and Taylor (1974). In the latter case, however, the alteration apparently causes a reduction in the magnetic susceptibility and so is opposite to the correlation in Idaho.

In order to directly test the correlation between hydrothermal alteration effects and magnetic properties, a few rapid measurements were made with a susceptibility bridge (Table 6.1). The data are extremely crude, but suggest that the unaltered Mesozoic rocks in the Idaho batholith commonly have lower (~ 0) magnetic susceptibilities than their altered equivalents. The data also show that the pink Eocene granites, which are typically highly altered, have high susceptibilities. As discussed in section 2.3.2, the pink color of the feldspar may result from iron (hematite) which was transferred from mafic minerals undergoing chloritization. This hematite may explain the high susceptibilities of the Eocene granites and possibly also of sample RB 209. Furthermore, the fact that positive aeromagnetic anomalies are not associated with the Lolo and Bungalow granites, which are Eocene plutons in the Bitterroot lobe, is consistent with their comparatively low degree of alteration as measured by Taylor and Magaritz (1976, 1978). This phenomenon requires additional study.

Overall, the geographic correlation between positive aeromagnetic anomalies and mapped or otherwise inferred Eocene granite plutons is better than the map correlation with altered rocks. Note in this connection (Fig. 6.3) that only a small positive anomaly exists in the Soldier Mts. area in the southeast portion of the batholith; this positive anomaly

Table 6.1 Relative Magnetic Susceptibility of Rocks from the Idaho Batholith Region

Sample Numbers	$\delta^{18}O_F$	Magnetic Susceptibility Arbitrary Units	Remarks*
"Normal" Mesozoic Rocks			
RH 8	8.4	~0	B-Mu QM, slightly alt.
RB 232	9.3	~0	Fresh B QM
RB 209	8.8	3.1	Gdr. with flesh colored MXL
Altered Mesozoic Rocks			
RH 10	-2.5	0.2	Strongly alt. Gdr
RH 24	-	~0	Strongly alt. QM
RB 235	0.6_{WR}	1.0	Strongly alt. QM
RB 237	4.3	~0	Alt. QM
Eocene Granites			
RK 36	-7.9	0.8	Pink Grt-Sawtooth Pluton
RK 37	-4.3	0.5	Pink Grt-Sawtooth Pluton
Tonalites, age uncertain			
RB 36	-	~0	
RK 40	7.9	~0	

*Abbreviations same as in Table 4.1

coincides with several outcrops of altered, pink Eocene rock, but does not extend appreciably into the large low- ^{18}O region further north which contains altered Mesozoic rocks and grey Eocene granodiorite. High susceptibility pink Eocene granites are thus considered to be primarily responsible for the aeromagnetic pattern, as originally proposed by Kiilsgaard et al (1970) and Cater et al (1973).

6.3 The Sawtooth Wilderness Anomaly - A Possible Giant Cauldron

The most striking feature of the 1:1,000,000 $\delta^{18}O$ map (Fig. 6.1) is the large low- ^{18}O anomaly, termed the Sawtooth Ring Zone (SRZ), associated with the Sawtooth batholith and its outliers. As discussed below, the detailed geometry of this anomaly is related to the topography and to the aeromagnetic pattern in the region. These considerations strongly suggest that the low- ^{18}O anomaly is coincident with zones of ring fracturing related to emplacement of the Eocene plutons. It is suggested that these systematic depletions in ^{18}O are related to structures produced by cauldron subsidence, which were then modified by resurgent doming.

The Sawtooth Ring Zone is a large elliptical annulus of low- ^{18}O rocks (Fig. 6.4), having an outer diameter of about 60 km (N-S) by 40 km (E-W). The western portion of the ring zone forms a broad belt about 20 km wide, approximately twice the width of the eastern and southern portions of the ring, and perhaps three times the width of the northern portion. The SRZ is centered on the Sawtooth batholith and smaller associated plutons immediately to the north, and encompasses the entire Sawtooth Wilderness Region.

Several of the plutons interior to the ring zone appear to exhibit

Figure 6.4 Detailed 1° x 1° map of the Sawtooth Ring Zone (SRZ), showing Eocene plutons (dashed pattern), feldspar $\delta^{18}O$ analyses (numbered dots; including a few whole-rock measurements), and $\delta^{18}O$ contours at +8 and +6 permil. The SRZ is a large, sharply bounded annulus of low $-^{18}O$ rocks which extends around the Sawtooth batholith and its outlying plutons. In a few small locations the +8 contour is omitted for clarity. T_{CV} indicates Challis Volcanic Rock.

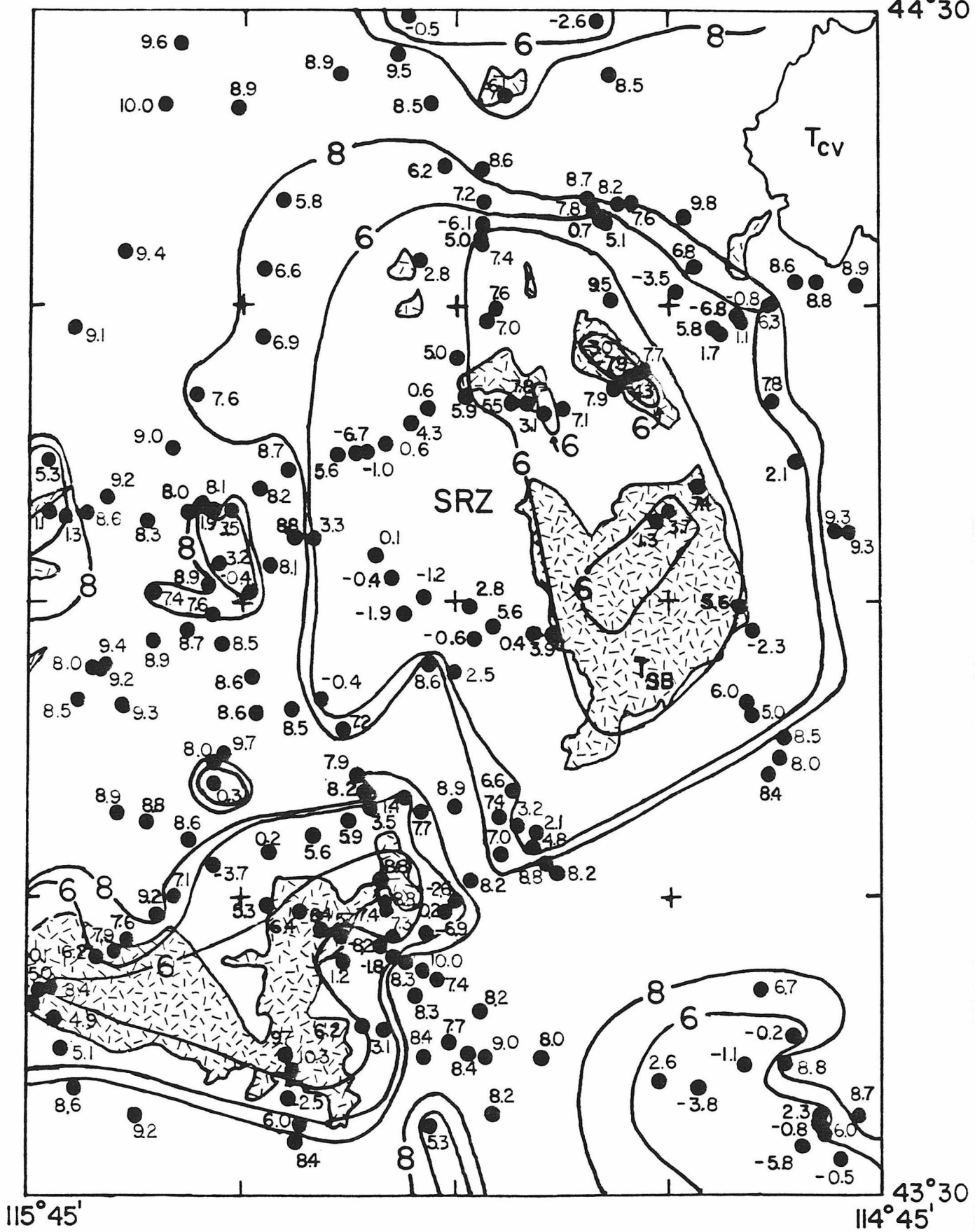
44°30'
43°30'
115°45'
114°45'
SRZ
T_{cv}
T_{sb}

local low- ^{18}O regions, but their margins and the adjacent wallrocks are higher in ^{18}O. This type of ^{18}O- geometry was observed on the east side of the Sawtooth batholith and also across the smaller Eocene plutons near Stanley Lake and near Grandjean. The contours on Fig. 6.4 have therefore been drawn assuming that a similar, radially-symmetric ^{18}O-geometry exists along all the contacts of these plutons, for example along the unsampled west side of the Sawtooth batholith.

The $\delta^{18}O$ pattern and the topography provide abundant evidence that the SRZ is structurally controlled. The anomalous region has a crude diamond shape. On the east the zone is coincident with the wide Sawtooth Valley, and on the northwest it adjoins a northeast-trending ridge which is at least partly fault bounded (Fig. 2.2). These topographic features, especially Sawtooth Valley, suggest that the SRZ is more easily eroded than adjacent rocks either within or outside the ring. The relation between topography and $\delta^{18}O$ is less pronounced on the west and south sides, and here it may be partly obscured by more recent faulting. However, in many places the valleys locally appear to widen and branch, and many topographic saddles occur, within these portions of the SRZ.

It is important to re-emphasize that the lowest ^{18}O rocks that make up the ring zone usually occur far outboard of the contacts of any of the Eocene plutons. This relation is best displayed within the wide (20 km) western portion of the SRZ. The analyses clearly show that the rocks in the 10 km-wide west half of this zone, those furthest from the Sawtooth batholith, are on the average lower in $\delta^{18}O$ ($\sim$ 0 permil) than rocks from the east half that is adjacent to the contact with the Sawtooth batholith (average $\delta^{18}O \approx +4$). In previously studied areas of meteoric-hydrothermal

alteration (e.g. see Taylor, 1971, 1974a), the zones of most intense ^{18}O depletion occur either: (1) at the margins of the pluton or "heat engine", or (2) in highly fractured caldera ring zones. Thus the most likely explanation for the SRZ isotopic anomaly is the latter, because the low- ^{18}O rocks occur at an appreciable distance from the large central plutons, and they also appear to coincide with a region of intrusive-related faults. Such faults are likely to have formed in the rigid country rocks as a result of subsidence during eruption of the Challis ash-flow tuffs associated with the Eocene plutons; these would have provided high-permeability zones and major conduits facilitating the flow of hydrothermal fluids. There is no other plausible explanation for the increase in $\delta^{18}O$ inward from the SRZ. For example, a model in which the water is simply assumed to undergo an ^{18}O shift to higher $\delta^{18}O$ values as it migrates radially inward cannot be reconciled with either the abrupt outer boundary of the SRZ, or with the low- ^{18}O zones in the cores of some of the Eocene plutons.

The detailed aeromagnetic map (Fig. 6.5) provides much additional information on the geological character of the Sawtooth ^{18}O anomaly. The features of interest are the large diamond-shaped magnetic high centered over the Sawtooth Mts., smaller internal zones of even higher magnetization, and the smaller associated magnetic low that coincides with Sawtooth Valley. As discussed in Section 6.2, many of the positive magnetic anomalies throughout the Idaho batholith are definitely associated with Eocene granite plutons, as is shown here for the Sawtooth batholith and the smaller plutons just to the north. Several of the other positive anomalies may be associated with unmapped plutons, especially those where pronounced

Figure 6.5 Detailed aeromagnetic map (1° x 1° region) showing the relationship between positive anomalies (shaded zone > 11,000 γ contour of Zietz et al, 1978) and the Eocene plutons (heavy outline). Same scale as Fig. 6.4. Note the large diamond-shaped positive anomaly in the Sawtooth Mts. region, and the smaller "square" zone of even higher magnetization associated with the outcrop of the Sawtooth batholith. The contour interval is 100 gammas.

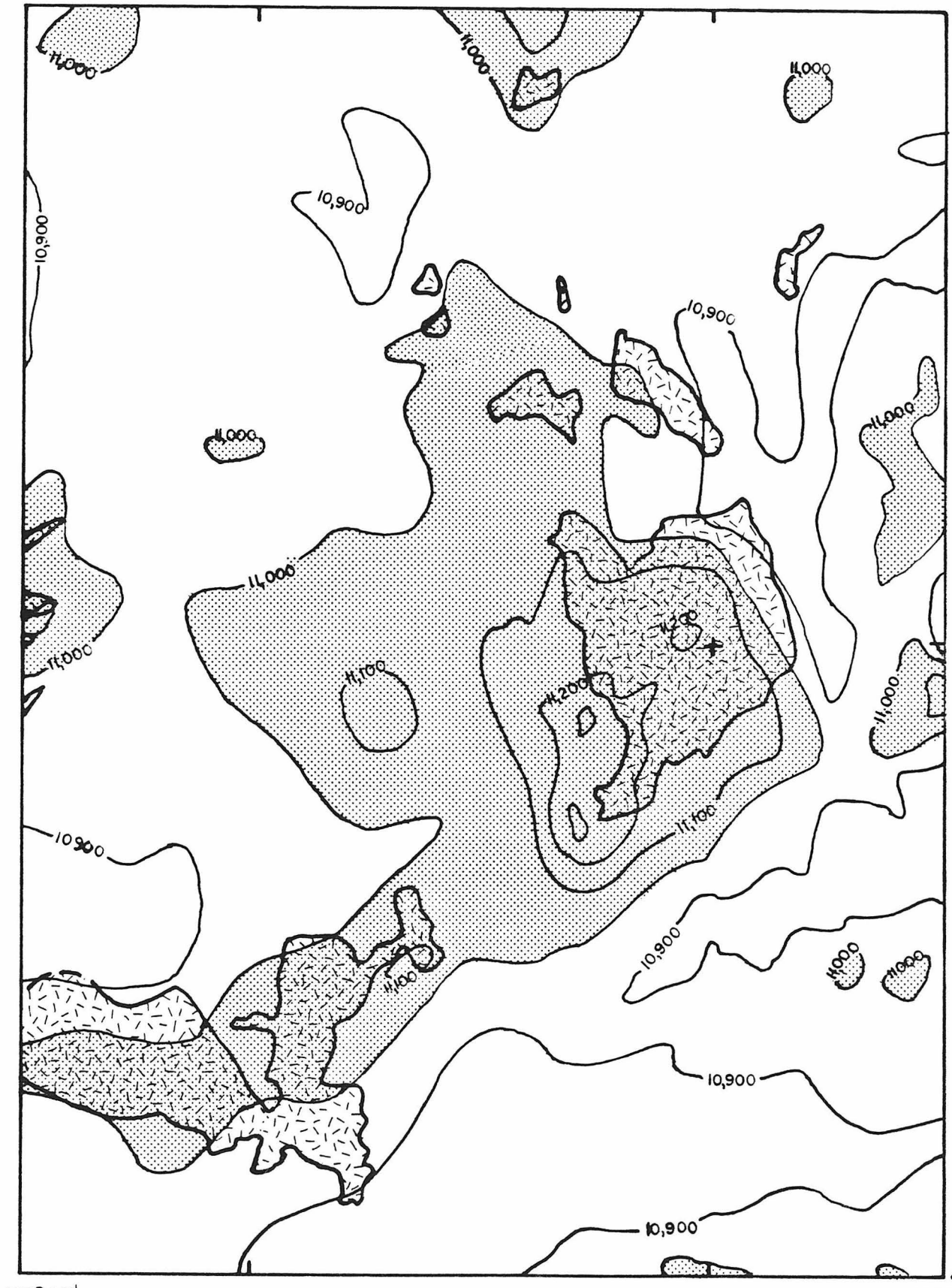
44°30'
43°30'
115°45'
114°45'
11,000
10,900
11,200
11,100
11,400

^{18}O depletions have been established (e.g. T7N, R9E).

The large diamond-shaped magnetic anomaly and the associated magnetic low over Sawtooth Valley are comparable in size and position to the anomalous $\delta^{18}O$ region encompassed by the SRZ. Although these magnetic features crudely mirror the topography, the extremely low susceptibilities of most Mesozoic rocks in the region suggest that these anomalies to first order reflect the large susceptibility contrast between Eocene (and altered?) rock and adjacent Mesozoic rock, rather than just topography. This conclusion is supported by the lack of correlation between the low amplitude aeromagnetic anomalies and the topography over the Bear Valley pluton in the northwest portion of Fig. 6.5, and over the Warm Lake pluton further west (see Fig. 6.3), both of which must therefore have very low susceptibilities. Given that the rocks in the Sawtooth block have higher susceptibilities than the normal rocks in the batholith, the topographic relief will influence the second order aspects of the anomaly pattern. In sum, the interpretation favored here is that the diamond-shaped Sawtooth block is largely comprised of magnetic rock, much of which may be Eocene granite in the shallow subsurface, with large outcrops of this granite being marked by even higher positive anomalies.

Figure 6.6 is a schematic geologic cross-section across the Sawtooth Mountains and adjacent areas. The figure shows a large Eocene batholith, inferred from the aeromagnetic anomaly in the region, whose conical top has been modified by formation of a large (40 km diameter) fault-bounded cauldron and by subsequent resurgent doming. Only small portions of this Eocene batholith are now exposed in the Sawtooth Mts. A thick sequence of associated volcanic rocks and caldera fill is inferred to have overlain

Figure 6.6 Interpretative cross section across the Sawtooth Ring Zone, showing large (~ 50 km diameter) cauldron block foundered into a gigantic Eocene batholith. Most of this hypothetical batholith lies below the present level of exposure (wavy line), except for the resurgent domes in the Sawtooth Mts. Arrows schematically illustrate fluid migration paths. A thick volcanic cover was formerly present. Graph shows somewhat generalized open-system oxygen W/R ratios across the structure.

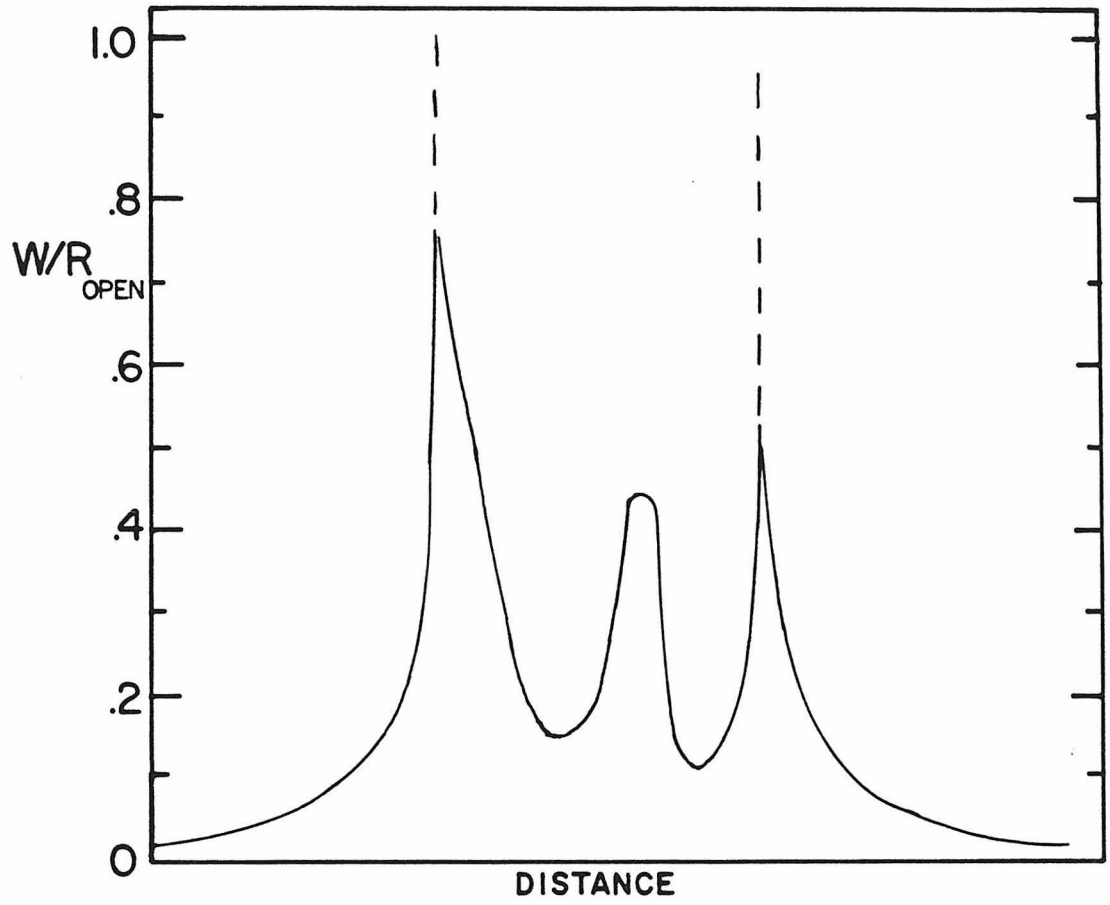
1.0
.8
W/R OPEN
.6
.4
.2
0
DISTANCE

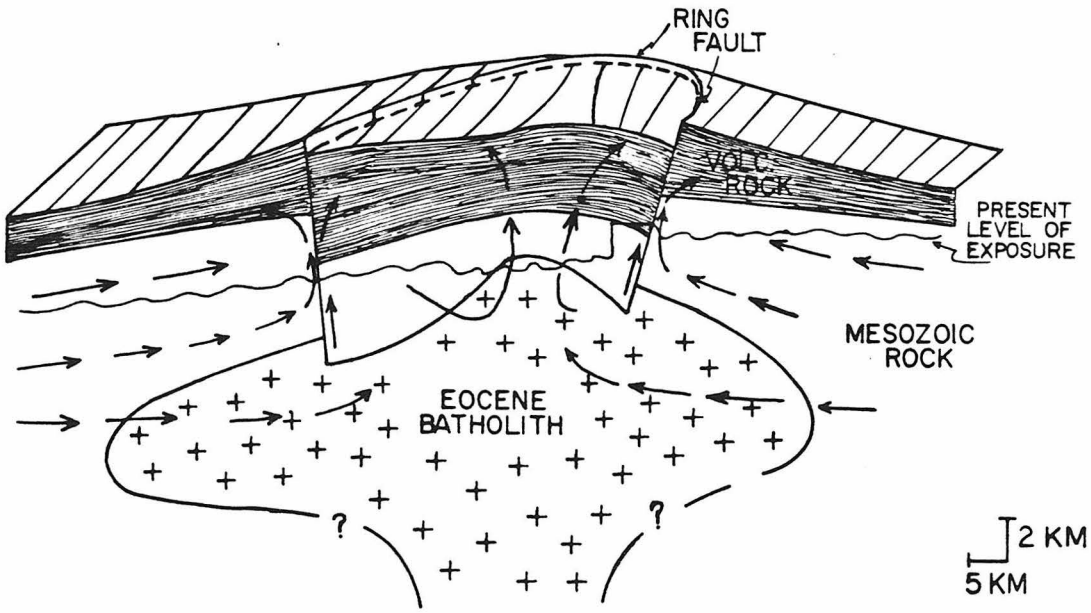
RING FAULT
VOLC. ROCK
PRESENT LEVEL OF EXPOSURE
MESOZOIC ROCK
EOCENE BATHOLITH
?
?
2 KM
5 KM

the epizonal Eocene batholith; this rock sequence has been removed from the immediate area, but thick exposures remain immediately to the east and it is possible that drilling would reveal such rocks in Sawtooth Valley. The graph above the cross-section somewhat schematically shows open system W/R ratios inferred from $\delta^{18}O$ and δD data along the present level of exposure. Extremely high ($\geq$ 1) W/R ratios are required by several of the low $\delta^{18}O$ values (down to -7 permil) near the outer margins of the SRZ. Peripheral to the zone of ring fracturing, the hydrothermal fluids must have migrated radially inward, as indicated by the fluid pathlines in the cross-section. It may appear from the W/R graph that the amount of radially migrating fluid is not sufficient to account for the high W/R ratios along and interior to the ring zone, but it must be remembered that the cylindrical geometry requires that the flux of these fluids falls off approximately as 1/r, as is shown. Note that this 1/r dependence fully explains the enormous scale of the D/H alteration effects in the Atlanta lobe. Fully fifty percent of these inwardly migrating fluids ascended through the ring fracture system. Some of the intercaldera hydrothermal activity could reflect deep circulating fluids which penetrated into the Eocene batholith after its solidification, but the most intense activity is thought to be due to subsequent intercaldera circulation systems developed about the resurgent domes, as is analogous to essentially all of the present-day geothermal activity inside the Yellowstone caldera system (see Eaton et al, 1975).

In summary, a large intrusive mass coincident with and underlying the diamond-shaped magnetic anomaly would explain the size and shape of the SRZ, and would be compatible with intrusion-related faulting and

perhaps with cauldron subsidence, as proposed by Criss and Taylor (1978). A cauldron model implicitly accounts for the annular shape of the low-^{18}O ring zone along the cauldron ring fracture, as shown by Taylor (1974a) for the Silverton cauldron in the San Juan Mts., Colorado. The model also accounts for the epizonal character of the Sawtooth batholith, and the thick pyroclastic units within the Challis volcanic sequence immediately to the east. It is in fact very likely that large amounts of rhyolitic volcanic rocks and ash-flow tuff once made up the roof rocks of the SRZ area, and have since been eroded away. In this model the Sawtooth batholith would represent a resurgent dome emplaced after caldera collapse and ash-flow tuff eruption, analogous to the model of Smith and Bailey (1968) for the Valles caldera. An unsatisfactory aspect of the model, however, is that more detailed work would be required to trace a definite, continuous ring structure completely around the Sawtooth Mts.

6.4 The Rocky Bar Anomaly: A Cross-Section through a Hydrothermal System

The best studied low-^{18}O area in the Idaho batholith is that developed around the Twin Springs-Dismal Swamp-Steel Mtn-Trinity Mtn. intrusive complex, here called the Rocky Bar Anomaly (RBA). This ^{18}O anomaly will be shown to be essentially a contact-zone phenomenon whose geometrical relations exhibit some major contrasts with those of the Sawtooth batholith and SRZ. More importantly, the rugged relief and large range in elevation in the vicinity of the Dismal Swamp stock and the nearby Rocky Bar mining camp allow construction of a fairly complete vertical cross-section through this particular hydrothermal system.

The Rocky Bar Anomaly (RBA) encompasses an area of 20 x 30 km, and

is comprised of a 3 km wide band of low- ^{18}O rock that conforms to the irregular boundary of the Rocky Bar intrusive complex. The RBA lies about 1 to 4 km outboard of the plutonic contact, as shown on Fig. 6.7. Interior to the low- ^{18}O RBA, both the wallrocks and the pluton margins show only minor ^{18}O depletions, and the core-zones of the Eocene plutons have ^{18}O contents characteristic of "normal"- ^{18}O igneous rocks. In contrast to the Sawtooth plutons, no zones of low- ^{18}O rocks were found interior to the RBA.

Although the Dismal Swamp, Twin Springs, and Steel Mtn. intrusives are composed largely of pink, commonly miarolitic granite and fine-grained granophyric rock, the Trinity Mtn. intrusive body immediately to the south consists of grey biotite-hornblende tonalite and granodiorite that is totally lacking in miarolitic cavities. The ^{18}O analyses indicate that the RBA extends around the Trinity Mtn. intrusive, and that the interior of this pluton has not been altered by the adjacent Dismal Swamp pluton. These two features represent the only compelling evidence for an Eocene age for the Trinity Mtn. pluton, although the presence of sphene and hornblende also distinguish it petrographically from typical Mesozoic igneous rocks in this portion of the Idaho batholith. Mutual cross-cutting relations between the Trinity Mtn. pluton and the other Eocene rocks have not yet been established (Bennett, pers. comm.).

Figure 6.5 shows that whereas the Dismal Swamp, Twin Springs, and Steel Mtn. granite intrusives are associated with a positive magnetic anomaly, the Trinity Mtn. pluton is not. Furthermore, the magnetic anomaly is much more closely associated with the granitic intrusives than with altered rocks in this region.

Figure 6.7 Detailed 1:250,000 map of the Twin Springs - Dismal Swamp - Steel Mtn. - Trinity Mtn. intrusive complex (geology from Rember and Bennett, 1979), showing $\delta^{18}O$ feldspar measurements (numbered dots; including a few whole-rock analyses) and $\delta^{18}O$ contours outlining the Rocky Bar Anomaly (RBA). T_{TS} (Twin Springs Pluton), T_{TM} (Trinity Mtn. Pluton), T_{DS} (Dismal Swamp Pluton), T_S (Steel Mtn. Pluton).

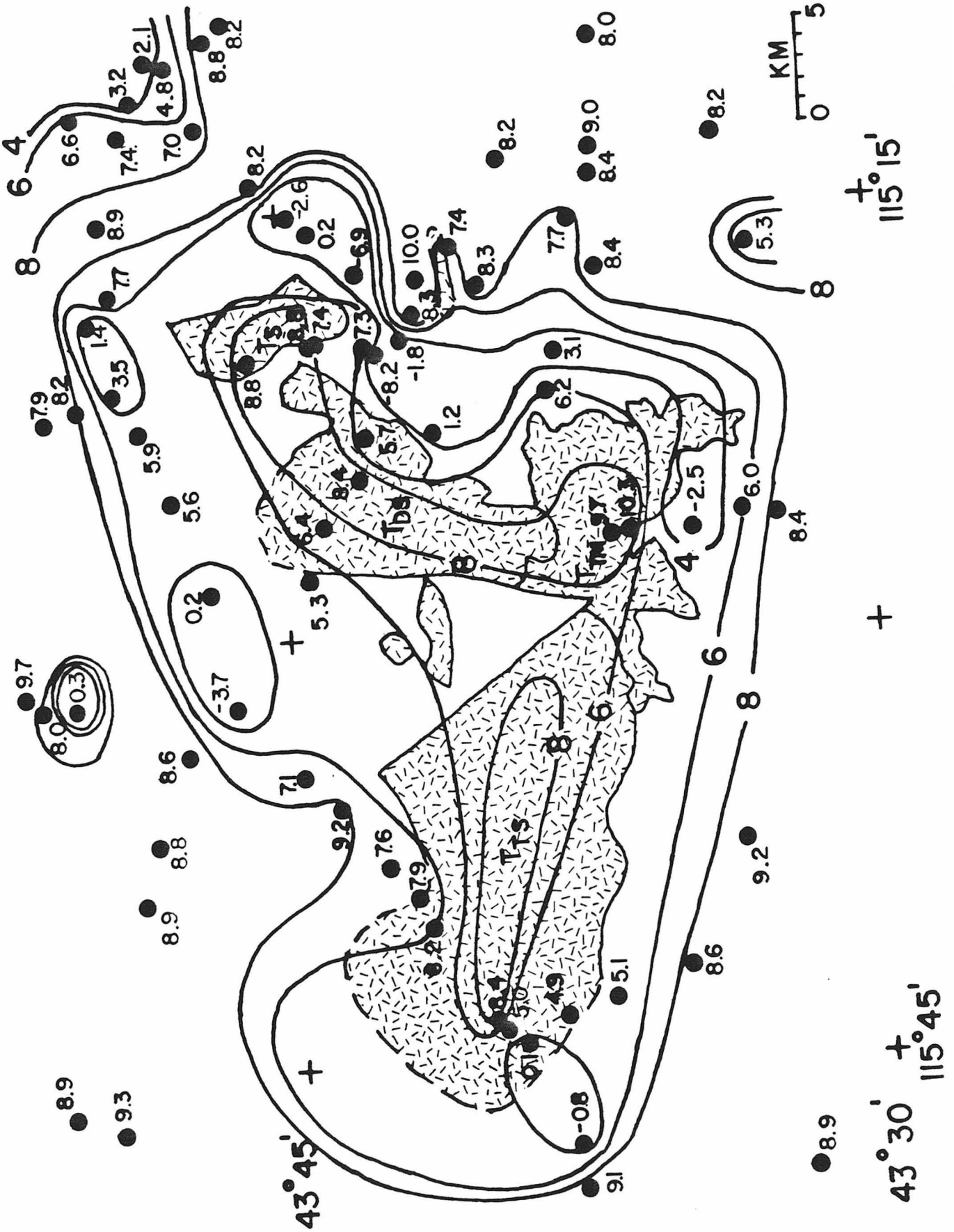
KM
0
5
115°15'
115°45'
43°30'
43°45'
Tds
Tts

Figure 6.8 shows an approximately NNW-SSE "cross-section" through the Dismal Swamp intrusive. The great relief in this area allows a significant vertical sampling of these rocks. The data points used in the plot probably all represent samples from one major fault block. Fig. 6.8 is not a true cross-section because the horizontal axis actually assumes radial symmetry and depicts the distance inward to the irregular pluton contact. Also, two of the points (triangles) have been projected from the north to the south side of the pluton, and the "contact distance" of two other points ($\delta^{18}O$ = 6.2; 3.1) was actually measured relative to the contact with the Trinity Mtn. pluton rather than to the contact of the Dismal Swamp intrusive, because the former was slightly closer. Furthermore, although the intrusive contact has been assumed to be everywhere vertical, the true attitude is not exactly known. Finally, note that the figure was drawn with significant vertical exaggeration.

Given the above qualifications and restrictions, the figure illustrates several properties of the low- ^{18}O RBA zone. As already mentioned, the lowest ^{18}O rocks occur a few kilometers outboard of the plutonic contacts, with the distance perhaps increasing slightly with increasing depth. Note that the vertical height of the low- ^{18}O zone is at least one-half of its width, which suggests that the original height far exceeded the width and has since been removed by erosion. Most importantly, the figure suggests that the present level of exposure lies somewhere near the middle of the zone of intense hydrothermal activity. At any level below an elevation of 6000', which is the elevation of the lowest- ^{18}O samples (-6.9; -8.2), the $\delta^{18}O$ values appear to increase as the depth increases.

Figure 6.8 Vertical SE-NW "cross-section" through the Dismal Swamp portion of the Rocky Bar Anomaly, somewhat schematically showing the relationship of the $\delta^{18}O$ values to the intrusive contact. Note that the lowest $\delta^{18}O$ values occur far outboard of the intrusive contact, and that the formerly productive mines (X) lie immediately outboard of the low $-^{18}O$ zone as discussed in Chapter 8. Triangles represent two points projected from the north to the south side of the Dismal Swamp pluton.

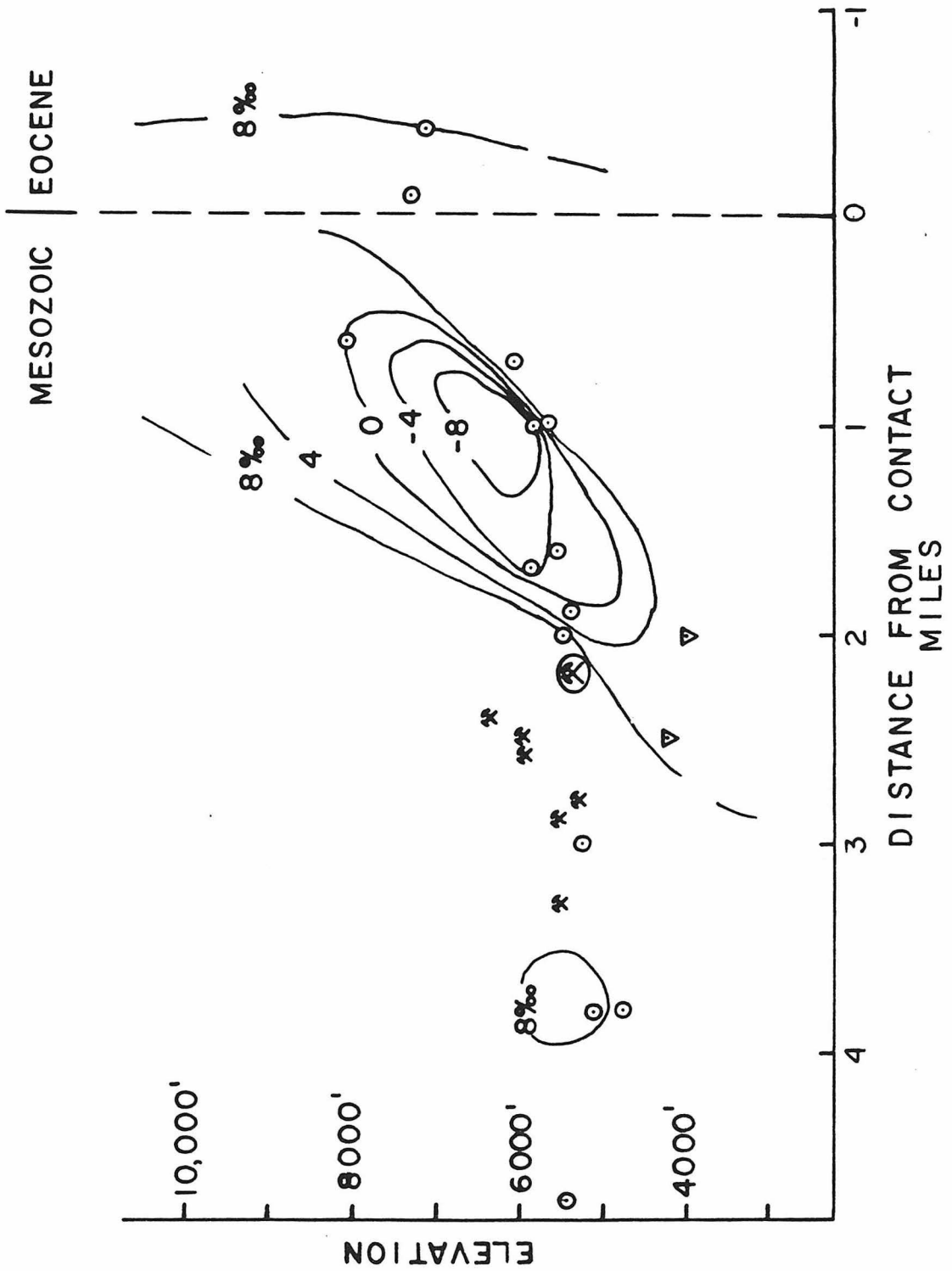
MESOZOIC
EOCENE
8‰
8‰
4
0
-4
-8
8‰
10,000'
8000'
6000'
4000'
ELEVATION
-1
0
1
2
3
4
DISTANCE FROM CONTACT
MILES

Thus the W/R ratios are probably decreasing with depth below this level, because of a drop in permeability as the fractures are closed by increased lithostatic pressure. This relationship is substantiated by the low-elevation points projected from the north side of the pluton (triangles), and also by relationships in surrounding rocks. For example, the low-elevation data points immediately NW of the Twin Springs pluton are generally higher in ^{18}O than typical rocks of the low- ^{18}O zone. However, points within the V-shaped (in plan) fault block immediately northeast of the Twin Springs intrusive are generally low in ^{18}O despite their low elevation. This indicates that this fault block has been downdropped, as is shown on the map by Rember and Bennett (1979).

6.5 Other Low- ^{18}O Areas

Several low- ^{18}O areas exist in the region which are not as well studied as the Sawtooth and Rocky Bar anomalies. This section briefly summarizes the known characteristics of these areas.

6.5.1 Casto Region

The largest of these low- ^{18}O areas, and perhaps the largest low-^{18}O zone in the entire region, is developed around the Casto and Crags plutons (CRZ, Fig. 6.1). Only a few reconnaissance samples from this low-^{18}O area have been studied. Similar to the SRZ and RBA, the anomaly is bounded by a steep ^{18}O gradient, with the lowest ^{18}O rocks occurring immediately inside the +8 permil contour. As in the case of the Sawtooth plutons, low-^{18}O rocks also occur in the interior of the Casto pluton. One sample (RSR 2) collected far inside the peripheral zone has a somewhat

higher $\delta^{18}O$ value (+7.8), perhaps indicating that a zone of higher ^{18}O exists interior to a low-^{18}O ring zone as in the Sawtooth Mts. A sample of a small biotite-hornblende diorite stock (RK 31) in the southernmost part of the area, of possible Eocene age (Armstrong, 1975), has a whole-rock $\delta^{18}O$ value of +6.1, which is essentially "normal" considering the relatively mafic composition. It is not known whether this pluton has a low-^{18}O aureole. Figure 6.3 shows a relatively good correspondence between a large positive aeromagnetic anomaly and this low-^{18}O zone.

6.5.2 Soldier Mts. Anomaly

More than 100 km^2 of highly altered rock occurs within and north of the Soldier Mts. in the southeast portion of the batholith (SM, Fig. 6.1). Several samples of highly altered, pink Eocene (?) rock were collected near Couch Summit (2-14-9, 2-13-1) and are probably responsible for the magnetic anomaly to the southwest. However, much of the Eocene rock in this region may be biotite-hornblende tonalite and granodiorite, an example being RH 85d (3-14-29). The Landsat photo suggests that a large (17 x 23 km) elliptical fault (?) encompasses this low-^{18}O area.

6.5.3 Anderson Ranch Anomaly

Another 100 km^2 region of altered rock occurs near Anderson Ranch Dam in the southernmost portion of the batholith (AR, Fig. 6.1). Lithologies are diverse in this region and numerous porphyry and aplite dikes occur. Although this region is not marked by a positive aeromagnetic anomaly, the Landsat photo reveals that this zone is coincident with

several conspicuous concentric "fractures" which are truncated on the southwest by a major NW trending fault system, as first pointed out to me by Jay Murray (pers. comm.).

6.5.4 Pine Anomaly

The Pine anomaly (P, Fig. 6.1) occurs north and east of Anderson Ranch reservoir. There is no evidence that the true shape of the anomaly is as shown on Fig. 6.3, or whether it is actually several small anomalies. One rock sample (3-10-13) apparently is pink Eocene granite.

6.5.5 Lucky Peak and Barber Flat Anomalies

The Lucky Peak and Barber Flat anomalies (LP, BF on Fig. 6.1) are small regions of low-^{18}O rock which occur near the contacts of small unmapped bodies of biotite-hornblende granodiorite. The detailed relationships are unknown, but the existence of the low-^{18}O rocks is strong evidence for an Eocene age for the associated plutons.

6.5.6 Banner Anomaly

The small (ca. 50 km^2) but relatively well mapped Banner anomaly (B, Fig. 6.1) occurs just west of the Sawtooth ring zone. No Eocene plutons were encountered along the traverse, but several porphyry, lamprophyre and aplite dikes occur in the area. The large "diamond-shaped" magnetic anomaly of the Sawtooth Mts. appears to extend into this region.

6.5.7 Boise Basin Anomaly

The Boise Basin anomaly (BB, Fig. 6.1) is associated with a dikelike

intrusion of quartz monzonite porphyry and with small diorite stocks mapped by Anderson (1947) and Ross and Forester (1947). Rocks adjacent to the low-^{18}O quartz monzonite porphyry are discernibly but not strongly depleted in ^{18}O compared to nearby rocks, expecially along the Grimes Pass Traverse (8-5-22, 8-5-15). However, the Grimes Pass rocks also occur immediately north of a small low-^{18}O pyroxene-biotite-hornblende quartz diorite pluton, itself adjacent to the quartz monzonite porphyry, which may be primarily responsible for the alteration. The better exposed but small intrusive zone further north is associated with strong ^{18}O depletion (9-6-33, 9-6-34, 9-6-35). Fig. 6.3 shows that a distinct positive aeromagnetic anomaly is associated with this region.

6.5.8 Pearl-Horseshoe Bend Anomaly

Last, a compositionally similar pyroxene-biotite-hornblende quartz diorite pluton mapped by Anderson (1934) is probably responsible for a small low-^{18}O zone (6-1-23) in the Pearl District, (PHB, Fig. 6.1). A specimen of granodiorite near the intrusive contact (7-2-33) did not show significant ^{18}O depletion but has a δD value of -100, significantly lower than the surrounding rock.

6.6 Implications Regarding the Characteristics of Deep Circulation in Modern Geothermal Systems

The $^{18}O/^{16}O$ and D/H data obtained in this work provide valuable insight into the nature of circulation in modern geothermal systems at deep levels that are presently inaccessible to study. This section thus attempts to relate the physical and historical characteristics of the Eocene "Sawtooth Mts." and "Rocky Bar" hydrothermal systems to those of

recent caldera-related geothermal systems, especially Yellowstone, Wyoming.

The most important information provided by the ancient, Sawtooth Mts. geothermal analogue is the tremendous scale of the hydrothermal circulation system. The regional D/H map (Fig. 6.2) proves that the circulation system developed about the Sawtooth Mts. involved an area of more than 8,000 km^2. The data from the Rocky Bar complex (Fig. 6.8) and evidence provided in Chapter 7 strongly suggests that much of this meteoric-hydrothermal activity penetrated to considerable depths, probably at least 7 km below the Eocene surface (c.f. Fig. 6.6). Thus, in the Idaho batholith about 50,000 km^3 of rock were apparently affected by the circulating hydrothermal fluids.

The amount of fluid which circulated through the Sawtooth hydrothermal system may be estimated from the $\delta^{18}O$ data. If all analyses are equally representative of the 2500 km^2 anomalous ^{18}O region, and if the former vertical height of this anomalous zone was only 7 km (compared to the ~ 55 km diameter), then this gigantic volume (17,500 km^3) of altered rock had an average $\delta^{18}O$ value of +3.2, which is fully 5.3 permil lower in $\delta^{18}O$ than its primary isotopic composition of +8.5. The minimum amount of fluid (with $\delta^{18}O$ initial = -16) required to balance this ^{18}O depletion in the rock can be calculated if the maximum possible ^{18}O shift (11 permil, to $\delta^{18}O$ = -5) is allowed in the fluid. This gives

$$W \times 11 = 5.3 \times R$$

$$\text{i.e.} \quad (W/R)_{\text{closed}} = 0.48 \; ; \quad (W/R)_{\text{open}} = 0.39$$

This calculation requires a minimum of 7,000 km^3 of hydrothermal fluid to cause the ^{18}O depletions observed in the Sawtooth area, and it is probable that the actual amount far exceeded this quantity. This gigantic volume of fluid could be supplied in 20,000 years by ordinary rainfall in the 8,000 km^2 recharge region even if only 5% of the rain sank deeply into the ground. The 7,000 km^3 figure also compares with the 0.1 km^3/yr discharge rate estimated by Fournier et al (1976) for the Yellowstone caldera. All other things being equal, the latter figure would require that the Sawtooth Mts. hydrothermal activity persisted for 70,000 years; this is a reasonable first-order value but could be too short by as much as a factor of 5 or 10.

It is clear that the relatively small (~ 400 km^2) exposures of Eocene granitic rock in the Sawtooth Mts. did not have enough thermal energy to heat these gigantic volumes of fluid and highly altered rock to temperatures of ~ 300°C. Most of the missing heat was provided by the hypothetical, large (~ 25,000 km^3; c.f. Chapter 7), Eocene magma chamber at greater depths, which was inferred from the aeromagnetic data (sec. 6.3). Furthermore, if the size and depth of the hydrothermal system are as great as here proposed, then as much as 50 percent of the required heat could have been provided by the ordinary, pre-Eocene geothermal gradient. This gradient was probably comparable to that of typical, modern continental crust (ca. 30°C/km), so that the rocks and fluid at 7 km depth would have had a temperature of 200°C before the Eocene magmatic event. This aspect of the deep circulation model is important, because it shows that not all of the thermal energy of geothermal systems need be provided solely by crystallizing magma, as is commonly assumed. Thus in the Sawtooth Mts.

model, the Tertiary magma chamber is considered to have provided the lateral thermal gradients and the driving energy that triggered the geothermal circulation, but only a fraction (perhaps 65%) of the total thermal energy of the fluid. The net result of the geothermal circulation system is for the fluid to abstract heat from large bodies of ordinary rock, as well as from the sides of the magma chamber, and to redistribute and release this energy in the central and upper portions of the system, similar to the models discussed by Norton and Knight (1977) and Norton and Taylor (1979).

One more aspect of the Sawtooth Mts. geothermal model needs to be described. It is considered probable that most (> 50 percent) of the inward-migrating, early-stage fluids ascended through the ring fracture system, and that much of the intercaldera activity was associated with later resurgent intrusion and doming of the foundered cauldron block. Note that the caldera-related modern geothermal systems discussed in Section 3.2 are all representative of the later, post-resurgence activity, and in fact the majority of hot springs lie geographically closer to the margins of the resurgent domes than to the ring fractures (Fig. 6.9). Although these latter systems probably have a deep-circulating component, they are best compared to the geographically small, primarily shallow, probably late-stage intercaldera circulation systems developed within the outcrops of the Sawtooth batholith and its outliers.

The evidence presented here for deep circulation in the ring fracture zones may imply that much of this type of activity has little or no surface expression (perhaps because of relatively impermeable cap-rocks). It is thus possible that geothermal reserves exist in young rhyolite

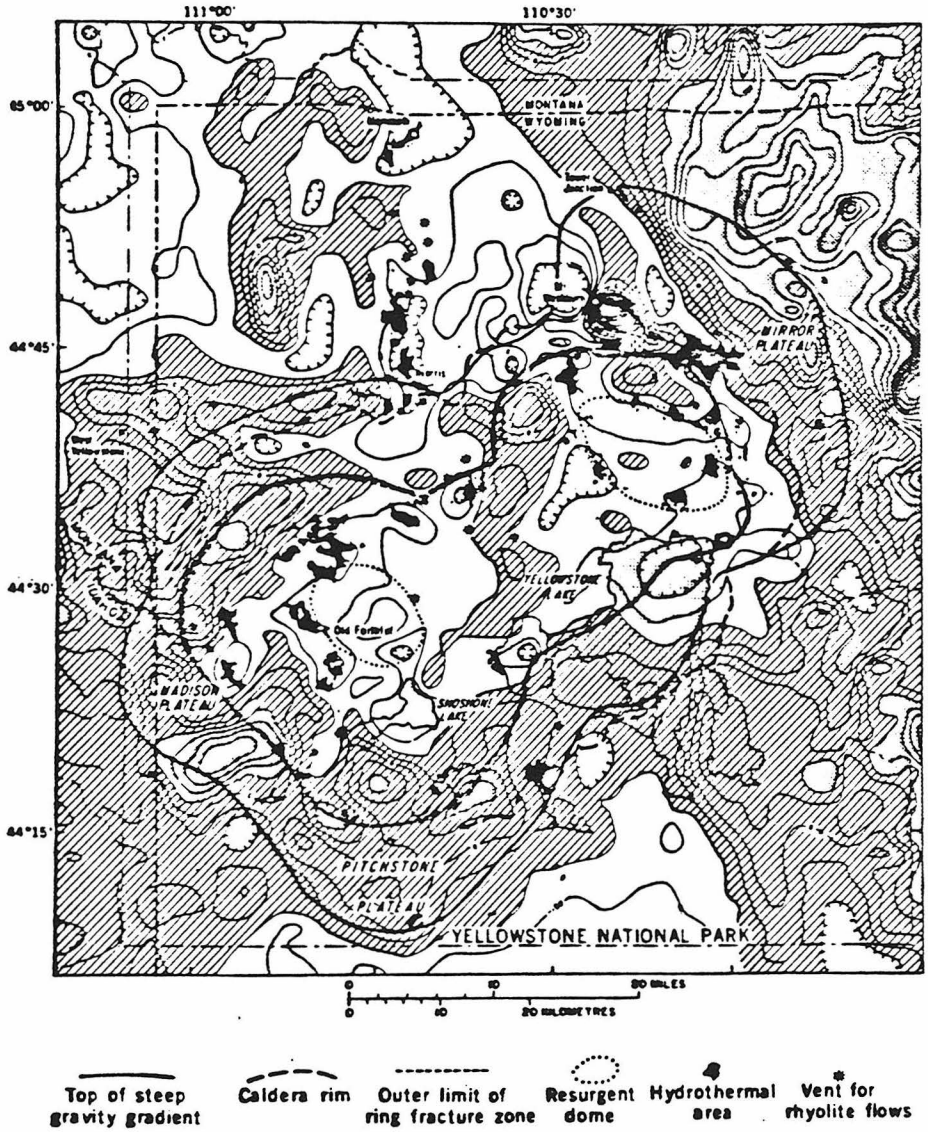

Figure 6.9 Map of the Yellowstone region, from Eaton et al (1975). Note that most of the zones of hydrothermal discharge are concentrated near the margins of the resurgent domes, while many of the exceptions occur near the outer limit of ring fracture.

plateau regions at depth along caldera ring fractures; these may exhibit little or no significant surficial expressions of hydrothermal activity. This matter deserves considerably more study.

CHAPTER 7

K-Ar RELATIONS IN THE IDAHO BATHOLITH

7.1 Biotite K-Ar Apparent Age Map (1:1,000,000): Relation to the Eocene Plutonic Event

K-Ar apparent ages of biotites in igneous plutons contain much information about rates of uplift, ancient geothermal gradients, and times of reheating, as well as giving some information about original emplacement ages. This section will describe the regional pattern of K-Ar apparent ages in the Idaho batholith, and will demonstrate their relationship to the areas of Eocene plutonium.

Figure 7.1 is a contour map of all presently available biotite K-Ar ages from granitic rocks of the Idaho batholith. The figure includes, and basically confirms and extends, the earlier data of McDowell and Kulp (1969), Armstrong (1974, 1975a), Armstrong et al (1977), and others (see Sec. 1.2.2). In particular the new K-Ar analyses confirm that the younger epizonal granitic plutons are all of Eocene age (38 to 44 m.y.), and that the K-Ar apparent ages in the rest of the Idaho batholith are 40 to 95 m.y. However, it should be noted that the diorite plutons near Boise Basin and Pearl-Horseshoe Bend are geologically of "intermediate" age (Sec. 2.2.4), and hence would probably be older than the Eocene. These bodies are shown as "Eocene plutons" on the maps because they seem to be responsible for at least some hydrothermal alteration and age resetting of the country rocks (see below).

Figure 7.1 also shows that the country rocks immediately adjacent to the pluton contacts are commonly similar in age ($\leq$ 45 m.y.) to the Eocene plutons. These Mesozoic country rocks undoubtedly lost essentially all radiogenic Ar during the heating event associated with Eocene intrusion. Exterior to these narrow contact zones the rocks appear to have suffered

Figure 7.1 Geologic map of the Atlanta lobe (1:1,000,000) showing Eocene plutons (ruled pattern), biotite K-Ar apparent ages (numbered points), and K-Ar age contours. Triangles represent K-Ar age determinations from the literature (see Table 4.6), and circles denote the analyses made in the current study; filled triangles and dots represent Mesozoic rocks, and half-filled points indicate Eocene rocks. The apparent ages appear to systematically decrease from the margins of the Idaho batholith toward the Eocene plutons, and in contact zones the Mesozoic rocks have Eocene apparent ages. About half of the plotted age data were determined in the present study; other determinations are due to Armstrong (1974, 1975a), Armstrong et al (1977), McDowell and Kulp (1969), Percious et al (1967), Marvin et al (1973), Berry et al (1976), and Hall (unpub.).

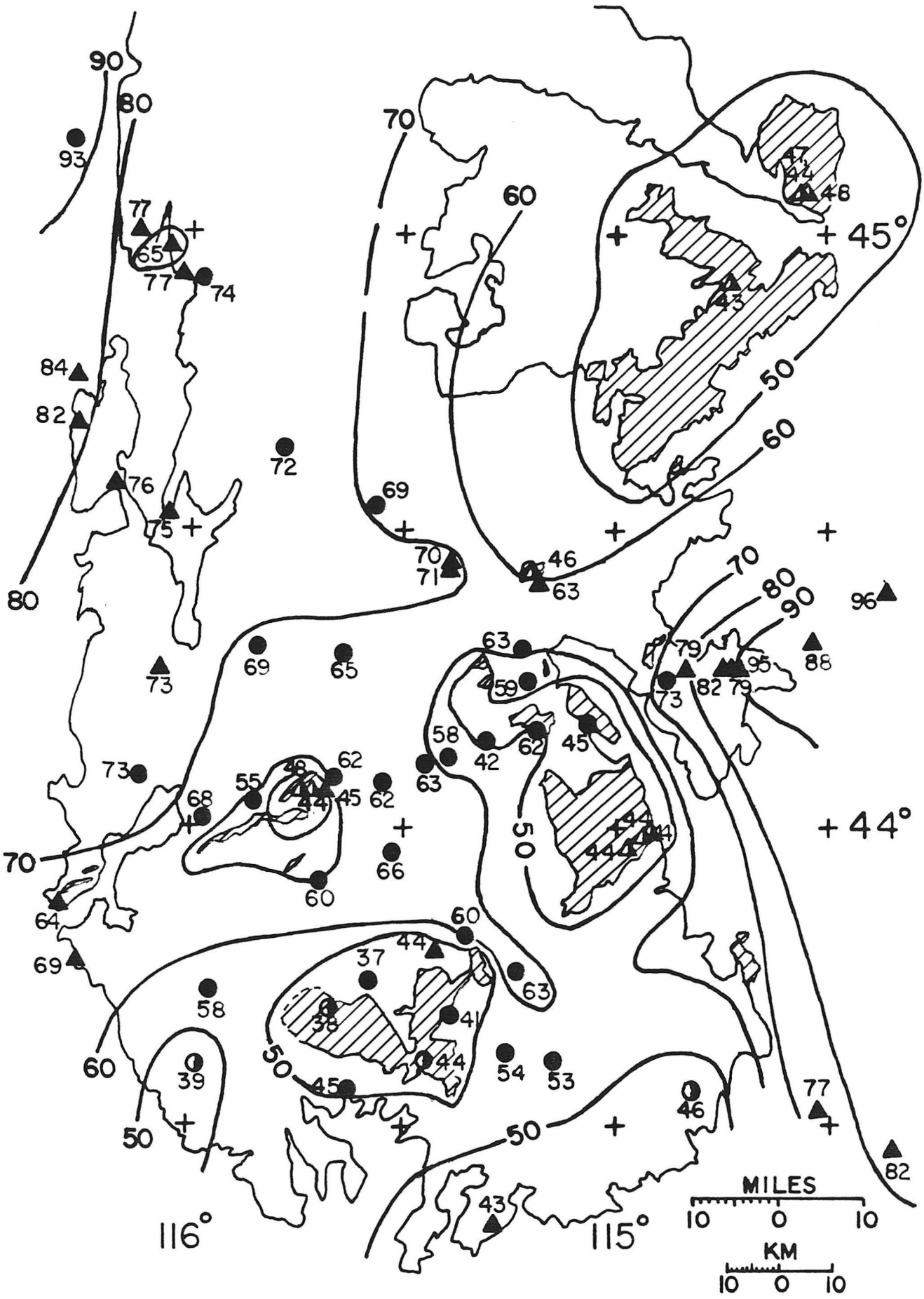
90
80
70
60
50
93
77
65
77
74
84
82
76
75
72
69
70
71
80
73
69
65
63
59
58
42
62
45
63
73
68
55
62
45
62
66
60
70
64
69
60
44
37
63
58
38
41
60
39
50
45
54
53
50
50
46
77
82
43
+45°
+44°
96
88
79
95
82
79
73
MILES
10 0 10
KM
10 0 10
116°
115°

only partial Ar loss, with the loss generally decreasing with increasing distance from the Eocene plutons, as originally suggested by McDowell and Kulp (1969) and Armstrong (1974). However, although the general K-Ar age relationships described by Armstrong (1974) are confirmed, the position of the 50 m.y. contour is drastically modified, and the area underlain by young (< 50 m.y.) apparent ages has been reduced to a small fraction of its former size (compare with Fig. 1.1).

The extensive new K-Ar results in this paper also indicate a major difficulty with any explanation based solely on partial Ar loss. This difficulty arises in part because of the absence of reset K-Ar ages in the interval 45 to 53 m.y., as compared to the essentially continuous and uniform distribution of ages from 53 to 82 m.y. (Fig. 7.2). It is clear that the zones of drastic K-Ar age resetting (i.e. $\leq$ 45 m.y.) are very narrow and confined to contact zones around the Eocene intrusives. Immediately outboard of this narrow zone the apparent ages discontinuously jump to generally $\geq$ 60 m.y. It is also difficult to reconcile the K-Ar age lowering of the more distant samples with the suggestion that most such rocks have undergone partial Ar loss during the Eocene plutonic event; note that the latter would imply that rocks more than 50 km from the Eocene plutons have lost Ar during the Eocene heat pulse.

These matters will be discussed in detail and resolved below. Evidence will be presented that throughout most of the terrane shown in Fig. 7.1, in the region where K-Ar ages are greater than 60 m.y., the K-Ar age pattern is basically a function of regional uplift and doming; this doming is thought to be attributable to the Eocene plutonic event. However, in regions near the Eocene plutons, and at low elevations, the young

Figure 7.2 Histograms of biotite K-Ar age determinations from plutonic rocks of the Atlanta lobe. Half filled squares denote the samples analyzed in the present study; diagonally ruled squares indicate previous data (see Table 4.6). The literature data for Mesozoic rocks are systematically older than the current data because most of the former analyses represent rocks from the batholith margins, whereas the present work concentrated on the "disturbed" regions near the center of the Atlanta lobe. Note that analyses from the Eocene plutons are clustered near 45 m.y., whereas data from the Mesozoic rocks fall into two distinct groups separated by a significant "age gap" between 45 and 53.4 m.y. The single analysis which appears to lie within the age gap is actually 45.0 m.y.

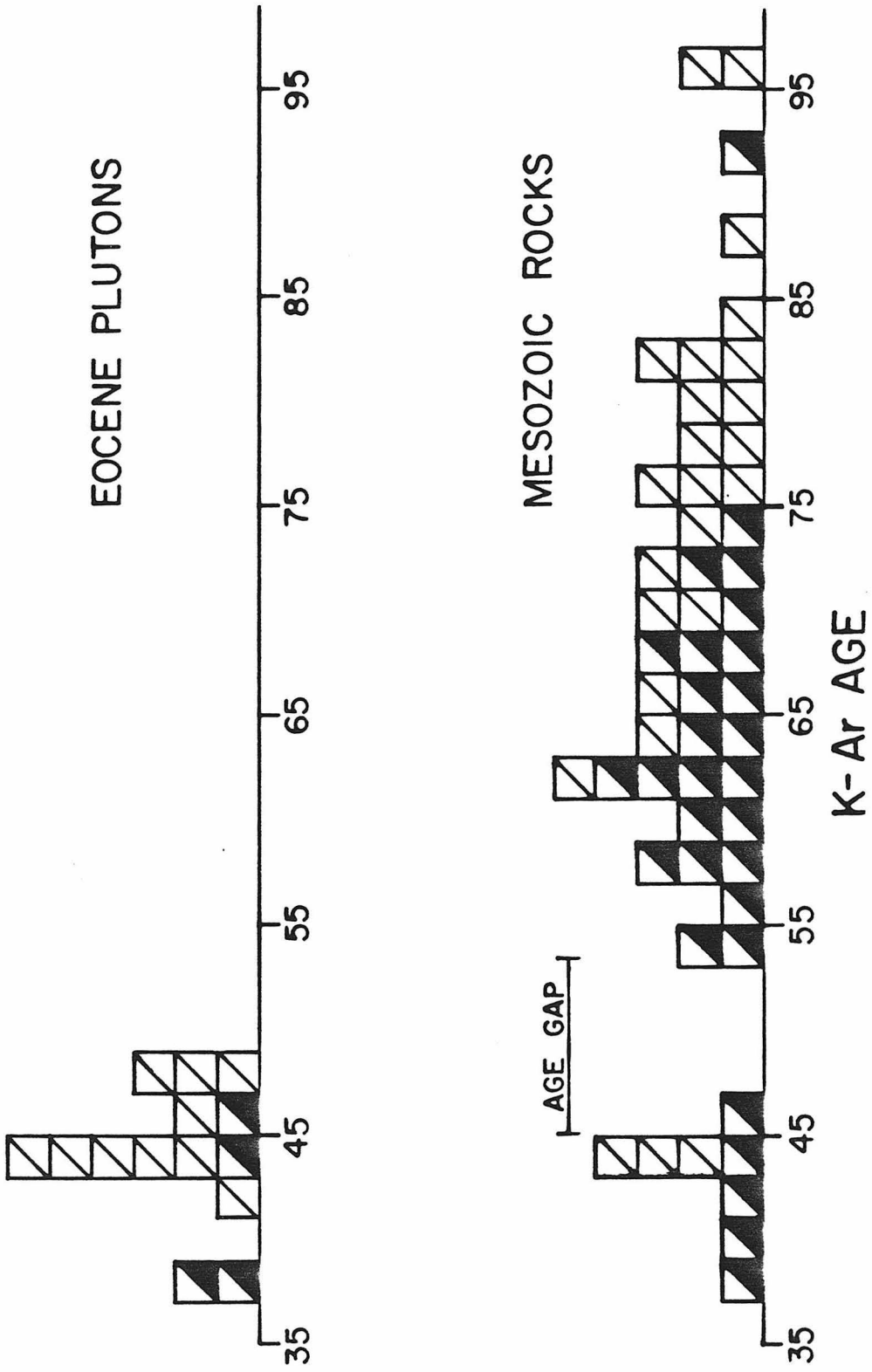
EOCENE PLUTONS
MESOZOIC ROCKS
AGE GAP
35
45
55
65
75
85
95
K-Ar AGE

(< 60 m.y.) K-Ar ages are a result of hydrothermal heating during the Eocene magmatic pulse.

7.2 Comparison of K-Ar Data with $^{18}O/^{16}O$ and D/H Measurements

The K-Ar contours in Fig. 7.1 show a good correspondence with the δD and $\delta^{18}O$ patterns discussed previously (Figs. 6.1, 6.2), such that all of the anomalously young "ages" are centered on regions of hydrothermally altered rocks, as originally noted by Taylor and Magaritz (1976). One of the principal goals of this investigation was to better document this phenomenon, and in particular to establish whether there is a direct relationship between hydrothermal alteration and radiogenic Ar loss in biotite. The discussion below demonstrates that although both the stable isotope and K-Ar apparent age patterns in the batholith are clearly a consequence of the Eocene plutonic event, over much of the area shown in Fig. 7.1 the K-Ar age patterns are only indirectly related to this event and to the D/H and $^{18}O/^{16}O$ effects.

7.2.1 $\delta^{18}O$ Correlation

Figure 7.3 shows the K-Ar apparent ages and $\delta^{18}O$ contents of the analyzed biotite-chlorite mixtures ("biotites"). For samples lying above the "age gap" (i.e. samples > 53 m.y.), a weak positive correlation exists between $\delta^{18}O$ and K-Ar age. In particular, if two samples collected close to the batholith margin are excluded, the normal $-^{18}O$ "biotite" samples ($\delta^{18}O > 5.5$) consistently exhibit older ($\geq$ 68 m.y.) K-Ar ages than samples with lower $\delta^{18}O$. However, the most highly ^{18}O-depleted and altered "biotite" above the age gap (RK 29a, 58 m.y., -1.9 permil) is

Figure 7.3 K-Ar apparent ages of "biotites" plotted against $\delta^{18}O$ analyses of aliquots of the same mineral separates. There is a weak positive correlation between these variables, such that high $\delta^{18}O$ biotites (unaltered) have relatively old K-Ar apparent ages. Circles denote Mesozoic rocks, and crosses indicate Eocene plutonic rocks.

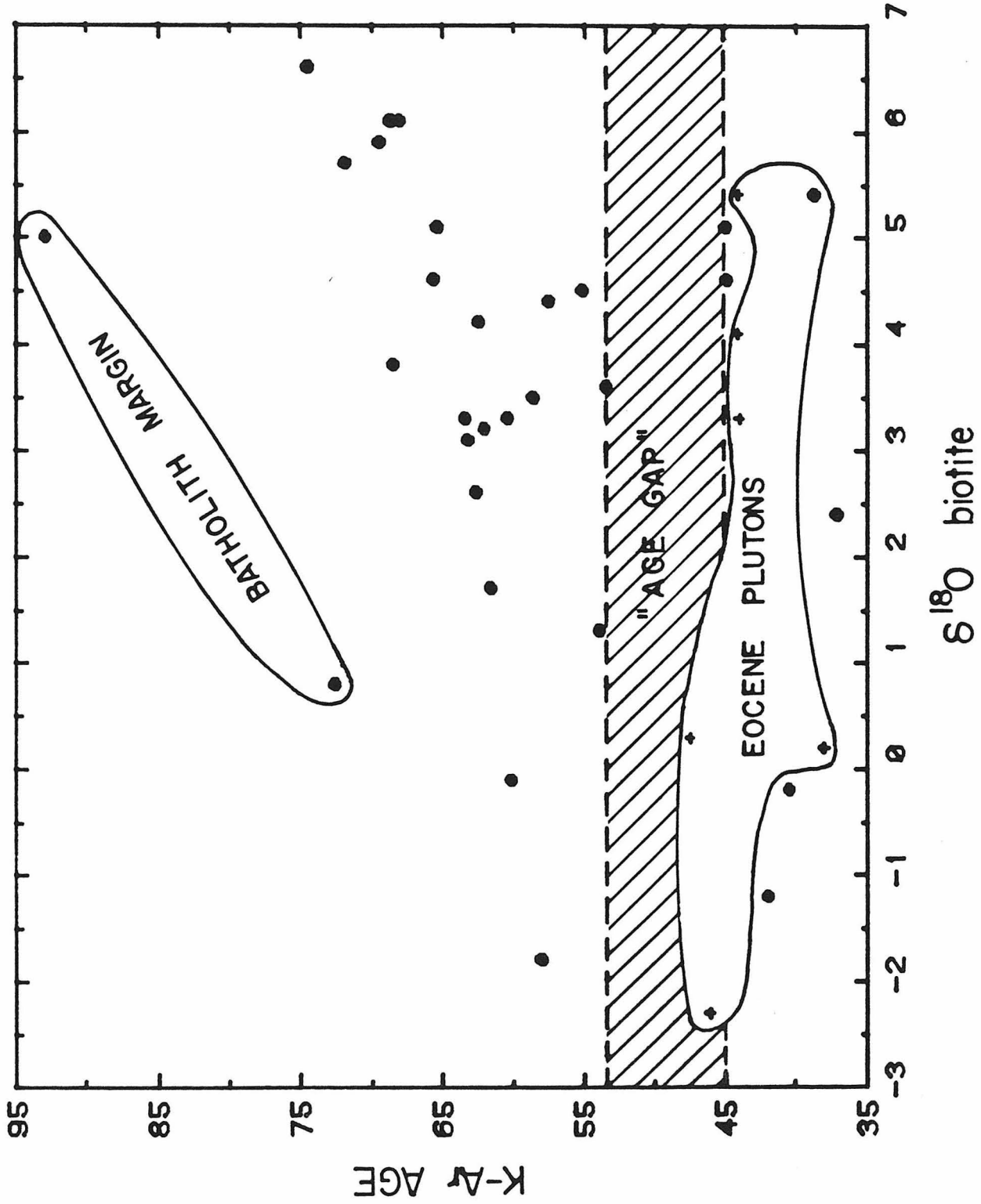
BATHOLITH MARGIN
"AGE GAP"
EOCENE PLUTONS
K-Ar AGE
95
85
75
65
55
45
35
-3
-2
-1
0
1
2
3
4
5
6
7
δ18O biotite

significantly "older" than some samples which show only weak ^{18}O alteration. Note that the Mesozoic samples that plot below the "age gap" clearly suffered almost complete Ar loss during the Eocene thermal event, thus these samples must have been heated to high temperatures (> 300°C).

7.2.2 K_2O Correlation

A plot of K-Ar age vs. K_2O content (Fig. 7.4) is similar in form to Fig. 7.3, which is to be expected because of the close linear correspondence between the $\delta^{18}O$ value and the K_2O content of "biotite" (Fig. 5.10). The lack of a strong correlation suggests that the chloritization process, which directly reduces the K_2O content of the "biotites", does not have a discernible effect on the K-Ar apparent ages. Inasmuch as the K_2O content enters directly into the K-Ar "age" calculation, reduction of the K_2O from 9.2 to 4.5 percent would drastically increase the apparent age (by approximately a factor of two), unless the radiogenic Ar content was proportionately reduced by the same process (chloritization) that affected the K_2O content. This rather remarkable result is explicable in terms of the experimental findings of Kulp and Engels (1963). They showed in hydrothermal experiments that biotite alteration is a layer by layer process that removes all radiogenic Ar and all potassium from the altered layers, while leaving other layers intact. Up to 80% of the K_2O could be removed under these conditions without significantly affecting the K-Ar "age" of the sample (Kulp and Engels, 1963).

There is some suggestion in Fig. 7.4 that the data-points above the "age gap" display an inverted L-shaped pattern. Most of the age lowering within the interval 63-96 m.y. is accompanied by little or no change in K_2O.

Figure 7.4 K-Ar apparent ages of "biotite" plotted against the K_2O content (in wt. %). There is a distinct positive correlation between these variables, such that biotites with high K_2O contents tend to have relatively high apparent ages. Circles denote Mesozoic rocks, and crosses represent Eocene plutons. All data shown in Fig. 7.1 are included; fully half of the determinations were made in other laboratories (see Table 4.6).

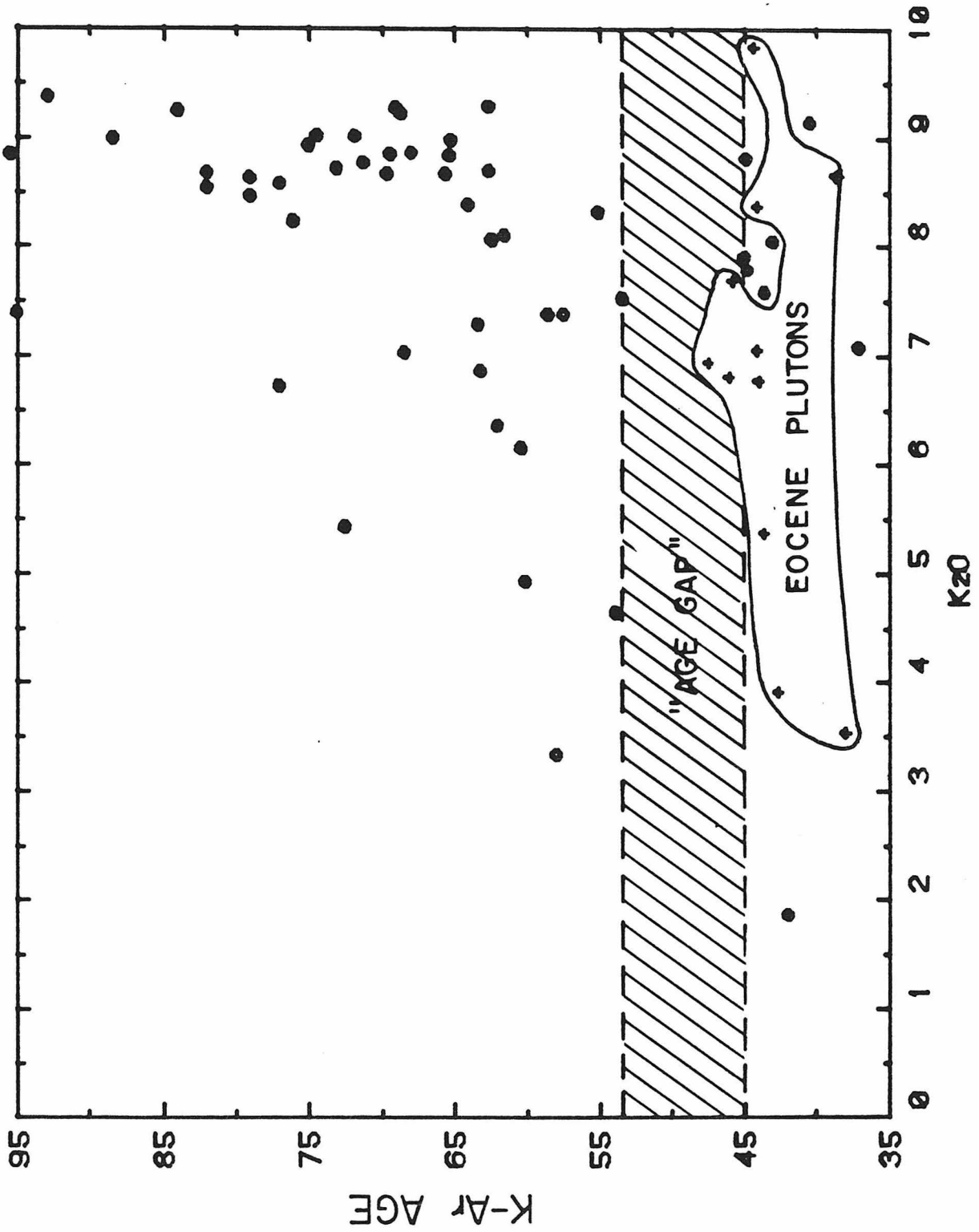
K-Ar AGE
95
85
75
65
55
45
35
0
1
2
3
4
5
6
7
8
9
10
K2O
"AGE GAP"
EOCENE PLUTONS

Only after the ages drop below 63 m.y. is there a marked tendency for the samples to show a decrease in K_2O; most of the samples with K-Ar ages between 53 and 63 m.y. have been significantly chloritized. It will be shown below that many of these samples have apparently suffered partial Ar loss during hydrothermal heating, whereas the K-Ar ages of most of the high K_2O samples were fixed by regional uplift (sec. 7.3).

The age gap probably results because of the exponential temperature dependence of the Ar diffusion coefficient. Above a narrow temperature interval (~ 300°C; the "blocking temperature") there will be complete Ar loss during the heating event. A few degrees below this temperature, there will only be partial Ar loss in the biotite, and at somewhat lower temperatures Ar loss will be negligible. Thus, closely constrained temperatures are required to produce apparent ages within the "age gap", and the regions where these exacting conditions were attained are understandably small.

7.2.3 D/H Correlation

A better overall correlation exists between the K-Ar ages and the δD values of "biotite" than with the $\delta^{18}O$ values (Fig. 7.5). This improved correlation results from the fact that all samples with ages below the "age gap" have been significantly depleted in deuterium, including samples from the Eocene plutons themselves. Figure 7.5 shows that all four rocks with "normal" δD values (> -75 permil) have systematically older K-Ar ages (> 68 m.y.) than all but one of the altered rocks (I 227). The δD - "age" correlation of all Mesozoic rocks (including the two from the batholith margin) is described by the least-squares line:

$$\text{Apparent Age} = 0.206 \times \delta D + 85.5$$

Figure 7.5 K-Ar apparent ages of "biotite" plotted against the δD value of the identical mineral separate. There is a distinct positive correlation between these variables. Circles denote Mesozoic rocks, and crosses represent Eocene plutons.

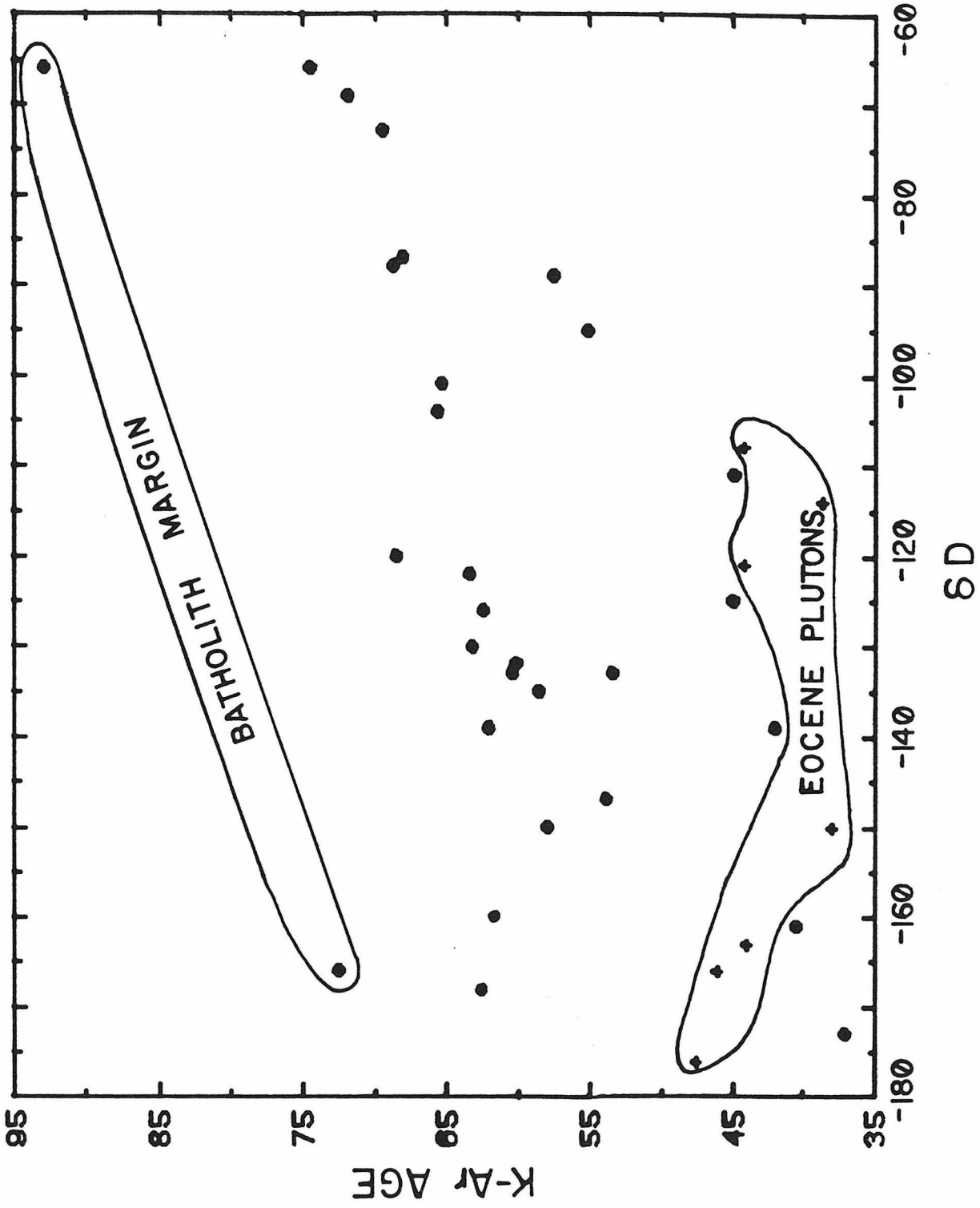
BATHOLITH MARGIN
EOCENE PLUTONS
K-Ar AGE
95
85
75
65
55
45
35
-60
-80
-100
-120
-140
-160
-180
δD

However, the ages do vary widely (± 15 m.y.) from the above least-squares line, particularly for any given δD value less than -100 permil.

It was hoped that the relatively poor isotopic systematics described above might be better elucidated if the δD content of each "biotite" concentrate was resolved into its pure chlorite and pure biotite components. This would then allow us to remove the chloritization effect which, as discussed above, has a strong influence on the bulk δD value but not on the K-Ar apparent age. Pertinent calculations and results are indicated on the following diagrams.

Figure 7.6 shows the relationship between the δD value and the K_2O contents of "biotite". The K_2O and H_2O contents (Fig. 5.9) allow the proportions of endmember biotite (9.2% K_2O) and chlorite (0% K_2O) to be determined for each mineral separate. If it is assumed that in each case the chlorite component formed in isotopic equilibrium with the meteoric water, so that its δD value would be approximately -150 permil, then the δD value of the biotite endmember can be calculated.

The mixing calculations are shown in Fig. 7.7, producing a family of mixing curves involving a single endmember chlorite (K_2O = 0; δD = -150) and various endmember biotites (K_2O = 9.2; δD = -60 to -180). The δD values of the biotite endmember in each analyzed mineral separate can then be estimated by extrapolation to the right-hand terminus of the appropriate curve; the actual calculated values are given in Table 7.1.

It is evident that this construction (Fig. 7.7) explains the wedge-shaped array of the data points. The "corrected" δD values of the "biotites" range from -206 to -22 permil (both extremes are poorly constrained, "inaccurate" values); most values range from a normal "primary magmatic" value of

Figure 7.6 δD value of "biotite" (i.e. biotite-chlorite mixtures) plotted against the K_2O content of the same mineral separate. Note the wedge-shaped distribution of data.

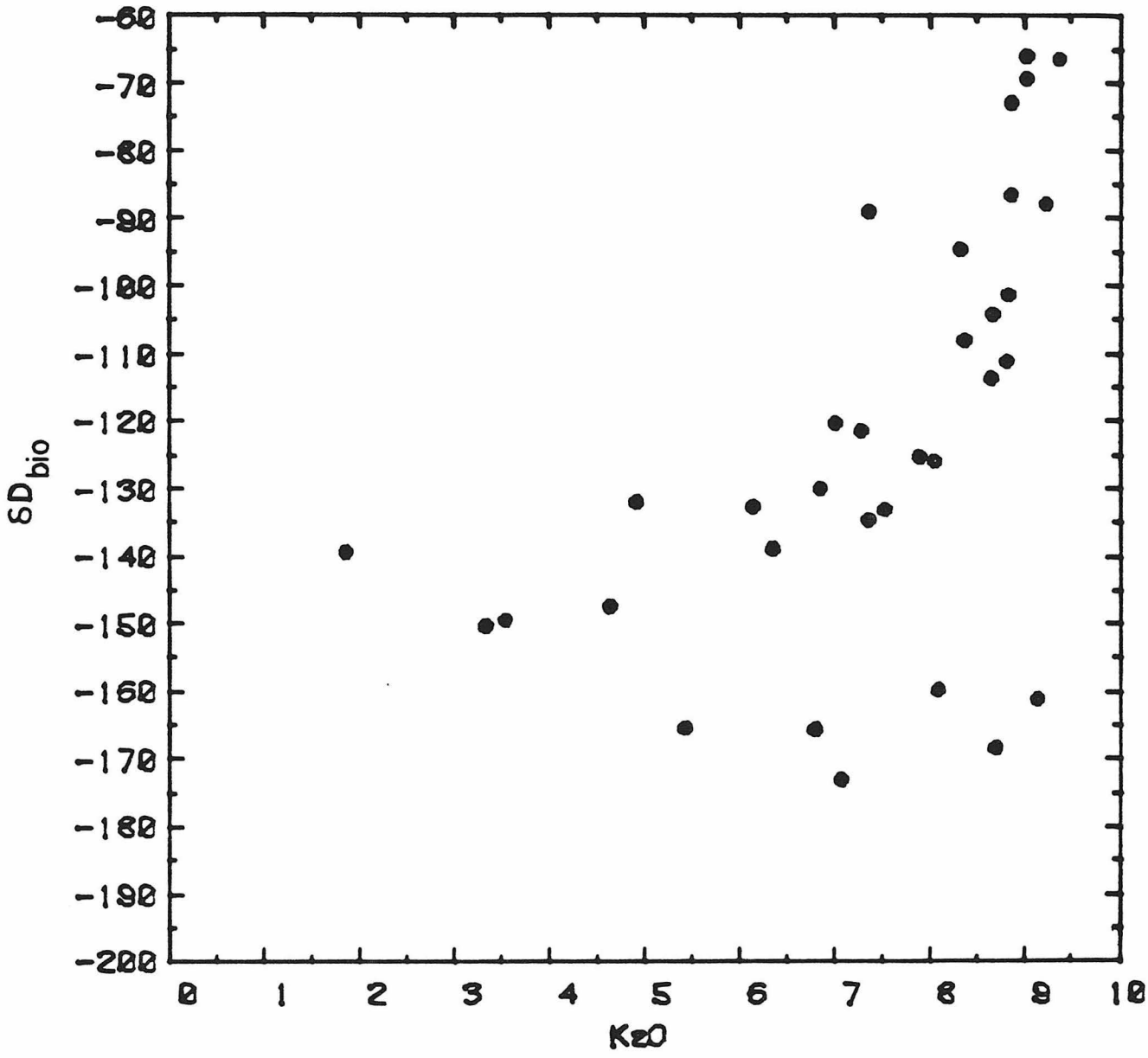
-60
-70
-80
-90
-100
-110
-120
-130
-140
-150
-160
-170
-180
-190
-200
δD_{bio}
0
1
2
3
4
5
6
7
8
9
10
K₂O

Figure 7.7 δD values of "biotites" (i.e. biotite-chlorite mixtures) plotted against the K_2O contents of the mineral separates. Only rocks with high ($\geq$ -75 permil) δD values can represent primary magmatic compositions. The majority of these "biotites" have interacted with heated meteoric waters; this has lowered the δD value and in most cases lowered the K_2O content as a result of conversion of biotite to chlorite. The family of curves represents theoretical mixing lines between one end-member represented by pure biotites (9.2 % K_2O) with δD values of -60, -80, -100, -120, -140, -160, and -180 permil, and another end-member composed of pure chlorite (0% K_2O) that is assumed to have a uniform δD value of -150 permil. The figure indicates that D/H exchange of some of the end-member biotites occurred during the hydrothermal process that converted part of the biotite to low-δD chlorite. See text.

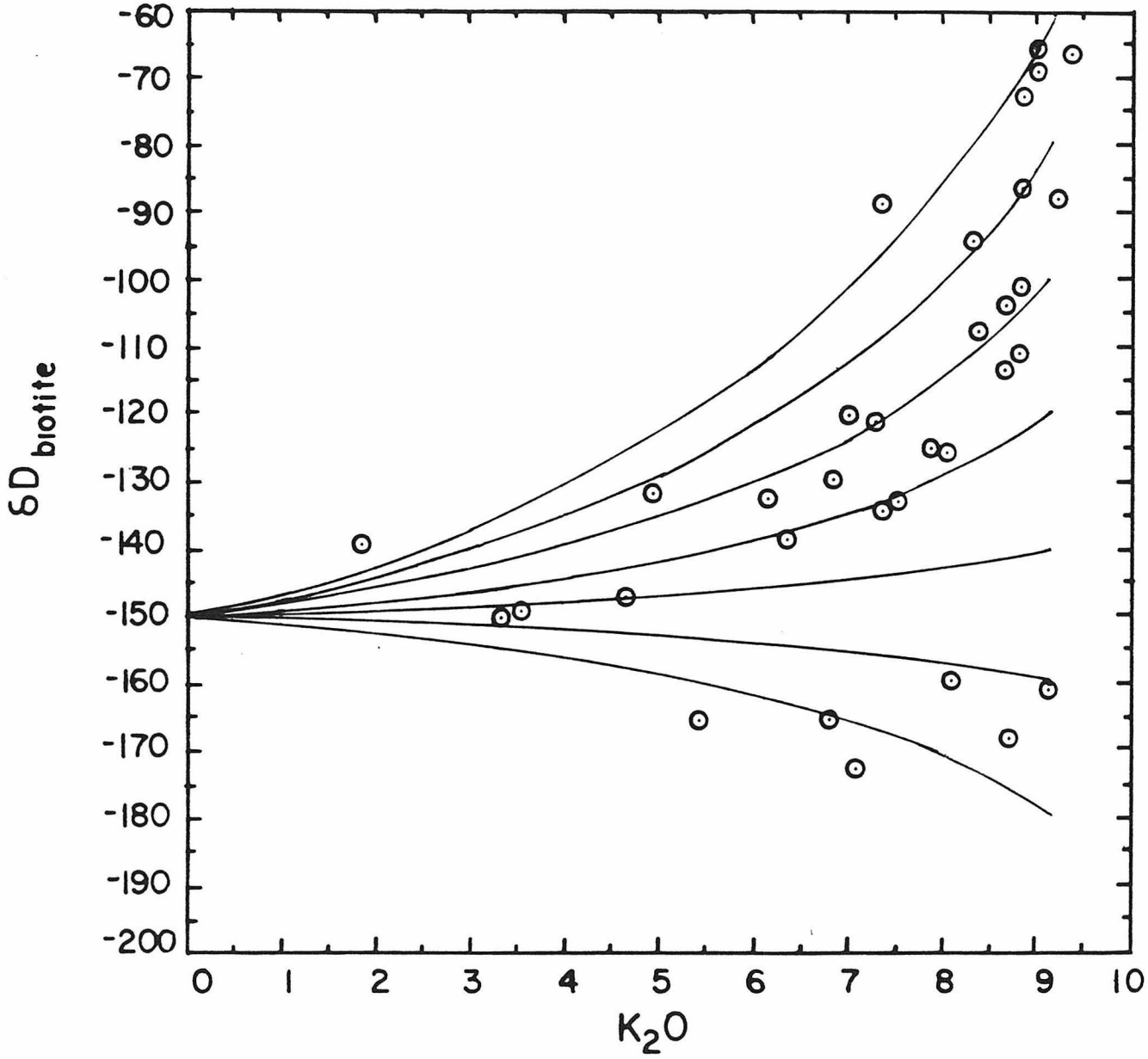
-60
-70
-80
-90
-100
-110
-120
-130
-140
-150
-160
-170
-180
-190
-200
δD biotite
0
1
2
3
4
5
6
7
8
9
10
K2O

Table 7.1

Calculation of δD Values of Endmember Biotites

Sample#	K-Ar Age	K_2O	H_2O#	δD	δD calc	Remarks
RB 45c	45.0	7.90	2.30	-125	-110 ± 6	
RB 68	57.5	7.37	2.52	- 89	- 41 ± 12	
RB 70	60.4	6.15	2.97	-133	-106 ± 17	inaccurate
RB 89f	68.5	7.02	2.78	-120	- 88 ± 14	
RB 134	65.3	8.83	1.92	-101	- 94 ± 3	
RB 148	68.6	9.22	1.71	- 88	- 88 ± 0	
RB 237a	42.1	1.87	4.02	-139	- 22 ± 107	inaccurate
RK 28a	63.4	7.29	2.35	-122	-101 ± 8	
RK 29a	58.0	3.33	3.87	-150	-150 ± 53	inaccurate
RK 40	44.9	8.81	1.79	-111	-107 ± 2	
RH 12	44.2	8.37	1.77	-108	- 98 ± 5	Eocene
RH 14a	40.5	9.14	1.63	-161	-161 ± 1	
RH 29	63.2	6.86	2.36	-130	-108 ± 13	
RH 43a	60.1	4.92	3.61	-132	- 81 ± 32	inaccurate
RH 57	65.6	8.67	1.89	-104	- 95 ± 4	
RH 85d	46.1	6.81	2.77	-166	-182 ± 16	Eocene; inaccurate
RH 95	53.4	7.52	2.18	-133	-123 ± 7	
RH 99	53.9	4.64	3.21	-147	-139 ± 29	inaccurate
RH 115	37.2	7.08	2.28	-173	-192 ± 9	
RH 120	38.0	3.54	3.10	-150	-150 ± 46	Eocene; inaccurate
RC 3a	62.4	8.06	1.99	-126	-117 ± 5	
RC 13	55.1	8.32	1.86	- 95	- 81 ± 6	
RC 18	68.0	8.86	1.74	- 87	- 82 ± 3	
RC 39e	61.5	8.10	2.46	-160	-165 ± 5	
I 7	62.6	8.69	1.81	-168	-171 ± 2	
I 9	58.6	7.37	2.14	-135	-125 ± 8	
I 14a	62.0	6.36	2.90	-139	-123 ± 15	
I 22	38.7	8.65	1.61	-114	-110 ± 4	Eocene
I 24a	71.8	9.01	1.81	- 69	- 64 ± 2	
I 32	92.9	9.37	1.63	- 66	- 66 ± 1	
I 205	74.4	9.01	1.53	- 66	- 66 ± 1	
I 210	69.4	8.85	1.97	- 73	- 64 ± 3	
I 227	72.5	5.43	3.64	-166	-206 ± 28	inaccurate

#H_2O content is given in μmoles/mg

-64 to a completely exchanged value of -192.

Although some of the extrapolations in Fig. 7.7 are poorly defined, it is clear that D/H exchange occurred in many of the "pure" biotite samples in the Atlanta lobe, in contrast to the general lack of discernible $^{18}O/^{16}O$ exchange in these endmember biotites (Fig. 5.10). The four samples that do show definite oxygen isotope exchange in the endmember biotite (I 7, RC 39e, RH 14a, RH 85d) also all display extreme D/H exchange, with the calculated δD value of the biotite endmember in each case being less than -160 permil. It is satisfying that the calculations in Table 7.1 demand marked deuterium depletions for these four samples, because theoretically the biotites must have undergone thorough D/H exchange if they have undergone strong ^{18}O exchange. It is unfortunate that the large variation in $^{18}O/^{16}O$ in the biotite and chlorite endmembers precludes treating the oxygen isotope data in a manner analogous to that carried out in Fig. 7.7 for the deuterium data.

Note that although the δD value of the biotite endmember can be rather accurately calculated for most of the points in Fig. 7.7, the estimates for those chlorite-rich separates with very low (< 5%) K_2O contents depend strongly on the assumptions because of the long extrapolation to the biotite endmember at 9.2 wt. % K_2O. If the δD value of the chlorite endmember was, for example, -139 rather than the assumed value of -150 permil, which is easily within permissible limits, the calculated δD value of the biotite endmember of sample RB 237a (1.8% K_2O, $\delta D = -139$) would be -139 rather than -22 permil. The calculation is obviously meaningless in such cases. Calculated "errors" are given in Table 7.1 assuming that the δD value of the endmember chlorite is known

only to $\pm$ 10 permil; analytical error in the δD and K_2O determinations would contribute only a few additional permil to the major uncertainties, which basically arise from the uncertainty in the actual chlorite δD value.

Returning now to the original purpose, the calculated δD values of the "pure" biotite endmembers are compared with the K-Ar apparent ages on Fig. 7.8. If Eocene rocks, probable Eocene rocks, and inaccurate points are excluded, a distinct positive correlation is seen to exist between these variables. However, the data scatter more widely than might be expected if the Ar loss was in all cases a <u>direct</u> consequence of the hydrothermal activity that caused the $^{18}O/^{16}O$ and D/H exchange. It is in fact possible that the D/H exchange in many of these endmember biotite samples occurred below the Ar "blocking temperature" of biotite ($\sim$ 300°C), as will be established more fully in Section 7.5.

Figure 7.8 Calculated δD values of end-member biotites plotted against the K-Ar apparent ages of the bulk mineral separate. Note the distinct positive correlation between these variables. Only Mesozoic rocks whose "δD" values could be confidently calculated to ± 15 permil are included. See text and Table 7.1.

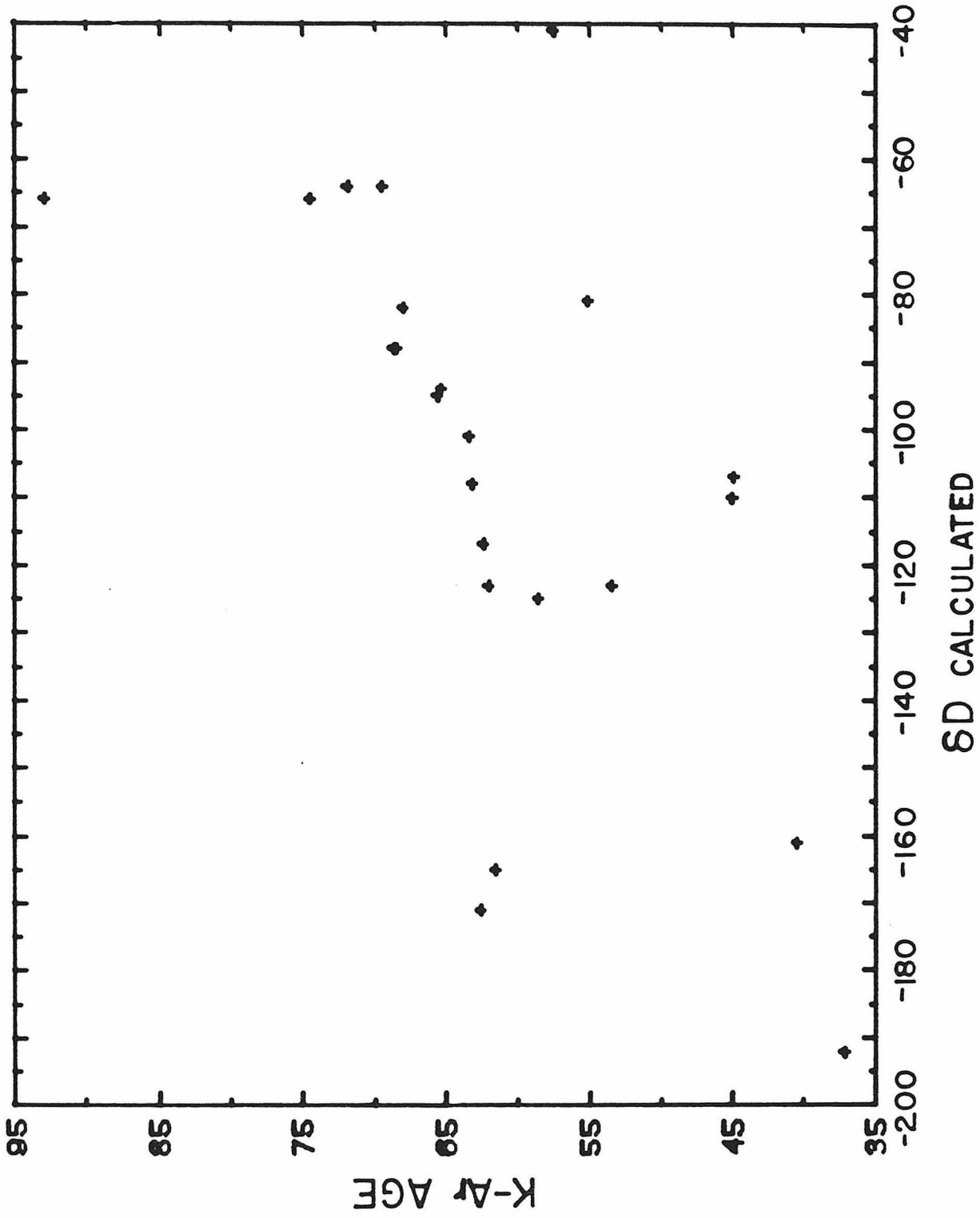
95
85
75
65
55
45
35
K-Ar AGE
-40
-60
-80
-100
-120
-140
-160
-180
-200
δD CALCULATED

7.3 Elevation Effect

Many studies, for example Armstrong (1966), Clark and Jäger (1969), Krummenacher et al (1975), and Turner and Forbes (1976), have shown that K-Ar ages in orogenic areas are often best interpreted as the time of uplift and cooling of the terrane (see Sec. 1.2.4). The discussion below will demonstrate the existence of a distinct vertical gradient in the K-Ar apparent ages in the Idaho batholith, and will propose that this uplift-related elevation effect, combined with a broad regional doming associated with emplacement of the Eocene batholiths, is one of the fundamental causes of the regional K-Ar age pattern. The other dominant K-Ar age-controlling mechanism in the batholith operated at the greatest depths now exposed by erosion (typically elevations below 3000') and also at short distances from Eocene plutonic contacts. This mechanism was clearly radiogenic Ar loss produced by the episode of hydrothermal (and contact) metamorphism that occurred during Eocene plutonism.

Figure 7.9 shows the relationship between the K-Ar apparent ages and the longitudes of analyzed Mesozoic biotite samples in the Atlanta lobe. This type of plot is employed because it utilizes readily available "objective" parameters, and does not require any geologic assumptions that are difficult to justify, such as would be the case with "distance to an intrusive contact"; the latter are often poorly known in this region, and in any case there is always the problem of buried plutons at shallow depths. The age data plotted in Fig. 7.9 display a distinct, parabola-like pattern as a function of distance; the minimum values are centered on the axis of Eocene plutonism, which trends roughly N-S between 114° 40' and 115° 30' and hence normal to the page. It might be argued that

Figure 7.9 K-Ar apparent ages of Mesozoic biotites from the Atlanta lobe plotted against the longitude of the sample. Note the distinct, parabola-like distribution with the minimum ages centered on the N-S trending axis of Eocene plutonism. The points are coded according to their elevation (feet above sea level), and it is apparent that at any longitude high elevation rocks (circles) tend to have older apparent ages than those collected at low elevations. The points with apparent ages of less than 45 m.y. almost invariably represent rocks collected near Eocene plutons, and the ages do not show a definite correlation with elevation. For the samples with ages older than the 45 to 53 m.y. "age gap", a stippled pattern outlines the distribution of samples collected between elevations of 5000 to 6000 feet. This contour separates all of the high-elevation points from the low-elevation points, as well as illustrating the parabola-like pattern.

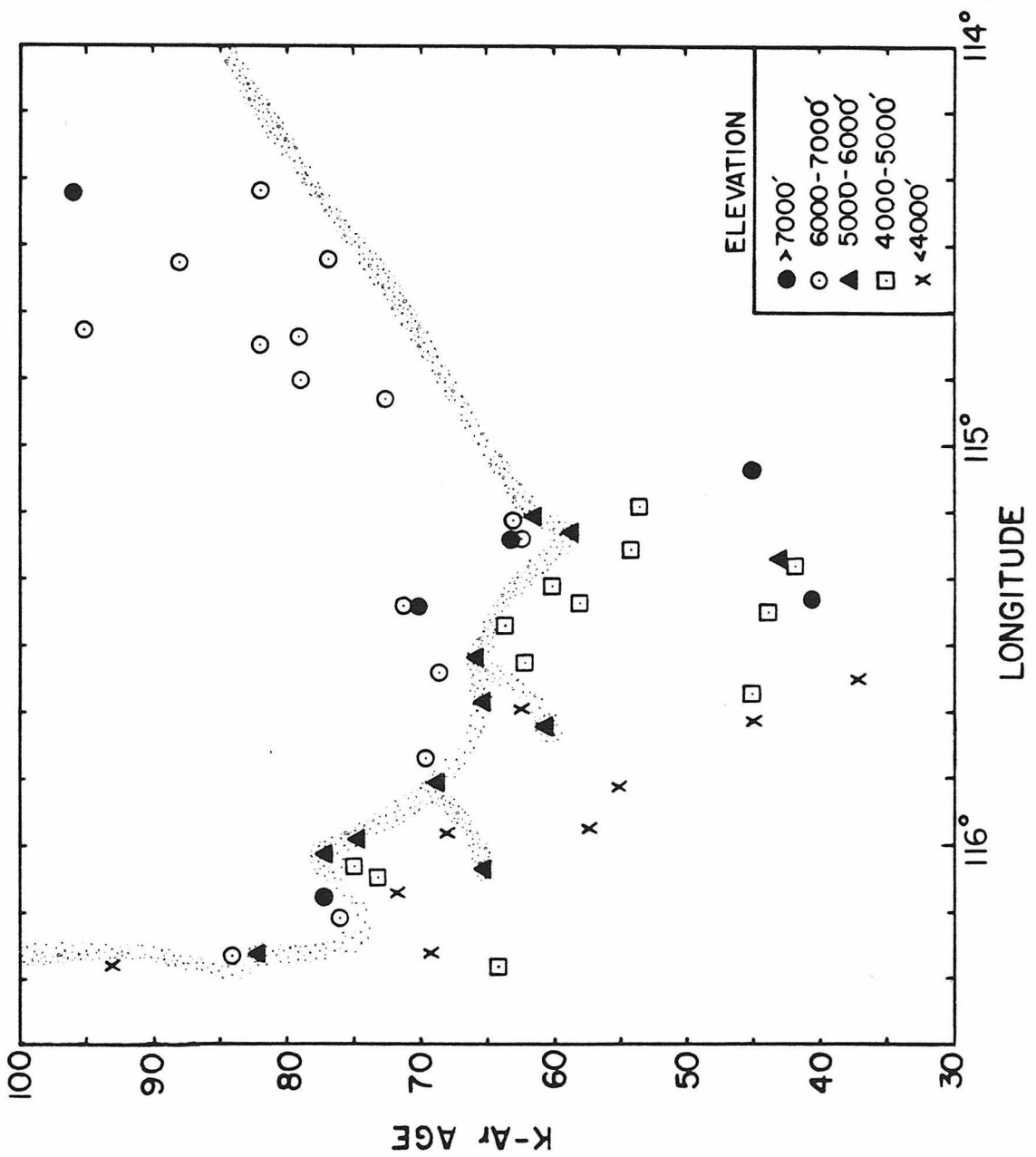
ELEVATION
>7000'
6000-7000'
5000-6000'
4000-5000'
<4000'
K-Ar AGE
100
90
80
70
60
50
40
30
116°
115°
114°
LONGITUDE

the relationship in Fig. 7.9 was entirely produced by partial loss of radiogenic Ar from the Mesozoic rocks during the Eocene hydrothermal event, particularly in view of the relationship shown in Fig. 7.8. However, as discussed previously, the great distances involved and the conspicuous age gap between 45 and 53 m.y. indicate that a combination of uplift and hydrothermal heating are required to explain the K-Ar age pattern.

Superimposed on the "parabolic" K-Ar pattern in Fig. 7.9 is an elevational dependence of the data points. At any longitude, high elevation points (circles) are "older" than middle elevation points (triangles and squares), which in turn generally have greater apparent ages than low elevation points (crosses). Numerous exceptions occur, especially where the distances to the Eocene intrusive contacts are short, as is demonstrably the case for almost all samples with apparent ages less than 45 m.y. Another example is a sample collected near the small Pearl-Horseshoe Bend diorite stock, at 116° 18', 64 m.y., reported by Armstrong (1975a). Overall, however, the correlation with elevation is astonishing when it is considered that the data have not been manipulated in any special way.

A complete analysis of the relationships shown in Fig. 7.9 requires the separation of the geographic and elevational dependences. The most straightforward and informative way of doing this is to divide the batholith into a series of 13 km wide (10' of longitude), N-S trending geographic strips, and to plot the apparent age vs. elevation for all the samples collected within each longitudinal strip. The results are shown on the following series of figures.

Strip "A" (Fig. 7.10) contains all points between 115° 8.9' and 115° 20', near to and just west of the major axis of Eocene plutonism. The series of "older" data points in the strip exhibit a clearcut, positive, almost linear correlation with elevation, such that the oldest apparent ages occur at the highest altitudes. However, two of the "younger" data-points (42, 43 m.y.) plot well off this correlation line and thus appear to have suffered total Ar loss during the Eocene heating event; two other points (53, 54 m.y.) appear to have partially lost radiogenic Ar. Note that all of these samples, from oldest to youngest, have very low δD values (-130 to -168) and hence have all been markedly exchanged with the meteoric-hydrothermal fluids. The calculated biotite endmember δD values are also all very low (-108 to -171, Table 7.1). There is no correlation between δD and K-Ar age for this subset of samples.

The data points within the next strip to the west ("B", 115° 20' - 115° 30') that exhibit the oldest apparent ages also display a positive correlation with elevation, although the distribution of data is not sufficient to prove the trend. Two of the data points (41, 44 m.y.) display complete Eocene Ar loss and do not correlate with elevation.

Most of the data points within the next strip "C", 115° 30' - 115° 40') exhibit a clearcut linear correlation with elevation, with a slope of 0.14 mm/yr (460 feet/m.y.). However, two points (37, 45 m.y.) collected near the Rocky Bar intrusive complex show the effects of pronounced Ar loss during the Eocene heating event.

The 3 data points within the adjoining strip ("D", 115° 40' - 115° 50') also seem to exhibit a positive elevational dependence, but the slope of the line is considerably different from the values in the above

Figure 7.10 A,B,C,D,E,F,G,b Plots of biotite K-Ar apparent ages vs. the elevation (in thousands of feet above sea level) of the Mesozoic rock samples in various ~ 13 km wide (10' of longitude), N-S trending geographic strips in the Atlanta lobe. Rocks with the oldest K-Ar apparent ages in each strip generally correlate positively with elevation, such that the oldest K-Ar ages occur at the highest elevations. Rocks with markedly younger apparent ages generally occur at low elevations, except those collected close to contacts with Eocene plutons, and their positions mark the truncation points ("elbows") of the age-elevation trends seen in "older" rocks. Data from eight geographic strips are shown on the following eight figures, all plotted within identical boxes to facilitate inter-comparisons. Sample numbers are indicated for each point (Tables 4.5 and 4.6). See text.

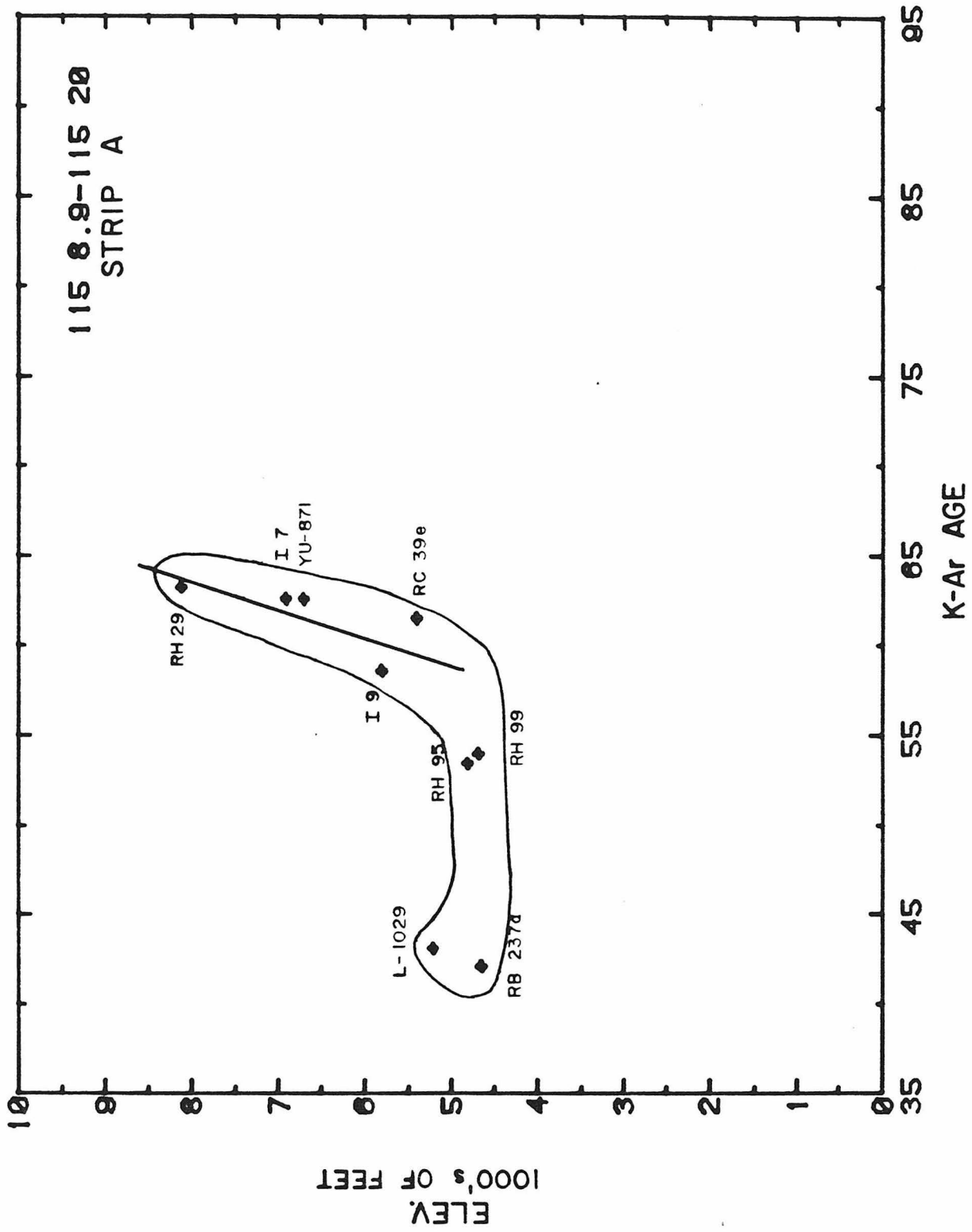
115 8.9-115 20
STRIP A
RH 29
I 7
YU-871
RC 39e
I 9
RH 95
RH 99
L-1029
RB 237d
ELEV.
1000's OF FEET
K-Ar AGE
10
9
8
7
6
5
4
3
2
1
0
95
85
75
65
55
45
35

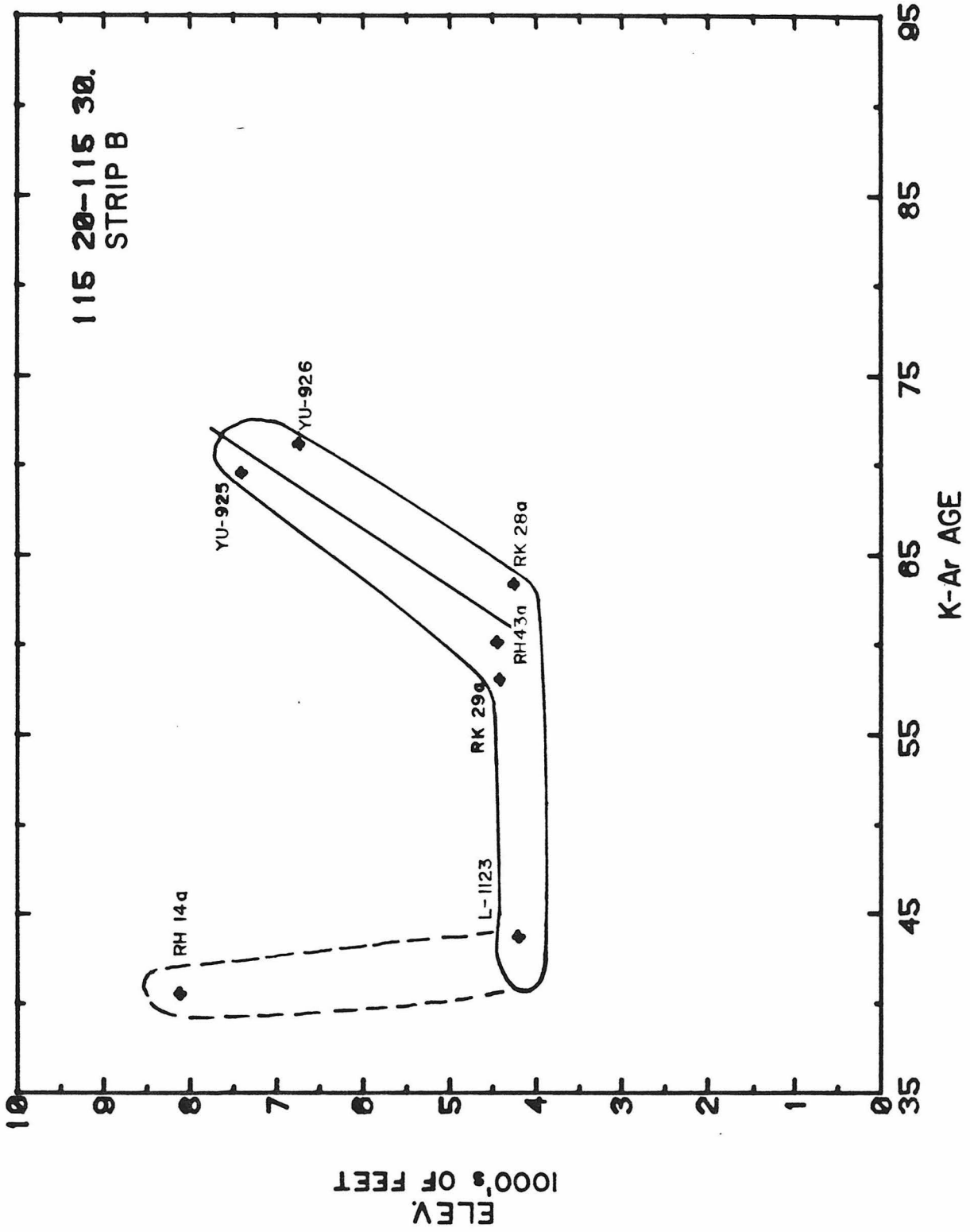
115 20-115 30.
STRIP B
YU-926
YU-925
RK 28a
RH43n
RK 29g
L-1123
RH 14a
10
9
8
7
6
5
4
3
2
1
0
35
45
55
65
75
85
95
K-Ar AGE
ELEV.
1000's OF FEET

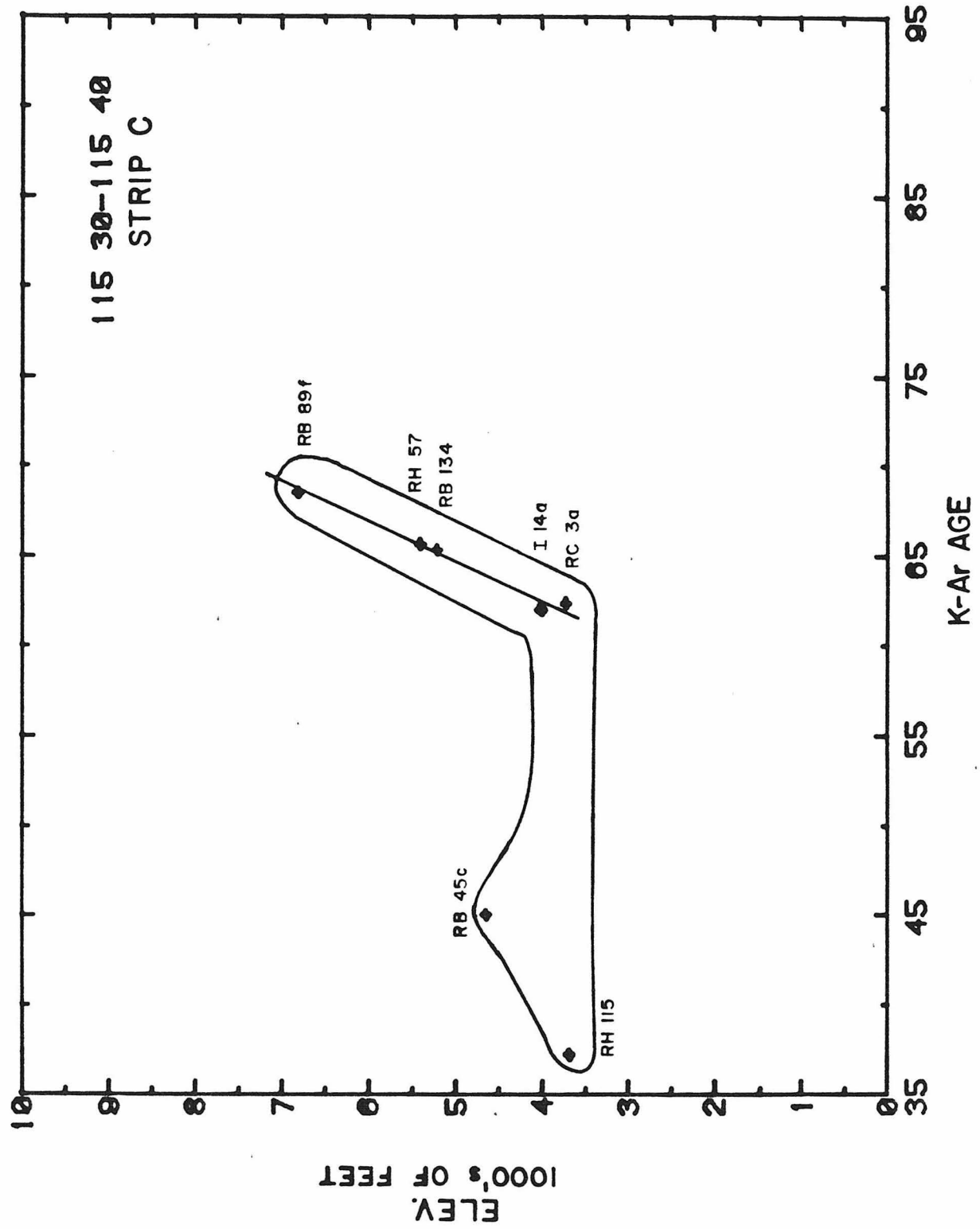
115 30-115 40
STRIP C
RB 89f
RH 57
RB 134
I 14a
RC 3a
RB 45c
RH 115
ELEV.
1000's OF FEET
K-Ar AGE
0
1
2
3
4
5
6
7
8
9
10
35
45
55
65
75
85
95

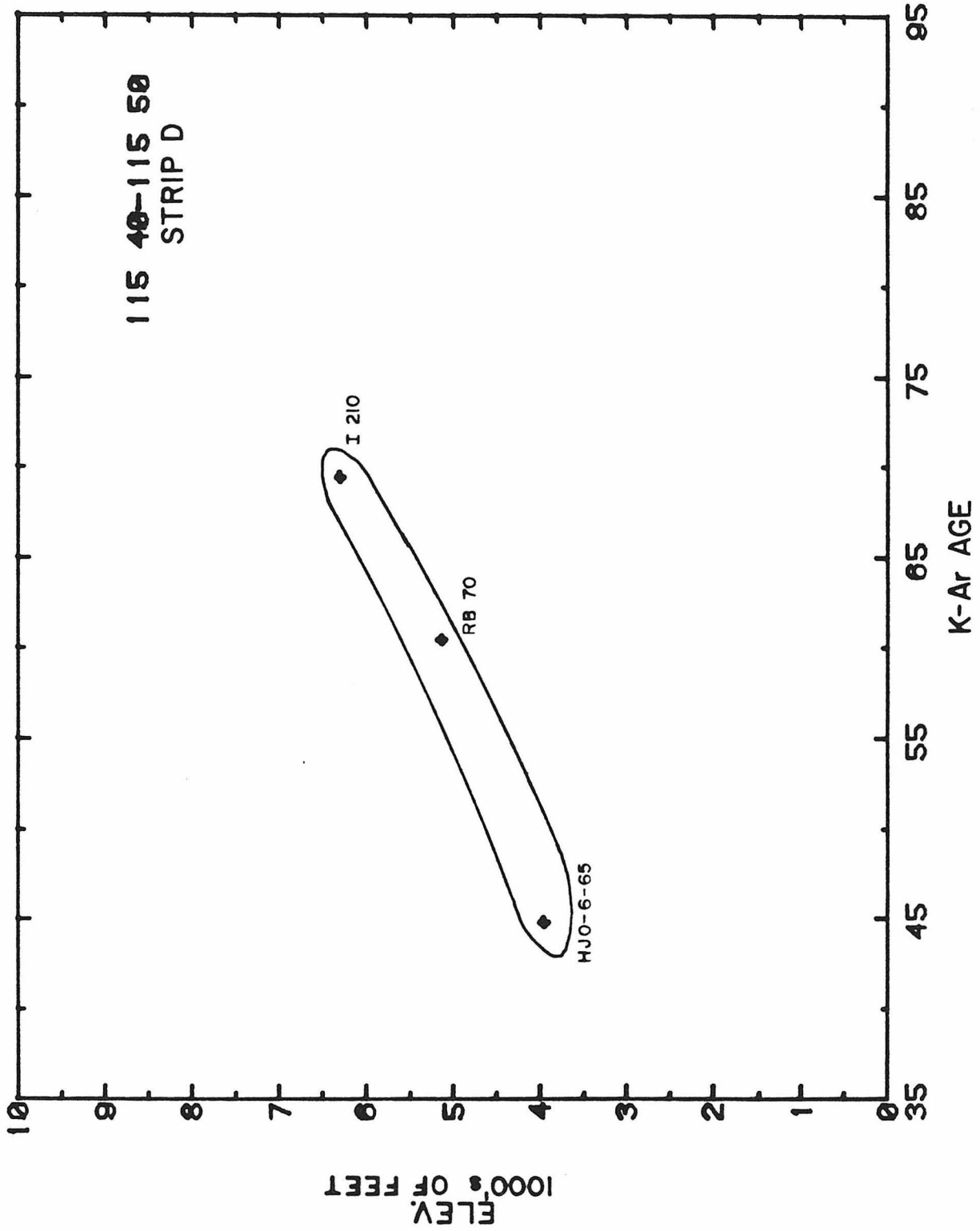
115 40-115 50
STRIP D
I 210
RB 70
HJ0-6-65
ELEV.
1000's OF FEET
K-Ar AGE
0
1
2
3
4
5
6
7
8
9
10
35
45
55
65
75
85
95

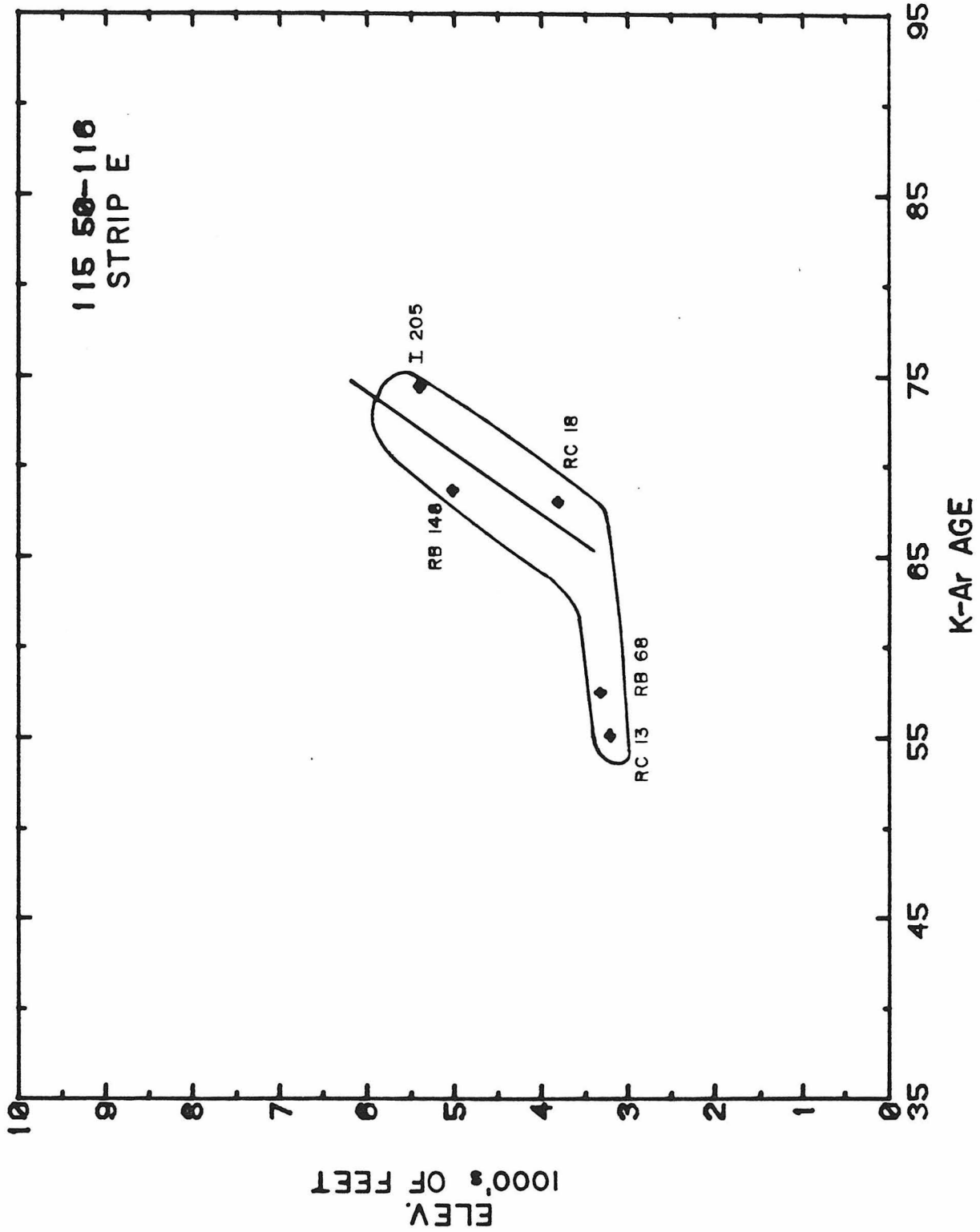
115 50-116
STRIP E
I 205
RC 18
RB 140
RB 68
RC 13
ELEV.
1000's OF FEET
K-Ar AGE
0
1
2
3
4
5
6
7
8
9
10
35
45
55
65
75
85
95

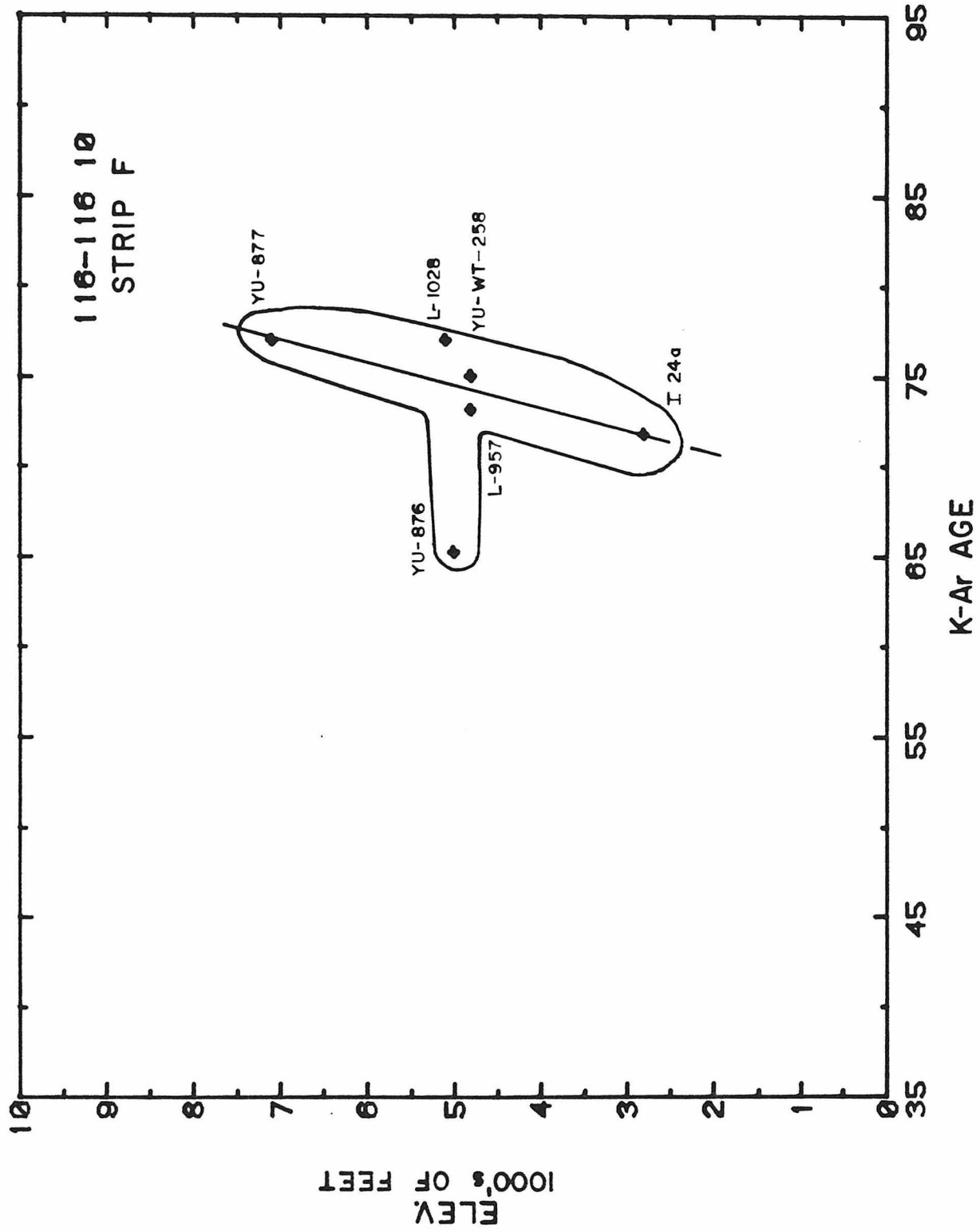
118-116 10
STRIP F
YU-877
L-1028
YU-WT-258
I 24a
L-957
YU-876
ELEV.
1000's OF FEET
K-Ar AGE
10
9
8
7
6
5
4
3
2
1
0
95
85
75
65
55
45
35

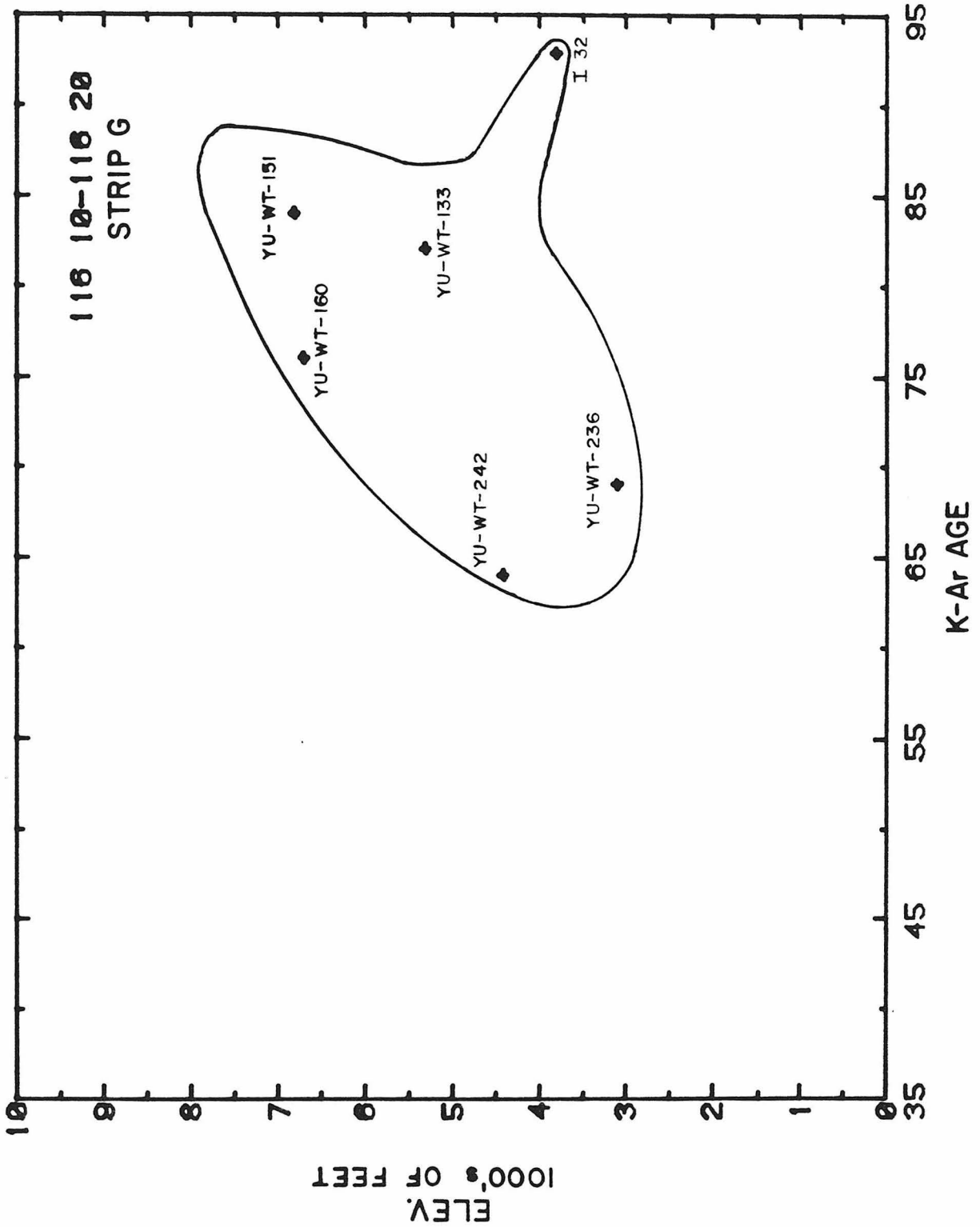
118 10-118 20
STRIP G
YU-WT-151
YU-WT-160
YU-WT-133
I 32
YU-WT-242
YU-WT-236
ELEV.
1000's OF FEET
K-Ar AGE
10
9
8
7
6
5
4
3
2
1
0
35
45
55
65
75
85
95

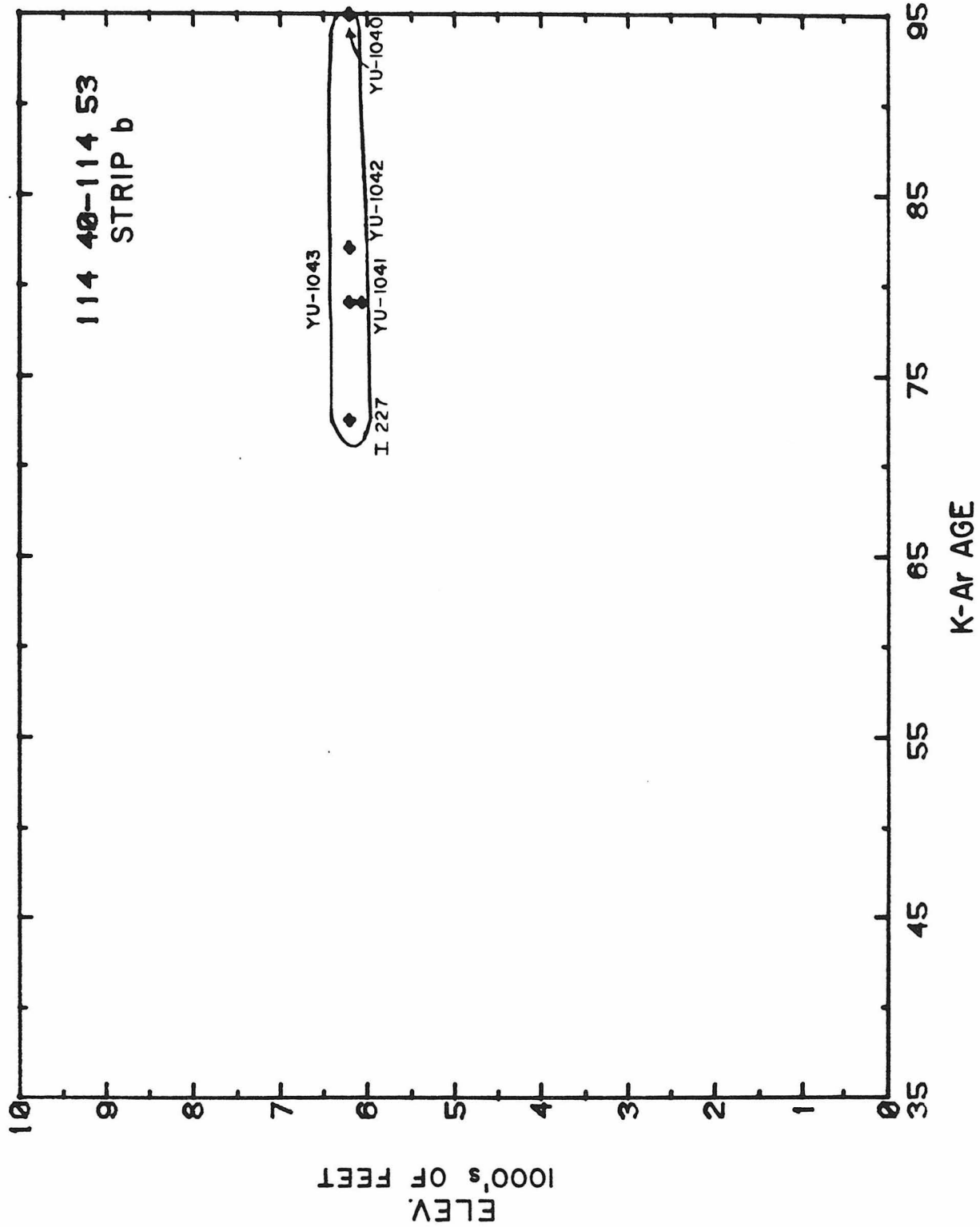
114 40-114 53
STRIP b
YU-1043
YU-1041
YU-1042
YU-1040
I 227
10
9
8
7
6
5
4
3
2
1
0
35
45
55
65
75
85
95
K-Ar AGE
ELEV.
1000's OF FEET

zones. Also this is the only strip where δD correlates well with the K-Ar age. It is suspected that the 45 m.y. point suffered total Ar loss, and the 61 m.y. point underwent partial Ar loss, due to nearby Eocene plutons. This unusual 3-point trend-line is considered to be fortuituous, and it is thought that only the point at 69 m.y. actually would lie on an age-elevation correlation line similar to those shown in Figs. 7.10a and 7.10c (see below).

The "oldest" rocks within the next strip ("E", 115° 50' - 116°) apparently fit a similar type of positive correlation with elevation, but the slope cannot be accurately determined because of the analytical uncertainty and the small range in elevation of the points. The "oldest" point (74.4), a tonalite, actually shows a closer relationship to the tonalites and granodiorites of strip "F" than to the other rocks of strip "E" which are quartz monzonites. The other points (55, 58 m.y.) in strip "E", the youngest of which was collected within 3 km of the Boise Basin intrusive, have apparently suffered partial Ar loss. It could be argued that all five rocks plot on a linear correlation line with a low slope, but in view of the above considerations and for overall consistency the preferred interpretation is as shown.

Points within strip "F" (116° - 116° 10') exhibit a good positive correlation with elevation. However, one point (65 m.y.) does not conform to this trend, possibly because of episodic Ar loss during the Eocene (although this cannot be documented geologically).

The apparent ages along the west margin of the batholith (strip "G", 116° 10' - 116° 20') show a poor positive correlation with elevation, and the slope may be different from the other zones. Similarly, samples from

the east margin of the batholith (strip "b", 114° 40' - 114° 53') show no correlation between apparent age and elevation. In these regions lateral changes in the apparent ages are also important, perhaps reflecting a boundary effect of batholithic emplacement or diapiric uplift. Considerable faulting and tilting has occurred along the western margin (strip "G") of the batholith (Kirkham, 1930; Hamilton, 1962), and this may have disturbed the age-elevation systematics in this region.

It is interesting to note that although (by inference) the K-Ar data suggest that the east margin of the batholith conforms to the mapped contact, the Bouguer gravity anomaly does not (Eaton et al, 1978). The latter closely follows the west and south contacts of the Atlanta lobe, yet does not follow the contact on the east side of the batholith but instead occurs much further east. Either the inference based on the K-Ar ages is wrong, or there is not a complete correspondence between the gravity anomaly and the batholith. The latter possibility would be in agreement with the relatively low metamorphic grade of much of the Paleozoic rock east of the batholith. Eaton et al (1978) in fact have suggested that large negative gravity anomalies need not perfectly coincide with low density batholithic rocks, since they may also reflect the density distribution of rocks at much greater depths.

Last, all analyzed rocks within one strip ("a", 114° 53' - 115° 8.9') represent Eocene rocks or probable Eocene rocks; the only possible exception (RK 40; 45 m.y.) was collected within 1 km of a Sawtooth pluton, and is either an Eocene rock or a Mesozoic rock which understandably lost all radiogenic Ar during the Eocene. These samples are thus inapplicable to the K-Ar age vs. elevation relation, and are not plotted.

The trend lines for the various 10' strips are shown together on Fig. 7.11, with the exception of strip "a" (no appropriate samples), strips "b" and "G" (batholith margin), and strip "D" (unusual and probably fortuitous trend). The figure shows that the "oldest" rocks in strips "A", "B", "C", "E", and "F" clearly display similar slopes of 0.09 to 0.23 mm/yr (300 to 800 ft/m.y.), with a best determined value of 0.14 mm/yr (strip "C"; 460 ft/m.y.). Note that both the positions of the trend lines and the elevations of the truncation points ("elbows") change systematically from west (strip F) to east (strip A). As discussed below, truncation points probably represent the position of the Ar blocking isotherm during Eocene time. The Ar blocking temperature is actually a narrow temperature interval, above which daughter (radiogenic) Ar diffuses away as fast as it is produced by decay, and below which diffusional losses are negligible; the "blocking temperature" depends on the type of mineral and also on the cooling rate, but for biotite is typically 300 $\pm$ 50°C (Dodson, 1973, 1979).

The interpretation favored for the trend lines is that all strips initially had the same age vs. depth relationship, which reflected slow (0.14 mm/yr) uplift and cooling of the Idaho batholith in pre-Eocene time. The writer envisages a model of continued, constant uplift from the late Mesozoic to the Eocene which caused successively deeper rocks to pass through the Ar blocking temperature, at levels below which Ar retention was impossible in biotite such that the rocks had a zero apparent age. At levels above this isotherm the biotite began to retain daughter Ar, and constant uplift resulted in the linear age vs. depth relation which was initially the same for all strips. Later, large scale doming of the region caused by emplacement of Eocene batholithic rocks (or

Figure 7.11 Elevation/Apparent-age trend lines of the "oldest" rocks within geographic strips A,B,C, E and F (c.f. figures 7.10). The slopes of all these trend lines vary from 0.09 to 0.23 mm/yr (300 to 800 feet per m.y.), with the trend given by strip C (0.14 mm/yr, or 460 feet/m.y.) being the best determined and close to the average value. The slopes of these lines are interpreted to represent uplift and cooling of the terrane in pre Eocene time, as discussed in text. Note that the positions of the various trend lines as well as the lower termination points (truncation points) change systematically as the longitude increases from strip A to strip F.

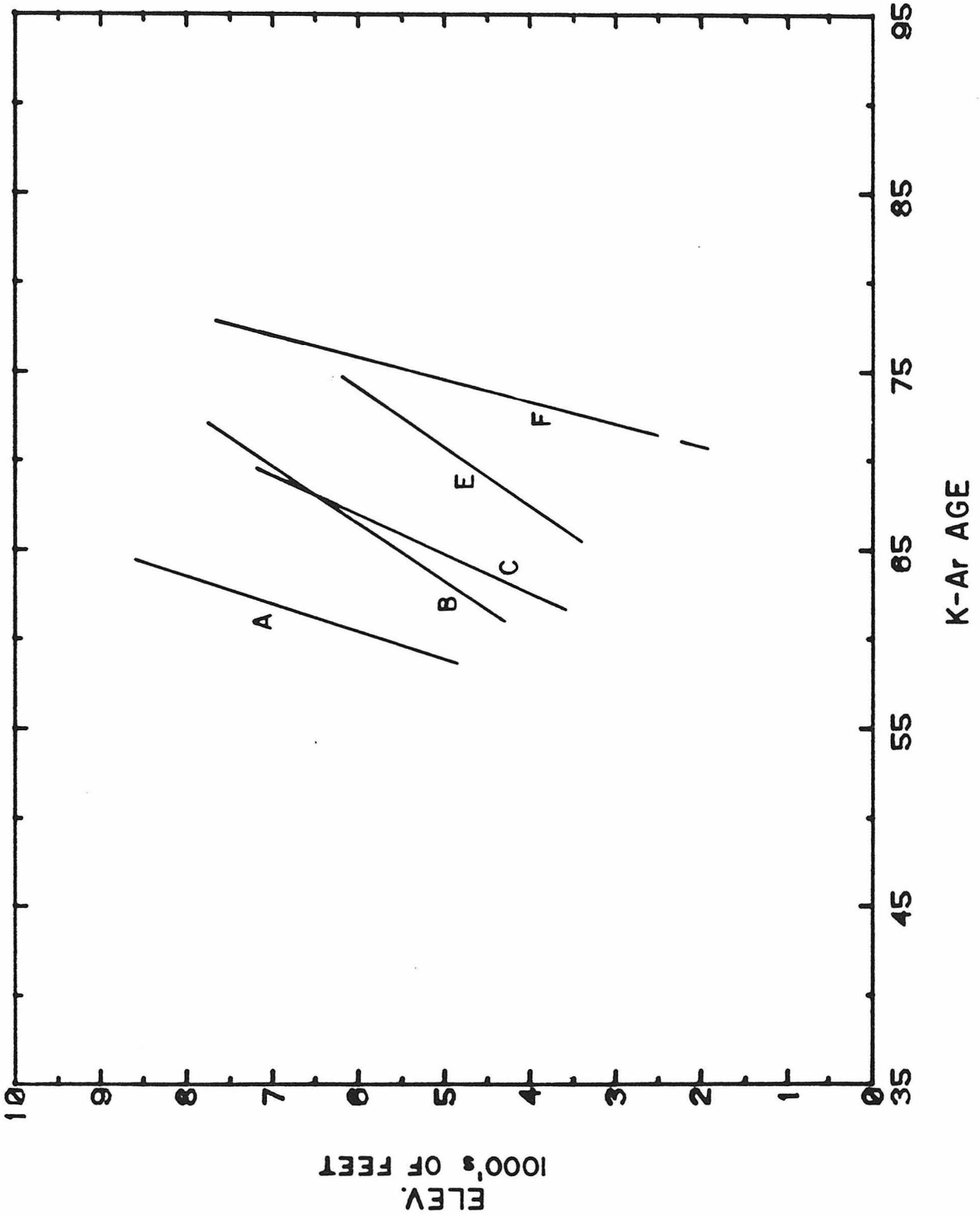
ELEV.
1000's OF FEET
10
9
8
7
6
5
4
3
2
1
0
95
85
75
65
55
45
35
K-Ar AGE
A
B
C
E
F

batholithic diapirism?) would have disturbed the elevation significance of the points, with the amount of change being directly related to the amount of doming at any locality, as schematically shown in Fig. 7.12. Thus, it appears that rocks within strip "A", near the axis of Eocene plutonism, were uplifted approximately 1 km relative to those of strips "B" and "C", which were in turn uplifted about 1 km relative to strips "D"(?) and "E", which were elevated about 1 km relative to strip "F" (Fig. 7.12). The above values could be in error by a factor of 2 given the uncertainty of the slopes of the correlation lines in Fig. 7.11, but even so they constrain several significant geologic parameters associated with the development of the Idaho batholith, as discussed in the section 7.5.

7.4 Hydrothermal Heating Effect

Previous studies (e.g. Hart, 1964; Hanson and Gast, 1967) have demonstrated that catastrophic Ar loss in older rocks commonly occurs in the reheated contact zones of crosscutting plutons. The following discussion shows that this phenomenon has also influenced many of the K-Ar ages of the Idaho batholith, notably at low elevations where temperatures were highest, and also in localities near contacts with Eocene plutons.

Figure 7.13 shows that the positions of the truncation points ("elbows") of the trend lines of Fig. 7.10 become systematically lower in elevation as the longitude increases from strip "A" (115° 8.9' - 115° 20') to strip "F" (116° - 116° 10'). These points probably represent the approximate position of the Ar "blocking" isotherm (~ 300°C) during the Eocene event, such that rocks heated to higher temperatures underwent

Figure 7.12 Schematic diagram comparing the vertical K-Ar apparent age gradients in a simplified cross-section through two terranes, one that underwent gentle symmetrical doming 40 m.y. ago and one that did not.

A. Present day cross-section through a terrane that has developed a uniform K-Ar apparent age gradient as a result of several million years of constant, uniform uplift through the Ar "blocking temperature" of biotite. This uplift could be due to any cause but a reasonable process might be isostatic readjustment after Mesozoic batholith formation. The rocks are assumed to have a present-day temperature of about 300° C and a zero age at a depth of 10.5 km, with an uplift rate of 0.15 mm per year and a geothermal gradient of 28.6° C per km. The "fossil" 300° C isotherm established in the rocks 40 m.y. ago is presently at a constant depth of 4.5 km.

B. Graph of K-Ar apparent ages vs. elevation for terrane A. At all positions I to VI the "age"/elevation trends are identical.

C. Symmetrical doming of terrane A over a short interval of time 40 m.y. ago was produced by magmatic intrusion at depth or by any other mechanism. This doming is superimposed upon a regional uplift identical to that in cross-section A, and produces a new terrane C where the observed apparent age of the rocks depends on both elevation and position relative to the dome axis.

D. Graph of K-Ar apparent ages vs. elevation for terrane C. Although the trend lines remain essentially parallel for gentle doming, the "age" /elevation trend lines are displaced according to their position. The slopes of the lines still reflect the ancient uplift rate and geothermal gradient, and the differential uplift of various positions due to doming may be reckoned by the displacements of the trend lines.

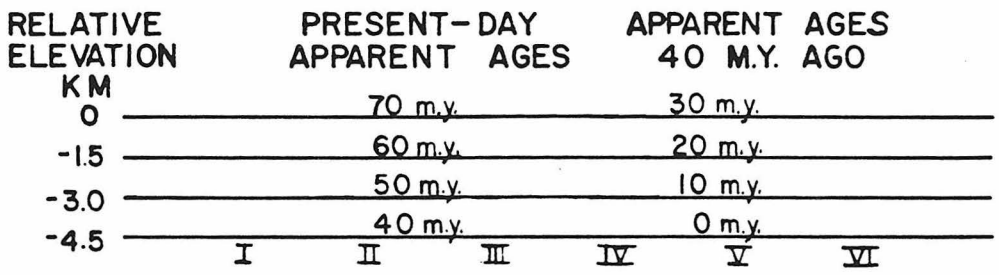
RELATIVE ELEVATION KM
PRESENT-DAY APPARENT AGES
APPARENT AGES 40 M.Y. AGO
0
-1.5
-3.0
-4.5
70 m.y.
60 m.y.
50 m.y.
40 m.y.
30 m.y.
20 m.y.
10 m.y.
0 m.y.
I
II
III
IV
V
VI

A

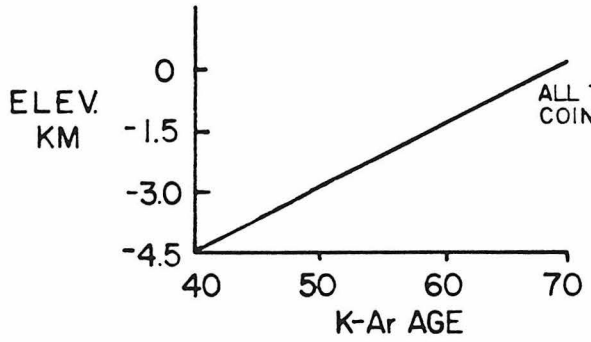
ELEV. KM
0
-1.5
-3.0
-4.5
40
50
60
70
K-Ar AGE
ALL TRENDS COINCIDENT

B

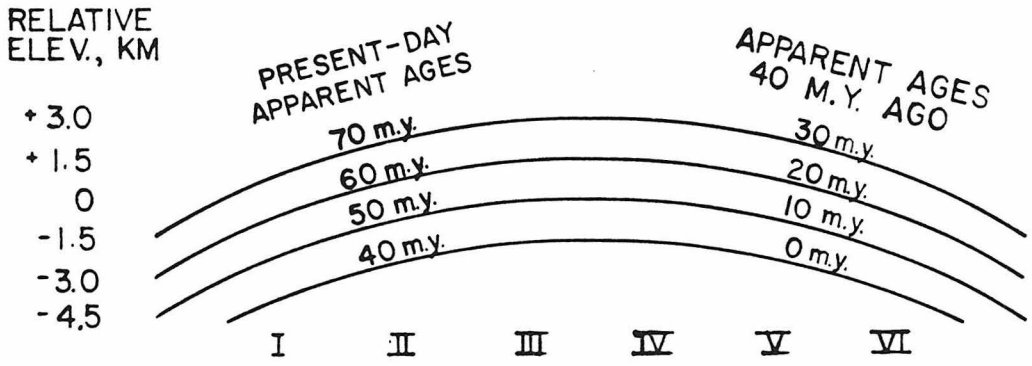
RELATIVE ELEV., KM
+3.0
+1.5
0
-1.5
-3.0
-4.5
PRESENT-DAY APPARENT AGES
APPARENT AGES 40 M.Y. AGO
70 m.y.
60 m.y.
50 m.y.
40 m.y.
30 m.y.
20 m.y.
10 m.y.
0 m.y.
I
II
III
IV
V
VI

C

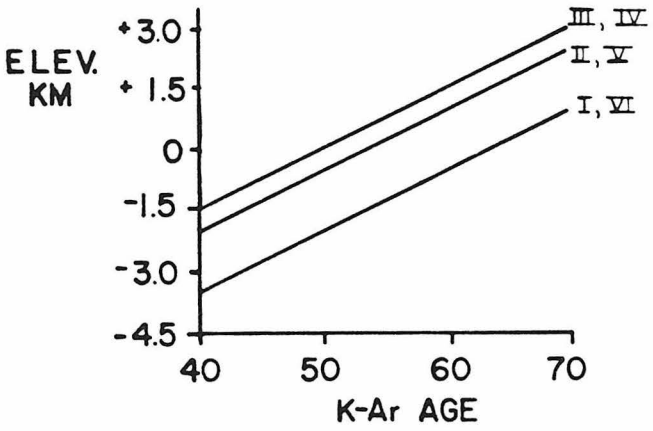
ELEV. KM
+3.0
+1.5
0
-1.5
-3.0
-4.5
40
50
60
70
K-Ar AGE
III, IV
II, V
I, VI

D

Figure 7.13 The elevations of the "truncation points" (elbows) of the K-Ar age/elevation trends of Fig. 7.10 seem to systematically increase from west to east across the Idaho batholith. The positions of these points are highly uncertain in strips b and D, cannot be determined for strips a and G, and must lie below the plotted triangle in strip F. The truncation point for strip b was determined on the assumption that all the K-Ar ages within this strip underwent partial Ar loss during the Eocene event, although this interpretation is not necessarily preferred. If the locus of Eocene plutonism is actually the axis of a regional dome, then the elevation of the truncation points should begin to systematically decrease on the east side of the batholith. Note, however, that the magnitude of elevation change of the truncation points from strip F to strip b is essentially identical to the change in average elevation across the batholith (Fig. 2.2).

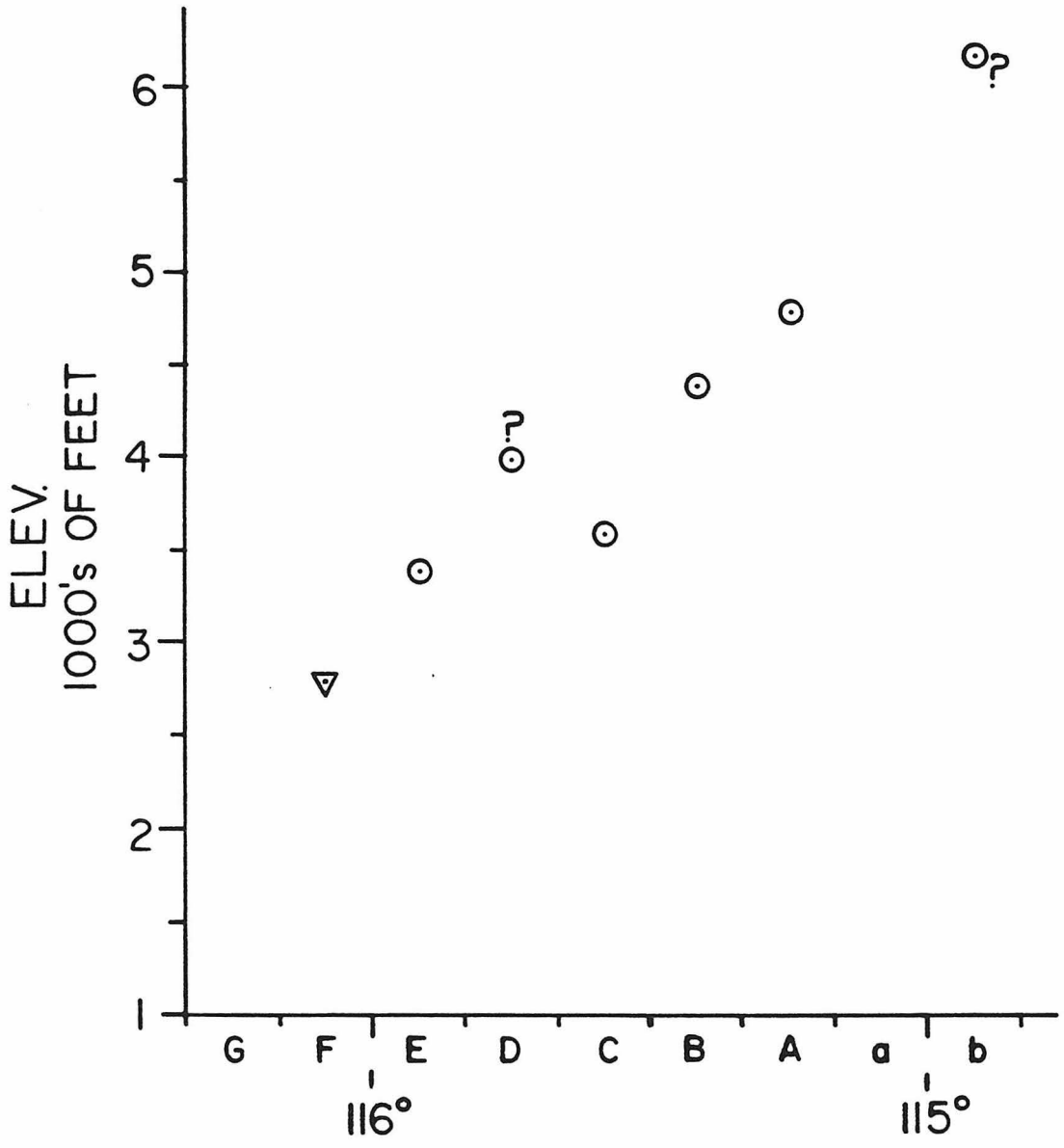
ELEV.
1000's OF FEET
6
5
4
3
2
1
G
F
E
D
C
B
A
a
b
116°
115°

partial or complete Ar loss at this time. The systematic variation in elevation of these points strongly suggests that the data reflect the regional distribution of the 300°C isotherm, and that all rocks at lower elevations (higher temperatures) suffered catastrophic Ar loss during the Eocene. However, an added complication is that many of the "young" K-Ar ages that define the truncation points could simply be from rocks collected close to contacts with Eocene plutons, as is demonstrable for the 45 m.y. rock within strip "D" and for at least one of the "young" (55 m.y.) rocks within strip "E" of Fig. 7.10. It is considered to be probable that the regional truncation points in these and possibly some other strips would have somewhat lower elevations - that is that rocks collected below the "elbows" in Fig. 7.10 could be found whose K-Ar ages still correlate positively with elevation.

Figure 7.14 is a modification of Fig. 7.12 which suggests that the systematic variation of the positions of the various "age" - elevation trend lines, as well as that of the truncation points, reflects an episode of doming produced by intrusion of the Eocene batholiths. If the Eocene magma chamber is as large as is suggested by the sketch, then regional magmatic heating of the country rocks must be considered in addition to simple doming of the pre-Eocene isotherms, as is shown. The similarity between the resultant trend lines of Fig. 7.14b and Fig. 7.11 strongly suggests that both doming and regional contact heating of the Idaho batholith occurred in Eocene time. A similar but more accurate model is presented in the next section.

Figure 7.14 Modification of the model of Fig. 7.12, assuming that doming of the batholithic terrane was produced by intrusion of a large Eocene batholith. Cross-section A shows that a large "zone of Ar loss" was produced close to the intrusive contact, where the rocks were reheated above the "blocking temperature" of biotite (~ 300° C) by the intrusive. All rocks within this zone would thus give young (generally < 45 m.y.) apparent ages. Graph B shows that the "age"/elevation trend lines of terrane A are "truncated" at the level of the zone of Ar loss, producing an "age gap" between 45 and 53 m.y. (dotted line). All rocks below the level of the truncation points ("elbows") of the trend lines in graph B would have young (< 45 m.y.) K-Ar ages.

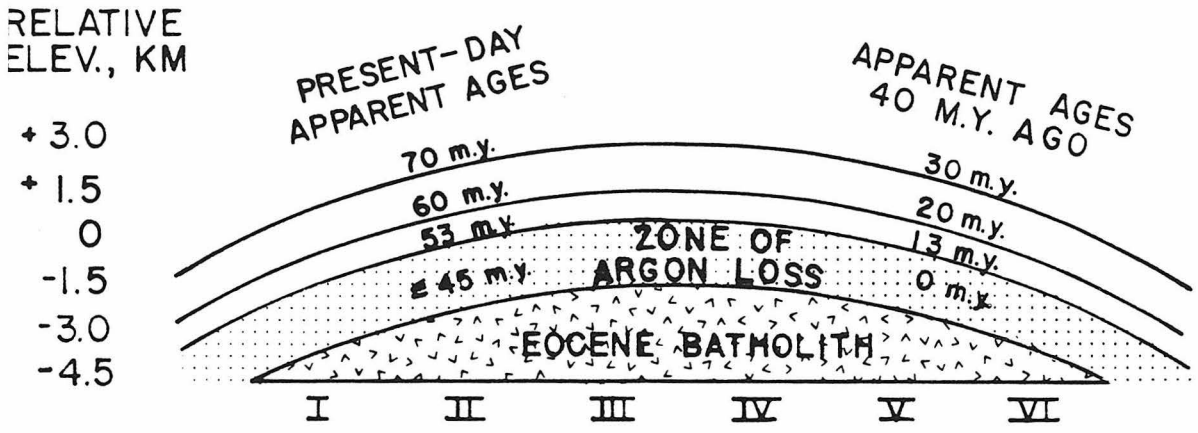
RELATIVE
ELEV., KM
+3.0
+1.5
0
-1.5
-3.0
-4.5
PRESENT-DAY
APPARENT AGES
APPARENT AGES
40 M.Y. AGO
70 m.y.
60 m.y.
53 m.y.
≤ 45 m.y.
30 m.y.
20 m.y.
13 m.y.
0 m.y.
ZONE OF
ARGON LOSS
EOCENE BATHOLITH
I
II
III
IV
V
VI

A

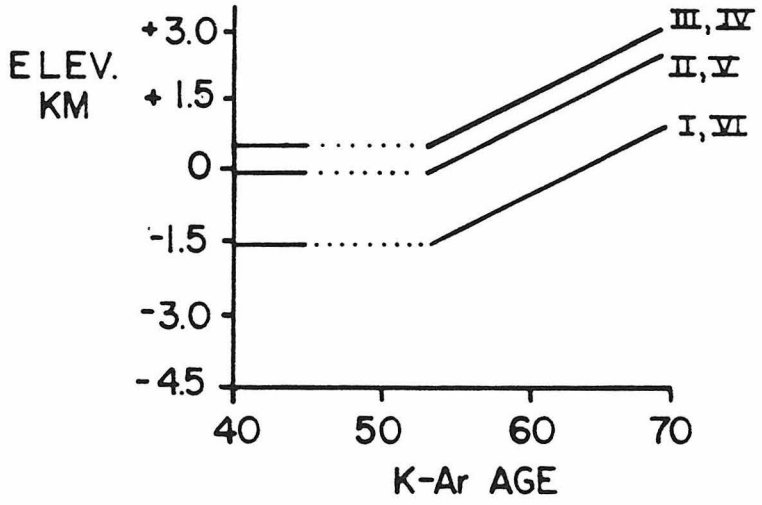
ELEV.
KM
+3.0
+1.5
0
-1.5
-3.0
-4.5
40
50
60
70
K-Ar AGE
III, IV
II, V
I, VI

B

7.5 Implications of K-Ar Apparent Ages to the Geology of the Eocene Event in Idaho

The K-Ar apparent ages bear significantly on many geologic and geophysical features of the Eocene igneous event of the Idaho batholith region. For example, they give some information about the approximate size and shape of the Eocene magma chambers, the depth of emplacement of the Eocene plutons, the magnitude of former geothermal gradients, and the minimum temperatures of the country rocks at the time of intrusion and hydrothermal alteration.

Figure 7.15 shows that if the K-Ar data in strip "C" (115° 30' to 115° 40') are extrapolated, the rocks would have an apparent age of zero at a depth of 7.6 km (25,000 feet) below sea level, or about 9.5 km below the present surface (this surface is presently at about 1.8 km, or 6000 feet elevation). Interpreted simply, this indicates that the rocks now at the surface were 9.5 km below the surface 66 m.y. ago, and also that the former temperature at that position in time and space was about 300°C, which is the approximate Ar "blocking temperature" for biotite. All other things being equal, this means that the pre-Eocene geothermal gradient was about 32°C per km. The graph also shows that at the inception of the Eocene event (~ 45 m.y. ago) these rocks would have exhibited apparent K-Ar ages of about 21 m.y. and they would have been about 6.5 km below the Eocene surface (at a temperature of about 200°C). Similar calculations could be made from the trend lines in each geographic strip, but inasmuch as the slopes of several of these trend lines are poorly controlled, it is probably most accurate to assume that the geothermal gradient derived from strip "C" applies to all areas.

Because the above conclusions have considerable importance to the

Figure 7.15 Long extrapolation of the strip C "age" vs. elevation trend line to a zero apparent age at 25,000 feet (7.6 km) below sea level, or about 31,000 feet (9.5 km) below the present level of exposure. The interpretation is that 66 m.y. ago the rocks currently exposed had a relative structural position 9.5 km below their current position, and were at the Ar "blocking temperature" of biotite (about 300°C). Uplift and erosion has brought these rocks to their current location. The fossil geothermal gradient indicated by these results is approximately 32°C per km, see text.

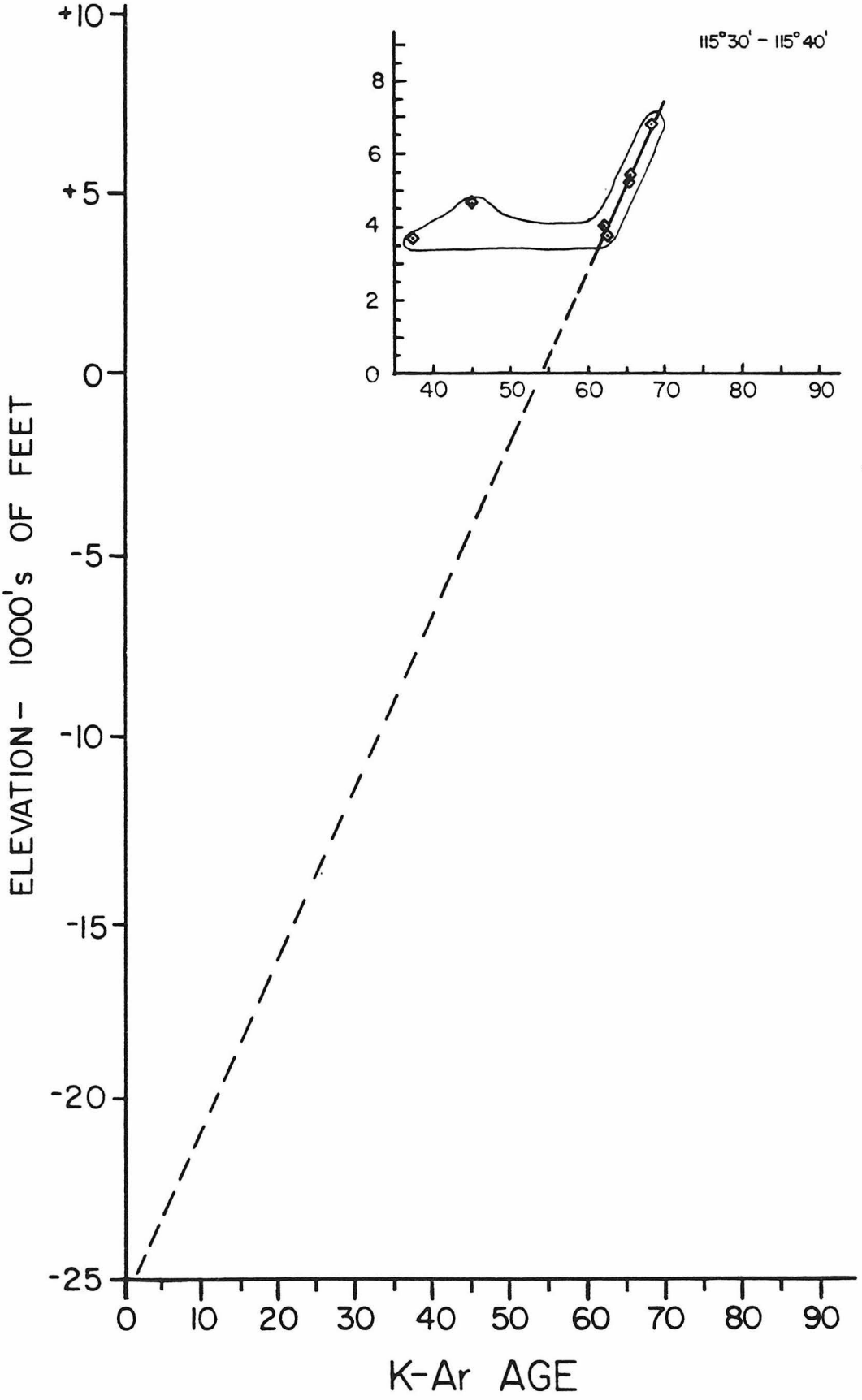
115°30' - 115°40'
8
6
4
2
0
40
50
60
70
80
90
+10
+5
0
-5
-10
-15
-20
-25
ELEVATION- 1000's OF FEET
0
10
20
30
40
50
60
70
80
90
K-Ar AGE

following discussion, it is important to document them with other geophysical data. Maps by Blackwell (1978) and Lachenbruch and Sass (1978) show that present-day heat flow in the Atlanta lobe region is comparable to, or slightly higher than, that typical of the Basin and Range province. Unpublished data of Blackwell show that the typical heat flow in strip "C" today is about 1.9 $\pm$ 0.2 h.f.u. Furthermore, Swanberg and Blackwell (1973) have shown that the average heat generation for the rocks (Bear Valley quartz monzonite) in this zone is 2.7 h.g.u. These data are consistent with a reduced heat flux of 1.6 h.f.u. and a depth constant of 10 km, which are similar to values observed in the Basin and Range province, according to the formulation of Birch et al (1968):

$$q = q_o + Ao\ D$$

where q is the surface heat flux, q_o is the basement contribution to the flux, D is the depth constant and Ao is the surface heat generation of the rocks.

If the exponential model of Lachenbruch (1968) is accepted, the above figures allow the computation of the heat generation value of the rocks formerly 9.5 km above those now exposed; i.e.:

$$A = Ao\ e^{-z/D}$$

$$\text{or}\quad 2.7 = Ao\ e^{-9.5/10}$$

which gives a value for the ancient Ao of 7.0 h.g.u. Assuming that the basement contribution to the heat flow (1.6 h.f.u.) was the same in the past, which is admittedly not obvious, then the Lachenbruch (1968) steady state model may be used to calculate the former temperature at a depth (z) of 9.5 km below the surface just prior to the Eocene plutonic event; i.e.:

$$T = \frac{q_o z}{K} + \frac{D^2 A_o}{K}\left(1 - e^{-z/D}\right)$$

using a conductivity (K) of 6.5×10^{-3} cal/cm-sec-°C, which is typical of quartz monzonite at moderate temperatures (c.f. Clark, 1966), this gives a temperature of 300°C at 9.5 km. The close agreement with the previous estimate is partly fortuituous. Had the ancient value of q_o been 0.5, 1.0 or 2.0 rather than the assumed 1.6, then the temperature at 9.5 km depth would have been 140°, 210°, and 360°C respectively. In any case, these considerations support the inferences drawn from the K-Ar data, and in a complementary manner the K-Ar data suggest that the ancient value of q_o was high and similar to that observed today.

Figure 7.16a was constructed given the geophysical results deduced from strip "C", as well as the amount of relative uplift of the various strips as taken from Fig. 7.11. Fig. 7.16a shows the distribution of temperature in the rock column at 65 m.y. before present, where it is assumed that the isotherms were essentially horizontal and that the geothermal gradient was 32°C per km. Deviations of the isotherms from horizontalily (relative to strip F) are shown in Fig. 7.16b at 45 m.y. before present, and are interpreted to represent the effects of distortion as a result of rapid doming and uplift during the Eocene intrusive period. The emplacement of the Eocene magmas is considered to have been instantaneous, such that the former isotherms have been domed but not otherwise influenced by the Eocene intrusives. If it is arbitrarily assumed that the subsurface Eocene contact is coincident with the 300°C isotherm, then the size and shape of the hypothetical Eocene batholith is as shown. In reality, of course, the actual series of Eocene intrusives could both crosscut the 300°C isotherm or lie at much greater depths.

Figure 7.16 Models of the isothermal surface in the Idaho batholith at 65, 45, and 40 m.y. before present.

A. Isotherms within the Idaho batholith 65 m.y before present. The geothermal gradient is 32°C per km. The elevation scale has relative significance but does not refer to the true elevation during the Eocene. Vertical exaggeration is about 4.4 : 1

B. Isotherms within the Idaho batholith 45 m.y. before present. The geothermal gradient is 32°C per km. The isotherms have been domed (relative to strip F) by instantaneous intrusion of a large, wedge shaped Eocene batholith, whose top is for clarity assumed to be coincident with the 300°C isotherm. The heat pulse from this intrusion has not yet influenced the temperatures of the country rocks. The elevation scale does not refer to the actual Eocene surface but rather to the position of this surface relative to the current land surface of about 1 to 3 km. Note that rocks currently exposed in the region had temperatures of 150° to about 300°C before the Eocene heat pulse.

C. Isotherms within the Idaho batholith 40–45 m.y. before present, as modified by the heat pulse of the Eocene intrusive. The position of the 300°C isotherm was calculated from the truncation points of the K-Ar age vs. depth relations. The elevation of this 300°C isotherm has probably been overestimated in strips D and E, and is probably closer to the dotted line except near contacts with Eocene plutons. Hydrothermal circulation would have been active during this stage; note that most rocks currently exposed (1 to 3 km elevation) would have had temperatures of 200 to 300°C. Incidentally, the uppermost few kilometers of rock were probably Challis volcanics, especially east of 115°30'. Note the steepened geothermal gradient, which over large areas exceeded 45°C per km.

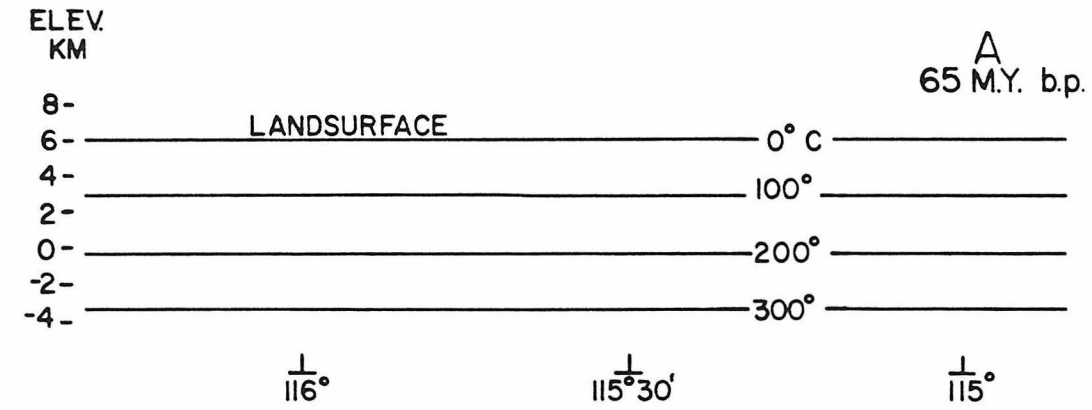
ELEV.
KM
A
65 M.Y. b.p.
8-
6-
4-
2-
0-
-2-
-4-
LANDSURFACE
0° C
100°
200°
300°
116°
115°30'
115°

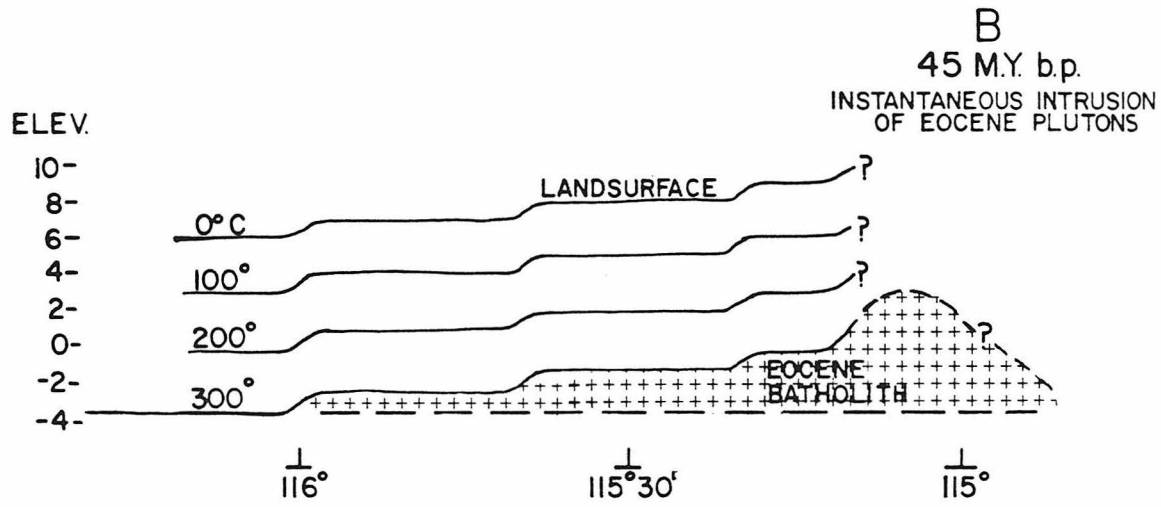
B
45 M.Y. b.p.
INSTANTANEOUS INTRUSION
OF EOCENE PLUTONS
ELEV.
10-
8-
6-
4-
2-
0-
-2-
-4-
LANDSURFACE
0° C
100°
200°
300°
?
EOCENE
BATHOLITH
116°
115°30'
115°

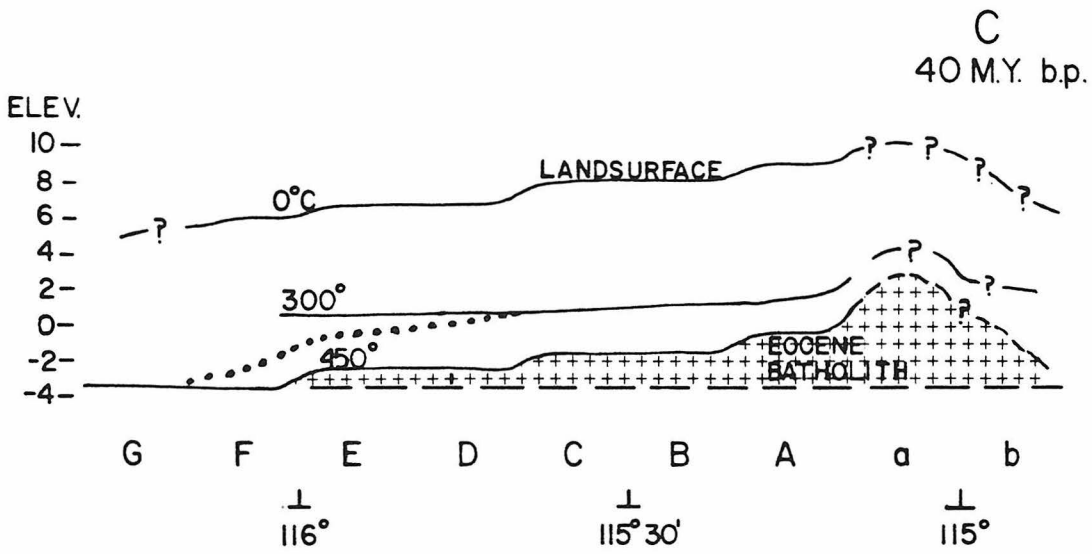
C
40 M.Y. b.p.
ELEV.
10-
8-
6-
4-
2-
0-
-2-
-4-
LANDSURFACE
0°C
300°
450°
?
EOCENE
BATHOLITH
G
F
E
D
C
B
A
a
b
116°
115°30'
115°

The simplest overall interpretation, however, is that the Eocene plutons originally made up a series of relatively thin magma sheets that wedge out and become thinner toward the west. Lawson (1914), Buddington (1959) and Hamilton and Myers (1967) have proposed that many batholith-sized plutons are essentially sheet-like (e.g. the Butte Quartz Monzonite pluton in the Boulder batholith in Montana), and Bennett (written comm. 1978) suggested that the Eocene plutons in Idaho also have a sheet-like form.

Note that the vertical scale in Fig. 7.16b does not refer to the actual Eocene surface (except in a relative sense) but actually refers to the modern land surface which lies between 1 and 3 km above sea level. The figure then shows that the rocks currently exposed in the region had temperatures of 150° to 300°C immediately before they were affected by the Eocene heat pulse. This result implies that a significant fraction (> 1/3) of the heat supplied to the ground waters responsible for the large scale hydrothermal alteration of these rocks would have come from the ordinary rocks of the cooling Mesozoic terrane, rather than just from the newly introduced Eocene magmas.

Figure 7.16c shows the isotherms within the Idaho batholith shortly after the intrusion of the Eocene magmas. The position of the 300°C isotherm was calculated from the truncation points ("elbows") of the K-Ar age vs. depth relations shown in Fig. 7.13, based on the inference that in each strip all rocks at or below the elevation of the various truncation points lost radiogenic Ar during the Eocene and hence were heated above the blocking temperature of biotite. However, some of the "young" K-Ar ages that define the truncation points could simply be from rocks collected close to Eocene plutons, as was discussed in Sec. 7.3 and 7.4.

Given the above qualifications, Fig. 7.16c shows how the isotherms

were modified by the Eocene heat pulse, such that the geothermal gradient was steepened to at least 45°C per km over large areas. Note that most rocks currently exposed in the region (1 to 3 km elevation) would have had temperatures of 200 to 300°C during this stage, which was the time of the most pronounced hydrothermal activity. These estimated temperatures are in good agreement with those independently inferred from the $\delta^{18}O$ and δD relationships of the hydrothermally altered rocks (c.f. Sec. 5.4.4), and with the large scale development of propylitic mineral assemblages.

The figure allows calculation of the amount of Eocene rock in the subsurface, if this simple interpretation (doming emplacement mechanism) is accepted and if the "cross section" truly represents the average condition of all E-W traverses in the Atlanta lobe. This gives a value of approximately 25,000 km^3 for the Eocene intrusives in the Atlanta lobe. This figure can be compared to the remaining amount of Challis volcanic rock in the region, which covers an area of about 7600 km^2, if it is assumed that the average thickness is 1 km (c.f. Sec. 2.3.3; this would imply 7600 km^3). Of course the former extent and thickness of the Challis volcanic field was unquestionably much greater than today, and so all that can be said is that the calculated volumes of intrusive rocks and volcanic rocks seem to be roughly comparable in magnitude.

The K-Ar results also bear on the depth of emplacement of the exposed Eocene plutons. At the present level of exposure these magma bodies apparently were intruded into country rocks that had cooled through the Ar blocking temperature millions of years earlier, and so were all considerably less than 300°C. The results discussed above imply that these rocks were intruded within about 5-7 km of the Eocene surface. In fact the upper portions of many of the Eocene plutons have miarolitic

cavities and granophyric textures (c.f. Sec. 2.3.2), so these plutons are known to have been emplaced at relatively high levels in the crust.

CHAPTER 8

RELATION OF ORE DEPOSITS TO THE HYDROTHERMAL SYSTEM

8.1 General Statement

Several important and widely separated Au-Ag ore bodies occur within the Idaho batholith. The discussion below will show that most of these ore deposits have a direct relation to the Tertiary meteoric-hydrothermal activity and that the $\delta^{18}O$ data obtained in this study have important implications with respect to the locations of mineralized areas in the batholith. In particular it will be shown below, purely from an empirical analysis of the $\delta^{18}O$ distribution, that large areas of the batholith probably have low Au-Ag potential, but that several narrow irregular zones in the batholith are favorable sites for future exploration.

In both a historic and economic sense the most significant ore deposits in the batholith are gold lodes and placers, and to a lesser extent silver lodes. Since the turn of the century, and especially during wartime, production has been extended to include antimony, mercury and tungsten. Current exploration interest in the region also includes molybdenum, uranium, pegmatite minerals (e.g. beryl, mica, feldspar, columbium) and blacksand placers (valued for Nb, Ta, Ti, Zr, Th, garnet, rare earths).

In a larger context Idaho is a major producing state of silver, lead and zinc, and in many years has led the nation in production (Weissenborn, 1964). The most important district, however, is the Coeur d'Alene, which lies far to the north of the study area. There is also significant production immediately east and southeast of the batholith in the Wood River, Bayhorse, and Yankee Fork Districts.

The following discussion will center on the gold, silver and antimony

deposits. These are the most important deposits within the batholith, and are the ones most clearly related to the Tertiary hydrothermal activity which is the focus of the present study. The Wood River and Yankee Fork Districts are given as examples of Tertiary deposits in non-granitic host rocks.

8.2 Geologic Setting of the Ore Deposits

The southeast portion of the Idaho batholith and the region immediately east comprises a portion of a huge metalliferous province which extends from eastern California into Montana (Noble, 1970). This arcuate province is distinguished by its Cu, Ag, Au, and Pb-Zn deposits, although production is not strictly confined to these metals. These deposits range in age from Precambrian to Pliocene, but Mesozoic, Laramide and Tertiary deposits are most common, and Paleozoic deposits are virtually unknown (Anderson, 1951; Noble, 1976). In common with many other metallogenic provinces of the world, then, this province is characterized by deposits with similar metal content having several different ages. This suggests that the ultimate source of the metals may lie within the mantle, and conversely that no single magmatic or tectonic event can account for the distribution of all the ore bodies (Noble, 1976).

Figure 8.1 shows the locations of all mineralized lodes in the vicinity of the Atlanta lobe which actually produced ore, based in large part on unpublished data provided by James A. Noble. The great majority of the localities within the batholith are Au-Ag deposits, commonly with significant but subordinate Pb, Zn, Cu, W and/or Sb values. Also shown on this figure are the low-^{18}O zones (shaded) determined from data obtained

Figure 8.1 Map of the Atlanta lobe, showing Eocene plutons (pattern), the +8 permil $\delta^{18}O$ contour which outlines the periphery of the low $-^{18}O$ zones, and productive lode mines (circles, large circles represent large producers). There is a distinct correlation between the +8 contour and mineralized zones within the batholith. Localities discussed in text are labeled. Note that the large, west-central portion of the batholith has negligible productivity; only weak hydrothermal effects operated here, as indicated by the deuterium data (compare Fig. 6.2).

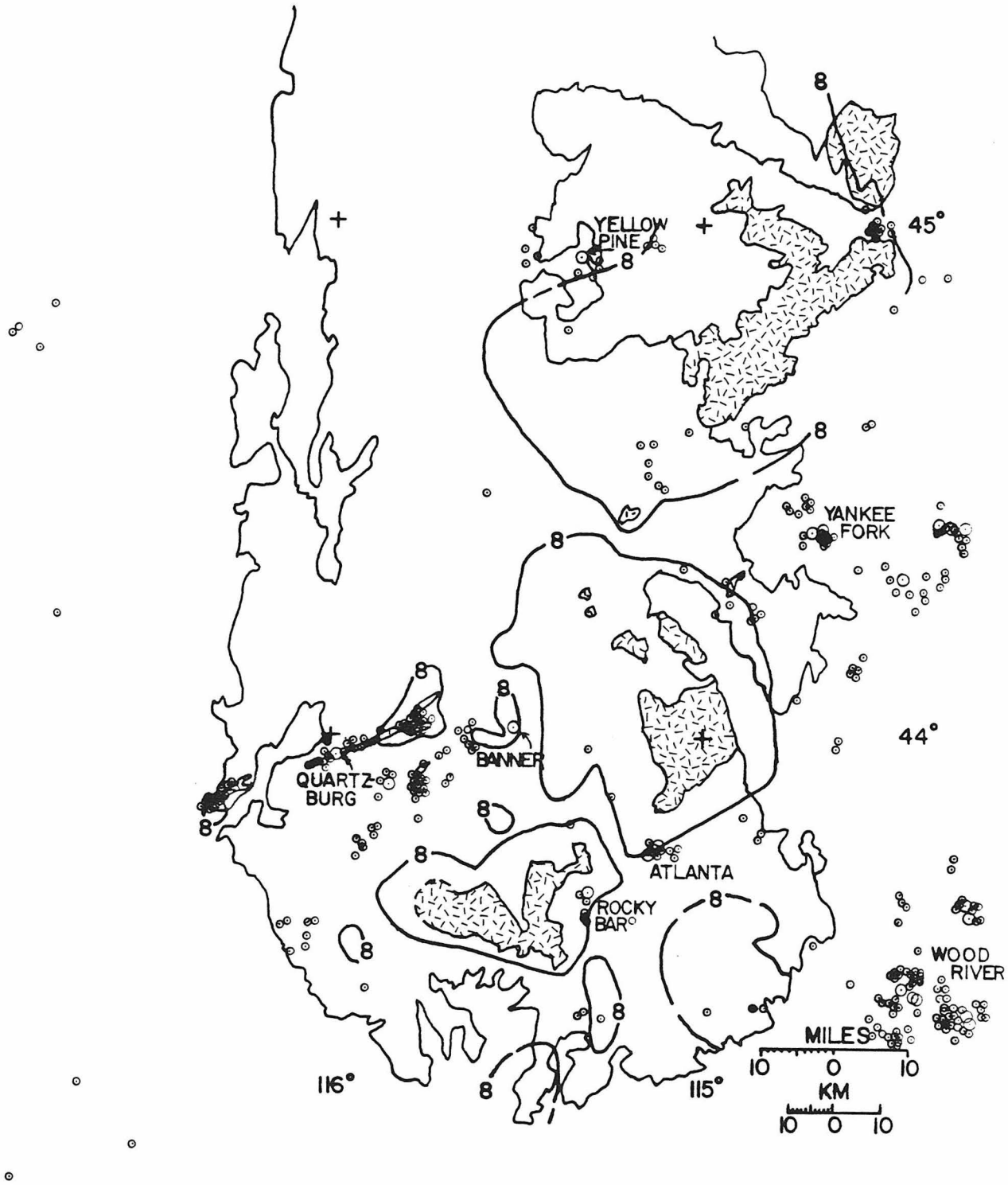
8
YELLOW PINE
45°
YANKEE FORK
QUARTZ-BURG
BANNER
44°
ATLANTA
ROCKY BAR
WOOD RIVER
MILES
10 0 10
KM
10 0 10
116°
115°

in this study.

Almost all of the Au-Ag deposits within the batholith are simple fissure veins which occupy shear zones within host granite. Exceptionally, some of the deposits in the Seafoam district (e.g. Mountain King Mine) occur as replacement bodies in small (stoped?) blocks of limestone (Ross, 1941), and ore in the Deadwood Mine reportedly occurs in schist inclusions in the granite (Campbell, 1931). A metasedimentary roof pendant also occurs in the Yellow Pine district, but the main Au (Sb, W) mine lies in granitic rock. Principal exceptions as to the nature of the ore are the Deadwood (Cu, Pb, Zn, Ag) and Hermada (Sb) mines, and the mines of the Seafoam District (Ag, Pb, Zn, Cu, with very little Au; Bergendahl, 1964). Furthermore, the Ag: Au ratio in the Banner and Vienna Districts is much higher than in most districts (Ross, 1941).

The ore deposits are commonly associated with pre-ore hypabyssal porphyry dikes and syn- and post-ore lamprophyre dikes which also cut the host granite. This proves that the ore deposits are Tertiary in age and not directly related to emplacement of the Mesozoic batholith (Anderson, 1951). In several papers Anderson (1947, 1951) has attempted to distinguish early and mid-Tertiary deposits on the basis of dike relations and also on the relation of the deposits to the Challis volcanic rocks. Such refinements are here regarded as premature, but the potential significance is recognized.

Most of the veins contain iron and base metal sulfides, often complex metal-S-As-Sb compounds, and precious metals which may be free or associated with the sulfides. The most common gangue materials are quartz and altered (usually sericitized) wallrock, but carbonates are commonly present

and adularia and albite have been reported in the Yankee Fork District. There is abundant evidence in all districts for relatively shallow ore deposition in that the veins and lodes were deposited in open spaces in the rocks; for example in most districts the gold is associated with late-stage quartz in drusy cavities. This is considered to be strong evidence for an epithermal origin of most of the veins.

It will be shown below in Section 8.4 that most of these ore deposits are spatially related to the giant meteoric-hydrothermal systems that have been mapped during the course of this study. The hydrothermal systems were in turn related to batholithic intrusion during the Eocene, which was accompanied by the formation of large calderas. The ring fractures of the calderas provided the principal conduits for dike emplacement, fluid circulation and ore deposition. The relation between dikes and veins is thus not regarded as direct in the sense implied by Anderson (1951).

Brief descriptions of selected mining districts of the region follow. The Atlanta, Rocky Bar, Quartzburg and Banner districts are representative of important precious metal deposits in the Idaho batholith, whereas the Yellow Pine deposits have a more complicated history. The Wood River district is illustrative of mineralization within Paleozoic host rocks, and the Yankee Fork district occurs within the Challis volcanic rocks.

8.3 Description of Selected Ore Deposits and Districts

8.3.1 Atlanta District

Location: T5N, R11E; Elmore Co.

Lode Production: 385,000 oz. Au, appreciable Ag (Bergendahl, 1964)

Occurrence: The Atlanta Mining District lies within a large silicified and brecciated shear zone in the Idaho batholith, along the southern edge of the Sawtooth Ring Zone. The main ore zone is 10 to 40 m wide and trends ENE for about 3 km, until it is truncated by the Montezuma Fault (Anderson, 1939). Several small WNW veins branch off the main shear.

The ore deposits are "characteristically epithermal" and are most productive within 300 m of the surface, in part due to supergene enrichment of Ag (Anderson, 1939). Vein minerals include pyrite and arsenopyrite, several base metal sulfides (e.g. chalcopyrite, enargite, galena, sphalerite, tetrahedrite), complex silver sulphosalts and free gold; the gangue is predominantly comb and drusy quartz and minor calcite (Anderson, 1939). Hobbs (1964) mentions that scheelite has been produced as a by-product of the gold mining.

Porphyry dikes are not known in the mineralized area, but dikes of syenite, diorite, and postore lamprophyre are associated with the deposits (Anderson, 1939, 1951). Wallrock alteration progresses toward the veins, from chloritization of biotite, to sericitization of chlorite, plagioclase and the K-feldspar, and finally to intense replacement of the completely sericitized rock by fine-grained quartz (Anderson, 1939).

8.3.2 Rocky Bar District

Location: T4N, R10E; Elmore Co.

Lode Production: 150,000 oz. Au, minor Ag (Bergendahl, 1964)

Occurrence: In the Rocky Bar District several gold-quartz veins occur within fissure zones in granitic rocks. The veins have a predominant E-W trend, and are usually associated with porphyry dikes (Anderson, 1943).

Some of the gold is free in the quartz, and some is associated with sulfide minerals. Other vein minerals include arsenopyrite, pyrite, sphalerite, galena, chalcopyrite and sericite (Anderson, 1943). Several stages of quartz deposition were identified, with the gold associated with late-stage comb and drusy quartz (Anderson, 1943). Some superficial, oxidized ore was extremely rich.

8.3.3 Quartzburg District

Location: T7N, R4E; Boise Co.

Lode Production: 400,000 oz. Au (Bergendahl, 1964)

Occurrence: The principal ore deposits in the Quartzburg District occur within a "porphyry belt" where numerous NE-trending Tertiary dikes cut the Idaho batholith (Ross, 1941). The ore deposits occur within shear zones in granitic rocks and as stockworks in the porphyry dikes, and also along the intersections of dikes and veins (Ross, 1941). The ore minerals include galenobismuthite, tetradymite, arsenopyrite, pyrite, native gold, galena and sphalerite; these are usually contained in quartz gangue but are sometimes disseminated in sericitized wall rock near the fissures (Ross, 1941).

Anderson (1947) distinguishes "early Tertiary (?)" and "Miocene" ore deposits in the Boise Basin region. The former deposits are generally WNW trending gold-quartz veins in fracture zones. Wall-rock alteration is reported to be slight, and the veins have no obvious relation to dikes. The more valuable "Miocene" deposits are characterized by their NE trend, common association with porphyry dikes, higher base metal content, and intense wallrock alteration (sericitization, silicification, pyritization)

near veins (Anderson, 1947). The principal lodes in the Quartzburg district are of this type, and are known to postdate emplacement of quartz monzonite porphyry and rhyolite porphyry dikes but to predate the lamprophyric dikes (Anderson, 1947). Their actual age is probably Eocene.

8.3.4 Banner District

Location: T8N, R8E; Boise Co.

Lode Production: 1,300,000 oz. Ag

Occurrence: Veins within the Banner District occur within N55E and N80E trending fissure zones in granodiorite and in rhyolite porphyry dikes (Anderson and Rasor, 1934b). The predominant metallic mineals are pyrargyrite and owyheeite, although proustite, miargyrite, tetrahedrite, galena, sphalerite, chalcopyrite, arsenopyrite, and pyrite also occur. Quartz is the principal gangue mineral, but calcite is locally abundant. At least one rhyolite porphyry dike is cut by a vein, but lamprophyric dikes appear to have been intruded near the end of ore deposition (Anderson and Rasor, 1934b).

8.3.5 Yellow Pine District

Location: T18 and 19N, R9E; Valley Co.

Lode Production: 310,000 oz. Au, with significant Ag, W, Sb (Bergendahl, 1964)

Occurrence: The Yellow Pine ore deposit consists of small quartz-stibnite veins and disseminated gold, antimony and tungsten ore. The deposit has produced considerable gold, significant silver, tungsten and antimony, and formerly was thought to contain the largest antimony reserve in the

United States (White, 1940; Cooper, 1951). The deposit is contained within a large (50 m) NE-trending shear zone in granitic rock, which bends abruptly south at the mine (White, 1940; Cooper, 1951). A large roof pendant of metasedimentary rock is nearby, and several pegmatite, aplite, porphyry, lamprophyre and basalt dikes occur in the area (White, 1940).

White (1940) noted that the antimony-silver mineralization, which occurs both as disseminated ore and as small quartz-stibnite veins, was superimposed on earlier sulfide mineralization characterized by disseminated gold-bearing pyrite and arsenopyrite. Cooper (1951) also describes scheelite-carbonate-quartz mineralization, which occurs disseminated in brecciated ore and also within small veinlets. This mineralization postdates the gold but predates the stibnite. Cooper also notes that basaltic dikes (previously called "lamprophyre") have chilled margins and that they postdate the gold but predate the stibnite mineralization, and considers that this relationship supports the Tertiary age for the mineralization suggested by White (1940).

Ross (1941) mentions that nearby mercury deposits are contained within the large block of metasedimentary rocks. The disseminated cinnibar-pyrite ore is concentrated in altered limestone which is locally converted to jasperoid.

8.3.6 Wood River District

Location: T.2 N, R.18 E and vicinity, Blaine Co.

Lode Production: Principally Pb-Ag, some Au, Cu, Zn

Occurrence: Ore deposits within the Wood River region usually occur as veins and replacement bodies along shear zones within hornfelsed argillite

and limestone of the Devonian Milligen Formation near granitic plutons (Hall et al, 1978). Occasionally the veins extend into the intrusive stocks, but with an increase in gold and a decrease in silver contents (Hall et al, 1978). Ross (1941) reports that Challis volcanic rocks in the region are locally mineralized, but Anderson (1950) implies that the volcanic rocks are postore. Anderson (1950) also states that andesitic and dacitic dikes in the region are pre-ore, and that lamprophyre dikes, which commonly occur along the ore bodies, are postore. Wallrock alteration is reported to be slight, and characterized by formation of sericite and addition of of carbonate and pyrite (Anderson, 1950).

The principal ore minerals are argentiferous galena and sphalerite in a siderite gangue, but arsenopyrite, bournonite, chalcopyrite, freibergite, gudmundite, marcasite, pyrite and pyrrhotite also occur. A shallow crustal source for the sulfur and lead is indicated by the positive and variable $\delta^{34}S$ values (+2 to +15 permil) of sulfide minerals, and by the radiogenic Pb isotope ratios (Hall et al, 1978). Fluid inclusions have homogenization temperatures of about 270°C and salinities of about 4 weight percent (Hall et al, 1978). δD values of these inclusions are about -115 permil and indicate that the ore fluids are predominantly of meteoric origin (Hall et al, 1978).

8.3.7 Yankee Fork District

Location: T12 and 13N, R15E; Custer Co.

Lode Production: 252,000 oz. Au, equal values in Ag (Bergendahl, 1964)

Occurrence: Ore deposits in the Yankee Fork district occur in veins in predominantly NE-trending fissures and as minor replacements along shear

zones in altered Challis volcanic rock (Ross, 1927). Much of the ore is concentrated within a few hundred feet of the surface, but there is no evidence for extensive supergene enrichment (Anderson, 1949). Several closely spaced dikes of dacite porphyry and subordinate granophyre, monzonite, quartz monzonite porphyry and pink granite intrude the Challis volcanics about a mile east of the General Custer Mine (Anderson, 1949).

Ore minerals include gold, electrum, argentite, gold and silver selenides, pyrite, galena, chalcopyrite, enargite and tetrahedrite, which generally occur in a gangue of fine-grained and drusy quartz with minor adularia, calcite and albite (Ross, 1927; Anderson, 1949). The silver to gold ratio of the ore is usually very high, often about 85 times by weight (Anderson, 1949). Wallrock alteration progresses from chloritization of dark minerals, to sericitization of feldspars and dark minerals within several meters of the veins, to silicification and pyritization along the veins (Anderson, 1949).

8.4 Evidence for a Meteoric-Hydrothermal Origin for the Ore Deposits

If deposits outside the batholith are ignored, Figure 8.1 shows that most of the mines are located in the southern and eastern portions of the Atlanta lobe, near the zones of Tertiary hydrothermal activity. Note specifically that in the large northwestern sector of the Atlanta lobe, where no low-^{18}O rocks were found and where only weak or non-existent deuterium depletions were noted, there is a complete lack of productive mineralized areas. This close spatial correlation between the $\delta^{18}O$ contours and the ore bodies is less conspicuous near Idaho City and in the western Boise Basin near Quartzburg. This might be attributable to

the paucity of isotopic data-points in these areas. It is worth noting that the δD values in the latter mineralized areas are generally lower than in surrounding rocks, and it is possible that a more detailed δD and $\delta^{18}O$ study would show good correlations on a smaller scale.

Figure 8.2 shows the relationship between the mine locations and the $\delta^{18}O$ contours in the best studied portion of the batholith, near the Sawtooth Ring Zone and the Rocky Bar anomaly. More than two-thirds of the mines, and probably 90% of the production, occurs within a narrow (~ 5 km wide) zone or strip that straddles the +8 permil $\delta^{18}O$ contour (Fig. 8.3). This winding, 5 km wide strip, portions of which outline the perimeter of the SRZ, constitutes only 30% of the total area shown in Figs. 8.2 and 8.3. Although this should be considered to be only an empirical relationship at the present time, the +8 $\delta^{18}O$ contour seems to coincide very well with the most productive ore zone in the batholith. This relationship has been accurately established for the Atlanta, Rocky Bar and Banner districts, which contain the most important deposits in this 10° x 10° region, and this constitutes strong evidence for a direct genetic relationship between ore deposition and the hydrothermal activity that produced the distribution of $\delta^{18}O$ contours in the batholith. The winding strip shown in Fig. 8.3 thus constitutes an obvious "target zone" for future mineral exploration in the batholith. Furthermore, more detailed $\delta^{18}O$ studies could probably refine this target zone much more precisely.

Note that, in addition to the barren areas that lie far outboard of the (strong) hydrothermal activity, large areas within and interior to the zones of extreme ^{18}O depletion also have negligible recorded production and probably low mineral potential. This statement, however,

Figure 8.2 Detailed map showing the correspondence between the $\delta^{18}O$ contours and the locations of productive mines (circles) in the vicinity of the Sawtooth Ring Zone and the Rocky Bar Anomaly. Compare Fig. 6.4.

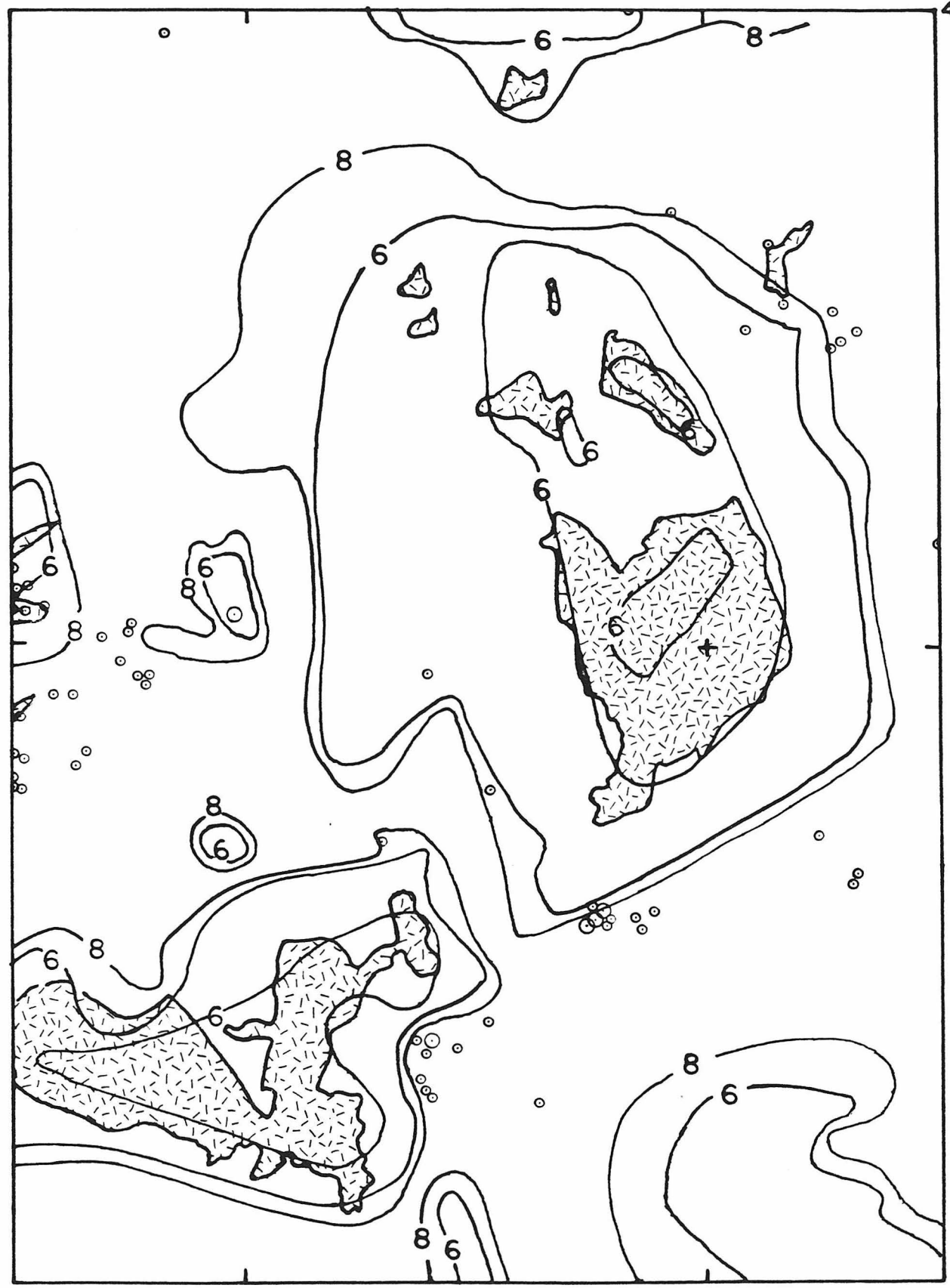
44°30'
43°30'
115°45'
114°45'
6
8

Figure 8.3 The prime prospecting area within the region shown in Fig. 8.2 is a ~ 3 km wide band that straddles the +8 $\delta^{18}O$ contour. Almost 3/4 of the mines, and all the important producers, lie within this narrow zone which constitutes only about 30% of the total area. More detailed study would probably improve these statistics. Note that large areas both within and exterior to the "target zone" have negligible recorded production.

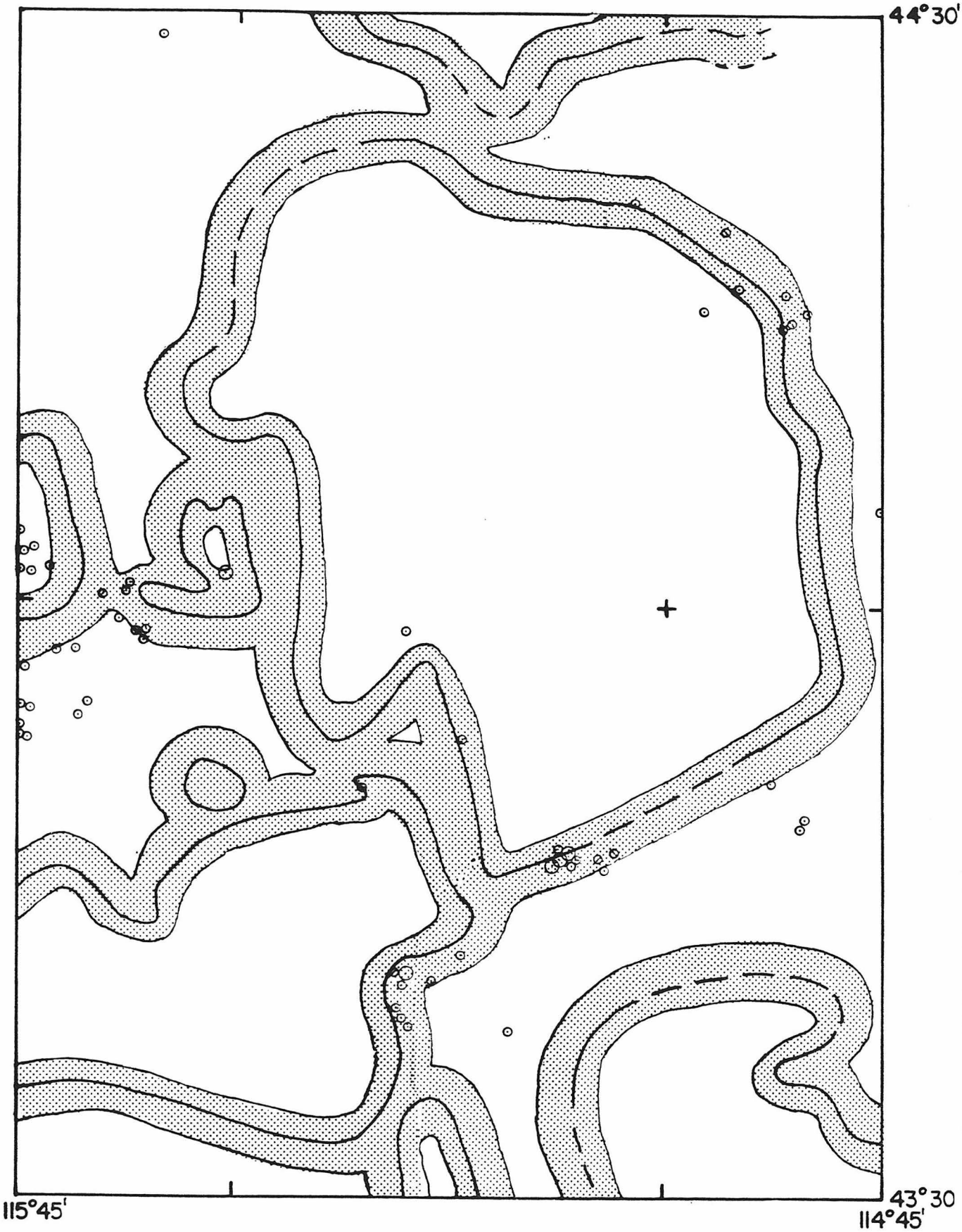
44°30'
115°45'
43°30
114°45'

neglects the current exploration interest in the Mo, U and Be associated directly with the Eocene granite plutons in these areas, and also the potential of blacksand placers (see Kiilsgaard et al, 1970; Armstrong, 1957). In any case, the empirical association of epithermal Au-Ag mineralization with the +8 $\delta^{18}O$ contour probably applies only to the outside contour, and not to the +8 contours interior to the ring zones. Overall, it is the writer's opinion that inferences based on new $^{18}O/^{16}O$ and D/H data confirm the decision of the United States Government to establish the boundaries of the Sawtooth Wilderness Area, which lies entirely within and interior to the Sawtooth Ring Zone.

Because the geochemistry of these ore deposits has not been studied in detail, only a simplified model of ore deposition will be attempted. The meteoric waters undoubtedly migrated radially inward toward the low-^{18}O zones, gaining heat and perhaps dissolving disseminated metals from large volumes of rock during transit. The hydrothermal fluids then apparently cooled and deposited quartz and metals near the giant ring structures described earlier in this report, probably during ascent along ring faults and other marginal fractures created by the central intrusives. The exact cause of the metal precipitation is not known, but none of the available evidence supports the involvement of any magmatic water. In this view the +8 permil $\delta^{18}O$ contour represents the location of favorable structures which existed near the zones of intense hydrothermal circulation at the appropriate time.

CHAPTER 9

SUMMARY AND CONCLUSIONS

The findings of this thesis bear on a broad variety of problems, including the nature of the Eocene event in south-central Idaho, the interactions of minerals with hydrothermal fluids, the characteristics of the deep portions of geothermal systems, the significance of K-Ar apparent ages in orogenic areas, and the genesis of epithermal ore deposits in the study area. The following discussion provides a brief synopsis of the critical geologic relationships in the southern half (Atlanta lobe) of the Idaho batholith, and enumerates the principal observations and conclusions of this study.

The Idaho batholith proper is a composite mass of plutons, which formed at relatively deep crustal levels presumably as a consequence of Mesozoic subduction at the edge of the North American craton. Most of the rocks are apparently Cretaceous in age and are a relatively uniform type of biotite quartz monzonite and granodiorite; however, the rocks of the western margin are primarily tonalite and granodiorite that commonly contain hornblende in addition to biotite. The primary isotopic composition of this mass is strikingly uniform, with whole rock $\delta^{18}O$ and biotite δD values almost invariably lying in the range of 9.5 ± 1.5 and -70 ± 5 permil respectively.

Following the development of the batholith, there was a 20-30 m.y. "quiet" period during which time the terrane experienced rather uniform uplift and cooling to temperatures somewhat below ~300°C. Immediately afterward was an intense episode of magmatism and tectonism termed the Eocene event, the effects of which are of paramount importance to the geology of the region and to which this study was principally directed.

The rocks produced during the Eocene event are calcalkaline, and thus are considerably more alkalic than the Mesozoic granitoids which comprise a calcic suite. During their emplacement the regional uplift was probably accelerated and accompanied by local doming. The Eocene magmas were either intruded at shallow levels in the continental crust, or were extruded on the surface as the Challis volcanic rocks; the latter cover an area of about 7600 km^2 in the region immediately east of the Idaho batholith (Ross, 1962b), and it is probable that these rocks formerly extended over the entire Atlanta lobe and thus provided the roof rocks for the epizonal Eocene plutons (Hamilton and Myers, 1967; Armstrong, 1974). Many of the petrographic features of the Eocene plutons reflect their shallow level of emplacement, the most obvious example being the common occurrence of miarolitic cavities which prove that a free fluid phase was present during their consolidation (Swanberg and Blackwell, 1973; Bennett, 1980).

An important consequence of the shallow emplacement of the Eocene plutons is that their heat pulse generated large-scale circulation of geothermal groundwaters, as was first discovered by Taylor and Magaritz (1976, 1978). Several independent lines of evidence prove that the bulk of these hot (generally 150°-350°C) fluids were derived from ordinary meteoric waters, which initially had $\delta^{18}O$ of about -16 and δD of about -120 permil. Although nothing remains of this activity today, the immense scale and intensity of these ancient geothermal systems is proved by $\delta^{18}O$ and δD measurements of the granitic rocks. Interaction and exchange of the rocks with these low $\delta^{18}O$ and low δD fluids produced major depletions in the isotopic ratios of the minerals, such that feldspar $\delta^{18}O$ and biotite δD values became as low as -8 and -176 permil, which contrast markedly with their respective primary values of about +9 and -70 permil. At least

7500 km^2 of the batholith was measurably depleted in ^{18}O (38% of the Atlanta lobe), and a much larger area, 15,200 km^2, was measurably depleted in deuterium (81% of the Atlanta lobe). The D/H effects are more widespread than the $^{18}O/^{16}O$ effects because deuterium exchange occurs even when the water/rock ratios are very low (<0.05).

Contour maps of the feldspar $\delta^{18}O$ and biotite δD measurements provide much information about the locations and characteristics of the ancient hydrothermal systems in Idaho. Areas of low-^{18}O rock which mark the zones of the most intense circulation occur as steep-walled annular rings which extend completely around the major Eocene plutons in the Atlanta lobe. Not only does this geographic relationship prove that heat from the Eocene plutons provided the driving force for the fluid circulation, but the marked circularity and abrupt outer boundary of the largest ^{18}O anomaly (the Sawtooth Ring Zone) provide good evidence that this feature is coincident with a zone of enhanced permeability along ring fractures related to a giant Eocene caldera.

Most of the important ore deposits within the batholith are simple fissure veins of the epithermal Au-Ag type. Anderson (1951) has shown that the majority of these deposits crosscut at least some of the Tertiary dikes of the region, and the current study has demonstrated that these deposits bear a spatial correspondence to the zones of intense hydrothermal alteration that have been mapped.

To ensure completeness, the principal findings of this study are restated and amplified below:

(1) There are many chemical and petrographic differences between the Mesozoic and the Eocene granitoids. In addition to those properties previously discovered, this study has determined that: a) Granophyric textures

are common in the Eocene rocks, whereas myrmekite is characteristic of the Mesozoic granitoids. b) Mesozoic rocks typically contain microcline whereas orthoclase is more characteristic of the Eocene rocks. c) Eocene rocks rarely if ever contain muscovite as a primary phase. d) The distinctive pink coloration of the Eocene granites appears to intensify with increasing hydrothermal alteration. e) The Mesozoic granitoids comprise a calcic suite, but the Eocene intrusives and the Challis volcanic rocks are calcalkaline. f) The existence of low-^{18}O aureoles around several distinctive bodies of biotite-hornblende granodiorite and tonalite suggests either that these intrusives also belong to the Eocene suite, or that there was another earlier period of shallow plutonism and meteoric-hydrothermal alteration.

(2) Although widespread meteoric-hydrothermal alteration was previously known in the region, the new results have amplified and quantified some remarkable systematics among the coexisting minerals. In practically all the rocks studied, oxygen isotopic exchange at subsolidus temperatures progressed at least four times as fast in feldspar as in coexisting quartz, and the $\delta^{18}O$ data for suites of related rocks plot on nearly linear trends which allow the primary isotopic composition to be deduced from altered rocks. Although the ^{18}O exchange rate of the "biotite" separates appears to be comparable to that of feldspar, most of the apparent ^{18}O depletions in these "biotites" are actually a consequence of transformation of part of the biotite to low ^{18}O chlorite. However, some D/H exchange of the endmember biotite typically occurred during alteration, and marked D/H and $^{18}O/^{16}O$ exchange is characteristic of those endmember biotites that were in close proximity to Eocene plutons and thus were strongly

heated in the presence of aqueous fluids. D/H exchange occurred at a much faster rate in biotite than in coexisting muscovite, but sericites have low δD values which suggest that they were formed in the presence of the hydrothermal fluid. There is a general correspondence between the degree of propylitization of the rocks and lowering of $\delta^{18}O$ produced by meteoric-hydrothermal alteration, although many exceptions are known which are probably attributable to differences in the temperature of alteration.

(3) The ranges of primary whole-rock $\delta^{18}O$ (9.5 ± 1.5) and biotite δD values (-70 ± 5) of rocks in the Atlanta lobe lie within the ranges observed in the other major Cordilleran batholiths. The primary $\delta^{18}O$ values observed in Idaho are in fact relatively restricted compared to the 5.3 to 12.8 permil range observed in the Peninsular Ranges batholith (Taylor and Silver, 1978), and this difference is probably explicable in terms of the types of source rocks from which the two batholiths were derived. In conjunction with previous data, such as the $^{87}Sr/^{86}Sr$ relationships of Armstrong et al (1977), the stable isotope data strongly suggest that the Mesozoic plutons of the Idaho batholith were derived in large part by melting of the lower continental crust (craton). These magmas cannot have been derived solely from either the mantle, the subducted oceanic slab, or from Mesozoic geosynclinal sedimentary rocks.

(4) The subsolidus depletions of D and ^{18}O produced by the hydrothermal activity in Idaho are similar to those observed in the Coast Range batholith of Alaska and British Columbia, which also were affected by widespread Eocene and later Tertiary plutonism (Magaritz and Taylor, 1976a,b). However, such ^{18}O and D depletions are rare in the Peninsular Ranges and Sierra Nevada batholiths, correlative with the lack of Tertiary epizonal plutonism in these area (Taylor and Silver, 1978; Masi et al,

1980). No definite evidence for the existence of low-^{18}O magmas has been found in the Idaho batholith or in the Eocene plutons; this, together with the documentation that appreciable volumes of such low-^{18}O extrusive magmas are commonly produced in regions of silicic vulcanism (Friedman et al, 1974; Lipman and Friedman, 1975; Hildreth et al, 1980), suggests that such low-^{18}O magmas typically exist only within the top few kilometers of the earth crust, and that the fate of most such magmas is to be erupted (commonly as H_2O-rich ash flow sheets).

(5) The zones of meteoric-hydrothermal alteration in the Idaho batholith were produced during and after the intrusion of the Eocene magmas and are fully as large as envisioned by Taylor and Magaritz (1976, 1978). Several thousand square kilometers of intensely altered rock have now been mapped, and discernible effects are present over more than three-quarters of the Atlanta lobe. The low-^{18}O zones which mark the regions of the most intense alteration occur as steep-walled annular rings that completely surround, but lie outboard of, the major Eocene plutons.

(6) The largest well-studied low-^{18}O area, the Sawtooth Ring Zone, is a 5 to 15 km wide annulus of altered rock which has an outer diameter of approximately 40 X 60 km. A positive aeromagnetic anomaly of similar dimensions characterizes the general region, and provides good evidence for the existence of a major Eocene batholith, of which the outcrop of the Sawtooth batholith comprises only a small part. These data, together with the thick sequence of Challis volcanic rocks immediately to the east, suggest that the low-^{18}O ring is coincident with a zone of ring fracture associated with a major Eocene caldera. Such a feature could have formed during major tectonic subsidence of overlying rock into the subjacent Eocene batholith, during an event associated with voluminous eruption of

ash flow tuff (Germer Tuff Member of the Challis Volcanic Sequence?). The Eocene plutons are thus regarded to be subvolcanic batholiths, whose emplacement was accompanied by the formation of major calderas of the type found at Valles, New Mexico and Yellowstone, Wyoming.

(7) Another well-studied low-^{18}O anomaly is developed around the Twin Springs-Dismal Swamp Steel Mtn.-Trinity Mtn. ("Rocky Bar") intrusive complex. The low-^{18}O rocks occur within a 20 X 30 km, ~3 km wide band which lies between 1 and 4 km outboard of the irregular contact of the Eocene intrusives, and extends over the ~2 km vertical range of the present topography.

(8) Several other zones of low-^{18}O rocks have been found in the Atlanta lobe. Tertiary intrusives have been previously mapped in several of these regions, and in the other areas at least some Eocene rocks were encountered along the traverses made during the present study. The spatial association between the low-^{18}O zones and the Tertiary intrusives is so good that this relationship provides an important mapping and interpretative tool in the region; even subsurface plutons which lie under a cover of older granitoids or Challis volcanic rocks can potentially be found with this isotopic mapping technique.

(9) The results of this study show that active fluid circulation and penetration of surface derived ground waters occurred to depths of at least 7 km below the surface, and involved extensive lateral migration of aqueous fluids; the circulation patterns of these fluids were affected for distances of at least 50 km away from the major Eocene plutons. At least 7000 km^3 of fluid are required to produce the isotopic depletions observed in the Sawtooth Ring Zone alone. At least 1/3 of the heat content of the geothermal waters was provided by the ordinary geothermal gradient in the

older rocks, which indicates that the Eocene magmas did not provide all the energy to these fluids. The annular distribution of intense, deep-level circulation observed in the Sawtooth Ring Zone contrasts with the inter-caldera discharge pattern associated with resurgent domes that is observed today on the surface at Yellowstone, Wyoming. Although ^{18}O depletions in Idaho are also observed in the presumed Eocene resurgent domes (e.g. the Sawtooth plutons) these are nowhere near as large as the ^{18}O effects associated with the ring zones. All the above properties bear on the properties of the deep levels of modern geothermal systems, and may indicate that, rather than just concentrating on the surface manifestations, significant geothermal reserves may be tapped at deep levels by drilling into the ring fracture zones of modern cauldron-related systems.

(10) The new K-Ar analyses in this thesis basically confirm and extend previous studies, and they prove that all of the epizonal granitic plutons in the Atlanta lobe are of Eocene age (38 to 44 m.y.). The data also demonstrate that K-Ar apparent ages of Mesozoic biotites decrease from about 95 m.y. along the east and west margins of the Atlanta lobe to 45 m.y. or less in the zones near the Eocene plutons. Although this relationship was formerly attributed to partial Ar loss on a large scale during the Eocene, the discovery of a distinct dependence of the ages on the present elevation and of a conspicuous "age gap" between 53 and 45 m.y. proves that most of the apparent ages were produced by constant, uniform uplift (~0.15 mm/yr) during the early Tertiary. The detailed geographic relationships suggest that the age pattern also reflects an episode of regional doming produced by intrusion of large volumes (~25,000 km^3) of Eocene magmas, and that only rocks collected near Eocene contacts or at the lowest elevations suffered catastrophic Ar loss during the Eocene.

The distribution of K-Ar apparent ages in the batholith allows reconstruction of the early Tertiary isotherms within the batholith and the history of uplift of the terrane, and these models are consistent with inferences drawn from the stable isotopic and petrographic data. For example, a simple interpretation of the data obtained from Mesozoic rocks preently exposed along a N-S strip between 115°30' and 115°40' west longitude is that 65 m.y. ago these rocks were located at a depth of about 9 to 10 km below the surface, and they had a temperature near the Ar "blocking temperature" for biotite (~300° C). Because of continuous uplift during the next 20 m.y., just prior to the Eocene event these rocks would have been at a depth of about 6 km and at a temperature of about 200° C; thus the pre-Eocene geothermal gradient was about 32° C/km. These temperature-depth relationships were then drastically modified over a relatively short time interval during the Eocene intrusive event, which was accompanied by large-scale doming and widespread hydrothermal activity.

(11) Although such relationships were specifically looked for, only very weak correlations were observed between the K-Ar apparent ages and the $\delta^{18}O$, δD and K_2O values of the "biotites". The major isotopic and K-Ar effect produced by the hydrothermal alteration of these biotites appears simply to be a layer by layer conversion to potassium- and argon-free chlorite. This generally occurred without markedly disturbing the K_2O and Ar concentrations in the remaining biotite, in the manner originally proposed by Kulp and Engels (1963). Thus the K-Ar ages of even heavily chloritized biotites (>50%) are not dramatically re-set by the hydrothermal alteration. The $\delta^{18}O$ values of the "unaltered" biotite end-members in these heavily chloritized samples also seem to be very little affected by the hydrothermal process, and although the D/H ratios of such biotites are

changed, they are usually not completely equilibrated with the coexisting hydrothermal fluids. The data in this thesis thus indicate that low-temperature hydrothermal alteration can markedly affect the D/H ratio of biotite without affecting either its $\delta^{18}O$ value or K-Ar age.

(12) The majority of the important ore deposits within the Atlanta lobe are of the epithermal Au-Ag type and are spatially associated with the periphery of the low-^{18}O zones. No significant orebodies have been discovered in the west-central portion of the Atlanta lobe, where isotopic exchange effects of the rocks are either weak or nonexistent. The $\delta^{18}O$ data thus provide a critical link between these deposits and the hydrothermal activity associated with the Tertiary intrusives, and permit the delineation of a "target zone" centered on the "outer" $\delta^{18}O = +8$ contour where future exploration will be most justified.

REFERENCES

Agricola, G. (1556). De Re Metallica. Translated from the Latin edition of 1556 by H.C. Hoover and L.H. Hoover, Dover Publications Inc., 1950.

Anderson, A.L. (1934) Geology of the Pearl-Horseshoe Bend Gold Belt, Idaho. Idaho Bur. Mines and Geology Pamph. 41, 36 p.

Anderson, A.L. (1939) Geology and ore deposits of the Atlanta district, Elmore County, Idaho. Idaho Bur. Mines and Geology Pamph. 49, 71 p.

Anderson, A.L. (1942) Endomorphism of the Idaho batholith. Geol. Soc. America Bull., V. 53, p. 1099-1126.

Anderson, A.L. (1943) Geology of the Gold-Bearing Lodes of the Rocky Bar District. Idaho Bur. Mines and Geology Pamph. 65, 39 p.

Anderson, A.L. (1947) Geology and ore deposits of Boise Basin, Idaho. U.S. Geol. Survey Bull. 944C, p. 119-319.

Anderson, A.L. (1949) Silver-gold deposits of the Yankee Fork District, Custer County, Idaho. Idaho Bur. Mines and Geology Pamph. 83, 37 p.

Anderson, A.L. (1950) Geology and Ore Deposits of the Hailey-Bellevue mineral belt. Idaho Bur. Mines and Geology Pamph 90, Part I, p. 1-38.

Anderson, A.L. (1951) Metallogenic epochs in Idaho. Econ. Geol., V. 46, p. 592-607.

Anderson, A.L. (1952) Multiple emplacement of the Idaho batholith. Jour. Geology, V. 60, p. 255-265.

Anderson, A.L. and Rasor, A.C. (1934a) Composition of a part of the Idaho batholith in Boise County, Idaho. Amer. Jour. Sci., V. 27, p. 287-294.

Anderson, A.L. and Rasor, A.C. (1934b) Silver mineralization in the Banner District, Boise County, Idaho. Econ. Geol. V. 29, p. 371-387.

Anderson, A.T., Jr., Clayton, R.N. and Mayeda, T.K. (1971) Oxygen isotope thermometry of mafic igneous rocks. Jour. Geol., V. 79, p. 715-729.

Armstrong, F.C. (1957) Dismal Swamp placer deposit, Elmore Co., Idaho. U.S. Geol. Survey Bull. 1042-K, p. 383-392.

Armstrong, F.C. and Oriel, S.S. (1965) Tectonic development of Idaho-Wyoming thrust belt. Amer. Assoc. Petroleum Geologists Bull., V. 49, p. 1847-1866.

Armstrong, R.L. (1966) K-Ar dating of plutonic and volcanic rocks in orogenic belts: in Potassium Argon Dating, eds. O.A. Schaeffer and J. Zähringer, Springer-Verlag, p. 117-133.

Armstrong, R.L. (1974) Geochronometry of the Eocene volcanic-plutonic episode in Idaho. Northwest Geology, V. 3, p. 1-15.

Armstrong, R.L. (1975a) The geochronometry of Idaho. Isochron/West, no. 14, 50 p.

Armstrong, R.L. (1975b) Precambrian (1500 m.y. old) rocks of central Idaho - the Salmon River arch and its role in Cordilleran sedimentation and tectonics. Amer. Jour. Sci., V. 275a, p. 437-467.

Armstrong, R.L. (1978) Cenozoic igneous history of the U.S. Cordillera from lat. 42° to 49° N. Geol. Soc. America Memoir 152, p. 265-282.

Armstrong, R.L. and Hansen, E. (1966) Cordilleran infrastructure in the eastern Great Basin. Amer. Jour. Sci., V. 264, p. 112-127.

Armstrong, R.L., Hollister, V.F. and Harakel, J.E. (1978) K-Ar dates for mineralization in the White Cloud-Cannivan porphyry molybdenum belt of Idaho and Montana. Econ. Geol., V. 73, p. 94-96.

Armstrong, R.L., Jäger, E. and Eberhardt, P. (1966) A comparison of K-Ar and Rb-Sr ages on Alpine biotites. Earth Planet. Sci. Lett., V. 1, p. 13-19.

Armstrong, R.L., Leeman, W.P. and Malde, H.E. (1975) K-Ar dating, Quaternary and Neogene volcanic rocks of the Snake River Plain, Idaho. Amer. Jour. Sci., V. 275, p. 225-251.

Armstrong, R.L. and Suppe, J. (1973) Potassium-argon geochronometry of Mesozoic igneous rocks in Nevada, Utah, and southern California. Geol. Soc. America Bull., V. 84, p. 1375-1392.

Armstrong, R.L., Taubeneck, W.H. and Hales, P.O. (1977) Rb-Sr and K-Ar geochronometry of Mesozoic granitic rocks and their Sr isotopic composition, Oregon, Washington, and Idaho. Geol. Soc. America Bull., V. 88, p. 397-411.

Atwater, T. (1970) Implications of plate tectonics for the Cenozoic tectonic evolution of western North America. Geol. Soc. America Bull., V. 81, p. 3513-3536.

Axelrod, D.I. (1966) Potassium-argon ages of some western Tertiary floras. Amer. Jour. Sci., V. 264, p. 497-506.

Axelrod, D.I. (1968) Tertiary floras and topographic history of the Snake River basin, Idaho. Geol. Soc. America Bull., V. 79, p. 713-734.

Bailey, R.A., Dalrymple, G.B., and Lanphere, M.A. (1976) Volcanism, structure, and geochronology of Long Valley caldera, Mono County, California. J. Geophys. Res., V. 81, p. 725-744.

Bally, A.W., Gordy, P.L. and Stewart, G.A. (1966) Structure, seismic data, and orogenic evolution of southern Canadian Rocky Mountains. Bull. Canadian Petroleum Geologists, V. 14, p. 337-381.

Becker, R.H. and Clayton, R.N. (1976) Oxygen isotope study of a Precambrian banded iron-formation, Hammersley Range, western Australia. Geochim. et Cosmochim. Acta., V. 40, p. 1153-1165.

Bennett, E.H. (1980) Granitic rocks of Tertiary age in the Idaho batholith and their relation to mineralization. Econ. Geol., V. 75, p. 278-288.

Bergendahl, M.H. (1964) Gold: in Mineral and Water Resources of Idaho. U.S. Geol. Survey Spec. Rept. No. 1, p. 93-101.

Berry, A.L. and others (1976) Summary of miscellaneous potassium-argon age measurements, U.S. Geological Survey, Menlo Park, California, for the years 1972-74. U.S. Geol. Survey Circ. 727, 13 p.

Birch, F., Roy, R.F., and Decker, E.R. (1968) Heat flow and thermal history in New England and New York: in Studies of Appalachian Geology-Northern and Maritime, eds. E. Zen, W.S. White, J.B. Hadley and J.B. Thompson, Jr. Interscience, p. 437-451.

Bishop, D.T. (1973) Petrology and geochemistry of the Purcell sills in Boundary County, Idaho. Belt Symposium, Dept. Geol., Univ. Idaho, Moscow, Idaho, V. II, p. 16-66.

Blackwell, D.D. (1978) Heat flow and energy loss in the western United States: in Cenozoic Tectonics and Regional Geophysics of the Western Cordillera, eds. R.B. Smith and G.P. Eaton. Geol. Soc. America Memoir 152, p. 175-208.

Blattner, P. and Bird, G.W. (1974) Oxygen isotope fractionation between quartz and K-feldspar at 600° C. Earth Planet. Sci. Lett., V. 23, p. 21-27.

Bond, J.G. (1978) Geologic map of Idaho. Idaho Bur. Mines and Geology.

Boone, G.M. (1969) Origin of clouded red feldspars: Petrologic contrasts in a granitic porphyry intrusion. Amer. Jour. Sci., V. 267, p. 633-668.

Bottinga, Y. and Javoy, M. (1973) Comments on oxygen isotope geothermometry. Earth Planet. Sci. Lett., V. 20, p. 250-265.

Bottinga, Y. and Javoy, M. (1975) Oxygen isotope partitioning among the minerals in igneous and metamorphic rocks. Rev. Geophys. and Space Phys. V. 13, p. 401-418.

Bowen, N.L. and Tuttle, O.F. (1950) The System $NaAlSi_3O_8$ - $KAlSi_3O_8$-H_2O. Jour. Geol., V. 58, p. 489-517.

Buddington, A.F. (1959) Granite emplacement with special reference to North America. Geol. Soc. America Bull., V. 70, p. 671-747.

Burchfiel, B.C. and Davis, G.A. (1972) Structural framework and evolution of the southern part of the Cordilleran orogen, Western United States. Amer. Jour. Sci., V. 272, p. 97-118.

Burchfiel, B.C. and Davis, G.A. (1975) Nature and controls of Cordilleran orogenesis, western United States: Extensions of an earlier synthesis. Amer. Jour. Sci., V. 275a, p. 363-396.

Campbell, S. (1931) Bunker Hill and Sullivan M. & C. Co., Hall-Interstate, Lost Pilgrim mines, Bernard, Deadwood Basin, Valley County. Thirty-second Annual Rept. Min. Industry of Idaho for 1930, p. 32-40.

Cater, F.W., Pinckney, D.M., Hamilton, W.B. Parker, R.L., Weldin, R.D., Close, T.J., Zilka, N.T., Leonard, B.F. and Davis, W.E. (1973) Mineral Resources of the Idaho Primitive Area and Vicinity, Idaho. U.S. Geol. Survey Bull. 1304, 431 p.

Chase, R.B., Bickford, M.E. and Tripp, S.E. (1978) Rb-Sr and U-Pb isotopic studies of the northeastern Idaho batholith and border zone. Geol. Soc. America Bull., V. 89, p. 1325-1334.

Chase, R.B. and Johnson, B.R. (1977) Border-zone relationships of the northern Idaho batholith. Northwest Geology, V. 6-1, p. 38-50.

Clark, S.P., Jr. (1966) Thermal conductivity: in Handbook of Physical Constants, ed. S.P. Clark, Jr. Geol. Soc. America Memoir 97, p. 459-482.

Clark, S.P. Jr. (1979) Thermal models of the central Alps: in Lectures in Isotope Geology, Jäger, E. and Hunziker, J.C. eds., Springer-Verlag, New York, p. 225-230.

Clark, S.P. Jr., and Jäger, E. (1969) Denudation rate in the Alps from geochronologic and heat flow data. Amer. Jour. Sci., V. 267, p. 1143-1160.

Clayton, R.N., Friedman, I., Graf, D.L., Mayeda, T.K., Meents, W.F. and Shimp, N.F. (1966) The origin of saline formation waters. J. Geophys. Res., V. 71, p. 3869-3882.

Clayton, R.N., Goldsmith, J.R., Karel, K.J., Mayeda, T.K. and Newton, R.C. (1975) Limits on the effect of pressure on isotopic fractionation. Geochim. et Cosmochim. Acta, V. 39, p. 1197-1201.

Clayton, R.N., Muffler, L.J.P., and White, D.E. (1968) Oxygen isotope study of calcite and silicates of the River Ranch No. 1. Well, Salton Sea geothermal field, California. Amer. Jour. Sci., V. 266, p. 968-979.

Clayton, R.N., O'Neil, J.R. and Mayeda, T.K. (1972) Oxygen isotpe exchange between quartz and water. J. Geophys. Res., V. 77, p. 3057-3067.

Compton, R.R. (1962) Manual of Field Geology. John Wiley and Sons, Inc., New York, 378 p.

Coney, P.J. (1978) Mesozoic-Cenozoic Cordilleran plate tectonics. Geol. Soc. America Memoir 152, p. 32-50.

Cook, E.F. (1954) Mining geology of the Seven Devils region. Idaho Bur. Mines and Geol. Pamph. 97, 22 p.

Cooper, J.R. (1951) Geology of the tungsten, antimony and gold deposits near Stibnite, Idaho. U.S. Geol. Survey Bull. 969-F, p. 151-197.

Craig, H. (1957) Isotopic standards for carbon and oxygen and correction factors for mass-spectrometric analysis of carbon dioxide. Geochim. et Cosmochim. Acta, V. 12, p. 133-149.

Craig, H. (1961) Isotopic variations in meteoric waters. Science, V. 133, p. 1702-1703.

Craig, H. (1963) The isotope geochemistry of water and carbon in geothermal areas: in Tongiorgi, E., ed., Nuclear Geology on Geothermal Areas, Spoleto, 1963. CNR, Lab. Geol. Nucl. Pisa., p. 17-53.

Craig, H. (1966) Isotopic composition and origin of the Red Sea and Salton Sea geothermal brines. Science, V. 154, p. 1544-1548.

Craig, H., Boato, G., and White, D.E. (1956) Isotopic geochemistry of thermal waters: in Proc. Conf. Nuclear Processes in Geol. Settings. Second Natl. Acad. Sci. Natl. Res. Council Publ. 400:29

Criss, R.E. and Taylor, H.P., Jr. (1978) Regional $^{18}O/^{16}O$ and D/H variations in granitic rocks of the southern half of the Idaho batholith and the dimensions of the giant hydrothermal systems associated with emplacement of the Eocene Sawtooth and Rocky Bar plutons. Geol. Soc. America Abst. with Prgms., V. 10, No. 7, p. 384.

Criss, R.E., Gregory, R.T. and Taylor, H.P., Jr. (in prep.) $\delta^{18}O$ systematics of coexisting minerals from hydrothermally altered plutonic rocks.

Dalrymple, G.B. and Lanphere, M.A. (1969) Potassium-Argon Dating: Principles, Techniques, and Applications to Geochronology. W.H. Freeman and Co., 1969, 258 p.

Dansgaard, W. (1964) Stable isotopes in precipitation. Tellus, V. 16, p. 436-468.

Deer, W.A., Howie, R.A., and Zussman, J. (1966) An Introduction to the Rock-Forming Minerals. Longman, 528 p.

Deines, P. (1977) On the oxygen isotope distribution among mineral triplets in igneous and metamorphic rocks. Geochim. et Cosmochim. Acta, V. 41, p.1709-1730.

DePaolo, D.J. (1979) Neodymium isotopic evidence on the origin of Sierra Nevada granites. Geol. Soc. America Abst. with Prgms. V. 11, No. 7, p. 412.

Dodson, M.H. (1973) Closure temperature in cooling geochronological and petrological systems. Contrib. Mineral. Petrol., V. 40, p. 259-274.

Dodson, M.H. (1979) Theory of cooling ages: in Lectures in Isotope Geology, eds. E. Jäger and J.C. Hunziker. Springer-Verlag, p. 194-202.

Doell, R.R., Dalrymple, G.B., Smith, R.L., and Bailey, R.A. (1968) Paleomagnetism, potassium-argon ages, and geology of rhyolites and associated rocks of the Valles caldera, New Mexico. Geol. Soc. America Memoir 116, p. 211-248.

Early, T.O. and Silver, L.T. (1973) Rb-Sr isotopic systematics in the Peninsular Ranges batholith of southern and Baja California. Trans. Amer. Geophys. Union, V. 54, p. 494.

Eaton, G.P., Christiansen, R.L., Iyer, H.M., Pitt, A.M., Mabey, D.R., Blank, H.R, Jr., Zeitz, I. and Gettings, M.E. (1975) Magma beneath Yellowstone National Park. Science, V. 188, No. 4190, p. 787-796.

Eaton, G.P. Wahl, R.R., Prostka, H.J., Mabey, D.R. and Kleinkopf, M.D. (1978) Regional gravity and tectonic patterns: Their relation to late Cenozoic epeirogeny and lateral spreading in the western Cordillera. Geol. Soc. America Memoir 152, p. 51-92.

Ellis, A.J. and Mahon, W.A.J. (1964) Natural hydrothermal systems and experimental hot-water/rock interactions. Geochim. et Cosmochim. Acta, V. 28, p. 1323-1357.

Evans, B.W. (1965) Application of a reaction-rate method to the breakdown equilibria of muscovite and muscovite plus quartz. Amer. Jour. Sci., V. 263, p. 647-667.

Fairchild, J.G.: in Wells, R.C. (1937) Analyses of rocks and minerals from the laboratory of the U.S. Geological Survey. U.S. Geol. Survey Bull. 878.

Ferguson, J.A. (1975) Tectonic implications of some geochronometric data from the northeastern border zone of the Idaho batholith. Northwest Geology, V. 4, p. 53-58.

Forester, R.W. and Taylor, H.P., Jr. (1976) ^{18}O-depleted igneous rocks from the Tertiary complex of the Isle of Mull, Scotland. Earth Planet. Sci. Lett., V. 32, p. 11-17.

Forester, R.W. and Taylor, H.P., Jr. (1977) $^{18}O/^{16}O$, D/H and $^{13}C/^{12}C$ studies of the Tertiary igneous complex of Skye, Scotland. Amer. Jour. Sci., V. 277, p. 136-177.

Fournier, R.O., White, D.E. and Truesdell, A.H. (1976) Convective heat flow in Yellowstone National Park. U.N. Symposium on the Development and Use of Geothermal Resources, 2d, San Francisco, Proc., p. 731-739.

Frey, M., Hunziker, J.C., O'Neil, J.R. and Schwander, H.W. (1976) Equilibrium-disequilibrium relations in the Monte Rosa granite, western Alps: Petrological, Rb-Sr and stable isotope data. Contrib. Mineral Petrol., V. 55, p. 147-179.

Friedman, I. (1953) Deuterium content of natural waters and other substances. Geochim. et Cosmochim. Acta, V. 4, p. 89-103.

Friedman, I. Lipman, P.W., Obradovich, J.D., Gelason, J.D. and Christiansen, R.L. (1974) Meteoric water in magmas. Science, V. 184, p. 1069-1072.

Friedman, I. Redfield, A.C., Schoen, B. and Harris, J. (1964) The variation of the deuterium content of natural waters in the hydrologic cycle. Rev. Geophys, V. 2, p.177-224.

Garlick, G.D. and Epstein, S. (1966) The isotopic composition of oxygen and carbon in hydrothermal minerals at Butte, Montana. Econ. Geol., V. 61, p. 1325-1335.

Giletti, B.J., Semet, M.P. and Yund, R.A. (1978) Studies in diffusion-III. Oxygen in feldspars: an ion microprobe determination. Geochim. et Cosmochim. Acta, V. 42, p. 45-57.

Gilluly, J. (1965) Volcanism, tectonism, and plutonism in the western United States. Geol. Soc. America Spec. Paper 80, 69 p.

Godfrey, J.D. (1962) The deuterium content of hydrous minerals from the east-central Sierra Nevada and Yosemite National Park. Geochim. et Cosmochim. Acta, V. 26, p. 1215-1245.

Grauert, B. and Hofmann, A. (1973) Old radiogenic lead components in zircons from the Idaho batholith and its metasedimentary aureole. Carnegie Inst. Washington Year Book 72, p. 297-299.

Greenwood, W.R. and Morrison, D.A. (1973) Reconnaissance Geology of the Selway-Bitterroot Wilderness Area. Idaho Bur. Mines and Geol. Pamph. 154, 30 p.

Gregory, R.T. and Taylor, H.P., Jr. (1981) An oxygen isotope profile in a section of Cretaceous oceanic crust, Samail ophiolite, Oman: evidence for $\delta^{18}O$-buffering of the oceans by deep (>5 km) seawater-hydrothermal circulation at mid-ocean ridges. J. Geophys. Res.

Hadley, J.B. (1964) Correlation of isotopic ages, crustal heating and sedimentation in the Appalachian region: in Tectonics of the Southern Appalachians, Lowry, W.D., ed. Va. Polytech. Inst. Dept. Geol. Sci. Mem., V. 1, p. 33-45.

Hall, W.E., Rye, R.O. and Doe, B.R., (1978) Wood River Mining District, Idaho- Intrusion-related lead-silver deposits derived from country rock source. Jour. Res. U.S. Geol. Survey, V. 6, No. 5, p. 579-592.

Hamilton, W. (1960) Metamorphism and thrust faulting in the Riggins Quadrangle, Idaho. U.S. Geol. Survey Prof. Paper 400-B, p. 230-231.

Hamilton, W. (1962) Late Cenozoic structure of west-central Idaho. Geol. Soc. America Bull., V. 73, p. 511-516.

Hamilton, W.B. (1963a) Metamorphism in the Riggins Region, western Idaho. U.S. Geol. Survey Prof. Paper 436, 95 p.

Hamilton, W. (1963b) Overlapping of late Mesozoic orogens in western Idaho. Geol. Soc. America Bull., V. 74, p. 779-788.

Hamilton, W. and Myers, W.B. (1967) The nature of batholiths. U.S. Geol. Survey Prof. Paper 554C, p. 1-30.

Hanna, W.F. (1969) Negative aeromagnetic anomalies over mineralized areas of the Boulder Batholith, Montana. U.S. Geol. Survey Prof. Paper 650-D, p. 159-167.

Hanson, G.N. and Gast, P.W. (1967) Kinetic studies in contact metamorphic zones. Geochim. et Cosmochim. Acta, V. 31, p. 1119-1153.

Harper, C.T. (1967) The geological interpretation of potassium-argon ages of metamorphic rocks from the Scottish Caledonides. Scott. J. Geol., V. 3, p. 46-66.

Harrison, J.E., Griggs, A.B., and Wells, J.D. (1974) Tectonic features of the Precambrian Belt Basin and their influence on post-Belt structures. U.S. Geol. Survey Prof. Paper 866, 15 p.

Harrison, J.E., Kleinkopf, M.D. and Obradovich, J.D. (1972) Tectonic events at the intersection between the Hope fault and the Purcell trench, northern Idaho. U.S. Geol. Survey Prof. Paper 719, 24 p.

Hart, S.R. (1964) The petrology and isotopic-mineral age relations of a contact zone in the Front Range, Colorado. Jour. Geol., V. 72, p. 493-525.

Hayden, R.J. and Wehrenberg, J.P. (1960) A^{40}-K^{40} dating of igneous and metamorphic rocks in western Montana. Jour. Geol., V. 68, p. 94-97.

Helgeson, H.C. (1968) Geologic and thermodynamic characteristics of the Salton Sea geothermal system. Amer. Jour. Sci., V. 266, p. 129-166.

Hietanen, A. (1962) Metasomatic metamorphism in western Clearwater County, Idaho. U.S. Geol. Survey Prof. Paper 344-A, 116 p.

Hietanen, A. (1963) Idaho batholith near Pierce and Bungalow, Clearwater County, Idaho. U.S. Geol. Survey Prof. Paper 344-D, p. 1-42.

Hietanen, A. (1968) Belt Series in the region around Snow Peak and Mallard Peak, Idaho. U.S. Geol. Survey Prof. Paper 344-E, p. 1-34.

Hietanen, A. (1969) Distribution of Fe and Mg between garnet, staurolite, and biotite in aluminum-rich schist in various metamorphic zones north of the Idaho batholith. Amer. Jour. Sci., V.267, p. 422-456.

Hildreth, W., Christiansen, R.L. and O'Neil, J.R. (1980) Catastrophic isotopic modification of rhyolite magma by creation of the Yellowstone caldera. Geol. Soc. America Abst. with Prgms., V. 12, No. 3, p. 111.

Hill, D.P. (1976) Structure of Long Valley caldera, California, from a seismic refraction experiment. J. Geophys. Res., V. 81, p. 745-753.

Hitchon, B. and Friedman, I. (1969) Geochemistry and origin of formation waters in the western Canada sedimentary basin - I. Stable isotopes of hydrogen and oxygen. Geochim. et Cosmochim. Acta, V. 33, p. 1321-1349.

Hobbs, S.W. (1964) Tungsten: in Mineral and Water Resources of Idaho. U.S. Geol. Survey Spec. Rept. No. 1., p. 223-233.

Hobbs, S.W. and Fryklund, V.C., Jr. (1968) The Coeur d'Alene District, Idaho: in Ore Deposits of the United States, 1933-1967. (Graton-Sales Volume), ed. J.D. Ridge. Amer. Inst. Mining Metallurgical and Petroleum Engrs., p. 1417-1435.

Howard, K.A. and Shervais, J.W. (1973) Geologic Map of Smith Prairie, Elmore County, Idaho. U.S. Geol. Survey Misc. Inv. Map I-818.

Hudson, T., Plafkir, G. and Lanphere, M.A. (1977) Intrusive rocks of the Yakutat-St. Elias area, south-central Alaska. Jour. Res. U.S. Geol. Survey, V. 5, p. 155-172.

Hunt, G. (1962) Time of Purcell eruption in southeastern British Columbia and southwestern Alberta. J. Alberta Soc. Petroleum Geologists, V. 10, p. 438-442.

Jaffe, H.W., Gottfried, D., Waring, C.L. and Worthing, H.W. (1959) Lead-alpha age determinations of accessory minerals of igneous rocks (1953-1957). U.S. Geol. Survey Bull. 1097-B, p. 65-148.

Jäger, E. (1962) Rb-Sr age determinations on micas and total rocks from the Alps. J. Geophys. Res., V. 67, p. 5293-5306.

James, R. (1968) Wairakei and Larderello; geothermal power systems compared.

New Zealand Jour. Sci. and Technology, V. 11, p. 706-719.

Kane, M.F., Mabey, D.R. and Brace, R. (1976) A gravity and magnetic investigation of the Long Valley caldera, Mono County, California. J. Geophys. Res., V. 81, p. 754-762.

Kiilsgaard, T.H., Freeman, V.L. and Coffman, J.S. (1970) Mineral Resources of the Sawtooth Primitive Area, Idaho. U.S. Geol. Survey Bull. 1319-D, 174 p.

King, P.B. (1969) The tectonics of North America - A discussion to accompany the tectonic map of North America: Scale 1:5,000,000. U.S. Geol. Survey Prof. Paper 628, 95 p.

King, P.B. (1977) The Evolution of North America. Princeton Univ. Press, 1977, 197 p.

King, P.B. and Beikman, H.M. (1974) Geologic map of the United States, exclusive of Alaska and Hawaii. U.S. Geol. Survey.

Kirkham, V.R.D. (1930) Old erosion surfaces in southwestern Idaho. Jour. Geol., V. 38, p. 652-663.

Krummenacher, D., Gastil, R.G., Bushee, J. and Doupont, J. (1975) K-Ar apparent ages, Peninsular Ranges batholith, southern California and Baja California. Geol. Soc. America Bull., V. 86, p. 760-768.

Kuellmer, F.J. (1960) X-ray intensity mesurements on perthitic materials, II. Data from natural alkali feldspars. Jour. Geol., V. 68, p. 307-323.

Kulp, J.L. and Engels, J. (1963) Discordances in K-Ar and Rb-Sr isotopic ages: in Radioactive Dating, Vienna, Intl. Atomic Energy Agency, p. 219-238.

Lachenbruch, A.H. (1968) Preliminary geothermal model of the Sierra Nevada. J. Geophys. Res., V. 73, p. 6977-6989.

Lachenbruch, A.H. and Sass, J.H. (1978) Models of an extending lithosphere and heat flow in the Basin and Range province: in Cenozoic Tectonics and Regional Geophysics of the Western Cordillera, eds. R.B. Smith and G.P. Eaton. Geol. Soc. America Memoir 152, p. 209-250.

Lachenbruch, A.H. Sorey, M.L., Lewis, R.E. and Sass, J.H. (1976) The near-surface hydrothermal regime of Long Valley caldera. J. Geophys. Res., V. 81, p. 763-768.

Lambert, S.J. (1976) Stable Isotope Studies of some Active Hydrothermal Systems. Unpub. Ph.D. thesis, California Institute of Technology, 362 p.

Larsen, E.S., Gottfried, D., Jaffe, H.W. and Waring, C.L. (1958) Lead-alpha ages of the Mesozoic batholiths of western North America. U.S. Geol. Survey Bull. 1070-B, p. 35-62.

Larsen, E.S., Jr. and Schmidt, R.G. (1958) A reconnaissance of the Idaho batholith and comparison with the southern California batholith. U.S. Geol. Survey Bull. 1070-A, p. 1-33.

Lawrence, J.R. and Taylor, H.P., Jr. (1971) Deuterium and oxygen-18 correlation: Clay minerals and hydroxides in Quaternary soils compared to meteoric waters. Geochim. et Cosmochim. Acta, V. 35, p. 993-1003.

Lawrence, J.R. and Taylor, H.P., Jr. (1972) Hydrogen and oxygen isotope systematics in weathering profiles. Geochim. et Cosmochim. Acta, V. 36, p. 1377-1393.

Lawson, A.C. (1914) Is the Boulder "batholith" a laccolith? - a problem in ore genesis. California Univ. Dept. Geol. Bull., V. 8, p. 1-15.

Lipman, P.W. and Friedman, I. (1975) Interactions of meteoric water with magma: an oxygen-isotope study of ash-flow sheets from southern Nevada. Geol. Soc. America Bull., V. 86, p. 695-702.

Lipman, P.W., Steven, T.A., Luedke, R.G. and Burbank, W.S. (1973) Revised volcanic history of the San Juan, Uncompahgre, Silverton, and Lake City calderas in the western San Juan Mountains, Colorado. Jour. Res. U.S. Geol. Survey, V. 1., No. 6, p. 627-642.

Lipman, P.W., Doc, B.R., Hedge, C.E. and Steven, T.A. (1978) Petrologic evolution of the San Juan volcanic field, southwestern Colorado: Pb and Sr isotope evidence. Geol. Soc. America Bull., V. 89, p. 59-82.

McBirney, A.R. (1980) Mixing and unmixing of magmas. Jour. Volcanol. Geotherm. Res., V. 7, p. 357-371.

McBirney, A.R. and Williams, H. (1969) A new look at the classification of calderas (abst). Intl. Assn. Volcanology and Chem. Earth's Interior, Symposium on Volcanoes and Their Roots. Oxford Univ., supp. absts.

McCulloch, M.T., Gregory, R.T., Wasserburg, G.J. and Taylor, H.P., Jr. (1980) A neodymium, strontium, and oxygen isotopic study of the Cretaceous Samail ophiolite and implications for the petrogenesis and seawater-hydrothermal alteration of oceanic crust. Earth Planet. Sci. Lett., V. 46, p. 201-211.

McDowell, F.W. (1966) Potassium-Argon Dating of Cordilleran Intrusives. Ph.D. thesis, Columbia University, 242 p.

McDowell, F.W., and Kulp, J.L. (1969) Potassium-argon dating of the Idaho batholith. Geol. Soc. America Bull., V. 80, p. 2379-2382.

McGookey, D.P., Haun, J.D., Hale, L.A., Goodell, H.G., McCubbin, D.G., Weimer, R.J. and Wulf, G.R. (1972) Cretaceous System: in Geologic Atlas of the Rocky Mountain Region, ed. W.M. Mallory. Rocky Mtn. Assn. of Geologists, A.B. Hirschfeld Press, p. 190-228.

Macdonald, G.A. (1972) Volcanoes. Prentice-Hall, Inc., Englewood Cliffs, New Jersey, 510 p.

Magaritz, M. and Taylor, H.P., Jr. (1976a) Isotopic evidence for meteoric-hydrothermal alteration of plutonic igneous rocks in the Yakutat Bay and Skagway areas, Alaska. Earth Planet. Sci. Lett., V. 30, p. 179-190.

Magaritz, M. and Taylor, H.P., Jr. (1976b) $^{18}O/^{16}O$ and D/H studies along a 500 km traverse across the Coast Range batholith and its country rocks, central British Columbia. Canadian Jour. Earth Sci., V. 13, p. 1514-1536.

Martin, R.F. and Lalonde, A. (1979) Turbidity in K-feldspars: Causes and implications. Geol. Soc. America Abst. with Prgms., V. 11, p. 472-473.

Marvin, R.F., Tschanz, C.M., Mehnert, H.H. and Mangum, J. (1973) Late Cretaceous age for molybdenite mineralization in Custer County, Idaho. Isochron/West, No. 7, p. 1.

Masi, U., O'Neil, J.R. and Kistler, R.W. (1976) Stable isotope systematics in Mesozoic granites near the San Andreas and Garlock fault systems, California. Geol. Soc. Amer. Abst. with Prgms., V. 8, p. 998.

Masi, U., O'Neil, J.R. and Kistler, R.W. (in press) Stable isotope systematics in Mesozoic granites of central and northern California and southwestern Oregon.

Matsuhisa, Y., Goldsmith, J.R., and Clayton, R.N. (1978) Mechanisms of hydrothermal crystallization of quartz at 250° C and 15 Kbar. Geochim. et Cosmochim. Acta, V. 42, p. 173-182.

Matsuhisa, Y., Goldsmith, J.R. and Clayton, R.N. (1979) Oxygen isotopic fractionation in the system quartz-albite-anorthite-water. Geochim. et Cosmochim. Acta, V. 43, p. 1131-1140.

Matthews, A. and Beckinsale, R.D. (1979) Oxygen isotope equilibration systematics between quartz and water. Amer. Minerologist, V. 64, p. 232-240.

Meyer, C., Shea, E.P. and Goddard, C.C. (1968) Ore deposits at Butte, Montana: in Ore Deposits of the United States, 1933-1967 (Graton-Sales Volume) ed. J.D. Ridge. Amer. Inst. Mining Metallurgical and Petro. Engrs., p. 1373-1416.

Moore, J.G. (1959) The quartz diorite boundary line in the western United States. Jour. Geol., V. 67, p. 198-210.

Noble, J.A. (1970) Metal provinces of the western United States. Geol. Soc. America Bull., V. 81, p. 1607-1624.

Noble, J.A. (1976) Metallogenic provinces of the Cordillera of western North and South America. Mineral. Deposita (Berlin), V. 11., p. 219-233.

Norton, D. and Knapp, R. (1977) Transport phenomena in hydrothermal systems: The nature of porosity. Amer. Jour. Sci., V. 277, p. 913-936.

Norton, D. and Knight, J. (1977) Transport phenomena in hydrothermal systems: Cooling plutons. Amer. Jour. Sci., V. 277, p. 937-981.

Norton, D. and Taylor, H.P., Jr. (1979) Quantitative simulation of the hydrothermal systems of crystallizing magmas on the basis of transport theory and oxygen isotope data: An analysis of the Skaergaard intrusion. Jour. Petrology, V. 20, p. 421-486.

Obradovich, J.D. and Peterman, Z.E. (1968) Geochronology of the Belt Series, Montana. Canadian Jour. Earth Sci., V. 5, p. 737-747.

Obradovich, J.D. and Peterman, Z.E. (1973) A review of the geochronology of Belt and Purcell rocks. Belt Symposium, Dept. Geol., Univ. Idaho, Moscow, Idaho, p. 8-9.

O'Neil, J.R. and Chappell, B.W. (1977) Oxygen and hydrogen isotope relations in the Berridale batholith. Jour. Geol. Soc. London, V. 133, p. 559-571.

O'Neil, J.R. and Clayton, R.N. (1964) Oxygen isotope geothermometry: in Isotopic and Cosmic Chemistry, eds. H. Craig, S.L. Miller and G.J. Wasserburg. North-Holland, p. 157-168.

O'Neil, J.R. and Kharaka, Y.K. (1976) Hydrogen and oxygen isotope exchange reactions between clay minerals and water. Geochim. et Cosmochim. Acta, V. 40, p. 241-246.

O'Neil, J.R., Silberman, M.L., Fabbi, B.P. and Chesterman, C.W. (1973) Stable isotope and chemical relations during mineralization in the Bodie mining district, Mono County, California. Econ. Geol., V. 68, p. 765-784.

O'Neil, J.R. and Silberman, M.L. (1974) Stable isotope relations in epithermal Au-Ag deposits. Econ. Geol., V. 69, p. 902-909.

O'Neil, J.R. and Taylor, H.P., Jr. (1967) The oxygen isotope and cation exchange chemistry of feldspars. Amer. Miner., V. 52, p. 1414-1437.

Pakiser, L.C., Kane, M.F. and Jackson, W.H. (1964) Structural geology and volcanism of Owens Valley region, California-a geophysical study. U.S. Geol. Survey Prof. Paper 438, 68 p.

Peacock, M.A. (1931) Classification of igneous rock series. Jour. Geol., V. 39, p. 54-67.

Percious, J.K., Damon, P.E., and Olson, H.J. (1967) Radiometric dating of Idaho batholith porphyries. U.S. Atomic Energy Comm. Annual Prog. Rept. No. COO-689-76, Appendix A-X.

Reid, R.R. (1963) Reconnaissance geology of the Sawtooth Range. Idaho Bur. Mines and Geol. Pamph. 129, 37 p.

Reid, R.R., Greenwood, W.R. and Morrison, D.A. (1970) Precambrian metamorphism of the Belt Supergroup in Idaho. Geol. Soc. America Bull., V. 81, p. 915-918.

Reid, R.R., Morrison, D.A., and Greenwood, W.R. (1973) The Clearwater orogenic zone: A relict of Proterozoic orogeny in central and northern Idaho. Belt Symposium, Dept. Geol., Univ. Idaho, Moscow, Idaho, p. 10-56.

Rember, W.C. and Bennett, E.H. (1979) Geologic Map of the Hailey Quadrangle, 1:250,000. Idaho Bur. Mines and Geology.

Roberts, R.J., Hotz, P.E., Gilluly, J. and Ferguson, H.G. (1958) Paleozoic rocks of north-central Nevada. Amer. Assn. Petroleum Geologists Bull., V. 42, p. 2813-2857.

Roberts, R.J. and Thomasson, M.R. (1964) Comparison of late Paleozoic depositional history of northern Nevada and central Idaho. U.S. Geol. Survey Prof. Paper 475-D, p. 1-6.

Ross, C.P. (1927) Ore deposits in Tertiary lava in the Salmon River Mountains, Idaho. Idaho Bur. Mines and Geol. Pamph. 25, 20 p.

Ross, C.P. (1928) Mesozoic and Tertiary granitic rocks in Idaho. Jour. Geol., V. 36, p. 673-693.

Ross, C.P. (1934) Geology and ore deposits of the Casto Quadrangle, Idaho. U.S. Geol. Survey Bull. 854, 135 p.

Ross, C.P. (1936) Some features of the Idaho batholith. Intl. Geol. Cong. Rept. 16 Sess., V. 1., p. 369-385.

Ross, C.P. (1941) The metal and coal mining districts of Idaho with notes on the nonmetallic mineral resources of the state. Idaho Bur. Mines and Geol. Pamph. 57, 263 p.

Ross, C.P. (1961) A redefinition and restriction of the therm Challis volcanics. U.S. Geol. Survey Prof. Paper 424-C, p. 177-180.

Ross, C.P. (1962a) Paleozoic seas of central Idaho. Geol. Soc. America Bull., V. 73, p. 769-794.

Ross, C.P. (1962b) Stratified rocks in south-central Idaho. Idaho Bur. Mines and Geol. Pamph. 125, 126 p.

Ross, C.P. (1963) Modal composition of the Idaho batholith. U.S. Geol. Survey Prof. Paper 475-C, p. C86-C90.

Ross, C.P. and Forrester, J.D. (1947) Geologic map of the state of Idaho. U.S. Geol. Survey and Idaho Bur. Mines and Geology, scale 1:500,000.

Ross, S.H. (1971) Geothermal potential of Idaho. Idaho Bur. Mines and Geol. Pamph. 150, 72 p.

Rostad, O.H. (1978) K-Ar dates for mineralization in the White Cloud-Cannivan porphyry molybdenum belt of Idaho and Montana - A discussion. Econ. Geol., V. 73, p. 1366-1368.

Ryan, B.D. and Benkinsop, J. (1971) Geology and geochronology of the Hellroaring Creek Stock, British Columbia. Canadian Jour. Earth Sci., V. 8, p. 85-95.

Ryder, R.T. and Ames, H.T. (1970) Palynology and age of Beaverhead Formation and their Paleotectonic implications in Lima region, Montana - Idaho. Amer. Assn. Petroleum Geologists Bull., V. 54, p. 1155-1171.

Ryder, R.T. and Scholten, R. (1973) Syntectonic conglomerates in southwestern Montana: Their nature, origin, and tectonic signficance. Geol. Soc. America Bull., V. 84, p. 773-796.

Savin, S.M. (1977) The history of the earth's surface temperature during the past 100 million years: in Ann. Rev. Earth Planet. Sci., 1977, V. 5, p. 319-355.

Schmidt, D.L. (1964) Reconnaissance petrographic cross section of the Idaho batholith in Adams and Valley Counties, Idaho. U.S. Geol. Survey Bull. 1181-G, 50 p.

Schmidt, D.L. and Mackin, J.H. (1970) Quaternary geology of Long and Bear Valleys, west-central Idaho. U.S. Geol. Survey Bull. 1311A, p. 1-22.

Scholten, R. (1968) Model for evolution of Rocky Mountains east of Idaho batholith. Tectonophysics, V. 6, p. 109-126.

Scholten, R. and Onasch, C.M. (1977) Genetic relations between the Idaho batholith and its deformed eastern and western margins. Northwest Geology, V. 6-1, p. 25-37.

Shenon, P.J. and Ross, C.P. (1936) Geology and ore deposits near Edwardsburg and Thunder Mountain, Idaho. Idaho Bur. Mines and Geol. Pamph. 44, 45 p.

Sheppard, S.M.F. and Epstein, S. (1970) D/H and $^{18}O/^{16}O$ ratios of minerals of possible mantle or lower crustral origin. Earth Planet. Sci. Lett., V. 9, p. 232-239.

Sheppard, S.M.F. and Taylor, H.P., Jr. (1974) Hydrogen and oxygen isotope evidence for the origins of water in the Boulder batholith and the Butte ore deposits, Montana. Econ. Geol. V. 69, p. 926-946.

Shieh, Y.N. and Taylor, H.P., Jr. (1969) Oxygen and hydrogen isotope studies of contact metamorphism in the Santa Rosa Range, Nevada and other areas. Contr. Mineral. and Petrol., V. 20, p. 306-356.

Siems, P.L. and Jones, R.W. (1977) The Challis volcanic field: A review. Geol. Soc. America Absts. with Prgms., V. 9, No. 6, p. 762.

Silver, L.T., Stehli, F.G. and Allen, C.R. (1963) Lower Cretaceous pre-batholithic rocks of northern Baja California, Mexico. Amer. Assn. Petroleum Geologists Bull., V. 47, p. 2054-2059.

Silver, L.T., Taylor, H.P., Jr. and Chappell, B. (1979) Some petrological, geochemical and geochronological observations of the Peninsular Ranges batholith near the international border of the U.S. and Mexico. Guidebook to field trip San Diego Geol. Soc. America Mtg. Mesozoic Crystalline Rocks: Peninsular Ranges batholith and pegmatites, Point Sal ophiolite. Dept. of Geol. Sci., San Diego State Univ. (1979). p. 83-110.

Slaughter, M. and Earley, J.W. (1965) Mineralogy and geological significance of the Mowry bentonites, Wyoming. Geol. Soc. America Spec. Paper 83, 116 p.

Smith, R.L. and Bailey, R.A. (1966) The Bandelier Tuff: A study of ash-flow eruption cycles from zoned magma chambers. Bull. Volcanol., Ser. 2, V. 29, p. 83-104.

Smith, R.L. and Bailey, R.A. (1968) Resurgent Cauldrons. Geol. Soc. America Memoir 116, p. 613-662.

Smith, R.L., Bailey, R.A., Ross, C.S. (1961) Structural evolution of the Valles caldera, New Mexico, and its bearing on the emplacement of ring dikes. U.S. Geol. Survey Prof. Paper 424-D, p. 145-149.

Smith, R.L. and Shaw, H.R. (1973) Igneous-related geothermal systems. U.S. Geol. Survey Circ. 726, p. 58-83.

Sorey, M.L. and Lewis, R.E. (1976) Convective heat flow from hot springs in the Long Valley caldera, Mono County, California. J. Geophys. Res., V. 81, p. 785-791.

Steeples, D.W. and Iyer, H.M. (1976) Low-velocity zone under Long Valley as determined from teleseismic events. J. Geophys. Res., V. 81, p. 849-860.

Steiger, R.H. (1964) Dating of orogenic phases in the central Alps by K-Ar ages of hornblende. J. Geophys. Res., V. 69, p. 5407-5421.

Steven, T.A., Lipman, P.W., Hail, W.J., Jr., Barker, F. and Luedke, R.G. (1974) Geologic map of the Durango Quadrangle, southwestern Colorado. U.S. Geol. Survey Misc. Inv. Map. I-764.

Stewart, J.H. (1978) Basin-range structure in western North America: A review. Geol. Soc. America Memoir 152, p. 1-32.

Streckeisen, A.L. (1973) Plutonic rocks: Classification and nomenclature recommended by the IUGS Subcommission on the systematics of igneous rocks. Geotimes, V. 18, No. 10, p. 26-30.

Suzuoki, T. and Epstein, S. (1976) Hydrogen isotope fractionation between OH-bearing minerals and water. Geochim. et Cosmochim. Acta, V. 40, p. 1229-1240.

Swanberg, C.A. and Blackwell, D.D. (1973) Areal distribution and geophysical significance of heat generation in the Idaho batholith and adjacent intrusions in eastern Oregon and western Montana. Geol. Soc. America Bull., V. 84, p. 1261-1282.

Talbot, J.L. (1977) The role of the Idaho batholith in the structure of the northern Rocky Mountains, Idaho and Montana. Northwest Geology, V. 6-1, p. 17-24.

Taubeneck, W.H. (1959) Age of granitic plutons in eastern Oregon. Geol. Soc. America Bull., V. 70, p. 1685 (Abst).

Taubeneck, W.H. (1971) Idaho batholith and its southern extension. Geol. Soc. America Bull., V. 82, p. 1899-1928.

Taylor, H.P., Jr. (1967) Oxygen isotope studies of hydrothermal mineral deposits: in Geochemistry of Hydrothermal Ore Deposits, ed. H.L. Barnes, 1967. Holt, Rinehart, and Winston Inc., p. 109-142.

Taylor, H.P., Jr. (1968) The oxygen isotope geochemistry of igneous rocks. Contrib. Mineral. Petrol., V. 19, p. 1-71.

Taylor, H.P., Jr. (1971) Oxygen isotope evidence for large-scale interaction between meteoric ground waters and Tertiary granodiorite intrusions, western Cascade Range, Oregon. J. Geophys. Res., V. 76, p. 7855-7874.

Taylor, H.P., Jr. (1973) O^{18}/O^{16} evidence for meteoric-hydrothermal alteration and ore deposition in the Tonopah, Comstock lode, and Goldfield mining districts, Nevada. Econ. Geol., V. 68, p. 747-764.

Taylor, H.P.,Jr. (1974a) Oxygen and hydrogen isotopic evidence for large-scale circulation and interactions between ground waters and igneous intrusions, with particular reference to the San Juan volcanic field, Colorado: in Geochemical Transport and Kinetics, eds. Hofmann, A.W., Giletti, B.J., Yoder, H.S., Jr. and Yund, R.A. Carnegie Institute of Washington Publication 634, 1974.

Taylor, H.P., Jr. (1974b) The application of oxygen and hydrogen isotope studies to problems of hydrothermal alteration and ore deposition. Econ. Geol., V. 69, p. 843-883.

Taylor, H.P., Jr. (1977) Water/rock interactions and the origin of H_2O in granitic batholiths. Jour. Geol. Soc. London, V. 133, p. 509-558.

Taylor, H.P., Jr. and Epstein, S. (1962) Relationship between O^{18}/O^{16} ratios in coexisting minerals in igneous and metamorphic rocks. Part I: Principles and experimental results. Geol. Soc. America Bull., V. 73, p. 461-480.

Taylor, H.P., Jr. and Epstein, S. (1962b) Relationship between O^{18}/O^{16} ratios in coexisting minerals of igneous and metamorphic rocks. Part II: Application to petrologic problems. Geol. Soc. America Bull., V. 73, p. 675-694.

Taylor, H.P., Jr. and Epstein, S. (1966) Deuterium-hydrogen ratios in coexisting minerals of metamorphic and igneous rocks(abst.) Trans. Amer. Geophys. Union, V. 47, No. 1, p. 213.

Taylor, H.P., Jr. and Forester, R.W. (1971) Low-^{18}O igneous rocks from the intrusive complexes of Skye, Mull, and Ardnamurchan, western Scotland. Jour. Petrology, V. 12, p. 465-497.

Taylor, H.P., Jr. and Forester, R.W. (1979) An oxygen and hydrogen isotope study of the Skaergaard intrusion and its country rocks: A description of a 55-m.y. old fossil hydrothermal system. Jour. Petrology, V. 20, p. 355-419.

Taylor, H.P., Jr. and Magaritz, M. (1976) An oxygen and hydrogen isotope study of the Idaho batholith (abst.). Trans. Amer. Geophys. Union, V. 57, p. 350.

Taylor, H.P., Jr. and Magaritz, M. (1978) Oxygen and hydrogen isotope studies of the Cordilleran batholiths of western North America: in Robinson, B.W., ed., Stable Isotopes in the Earth Sciences, DSIR Bull. 220, p. 151-173, New Zealand Dept. of Scientific and Ind. Res., Wellington, New Zealand.

Taylor, H.P.,Jr. and Silver, L.T. (1978) Oxygen isotope relationships in plutonic igneous rocks of the Peninsular Ranges batholith, southern and Baja California. Short papers of the Fourth Intl. Conf. on Geochron., Cosmochron., and Isotope Geol., U.S. Geol. Survey Open File Rept. 78-701, p. 423-426.

Thayer, T.P. and Brown, C.E. (1964) Pre-Tertiary orogenic and plutonic intrusive activity in central and northeastern Oregon. Geol. Soc. America Bull., V.75, p. 1255-1262.

Tilling, R.I., Klepper, M.R., and Obradovich, J.D. (1968) K-Ar ages and time span of emplacement of the Boulder batholith, Montana. Amer. Jour. Sci., V. 266, p. 671-689.

Todd, V.R. and Shaw, S.E. (1979) Structural, metamorphic and intrusive framework of the Peninsular Ranges batholith in southern San Diego County, California. Guidebook to field trip San Diego Geol. Soc. America Mtg., Mesozoic Crystalline Rocks: Peninsular Ranges Batholith and Pegmatites, Point Sal Ophiolite. Dept. of Geol. Sci., San Diego State Univ. (1979), p. 177-232.

Truesdell, A.H. (1974) Oxygen isotope activities and concentrations in aqueous salt solutions at elevated temperatures: Consequences for isotope geochemistry. Earth Planet. Sci. Lett., V. 23, p. 387-396.

Truesdell, A.H. and White, D.E. (1973) Production of superheated steam from vapor-dominated geothermal reservoirs. Geothermics, V. 2, p. 154-173.

Tschanz, C.M., Kiilsgaard, T.H., Seeland, D.A., VanNoy, R.M., Evans, R.D., Federspiel, F.E., Ridenour, J., Zilka, N.T., Tuckek, E.T. and McMahon, A.G. (1974) Mineral resources of the eastern part of the Sawtooth National Recreation Area, Custer and Blaine Counties, Idaho. U.S. Geol. Survey Open File Rept., 648 p.

Turi, B. and Taylor, H.P., Jr. (1971) An oxygen and hydrogen isotope study of a granodiorite pluton from the southern California batholith. Geochim. et Cosmochim. Acta., V. 35, p. 383-406.

Turner, D.L. and Forbes, R.B. (1976) K-Ar studies in two deep basement drill holes: A new geologic estimate of argon blocking temperature for biotite (abst.). Trans. Amer. Geophys. Union, V. 57, p. 353.

Vacquier, V., Steeland, N.C., Henderson, R.G. and Zeitz, I. (1951) Interpretation of Aeromagnetic Maps. Geol. Soc. America Memoir 47, 151 p.

Vallier, T.L. (1977) The Parmian and Triassic Seven Devils Group, western Idaho and northeastern Oregon. U.S. Geol. Survey Bull. 1437, 58 p.

Weissenborn, A.E. (1964) The mineral industry in Idaho: in Mineral and Water Resources of Idaho, U.S. Geol. Survey Spec. Rept. No. 1, p. 13-22.

Wenner, D.B. and Taylor, H.P., Jr. (1971) Temperatures of serpentinization of ultramafic rocks based on O^{18}/O^{16} fractionation between coexisting serpentine and magnetite. Contr. Mineral. Petrol., V. 32, p. 165-185.

White, D.E. (1940) Antimony deposits of a part of the Yellow Pine district, Valley County, Idaho. U.S. Geol. Survey Bull. 922-I, p.247-279.

White, D.E. (1973) Characteristics of geothermal resources: in P. Kruger and C. Otte, eds., Geothermal Energy: Resources, Production, Stimulation. Stanford Univ. Press, Stanford, California, p. 69-94.

White, D.E., Barnes, I. and O'Neil, J.R. (1973) Thermal and mineral waters of nonmeteoric origin, California Coast Ranges. Geol. Soc. America Bull., V. 84, p. 547-560.

White, D.E., Hem, J.D. and Waring, G.A. (1963) Chemical compositions of subsurface waters: in Data of Geochemistry: U.S. Geol. Survey Prof. Paper 440-F, 67 p.

White, D.E., Muffler, L.J.P, and Truesdell, A.H. (1971) Vapor-dominated hydrothermal systems compared with hot water systems. Econ. Geol., V. 66, p. 75-97.

Williams, H., Turner, F.J. and Gilbert, C.M. (1954) Petrography: An Introduction to the Study of Rocks in Thin Section. W.H. Freeman and Co., San Francisco, 406 p.

Williams, L.D., (1979) General geology of a section across the Bitterroot lobe of the Idaho batholith. Northwest Geology, V. 8, p. 29-39.

Williams, P.L. (1961) Glacial Geology of Stanley Basin. Idaho Bur. Mines and Geol. Pamph. 123, 29 p.

Yoder, H.S. and Eugster, H.P. (1955) Synthetic and natural muscovites. Geochim. et Cosmochim. Acta, V. 8, p. 225-280.

Zietz, I. Gilbert, F.P. and Kirby, J.R., Jr. (1978) Aeromagnetic map of Idaho: color coded intensities. U.S. Geol. Survey Geoph. Inv. Map GP-920.

Appendix 1 — δD determinations of Modern Thermal Waters from the Idaho Batholith

A few δD determinations were made of thermal springs from the Atlanta lobe:

Name	T-R-S	δD	Elevation	Temp° C*	Discharge gpm*
Kirkham Hot Spr.	9-8-32	-141	4000'	49-64	250
Sacajawea Hot Spr.	10-11-33	-142	5000'	68	100
Preis Hot. Spr.	3-14-19	-149	5680'	41	10
Sunbeam Hot Spr.	11-15-19	-154	5960'	76	200

*from Ross (1971)

These values compare closely with δD analyses for the S. Fork of the Payette River (-130) and for a rainstorm near Boise (-153), which is strong evidence that the thermal waters are heated meteoric waters. A decrease in δD with increasing elevation, as shown by the thermal springs, is also a characteristic of meteoric waters in many localities (see Dansgaard, 1964). The differing δD contents of these thermal springs proves that a significant proportion (or all) of the waters in each hot spring system are derived from independent, localized recharge areas. Many of the modern thermal springs appear to be utilizing the fracture zones of the ancient (Eocene) geothermal systems.

Appendix 2 $\delta^{18}O$ Determinations of Challis Volcanic Rocks

A few $\delta^{18}O$ measurements were made of Challis volcanic rocks. As the thesis was near completion when the analyses became available, these numbers are not discussed in the text. All samples were collected immediately east of the Atlanta lobe.

Field #	Rock Type	$\delta^{18}O_{WR}$	LAT.	LONG.
RC 32	Andesite	-1.4	44°22.80'	114°43.18'
RC 33	Andesite	4.8	44°23.84'	114°38.79'
RC 34b	Andesite	0.9	44°23.65'	114°38.30'
RH 76	Dacite Porphyry	5.3	43°52.68'	114°43.39'

The analyses show that two rocks have been strongly depleted in ^{18}O compared to their primary values which were probably about +6 or higher. One of these low ^{18}O rocks (RC 34b) was collected within 4 km of the General Custer Mine; this sample lies within one hundred meters of a dacite porphyry dike (RC 34a) which has a similar $\delta^{18}O$ value (0.1). Undoubtedly a sizeable, post early Challis hydrothermal system was established at this locality, and is probably related to the mineralization. It is considered likely that the convective system was established around a crosscutting, ~3 km diameter intrusive mass of dacite porphyry located immediately to the west (see map by Anderson, 1949).